AD-A044 031 SOUTHERN RESEARCH INST BIRMINGHAM ALA F/G 11/9
EVALUATION OF THE COMPRESSIVE PROPERTIES OF A SPECIAL 3DQP.(U)
SEP 76 J R KOENIG, G F FORNARO DNA001-75-C-0037
UNCLASSIFIED SORI-76-483-3406-9-I-F DNA-4174F NL

1 OF 2
AD A044031

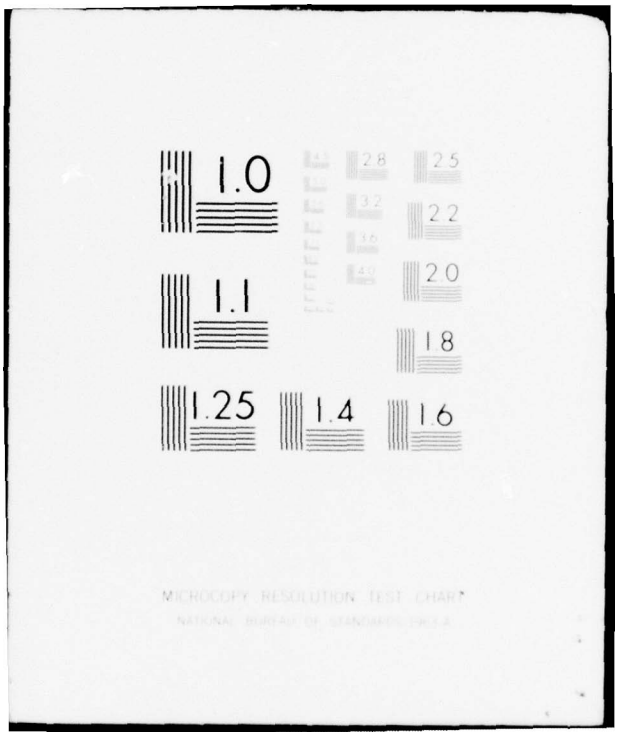
1.0
1.1
1.25
1.4
1.6
2.8
2.5
3.2
2.2
3.6
2.0
4.0
1.8
MICROCOPY RESOLUTION TEST CHART
NATIONAL BUREAU OF STANDARDS 1963-A

DNA 4174F

EVALUATION OF THE COMPRESSIVE PROPERTIES OF A SPECIAL 3DQP

Southern Research Institute
2000 Ninth Avenue South
Birmingham, Alabama 35205

16 September 1976

Final Report for Period October 1975—August 1976

CONTRACT No. DNA 001-75-C-0037

THIS WORK SPONSORED BY THE DEFENSE NUCLEAR AGENCY
UNDER RDT&E RMSS CODE B342075464 N99QAXAC31320 H2590D.

Prepared for
Director
DEFENSE NUCLEAR AGENCY
Washington, D. C. 20305

Destroy this report when it is no longer needed. Do not return to sender.

UNCLASSIFIED

SECURITY CLASSIFICATION OF THIS PAGE (When Data Entered)

REPORT DOCUMENTATION PAGE	READ INSTRUCTIONS BEFORE COMPLETING FORM
1. REPORT NUMBER: DNA 4174F	2. GOVT ACCESSION NO. / 3. RECIPIENT'S CATALOG NUMBER
4. TITLE (and Subtitle): EVALUATION OF THE COMPRESSIVE PROPERTIES OF A SPECIAL 3DQP	5. TYPE OF REPORT & PERIOD COVERED: Final Report for Period Oct 75—Aug 76
	6. PERFORMING ORG. REPORT NUMBER: 76-483-3406-9-I-F
7. AUTHOR(s): J. R. Koenig, G. F. Fornaro	8. CONTRACT OR GRANT NUMBER(s): DNA 001-75-C-0037
9. PERFORMING ORGANIZATION NAME AND ADDRESS: Southern Research Institute, 2000 Ninth Avenue South, Birmingham, Alabama 35205	10. PROGRAM ELEMENT, PROJECT, TASK AREA & WORK UNIT NUMBERS: Subtask N99QAXAC313-20
11. CONTROLLING OFFICE NAME AND ADDRESS: Director, Defense Nuclear Agency, Washington, D.C. 20305	12. REPORT DATE: 16 September 1976
	13. NUMBER OF PAGES: 188
14. MONITORING AGENCY NAME & ADDRESS (if different from Controlling Office): DCASD Birmingham, 908 South 20th Street, Birmingham, Alabama 35205	15. SECURITY CLASS. (of this report): UNCLASSIFIED
	15a. DECLASSIFICATION/DOWNGRADING SCHEDULE

16. DISTRIBUTION STATEMENT (of this Report)

Approved for public release; distribution unlimited.

17. DISTRIBUTION STATEMENT (of the abstract entered in Block 20, if different from Report)

18. SUPPLEMENTARY NOTES

This work sponsored by the Defense Nuclear Agency under RDT&E RMSS Code B342075464 N99QAXAC31320 H2590D.

19. KEY WORDS (Continue on reverse side if necessary and identify by block number)

Compression
3DQP
Test Techniques
Composites

20. ABSTRACT (Continue on reverse side if necessary and identify by block number)

The compression properties of two cylinders of 3DQP composites were evaluated in the axial and hoop directions using two test techniques.

DD FORM 1 JAN 73 1473 EDITION OF 1 NOV 65 IS OBSOLETE

UNCLASSIFIED

SECURITY CLASSIFICATION OF THIS PAGE (When Data Entered)

TABLE OF CONTENTS

LIST OF ILLUSTRATIONS

LIST OF ILLUSTRATIONS (Continued)

LIST OF ILLUSTRATIONS (Continued)

LIST OF TABLES

EVALUATION OF THE COMPRESSIVE PROPERTIES OF A SPECIAL 3DQP

INTRODUCTION

The intent of this program was the evaluation of the hoop and axial compressive properties of two cylinders of three dimensional quartz phenolic. Both cylinders were manufactured by the C process/slat technique and both had an A_r/A_t of roughly 0.7. Cylinder 6.1.4 was seven inches in diameter and cylinder 4.1.18 was approximately 14 inches in diameter.

Two basic specimen configurations were utilized. One was the curved coupon as originally designed by Southern Research Institute (SoRI) in the conduction of the Composite Response Study (CRS). The other was a somewhat shorter and thinner specimen with straight edges and no reduced gage section. These will be referred to as the SoRI design, and the rectangular design, respectively, throughout this report. The resulting data enabled a direct comparison of specimen types, as well as the associated test techniques, to be made. This program was conducted under DNA Contract DNA001-75-C-0037.

TEST MATRIX

SoRI received 2 in. x 2 in. arcs from cylinder 6.1.4 from which hoop and axial specimens of the two design types were machined. In addition specimens of the rectangular design were premachined and sent to SoRI. The test matrix indicating the type and quantity of specimens is shown in Table 1.

CUTTING PLAN

The cutting plan for excising the specimen blanks from cylinder 6.1.4 is shown in Figure 1. From this cylinder SoRI received the twelve arcs labeled SoRI 1 through 12. Arcs 1, 3, 6, 7, 9, and 11 were labeled for use in making

circumferential specimens and arcs 2, 4, 5, 8, 10 and 12 were labeled for making axial specimens.

After NDC of the arcs, these were machined by SoRI into specimens per the following table.

	Side One	Side Two
C-1	1 SoRI[1] Circ	2 Rectangular Circs[2]
A-2	1 SoRI Axial	-
C-3	1 SoRI Circ	2 Rectangular Circs[2]
A-4	1 SoRI Axial	-
A-5	1 SoRI Axial	1 Rectangular Axial[3]
C-6	-	1 SoRI Circ
C-7	1 SoRI Circ	1 SoRI Circ
A-8	1 SoRI Axial	1 Rectangular Axial[3]
C-9	-	1 SoRI Circ
A-10	1 SoRI Axial	-
C-11	1 SoRI Circ	1 SoRI Circ
A-12	1 SoRI Axial	

[1] Refers to specimen design - see Test Technique section

[2] Consisted of four pieces - two from inside and two from outside (labeled In and Out)

[3] Labeled 5-AC-Rect* and 8-AC-Rect*

In addition, SoRI received six axial specimens of the rectangular design pre-machined by the sponsor from the segments directly below arcs 2, 4, 5, 8, 10 and 12, which were labeled 2-AC-Rect, 4-AC-Rect, etc. The remainder of the material was retained for further use by the sponsor.

The cutting plan used by the sponsor for cylinder 4.1.1ð is shown in Figure 2. Of the specimens indicated, SoRI received axial specimens A4, A13, A19, A30, and A39,

and hoop specimens H7, H16, H24, H32, and H33. In addition, axial specimens A43, A46, A48 and A50 were machined from the portion indicated as spare and sent to SoRI.

NONDESTRUCTIVE TEST TECHNIQUES

Radiography

Radiography was performed using state-of-the-art X-ray techniques for low absorptive materials. The radiography unit is a Radiflour 360 manufactured by Torr X-Ray Corporation, rated for operation from 0 to 120KV at either 3 or 5 MA. A beryllium window and small focal spot size (0.35mm) are two characteristics which enable it to examine low absorptive materials with high resolution and sensitivity. Radiographic sensitivity using extra-fine grain film is less than two percent.

The twelve arcs from cylinder 6.1.4 were radiographed simultaneously using a turntable technique before machining into finished specimens. After machining, the SoRI design, the rectangular design, and the premachined specimens were radiographed in groups of varying size. All arcs and specimens were positioned with the axial fibers parallel to the source to enable variations in the circumferential fibers to be viewed. In addition the SoRI design axial specimens were also X-rayed in the circumferential direction.

Gravimetric Bulk Density

Bulk density was determined from direct measurements of weight and dimensions. Weight measurements were made on an analytical balance having a sensitivity of +0.0001 gram. Dimensional measurements were made to the nearest 0.0005 inch using micrometers.

The densities of the twelve arcs were determined before final machining, while those of the additional specimens received by SoRI were calculated for each individual specimen.

Ultrasonic Velocity

Acoustic velocity was measured using the through-transmission, elapsed-time technique. In this method, an electrical pulse originated in a pulse generator and was applied to a ceramic piezo-electric crystal (SFZ). The pulse generated by this crystal was transmitted through a short delay line and inserted into the specimen. The time of insertion of the leading edge of this sound beam was the reference point on the time base of the oscilloscope, which was used as a high speed stop watch. When the leading edge of this pulse of energy reached the other end of the specimen, it was displayed on the oscilloscope. The difference between the entrance and exit times was used with the specimen length in calculating ultrasonic velocity. Appendix B should be consulted for a more extensive explanation of the ultrasonic velocity technique.

For Arcs 1, 3, 6, 7, 9, 11, those from which hoop specimens were to be machined, velocity was determined in both the radial and circumferential directions. The remaining arcs, designated for axial specimens, had velocity calculated in the axial direction only.

COUPON COMPRESSION TEST TECHNIQUE

The basic compressive test apparatus had three structural components: a sleeve, a lower grip, and an upper grip as shown in Figures 3 and 4. The lower grip rested on the fixed platform of a conventional loading

frame, while the upper grip was located between the specimen and the moving crosshead. A Tinius Olsen screw-driven compression machine, with a maximum capacity of 30,000 pounds was used in this program. The applied load was monitored directly from the built-in load cell in the platform of the machine. Perpendicular alignment of the load was ensured by the guiding action of the sleeve which fits (within 0.001 in.) around the upper and lower grips. The specimen was held firmly in place in precision inserts which were bolted into the grips. A separate set of inserts was designed to exactly match each of the four specimen configurations used.

SoRI Axial Specimen Configuration

The axial compressive test was used to determine the axial compressive modulus and axial ultimate compressive strength. The axial specimen designed at SoRI having an overall length of 2 in. with a 0.5 in. x 0.6 in. x 0.7 in. gage section is shown in Figure 5. The inside and outside radii of the specimen were approximately the same as the original cylinder which allowed the circumferential fibers to remain intact across the gage section of the specimen.

Axial strain was measured by two independent systems. Clip-ons and surface strain gages were mounted on both edges of the specimens (see Figure 6). Each set of gages was wired in series and the signals from each were monitored on individual x-y recorders. This provided an immediate indication of the relative accuracy of the two strain measuring techniques.

SoRI Circumferential Specimen Configuration

The SoRI circumferential specimen (Figure 7) was designed to enable the determination of circumferential

compressive modulus and ultimate strength. Ideally, inside and outside radii would have been carefully machined in order to provide a uniform distribution of circumferential fibers. However, due to time constraints, the specimens were machined to accommodate the 4.5 in. radius hardware developed for the CRS program. This change from the optimal design allowed approximately one-half ply to "run out" over the length of the gage.

The loading apparatus was the same as used in the axial compressive test with the addition of a lateral support arm. As compressive loads were applied to the grips, the gage section of the specimen experienced both bending and axial compressive loads. However, the support arm, which was inserted through a cutout in the sleeve, was applied in a manner which negated the bending effect. Clip-on gages on the inner and outer faces continuously monitored the displacements there. By adjusting the support arm both displacements were maintained equal and the stress in the gage section was considered nominally uniform. The modulus and ultimate strength were determined as though the loading were simple uniaxial.

Again, both clip-ons and strain gages were mounted on the edges of the specimen. Figure 8 shows a schematic view of the overall instrumentation including a total of four clip-ons and two surface strain gages per specimen.

Rectangular Axial Specimen Configuration

The rectangular axial compressive specimen is shown in Figure 9. It was tested in the same apparatus as described above with a similar arrangement of clip-ons and strain gages as described previously. Except for a miniaturized set of clip-on arms designed to fit the smaller specimen size, the instrumentation (Figure 10) and recording procedures were identical to those used for the SoRI designed axial specimen.

Rectangular Circumferential Specimen Configuration

The rectangular designed circumferential specimen consisted of two separate 1.00 in. x 0.300 in. x 0.150 in.

pieces cut from a circumferential chord of a cylinder. They were mounted face to face in the inserts, with the circumferential fibers from each "half-specimen" bowing towards the center (see Figure 11). This eliminated most bending moment as the two halves tended to apply lateral support to one another during compression. This specimen is often referred to as the "belly to belly" configuration.

The instrumentation was again similar to that described before with a few minor changes. The clip-ons were mounted on opposing sides of the specimen rather than on the edges. Furthermore, a surface strain gage was located on each edge of each "half-specimen" resulting in a total of four gages per specimen (Figure 12). The four gages were monitored two at a time until it was determined that negligible discrepancies occurred between the signals. In subsequent testing all four gages were wired together in series, producing one recorded signal.

NONDESTRUCTIVE CHARACTERIZATION OF 3DQP ARCS AND SPECIMENS

The twelve arcs received were examined using ultrasonic velocity, visuals and X-rays. The gravimetric density of each arc was also determined. For the ultrasonic data three points were measured in both the axial and circumferential directions at 0.25L, 0.5L and 0.75L along the surface. In the radial direction five points were measured, one at the center and one each at the center of four quadrants. These data are shown in Table 2 which reports only the average of the velocity data for each arc. Table 3 shows the density values for each of the specimens from 4.1.18 and Table 4 shows the densities of the six pre-machined specimens from 6.1.4. The average

data for the density of the arcs from 6.1.4 was 1.685 gm/cm^3 and for the specimens from 4.1.18, 1.625 gm/cm^3. The difference in the densities between the cylinders probably was not as great as this would indicate since the specimens from 4.1.18 came from near the inside of the arc. Similar specimens taken adjacent to the arcs in 6.1.4 had an average density of 1.662 gm/cm^3. The average velocities of the 6.1.4 arcs were 0.1798, 0.1809, and 0.1937 in./μsec in the axial, circumferential and radial directions, respectively.

Prints of the X-rays of both the specimens and the arcs are included as Figures 13 through 16. Notice the nature of the circumferential yarns, especially towards the center on the arcs from 6.1.4. This bending and waving of the circumferential yarns was evident in the visual examinations and is documented in a 20X photomicrograph in Figure 17. The montage was taken through the center of the arc viewing in the axial direction.

COMPRESSIVE TEST RESULTS

The results of the compressive tests are reported in tabular form in terms of three parameters - tangent modulus, ultimate stress, and ultimate strain. The modulus for each specimen was determined by calculating the slope of a tangent to the linear portion of the stress-strain curve. In many cases a slight nonlinear portion of the curve at low stress levels was ignored in the calculations. Since two independent strain measuring systems were utilized, moduli values as determined from both clip-ons and surface strain gages are reported. The strain-to-failure data are reported from clip-ons only, since strain gages typically give ambiguous results near the end of the run. The ultimate strain reported is the strain value corresponding to the ultimate stress.

The results of the six axial compressive tests using the SoRI design are summarized in Table 5. The average modulus was 2.06 x 10^6 psi (clip-ons) and 2.15 x 10^6 psi (strain gages), the average strength 55,733 psi and the average strain-to-failure 35 mils/in. The composite stress-strain curves from these six runs are shown in Figures 18 and 19 (clip-on and strain gage data, respectively). Repeatability is demonstrated by the narrow range within which all curves lie. Individual raw data curves are provided in Appendix A.

The results from the rectangular design axial compressive tests from cylinder 6.1.4 are shown in Table 6. The average modulus for these eight runs was 2.17 x 10^6 psi (both methods). The average strength was 52,338 psi and the average ultimate strain 28 mils/in. These data include results from two specimens which were machined at SoRI from arcs 5 and 8. Only limited significance may be attributed to the slightly higher values from these runs due to the small sample size. The composite stress-strain curves from these eight runs are shown in Figures 20 and 21.

The results from the rectangular design axial compressive tests on material from cylinder 4.1.18 are shown in Table 7. The average moduli from these nine tests was softer than that for the 6.1.4 material, 1.93 x 10^6 psi (clip-ons) and 1.86 x 10^6 psi (strain gages). The average strength was less than that from 6.1.4, 43,656 psi and the ultimate strain was lower, 24.3 mils/in. The composite plots for these runs are shown in Figures 22 and 23. Again, a very tight envelope may be constructed around the stress-strain curves.

The circumferential compressive test data using the

SoRI design specimen for material from cylinder 6.1.4 is given in Table 8. The average modulus, as calculated from the clip-on data was 3.54×10^6 psi and 3.78×10^6 psi per strain gages. The ultimate strength was 75,050 psi and ultimate strain 23.7 mils/in. The composite plot of the stress-strain curves is shown in Figures 24 and 25.

The rectangular design circumferential data on material from cylinder 6.1.4 is given in Table 9. These were machined by SoRI from Arcs 1 and 3. One inner and one outer specimen was obtained from each arc. The average modulus using both inners and outers was 3.77×10^6 psi (clip-ons), average strength, 59,050 and average ultimate strain 17.3 mils/in. In this case the clip-ons were attached to the faces rather than the edges of the specimens. The average strain gage modulus measured was 3.61×10^6 psi. The distinction between the inner and outer specimens is evident, the inners being stronger (average strength, 61,600 psi) than the outers (56,500 psi) and, perhaps, stiffer (per clip-ons). Notice that the same trend exists for these data points as for the SoRI design specimens, arc 1 was stronger but less stiff than arc 3 (arc 3 was denser). These comparisons will be discussed further later. The composite plot of the stress-strain curves are shown in Figures 26 and 27.

The circumferential compressive data (rectangular design specimen) from cylinder 4.1.18 are given in Table 10. The moduli data from the clip-on gages vary widely due, apparently, to bending in some of the specimens. Again, the clip-ons were mounted on the faces while the strain gages were on the edges. The average modulus per the clip-ons was 4.00×10^6 psi and per the strain gages was 3.53×10^6 psi. The average strength was 63,420 psi

and ultimate strain, 17.3 mils/in. The composite stress-strain curves are shown in Figures 28 and 29. Evidence of relatively severe bending is obvious at low stress levels for specimen H32-CC-Rect. The apparent negative strain was verified by visual observation of the specimen during the test. As the load was initially applied, slight gaps, which were observed visually, opened between the two "half-specimens". This indicated that they were actually bending away from each other instead of applying mutual lateral support, as intended. The modulus as calculated from the subsequent linear portion of the curve (4.25×10^6 psi), still falls within the range of values from the other specimens in this group.

Prior Data and Materials

A summary of some prior experience with this class of materials is provided in Tables 11 (Axial) and 12(Hoop). As is evident, material differences make the comparison difficult. A large segment of the prior data was conducted on Process A materials. The best comparisons came from the CRS program. This program was conducted on Process C material (pineapple) on which optimal test techniques were developed. Examples of the data generated are given in Figures 30 (Axial) and 31 (Hoop). The 6.1.4 material is less stiff but stronger than the CRS material.

Clip-on Gages versus Strain Gages

As was mentioned earlier, both clip-on gages and surface mounted strain gages were used to monitor strain for each run. In general, good agreement has been achieved between the two techniques. This is shown graphically in Figures 32 through 37 in which the moduli calculated from both techniques are displayed for the various specimen types. Excellent agreement can be seen for specimens from the

axial direction (both designs) where, in many cases, data points from the two methods fall directly on top of one another (Figures 32 through 34). Slightly more variation is evident in the data from the circumferential direction specimens (Figures 35 through 37) with differences typically ranging up to approximately 10 percent. The fact that specimens H32 and H33 (Figure 37) vary by more than this amount can be attributed to bending in the specimens. Since the specimen halves tended to bow toward the clip-ons, the apparent strain for a given stress level was less than that recorded by surface strain gages mounted on perpendicular sides. This produced an uncharacteristically high modulus in these cases.

For composite materials of this type, clip-on data is considered to be more representative of the true material response than surface strain gages. This data does have the question of effective gage length since the clip-on flags span 0.1 inch of the gage section. However, from previous experience with composite materials, this difference has been found to be negligible. Clip-ons enable local effects, if any, to be avoided by measuring strain over a longer gage length than surface strain gages. Nevertheless, strain gages do provide valid data for comparison purposes if the cell size is sufficiently small in relation to the gage length. Proper application and alignment promotes repeatability and a degree of confidence in the data.

For specimens of both designs from the axial direction either method is suitable as was demonstrated previously, while the clip-on method is desired for the SoRI design circumferential specimen. For the case of the rectangular design circumferential specimen, the strain gage data are

preferable since the clip-on data were more adversely affected by bending in the specimen.

Inside versus Outside

The CRS program showed the distinction to be very small between the material near the ID and material near the OD. It appears to be somewhat stronger in the case of cylinder 6.1.4 but the data gathered are insufficient for a strong conclusion. A summary of pertinent data are shown in Table 13. Further study would be required to develop a correlation.

Effect of Specimen Design

The moduli of specimens from cylinder 6.1.4, as calculated from both the clip-on gages and the strain gages agree very well between the SoRI specimen design and test technique and the rectangular specimen design and test technique. A comparison is shown in Figures 38 (clip-on) and 39 (strain gage) and in Table 14. The ultimate stresses and strains do not correlate well, the SoRI technique showing the material to be stronger with a higher strain ultimate. A comparison of this data is shown in Figures 40 and 41.

Seven Inch (6.1.4) versus Fourteen Inch (4.1.18) Cylinder Data

The comparison between cylinders 6.1.4 and 4.1.18 can be made using data generated on the rectangular design specimens. These data are summarized in Table 15. The larger cylinder appears to be slightly softer and weaker than the 7 inch cylinder. However, the circumferential strength of the 4.1.18 cylinder is actually higher. This may not actually be true based on the comparison of rectangular and SoRI test techniques. The difference in the ultimate

strengths measured between the two techniques is less for the axial specimens than for the circumferential specimens. Taking this a step further, the fourteen inch cylinder with less curvature may be showing less degradation of its true strength vis a vis the 6.1.4 specimens. These data are plotted by specimens in Figures 42 through 46.

CONCLUSIONS

Several general conclusions may be drawn from the test data which has been reported and analyzed in this report. Material from cylinder 6.1.4 can be compared to that from cylinder 4.1.18 by considering results from the rectangular design specimens. Cylinder 6.1.4 is definitely stiffer and stronger in the axial direction. In the circumferential direction the moduli values are more nearly equivalent while the ultimate strength of cylinder 4.1.18 is slightly higher. Further testing of material from cylinder 4.1.18 using the SoRI design specimen would be necessary to validate the legitimacy of the circumferential strength.

The results from cylinder 6.1.4 may be compared with previous SoRI data from the CRS program since identical specimen configurations were used. The 6.1.4 material is less stiff but stronger in both directions than the CRS materials. Also the 6.1.4 material showed extreme "waviness" of the circumferential yarns, especially near the center of the original arcs. This is considered atypical when compared to the CRS material. The processing differences between the materials obviously contributed to the data variability.

Clip-on extensometers and surface mounted strain gages are both viable methods of measuring deformation in the

type of materials considered here. Results from the two techniques vary minimally except in the case of circumferential specimens. These discrepancies were able to be traced directly to specimen design. Except where other factors are involved, the clip-on data are considered to give slightly more representative results.

The SoRI and rectangular design specimens showed similar moduli values in both directions, when measured by either strain device. However, the ultimate strength values from the SoRI specimen are much higher especially in the circumferential direction, where the SoRI type produced a maximum stress approximately 27 percent higher than the rectangular specimen. Apparently, the utilization of lateral support during the test enabled an accurate assessment of the material's resistance to uniaxial compressive loads without the introduction of unknown bending stresses. The curved coupon and its associated test technique must be considered more valid than the smaller rectangular specimen test technique.

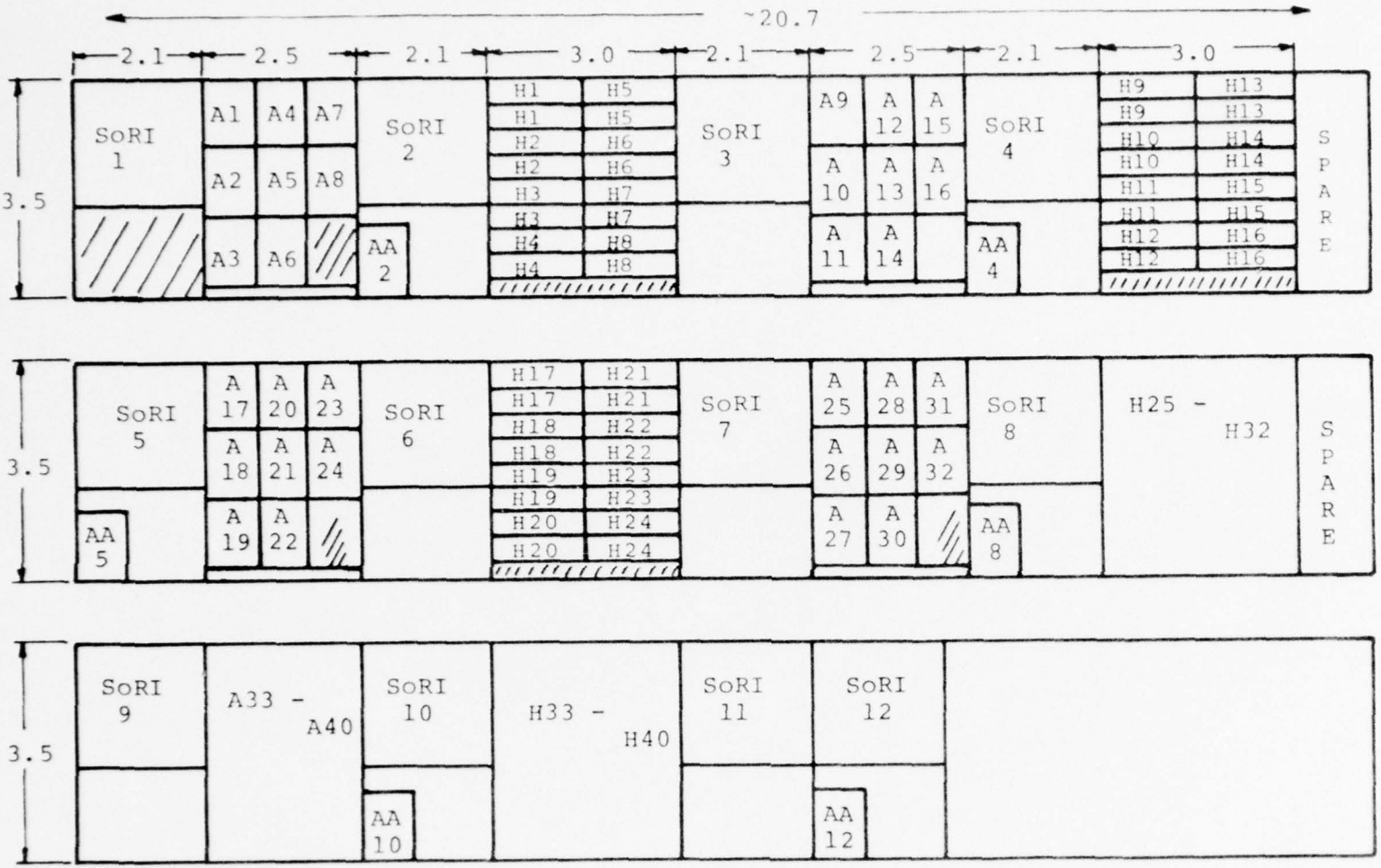

Figure 1. Cut Up of 6·1·4

Dimensions of Specimens

Axial Compression: 1 inch long x 2 cells wide x 0.2 inch thick

Hoop Compression: 1 inch long x 0.3 inch wide x 0.15 inch thick

SoRI Blanks: 2 inches long x 2 inches long x full wall thickness

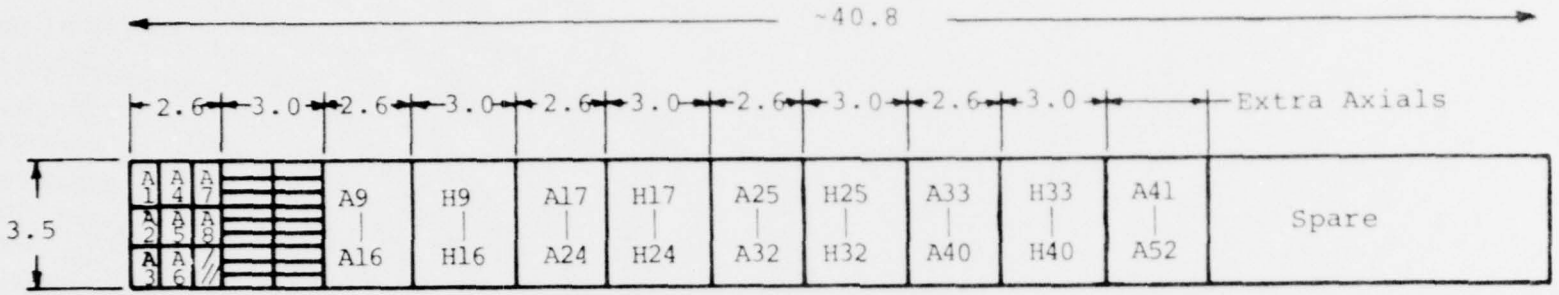

Dimensions of Specimens

Axial Compression: 1 inch long x 2 cells wide x 0.2 inch thick
Hoop Compression: 1 inch long x 0.3 cells wide x 0.15 inch thick

Figure 2. Cut up of 4·1·18

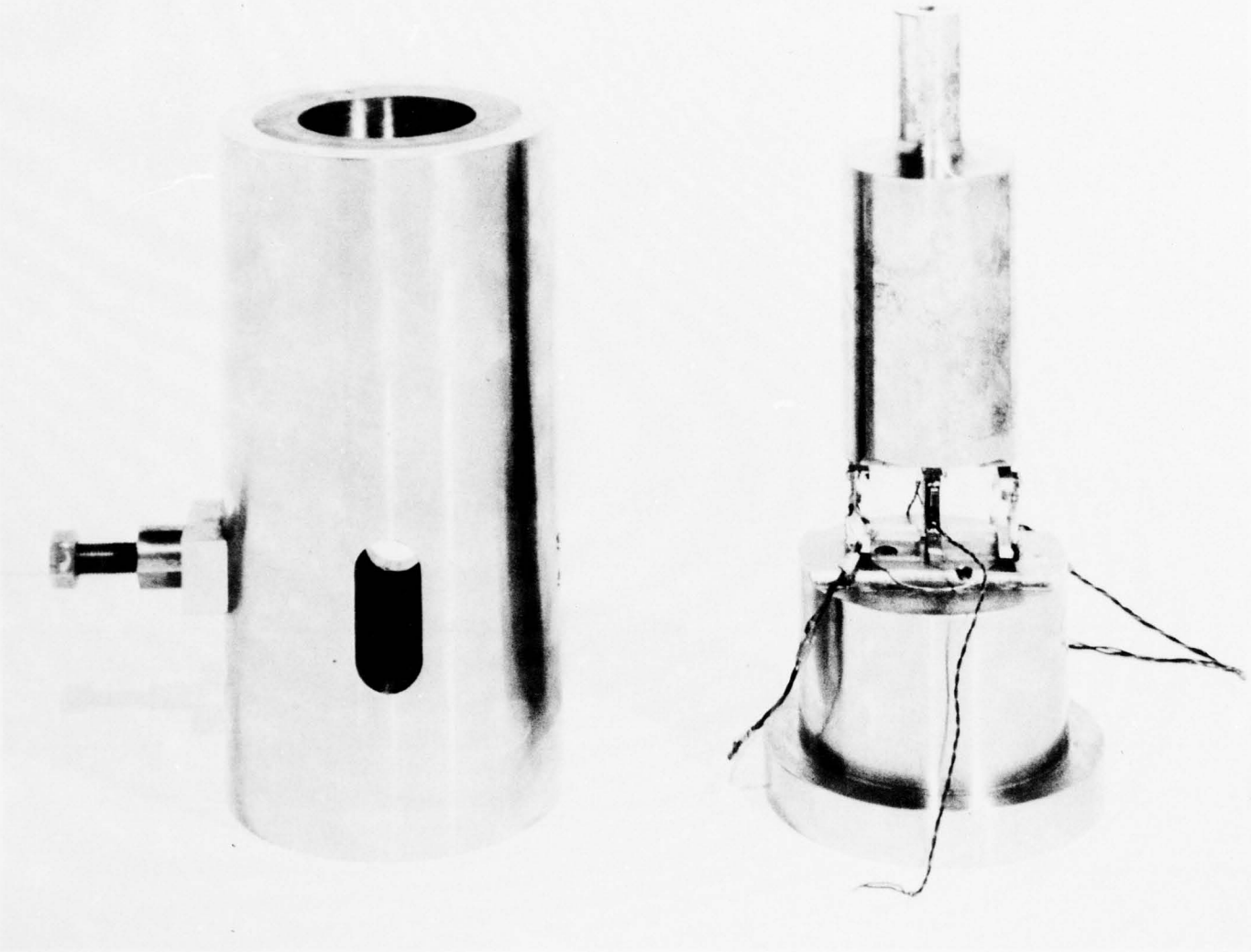

Figure 3. Compressive Test Apparatus for Curved, Circumferential and Axial Coupons

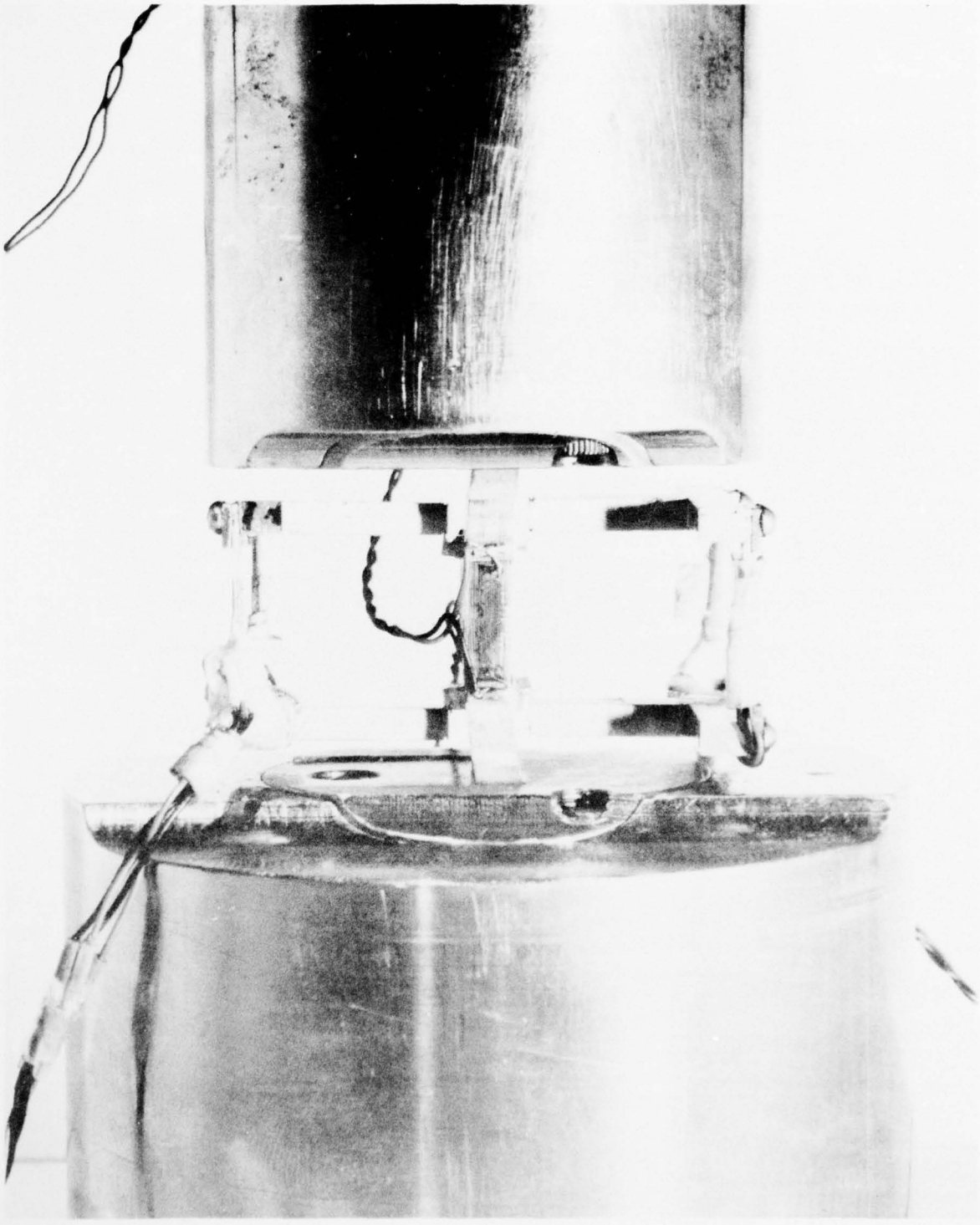

Figure 4. Details of the Curved Circumferential, Compressive Test (Additional Clip-On Gages Were Mounted on the Edges [not shown in photo])

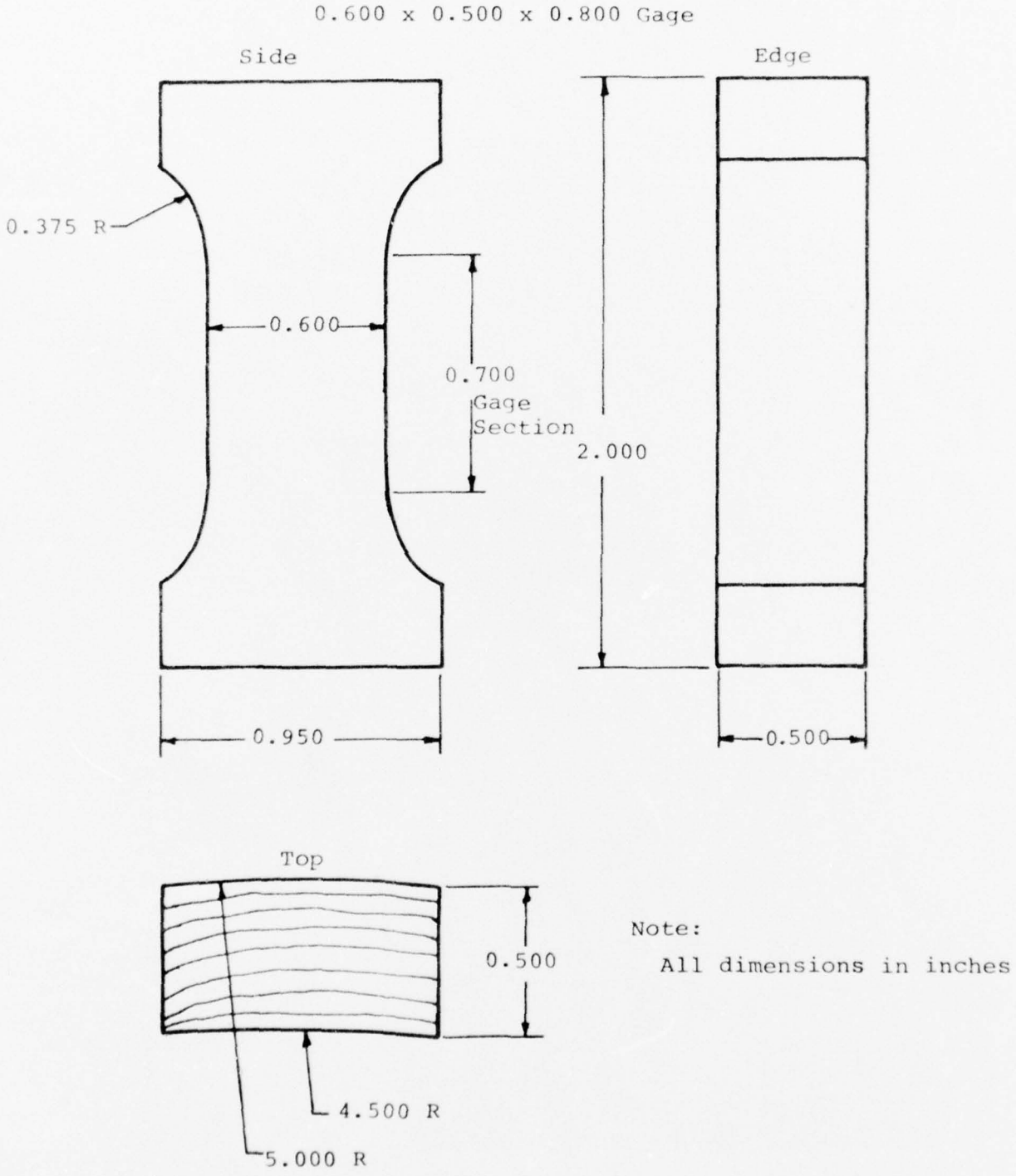

Figure 5. SoRI Design Axial Specimen

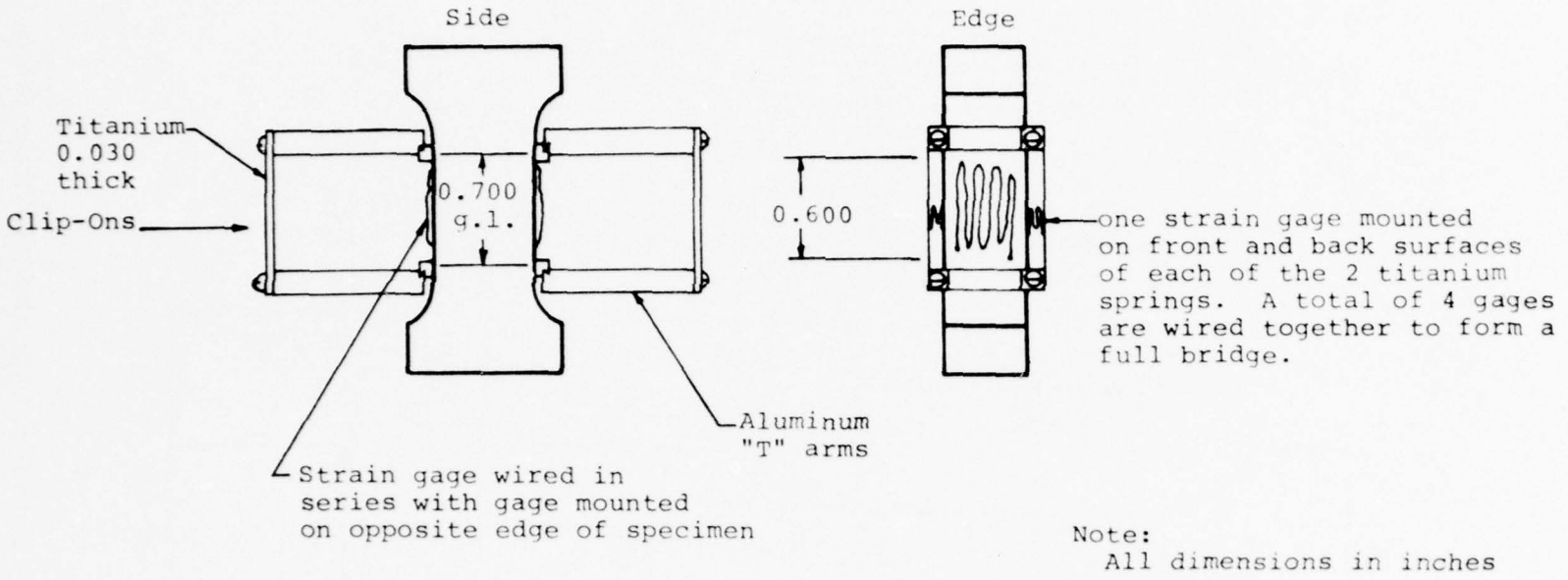

Figure 6. SoRI Design Axial Specimen - Clip-On and Strain Gage Configuration

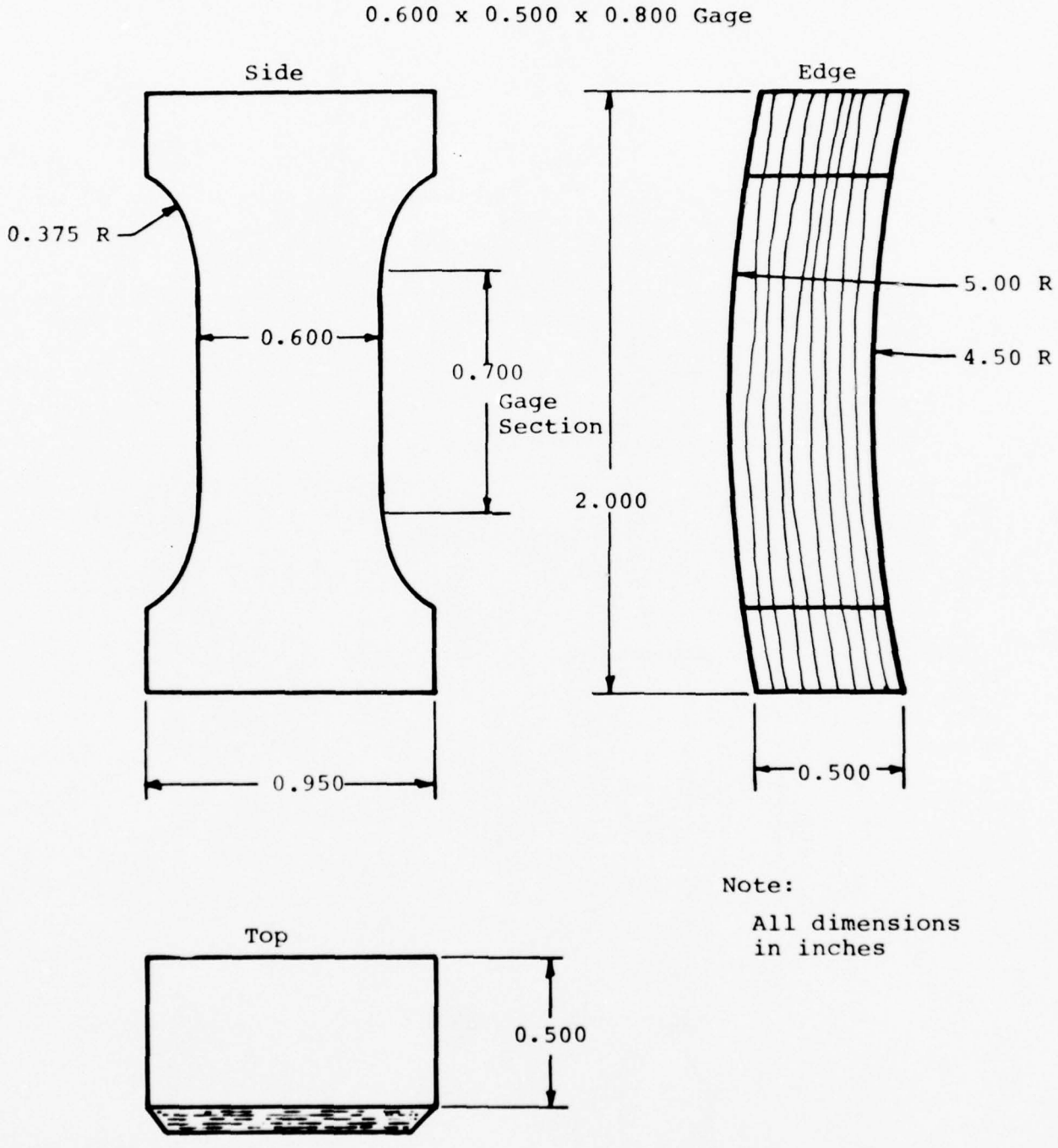

Figure 7. SoRI Design Circumferential (Hoop) Specimen

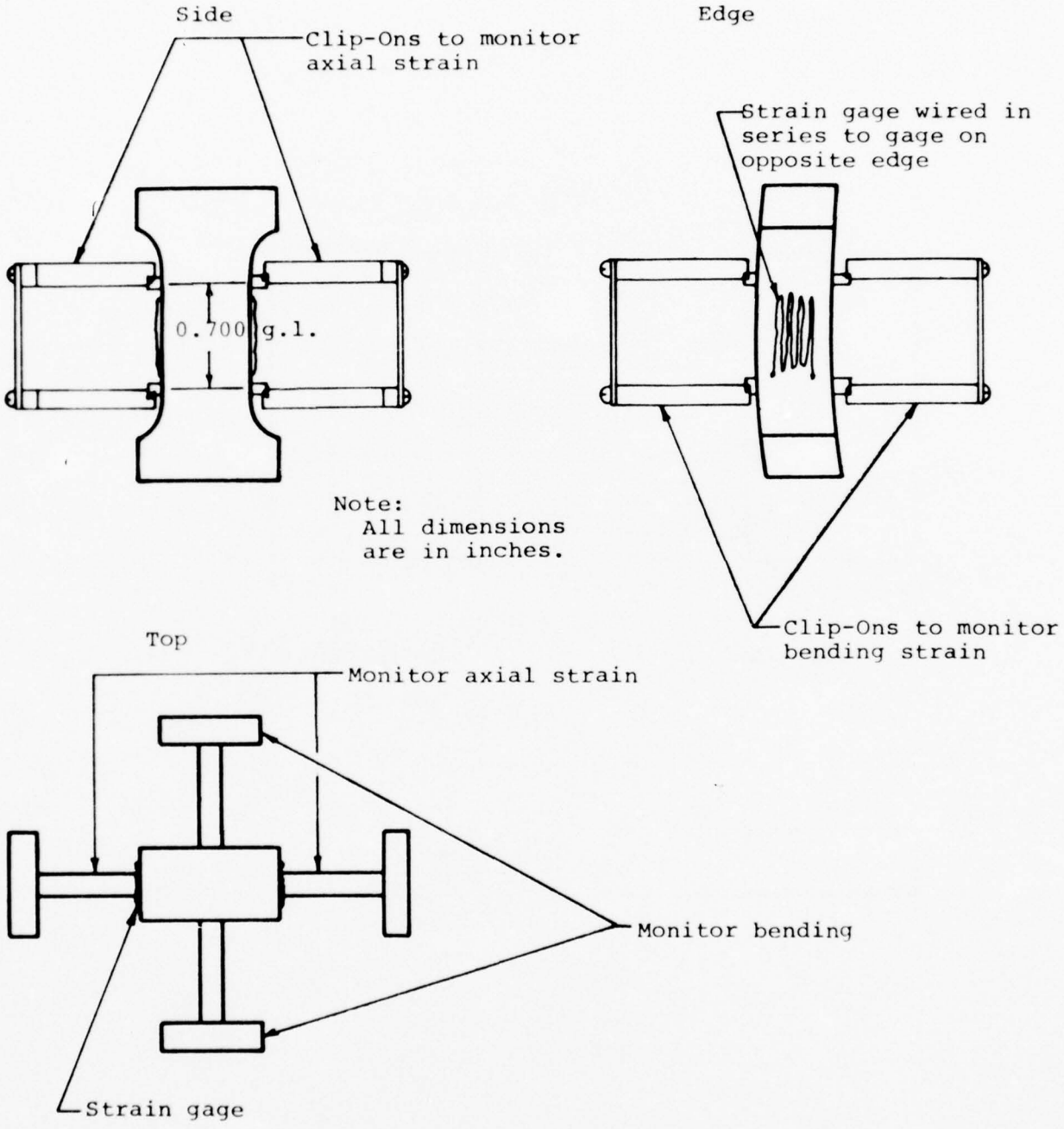

Figure 8. SoRI Design Circumferential Specimen - Clip-On and Strain Gage Configuration

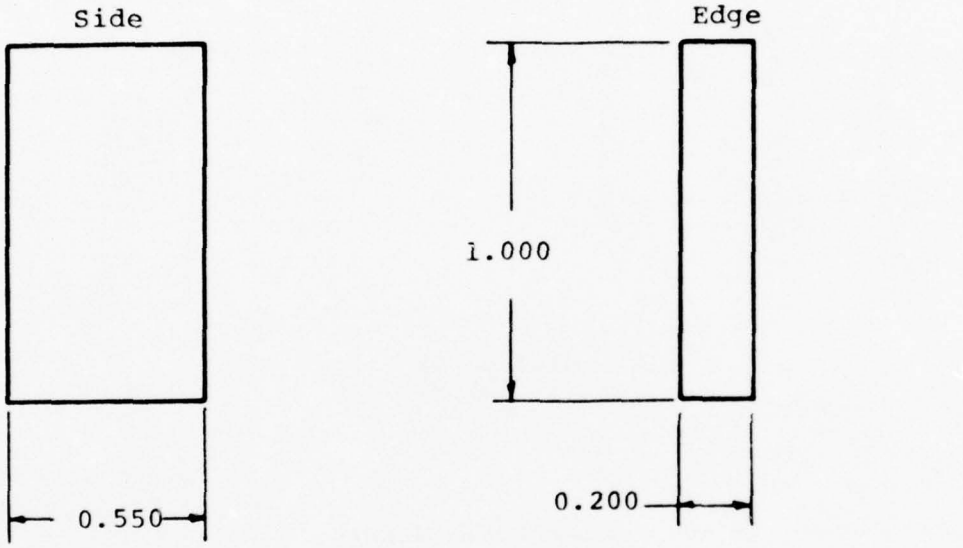

Figure 9. Rectangular Design Axial Specimen 1.000 x 0.550 x 0.200

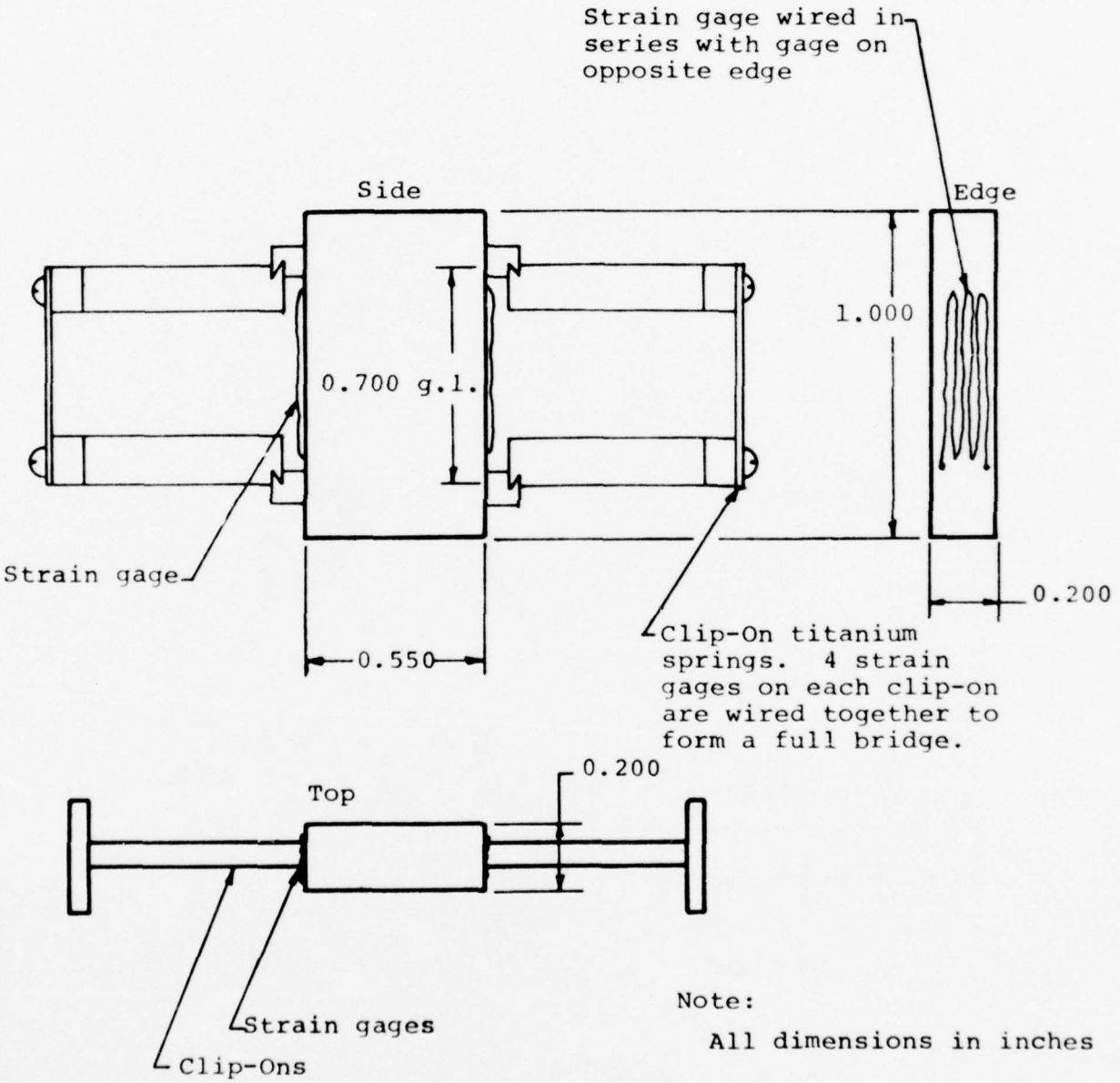

Figure 10. Rectangular Design Axial Specimen - Clip-On and Strain Gage Configuration (1.000 x 0.550 x 0.200)

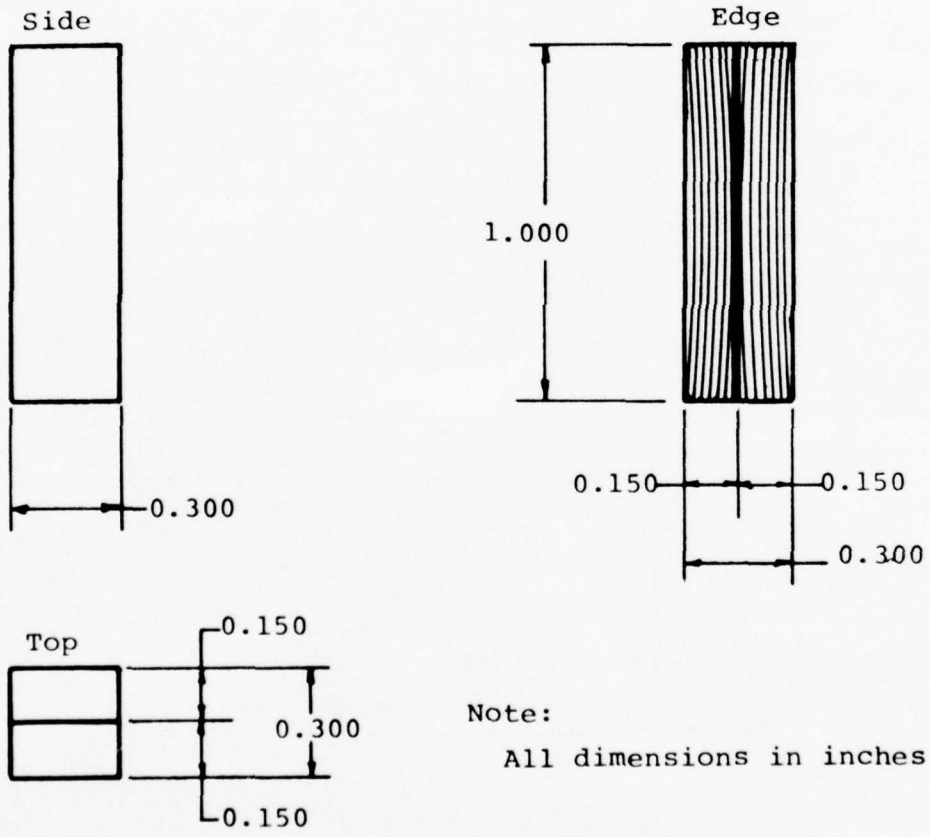

Figure 11. Rectangular Design Circumferential (Hoop) Specimens (1.000 x 0.300 x 0.300)

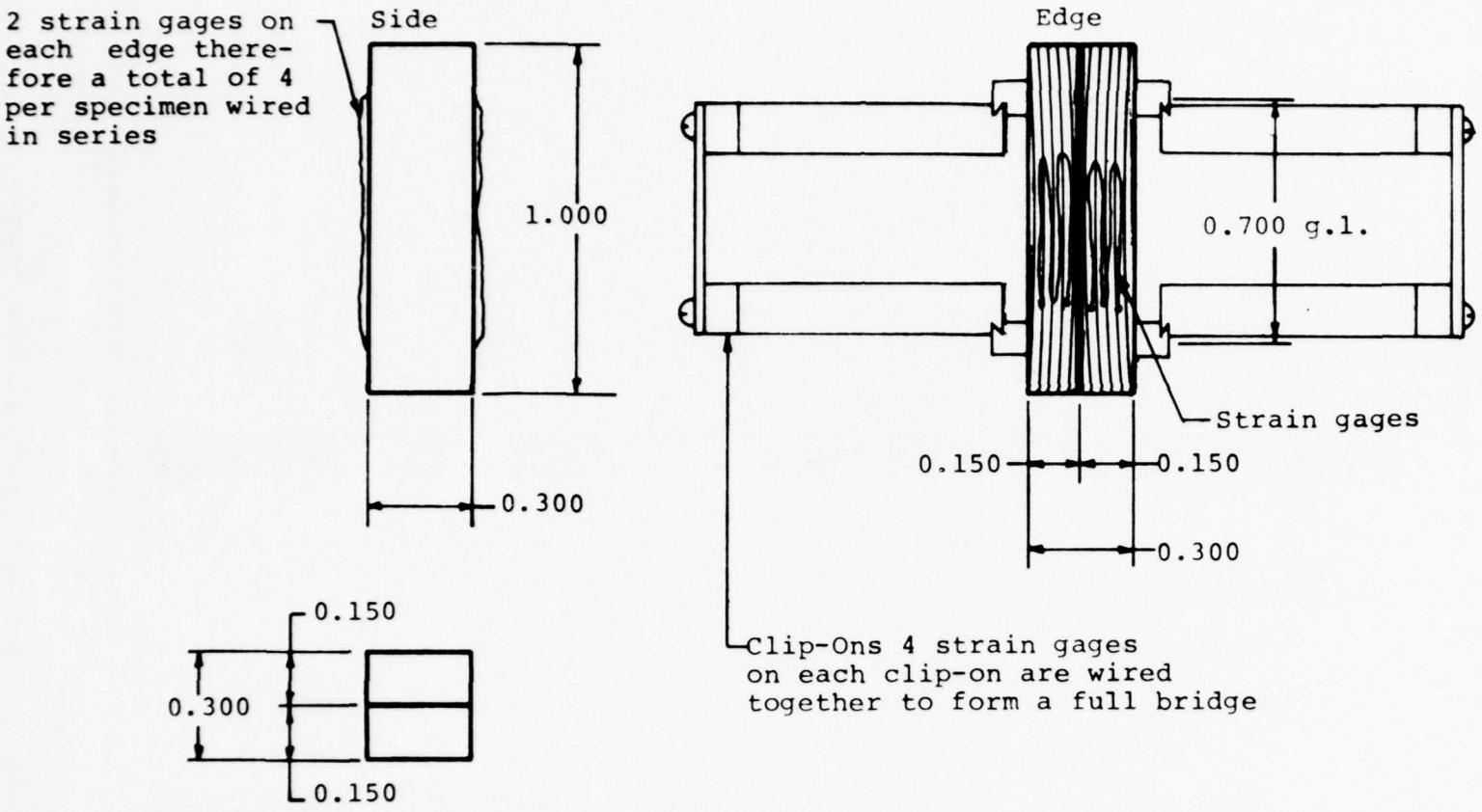

Figure 12. Rectangular Design Circumferential (Hoop) Specimens - Clip-On and Strain Gage Configuration (1.000 x 0.300 x 0.300)

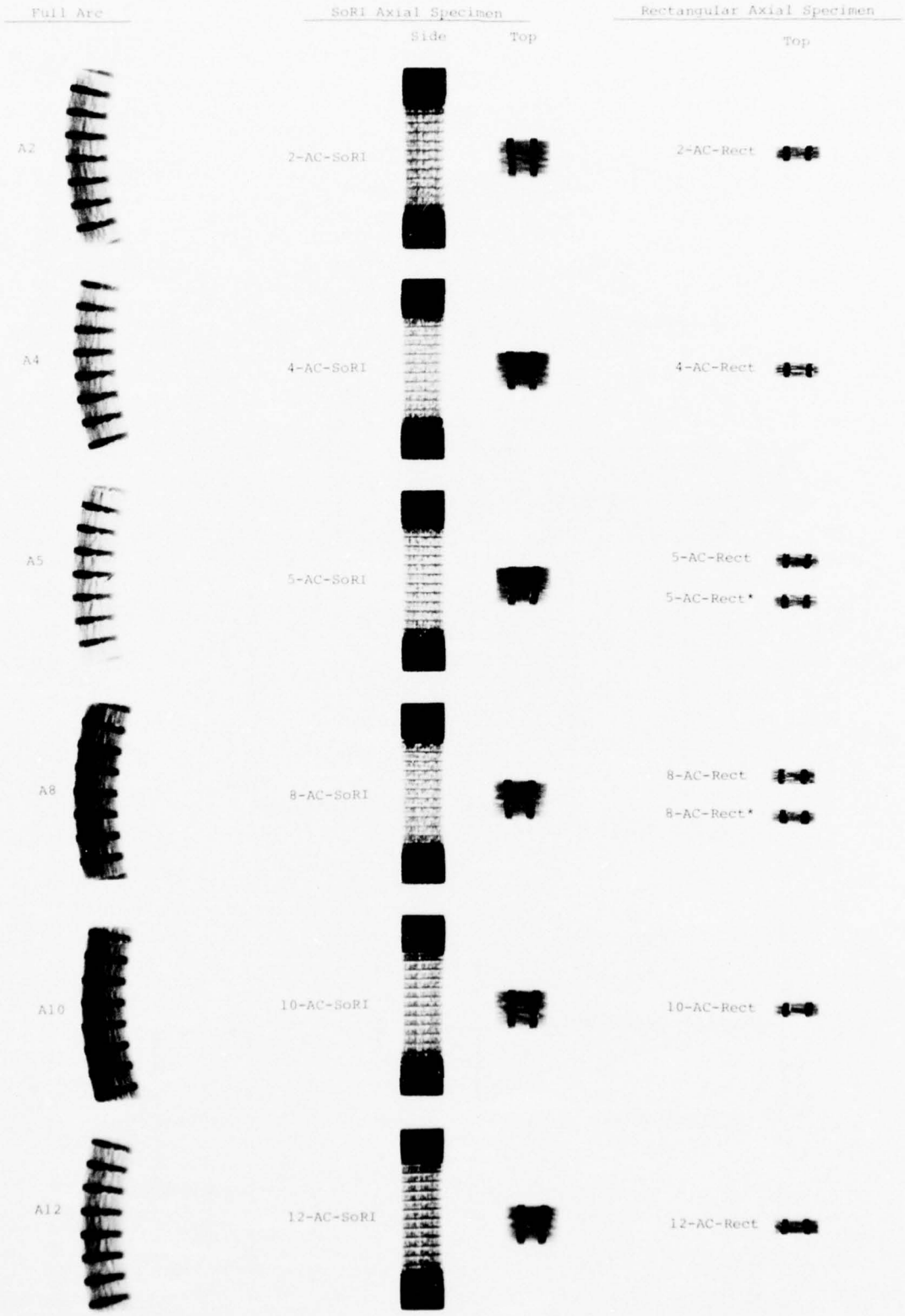

*Machined at SoRI from arc. All other rectangular specimens pre-machined from material adjacent to the respective arc.

Figure 13. X-ray Print of Axial Specimens from Cylinder 6.1.4

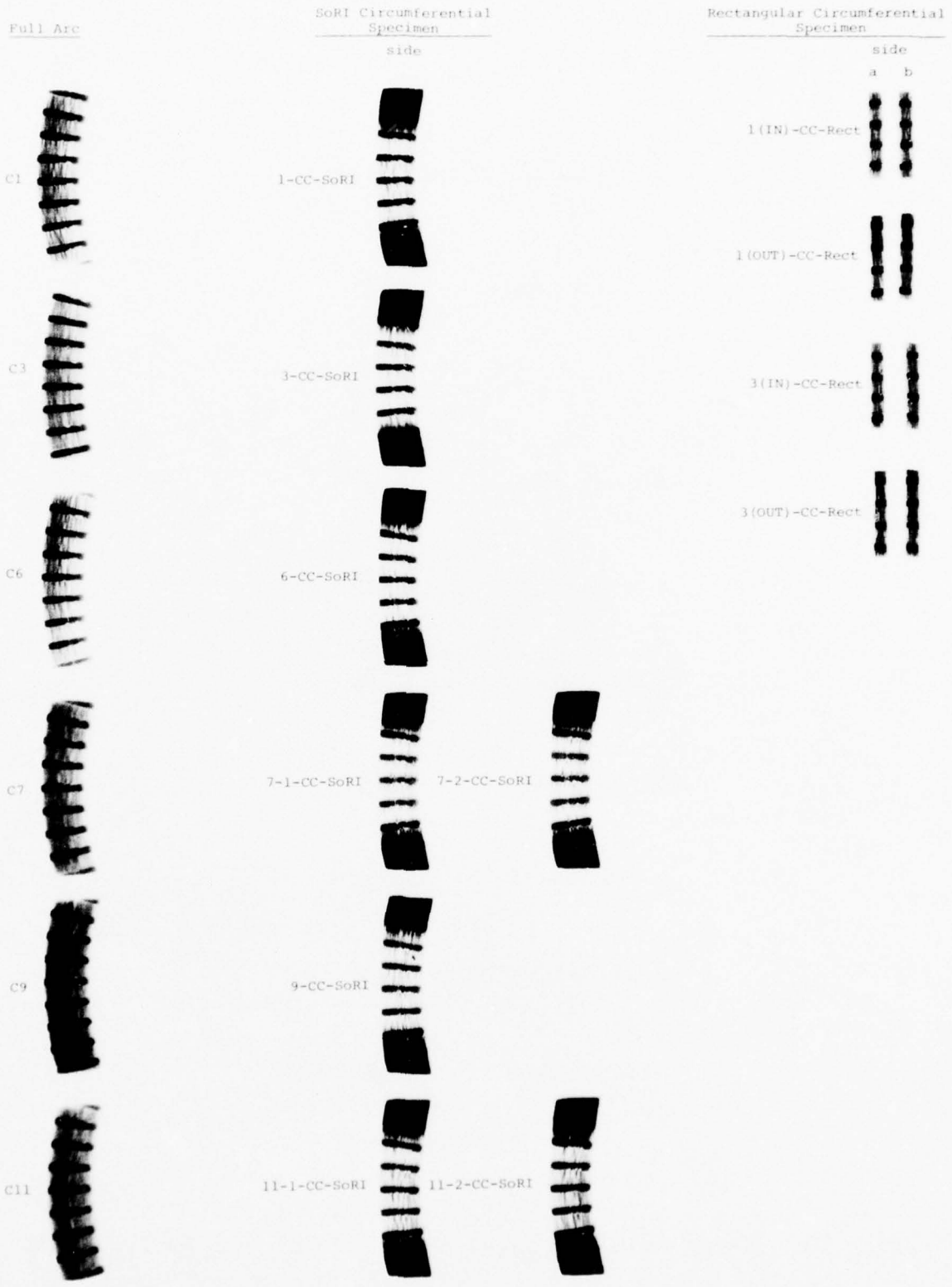

Figure 14. X-ray Print of Circumferential Specimens from Cylinder 6.1.4

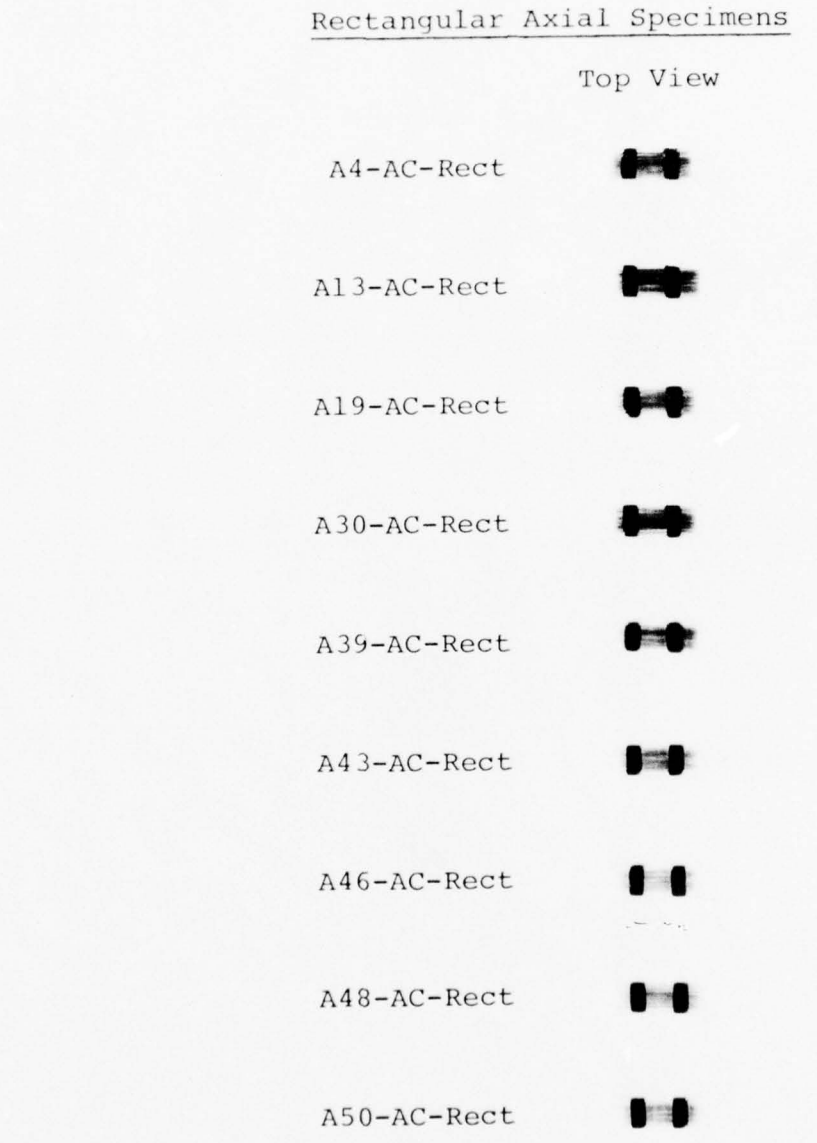

Figure 15. X-ray Print of Axial Specimens from Cylinder 4.1.18

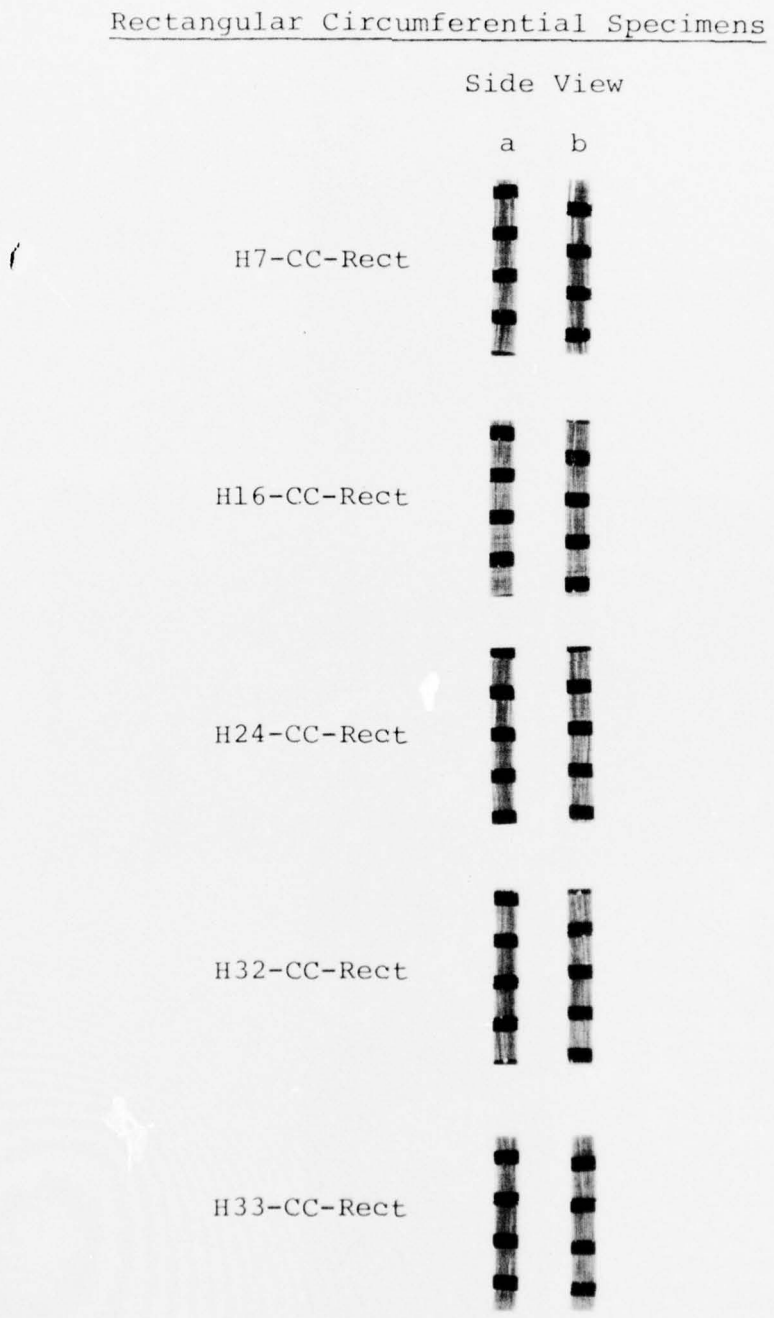

Figure 16. X-ray Print of Circumferential Specimens from Cylinder 4.1.18

Figure 17. 20X Photomicrograph Showing Circumferential "Waviness" in Arc 6

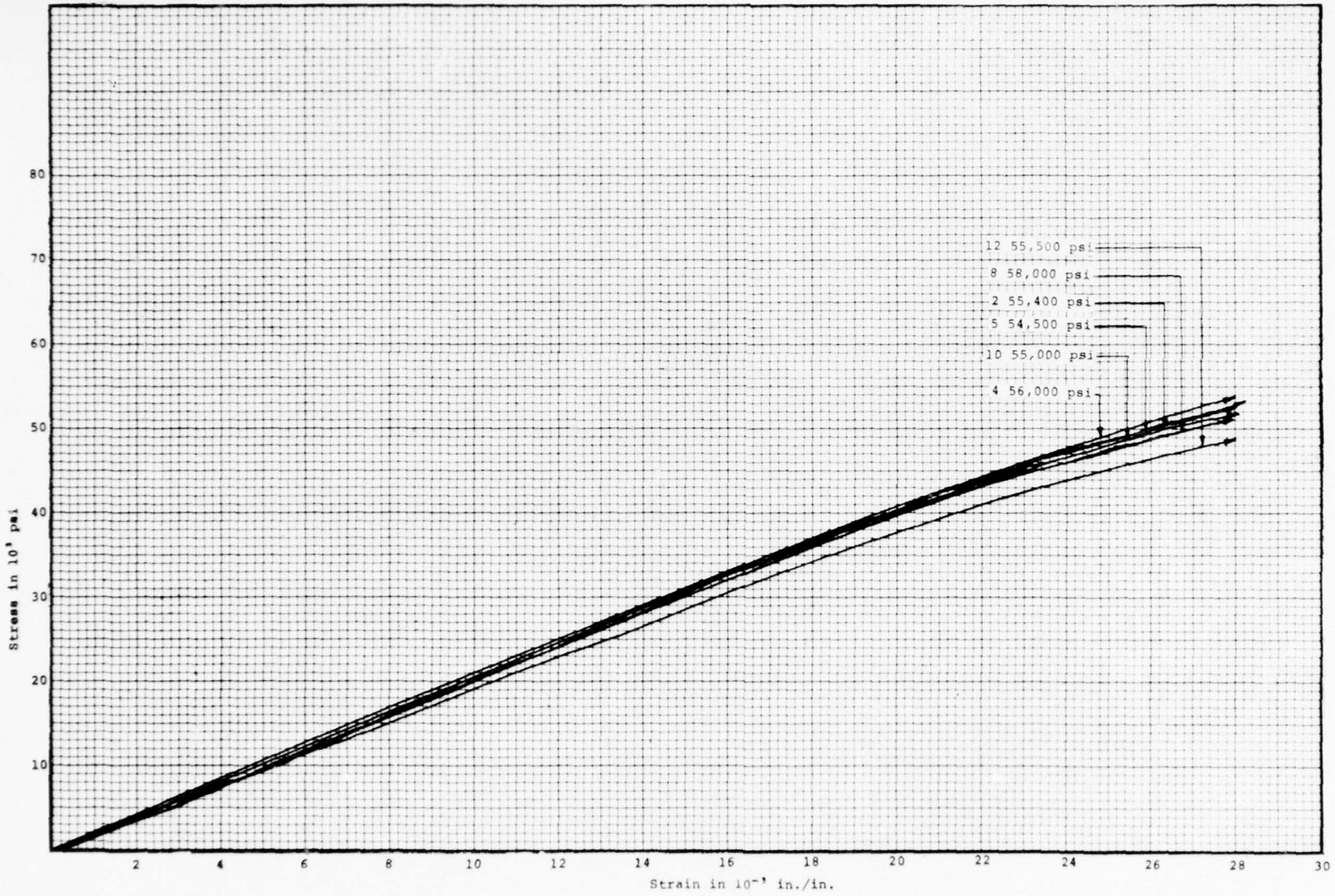

Figure 18. Composite Plot Axial Compression SoRI Specimen Configuration 3DQP - 6·1·14 (Clip-On Data)

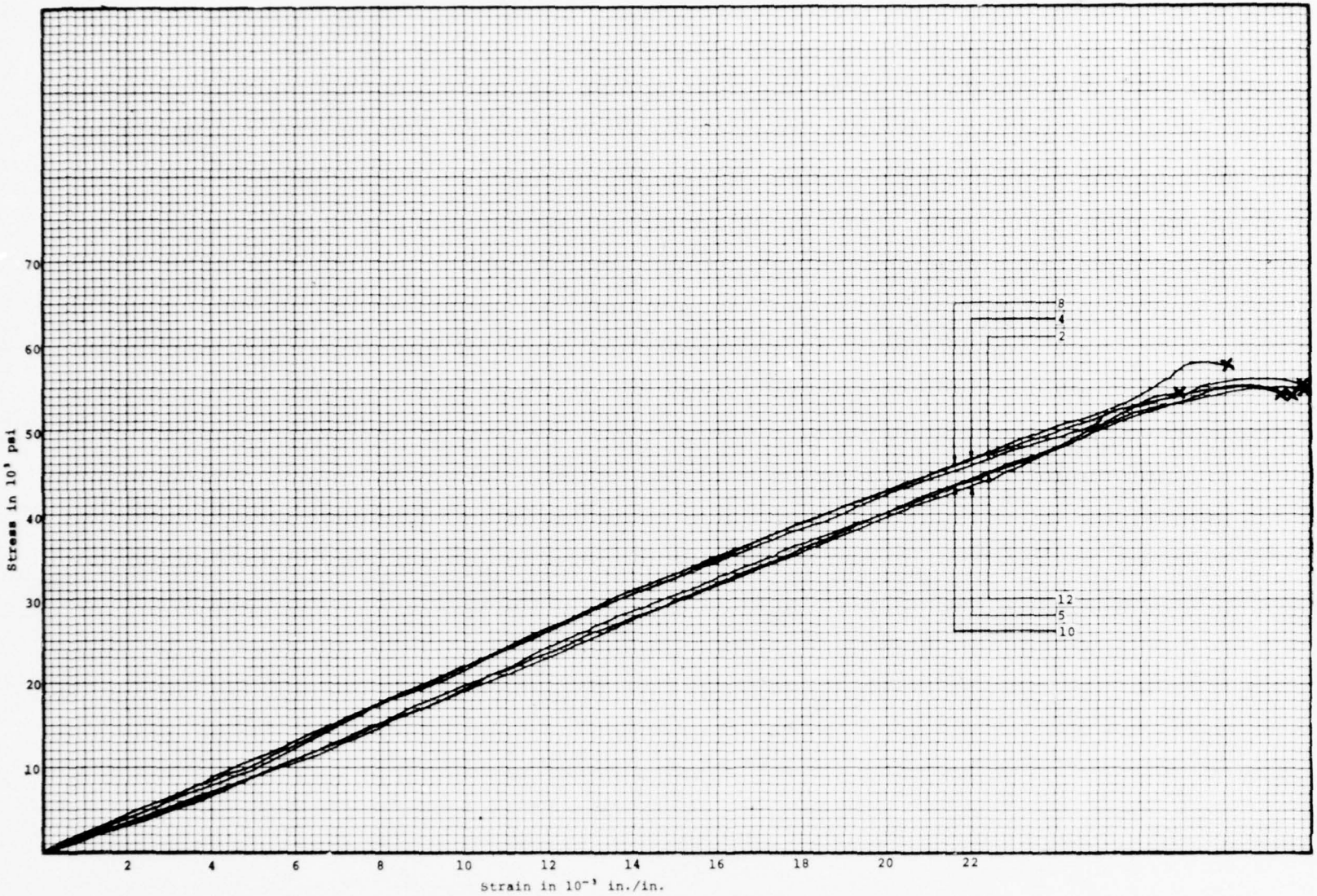

Figure 19. Composite Plot Axial Compression SoRI Specimen Configuration 3DQP - 6·1·4 (Strain Gage Data)

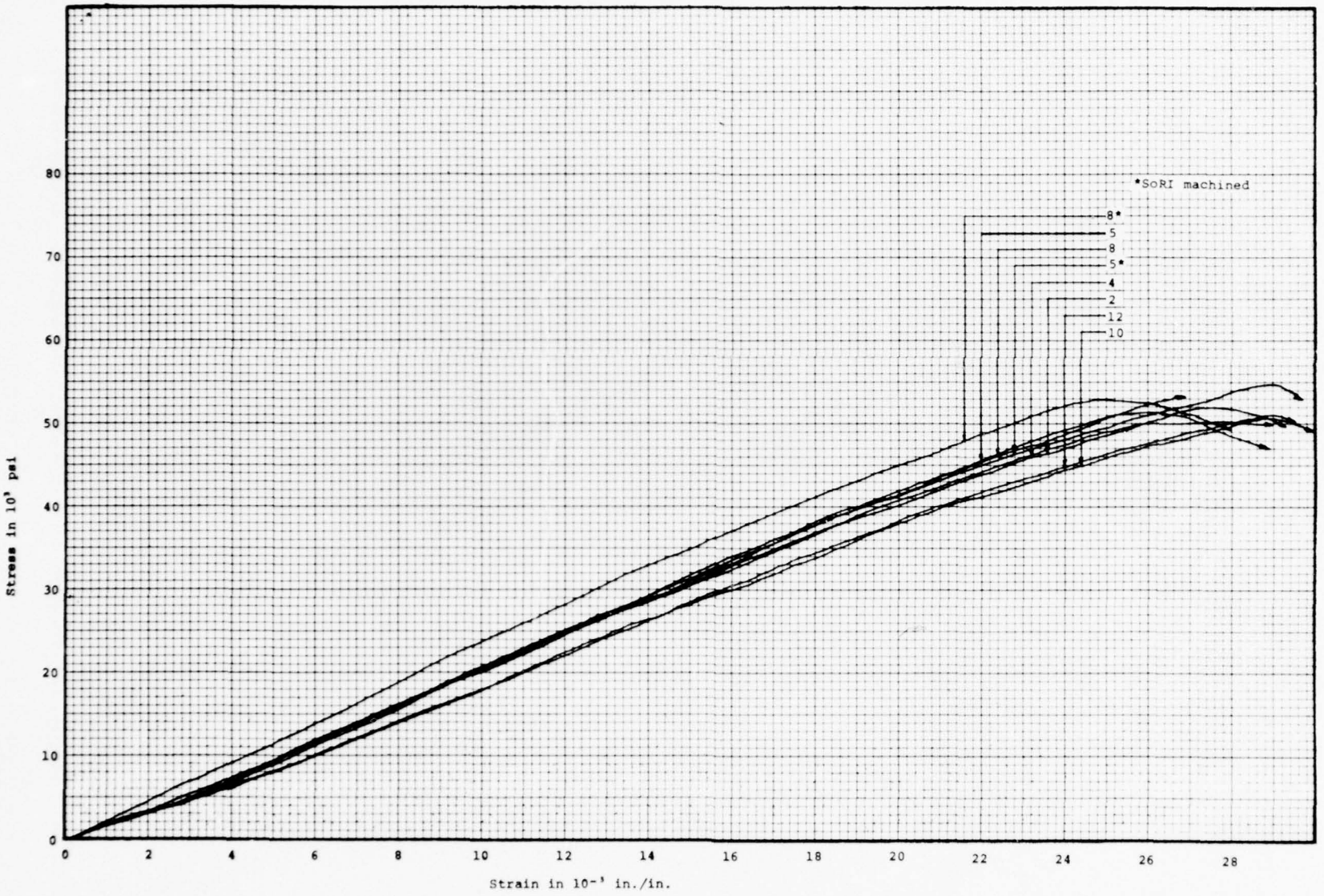

Figure 20. Composite Plot Axial Compression-Rectangular Specimen Configuration 3DQP-6.1.4 (Clip-on Data)

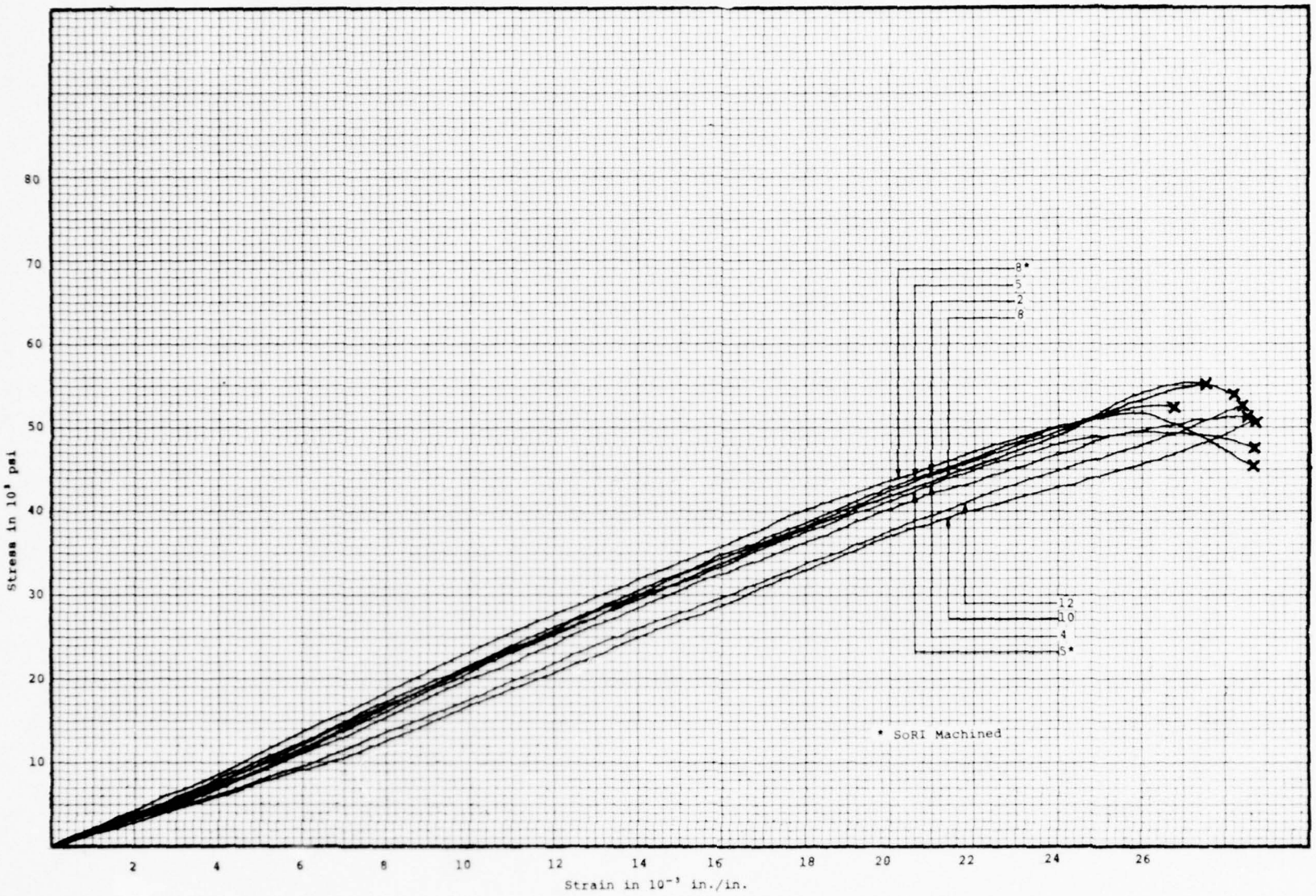

Figure 21. Composite Plot Axial Compression-Rectangular Specimen Configuration 3DQP-6.1.4 (Strain Gage Data)

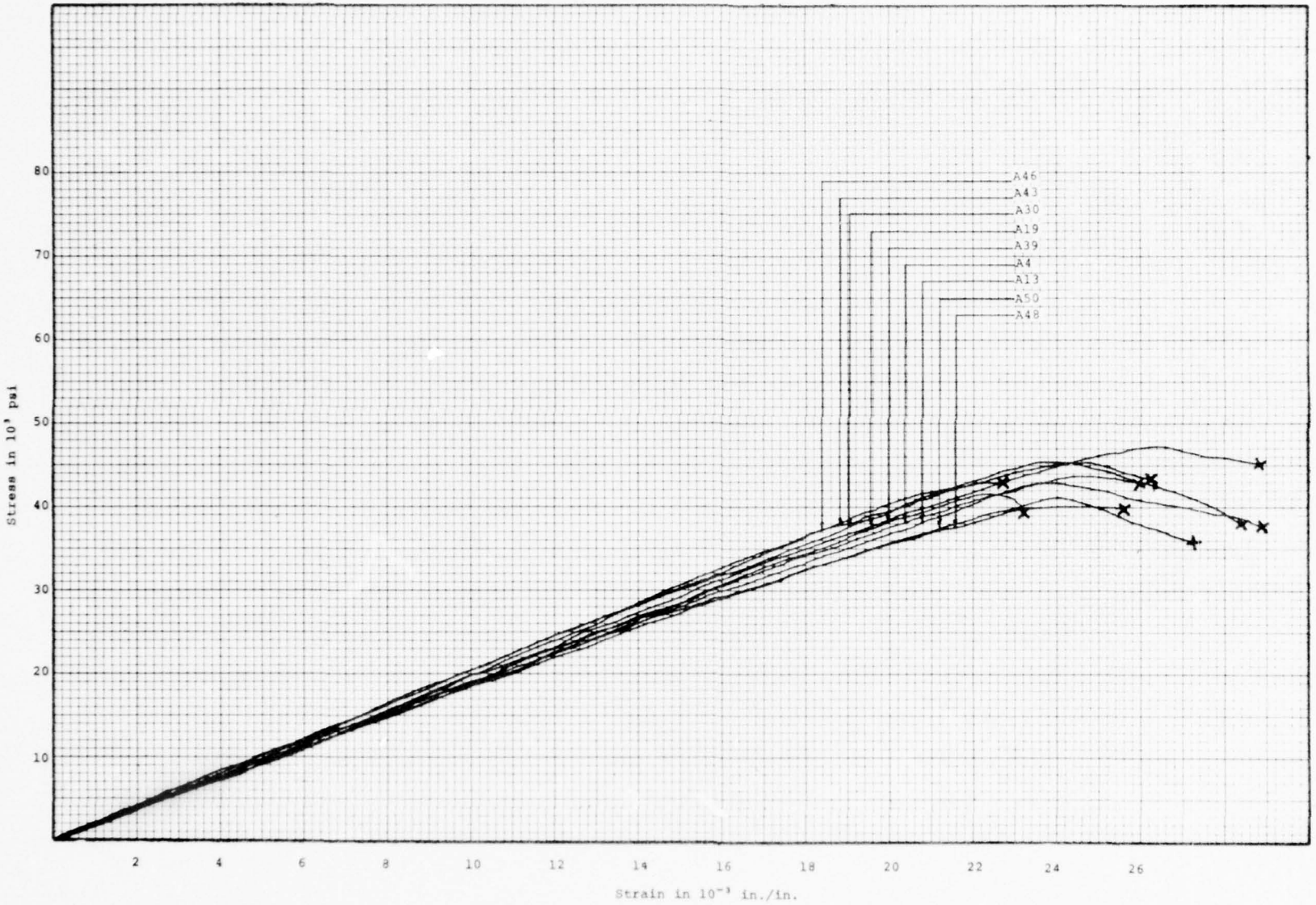

Figure 22. Composite Plot Axial Compression-Rectangular Specimen Configuration 3DQP-4.1.18 (Clip-on Data)

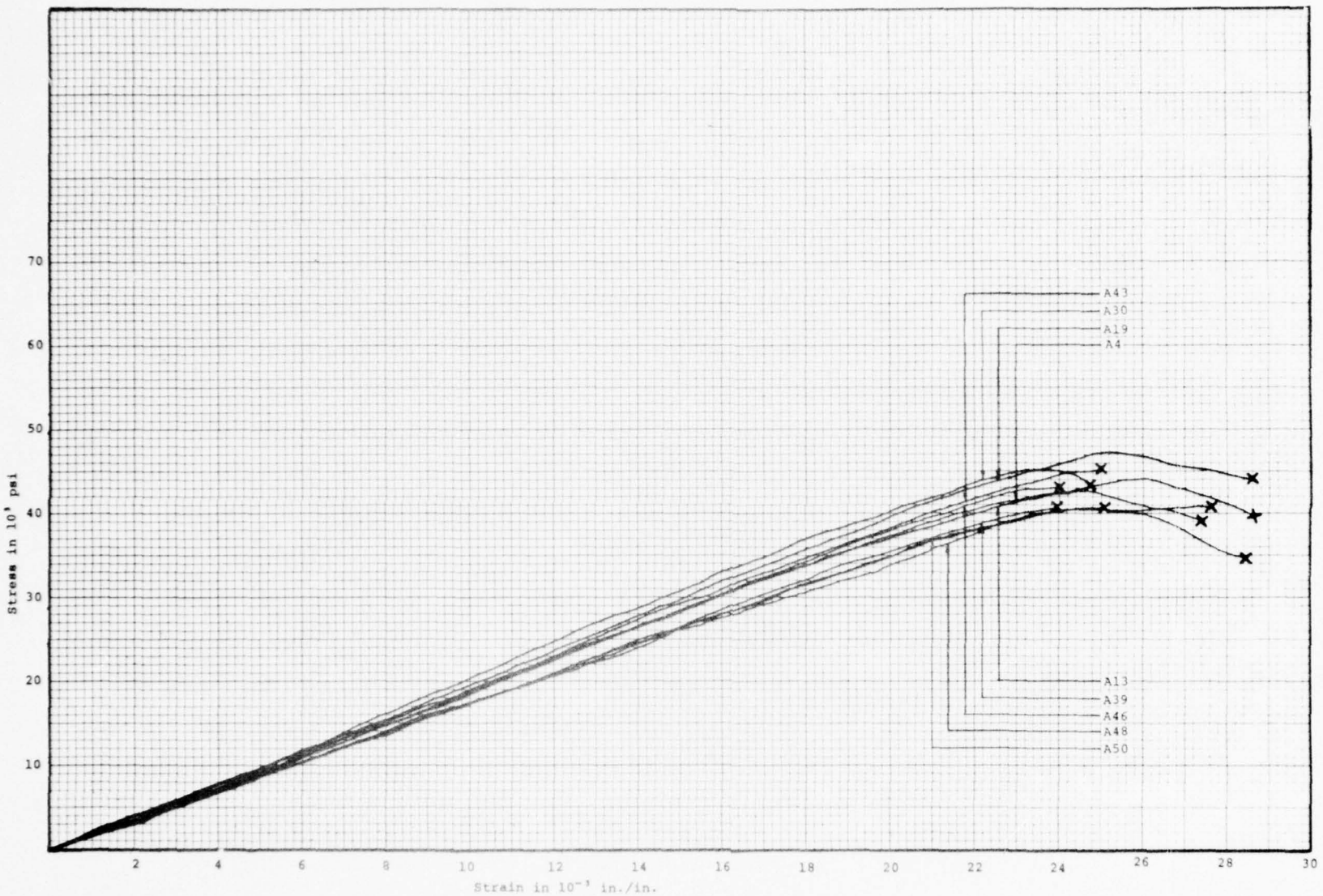

Figure 23. Composite Plot Axial Compression-Rectangular Specimen Configuration 3DQP-4.1.18 (Strain Gage Data)

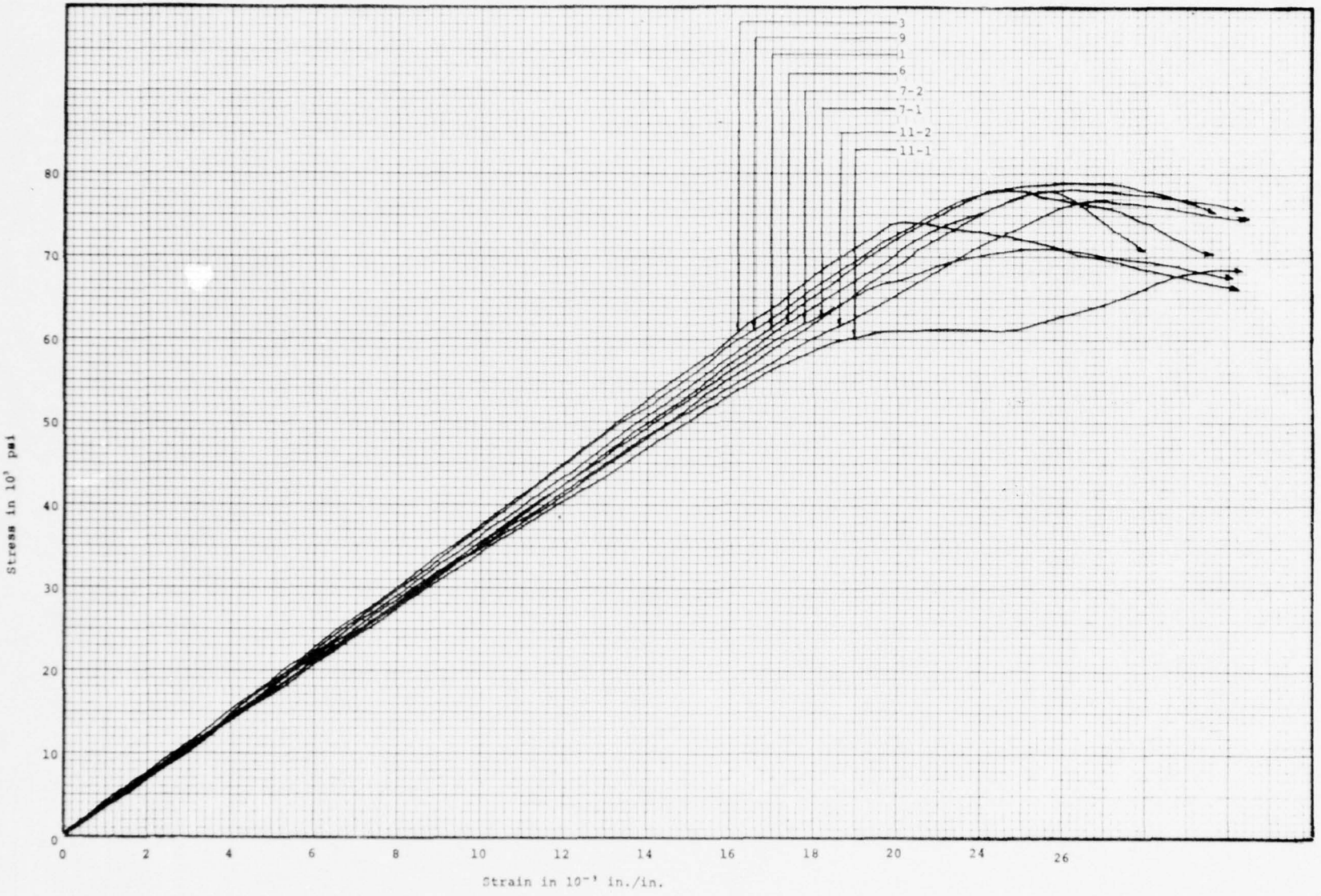

Figure 24. Composite Plot Circumferential Compression-SoRI Specimen Configuration 3DQP-6.1.4 (Clip-on Data)

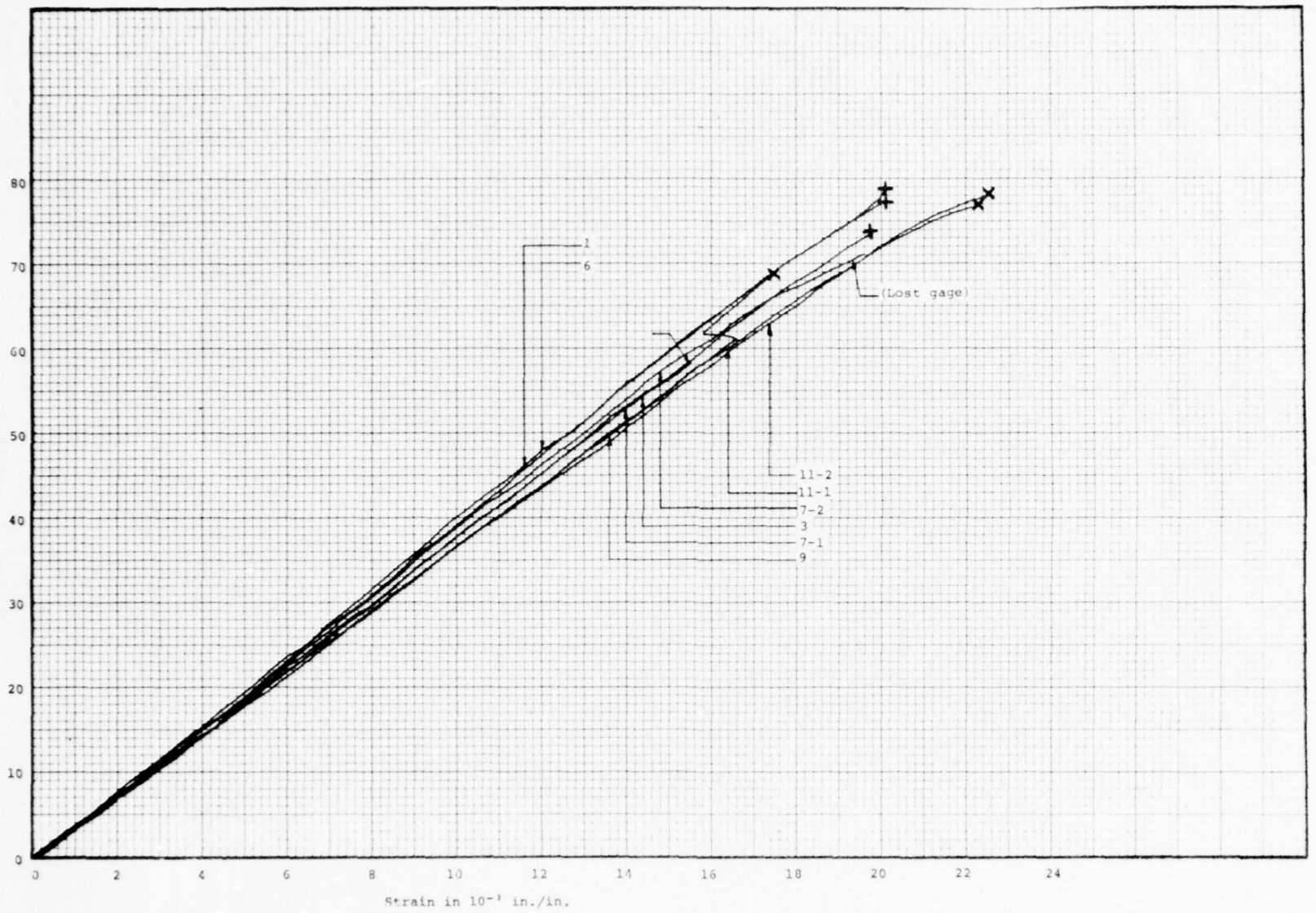

Figure 25. Composite Plot Circumferential Compression-SoRI Specimen Configuration 3DQP-6.1.4 (Strain Gage Data)

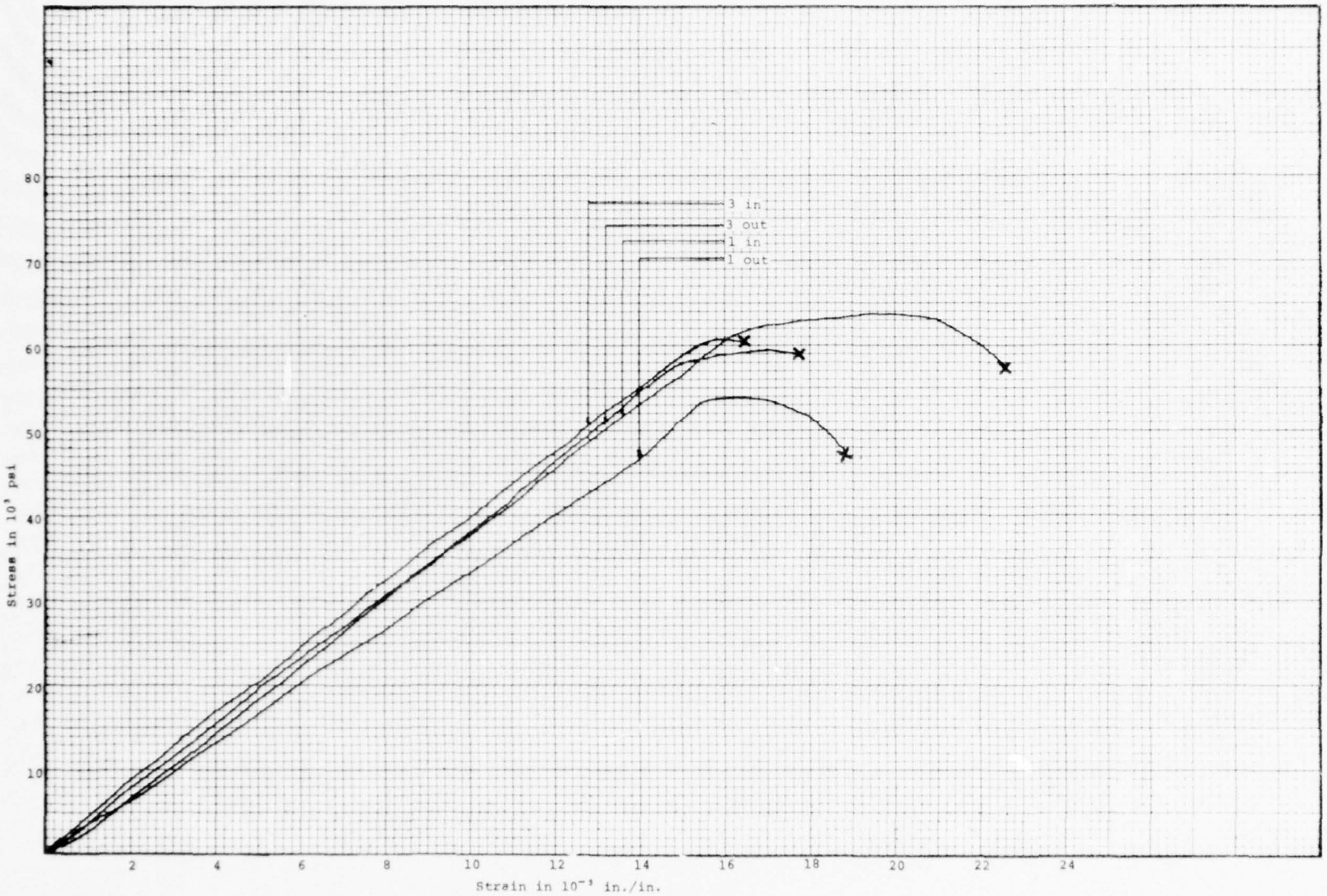

Figure 26. Composite Plot Circumferential Compression-Rectangular Specimen Configuration 3DQP-6.1.4 (Clip-on Data)

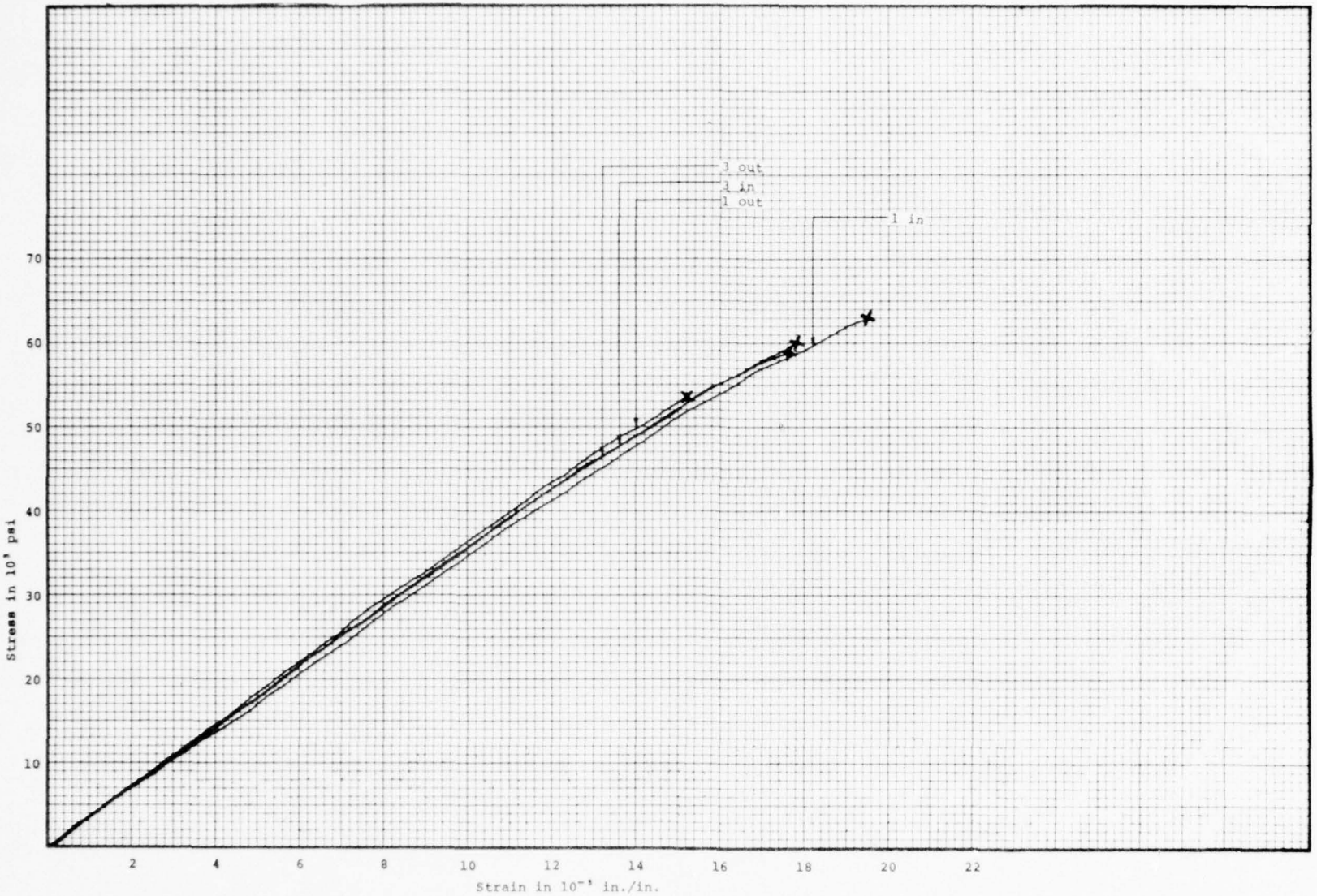

Figure 27. Composite Plot Circumferential Compression-Rectangular Specimen Configuration 3DQP-6.1.4 Strain Gage Data

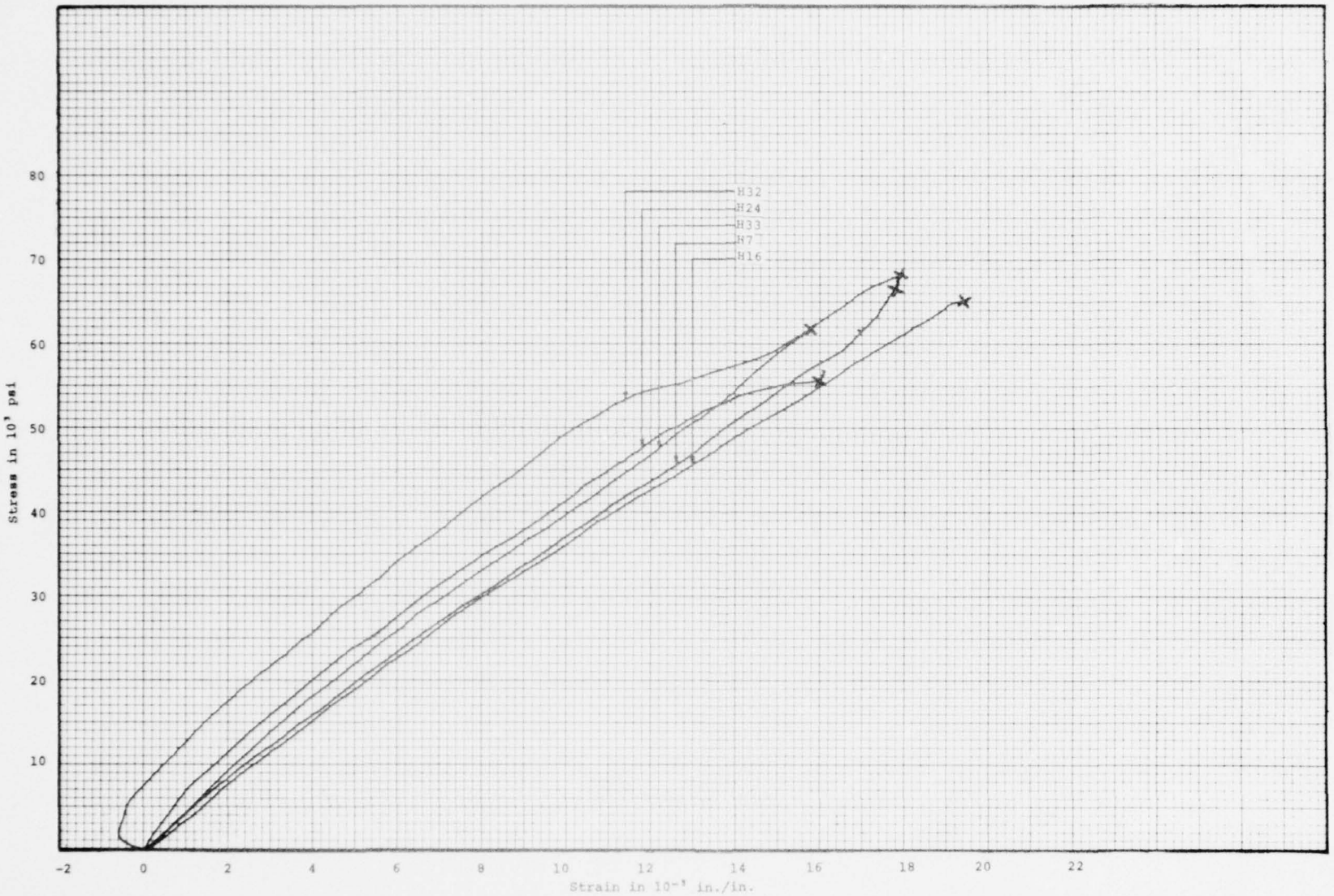

Figure 28. Composite Plot Circumferential Compression-Rectangular Specimen Configuration 3DQP-4.1.18 (Clip-on Data)

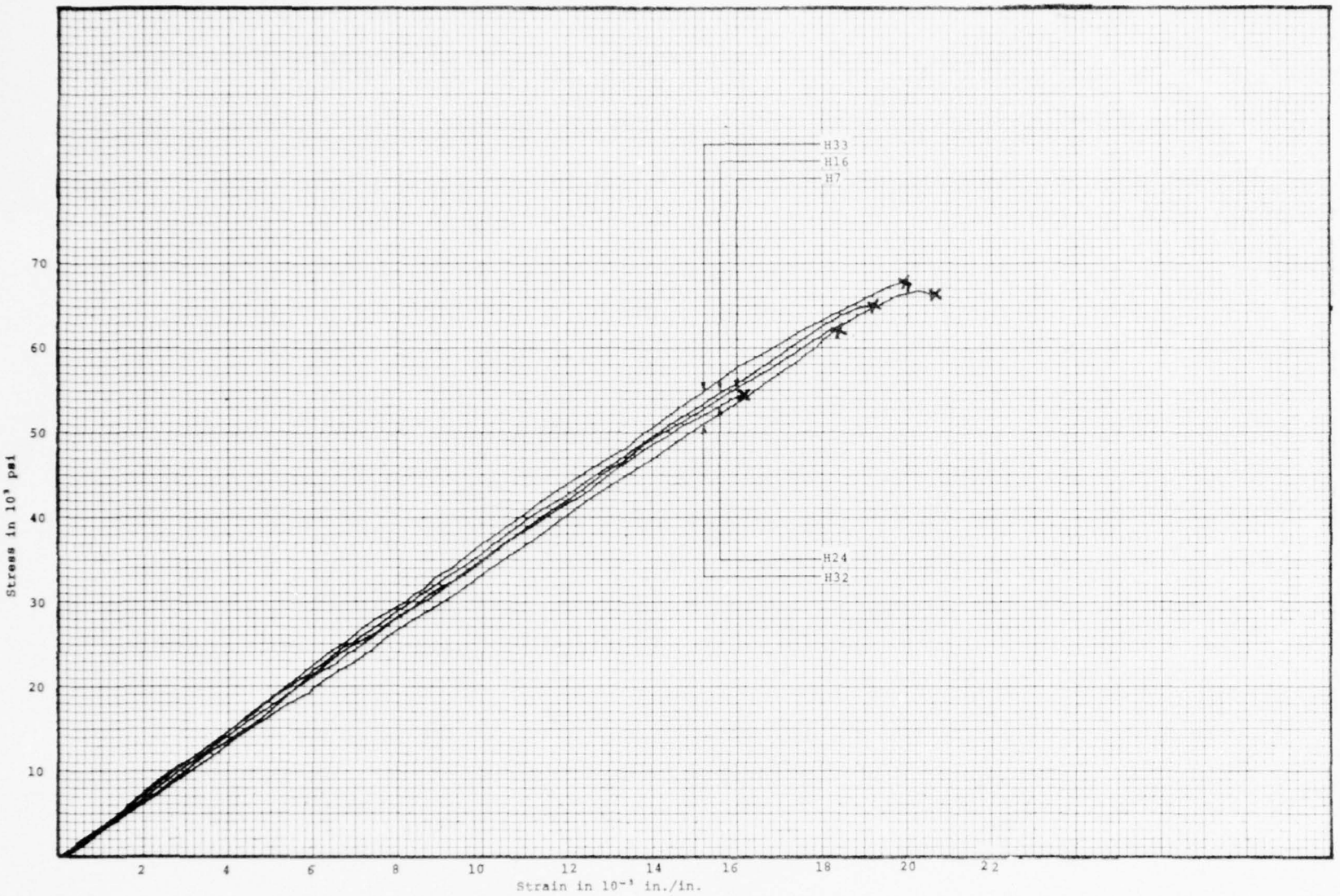

Figure 29. Composite Plot Circumferential Direction-Rectangular Specimen Configuration 3DQP-4.1.18 (Strain Gage Data)

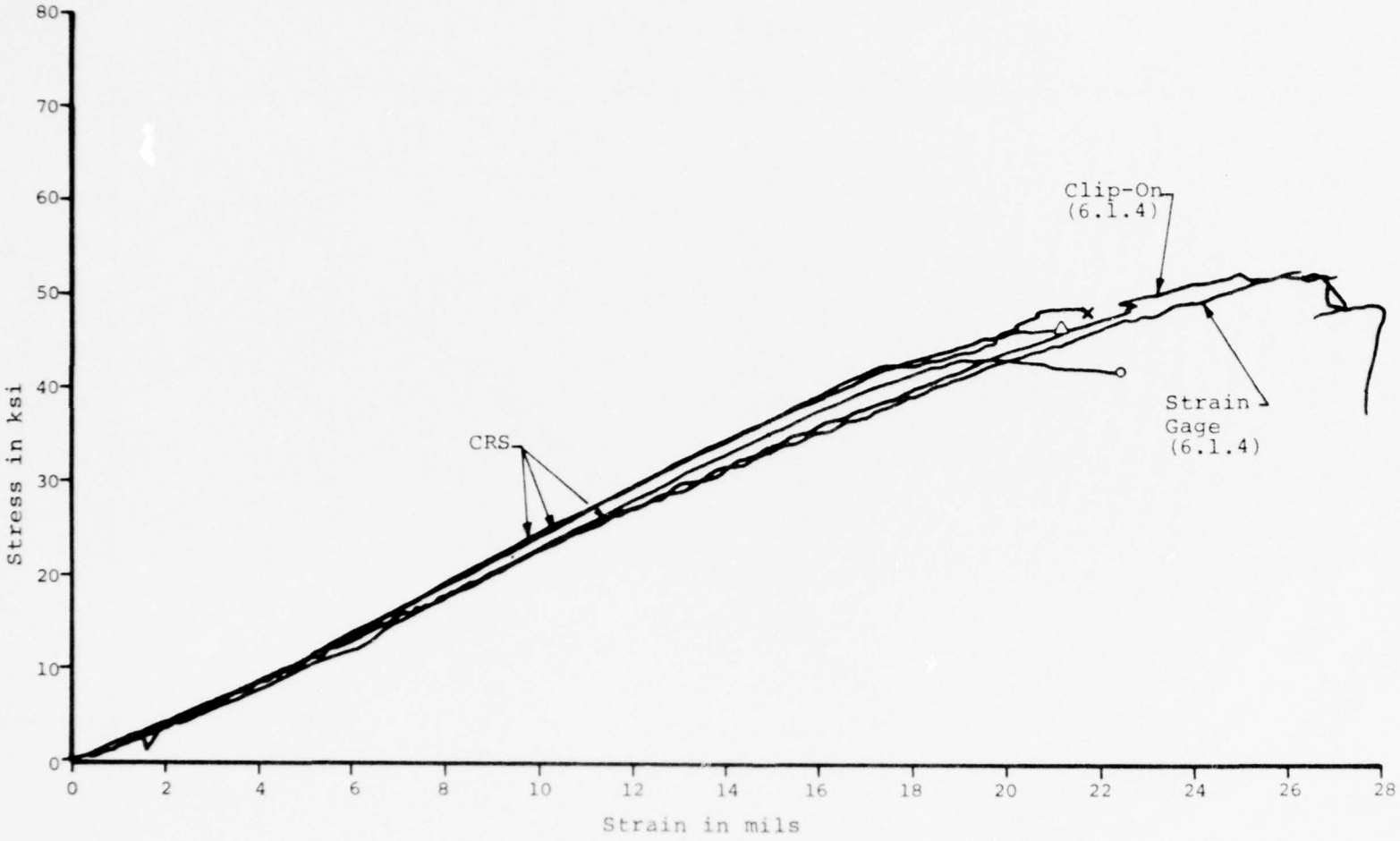

Figure 30. Typical Axial Compression Data from CRS (with one run from 6·1·4)

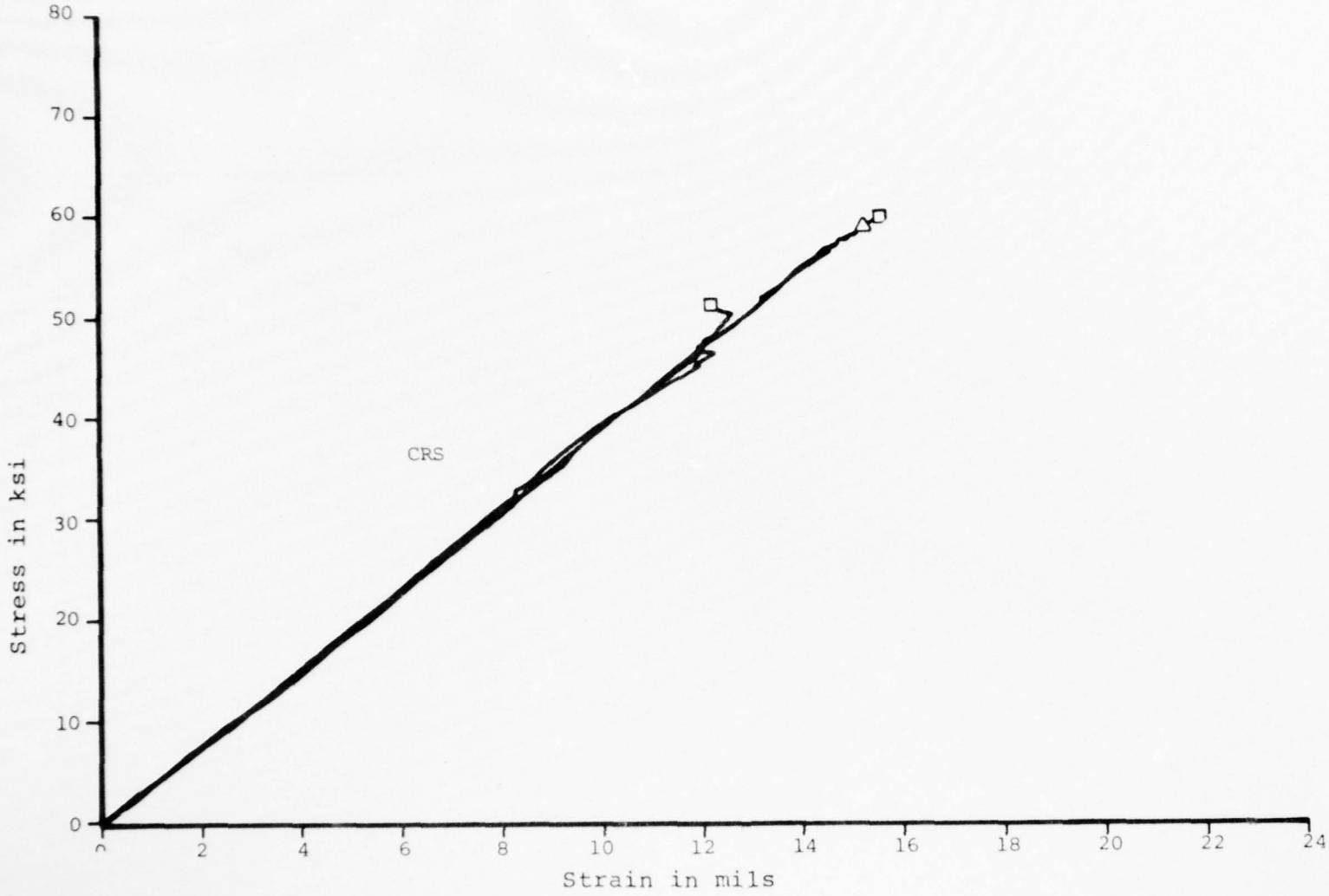

Figure 31. Typical Circumferential Compression Data from CRS

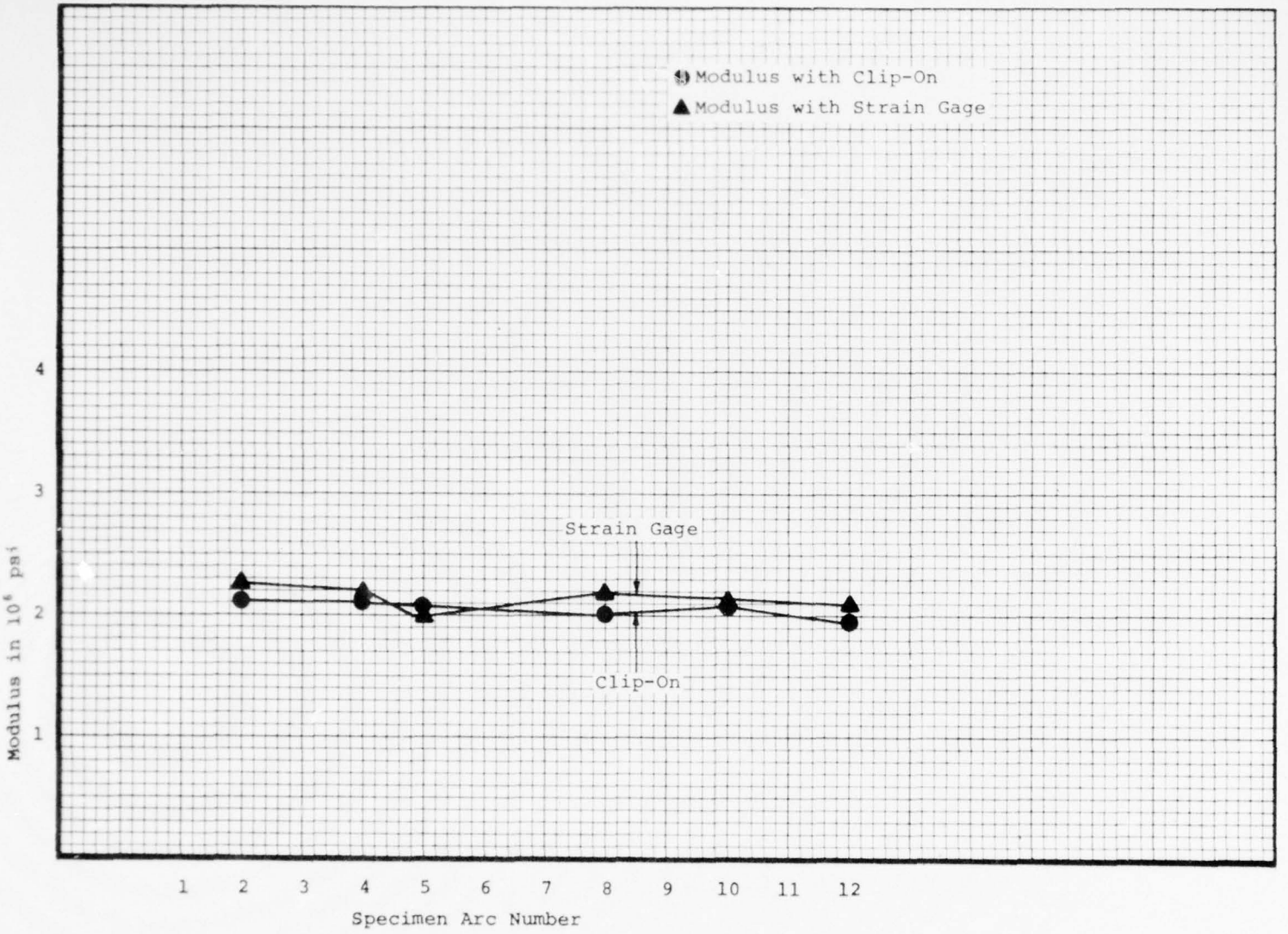

Figure 32. Comparison of SoRI Axial Clip-On versus Strain Gage Data 6·1·4

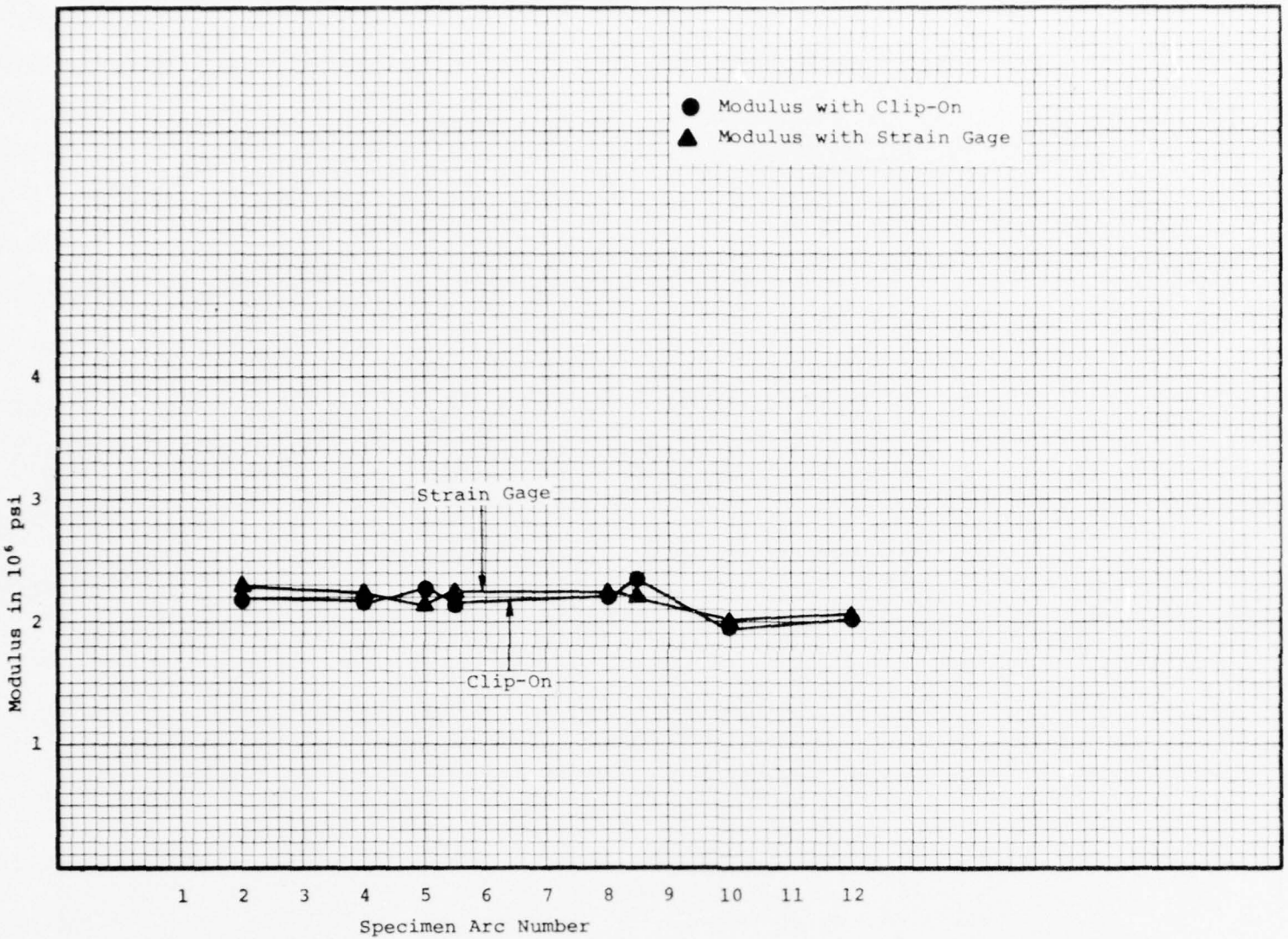

Figure 33. Comparison of Rectangular Axial Clip-on versus Strain Gage Data 6.1.4

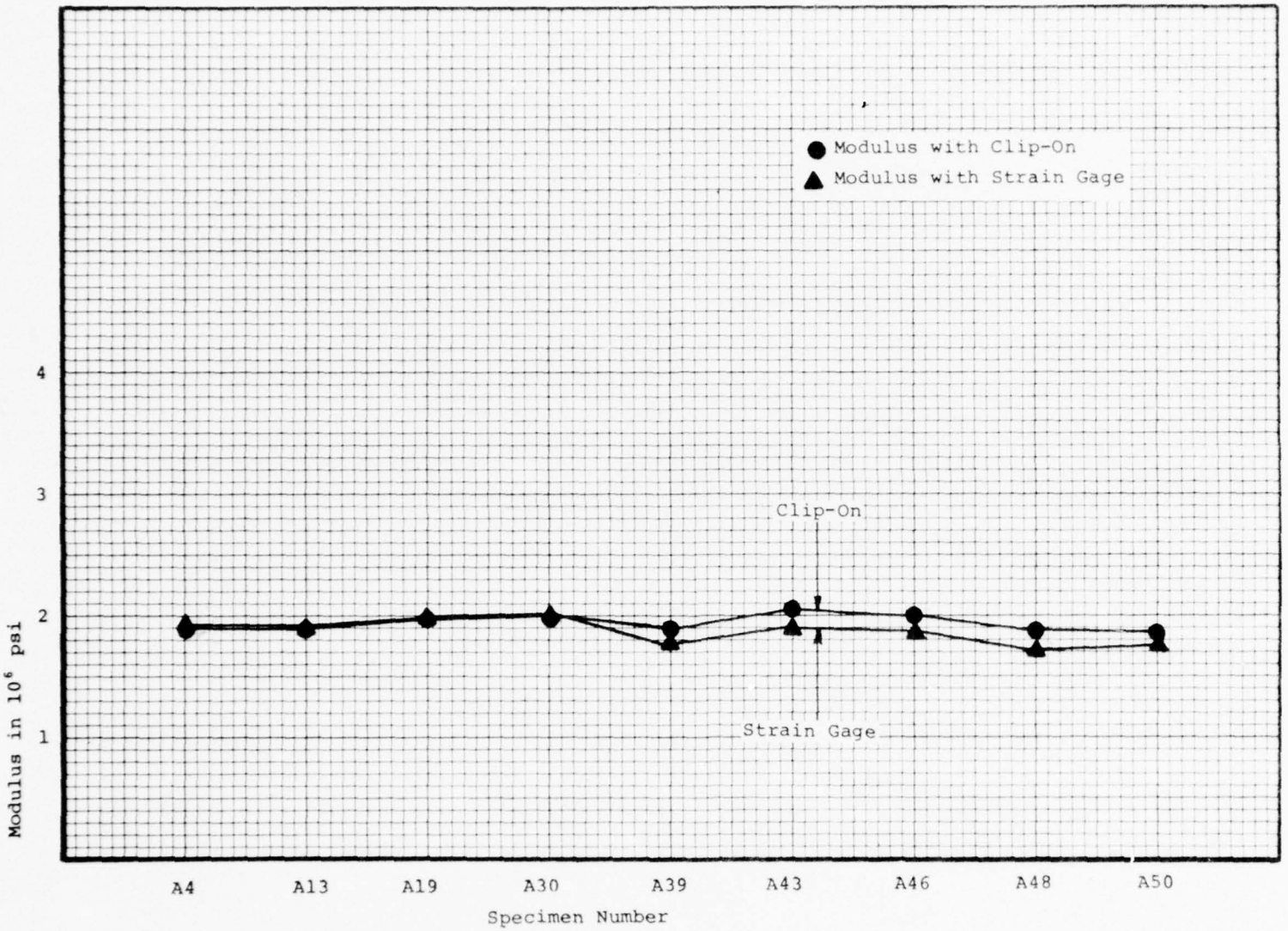

Figure 34. Comparison of Rectangular Axial Clip-On versus Strain Gage Data 4.1.18

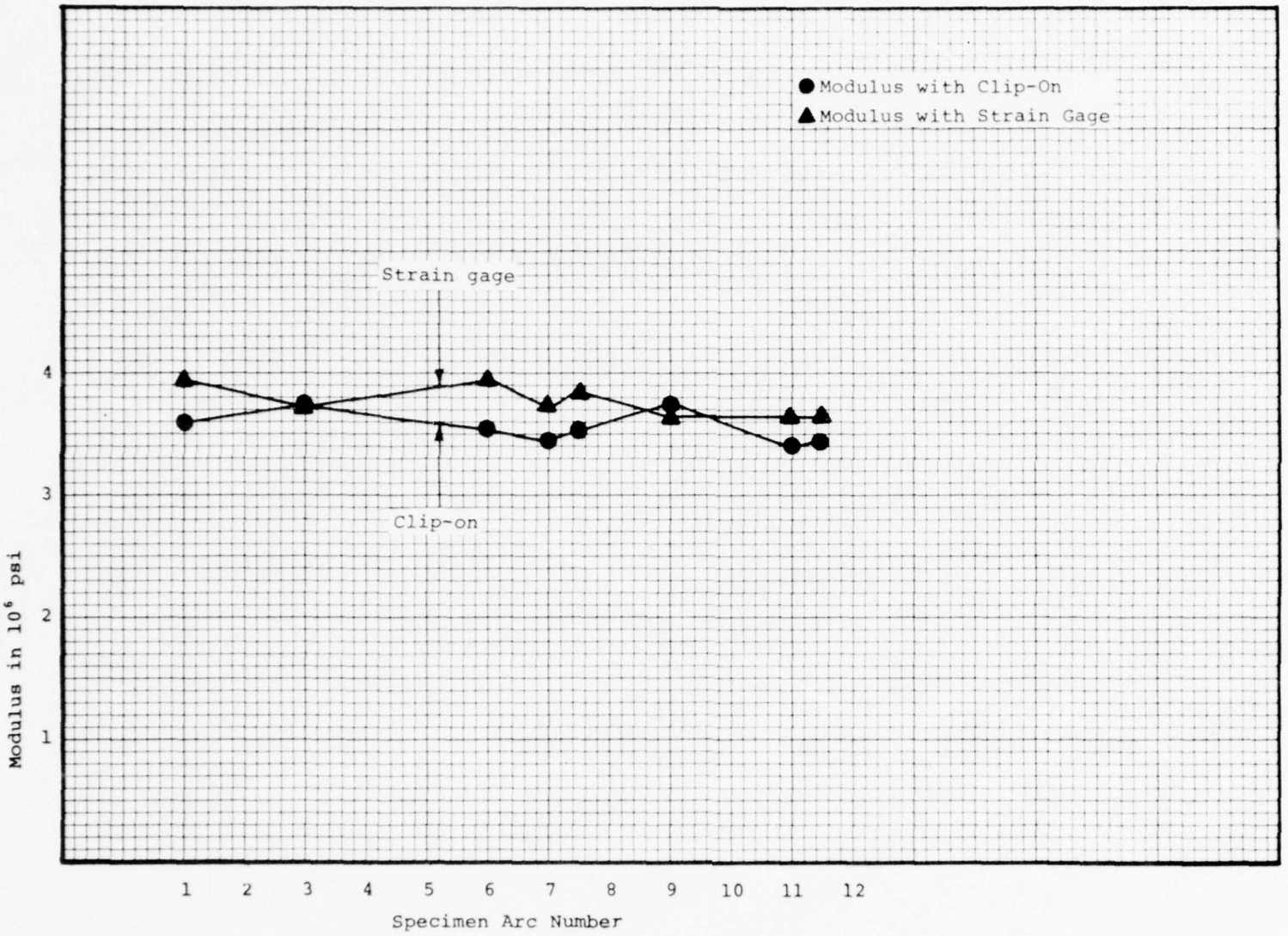

Figure 35. Comparison of SoRI Circumferential Clip-On versus Strain Gage Data 6·1·4

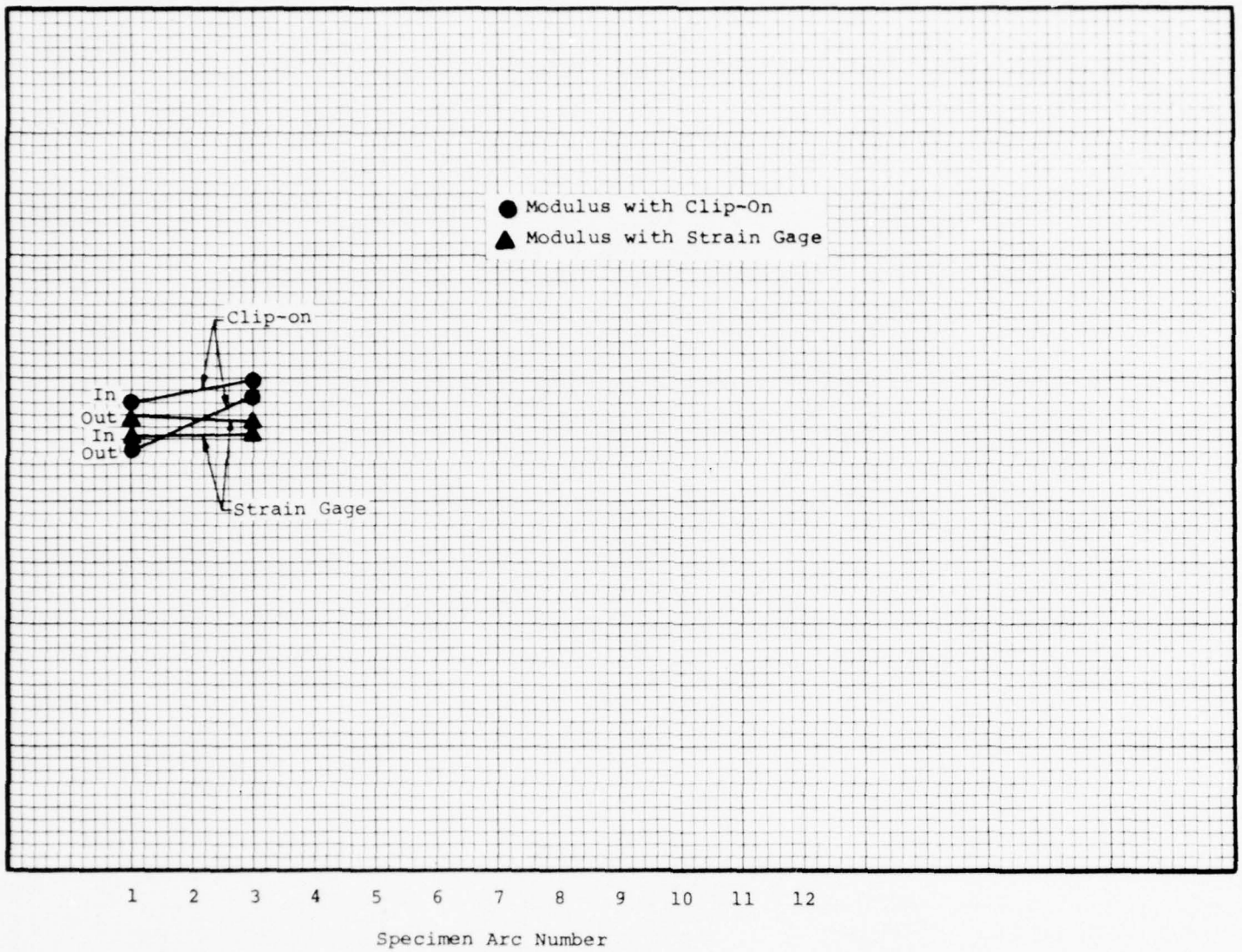

Figure 36. Comparison of Rectangular Circumferential Clip-on versus Strain Gage Data 6.1.4

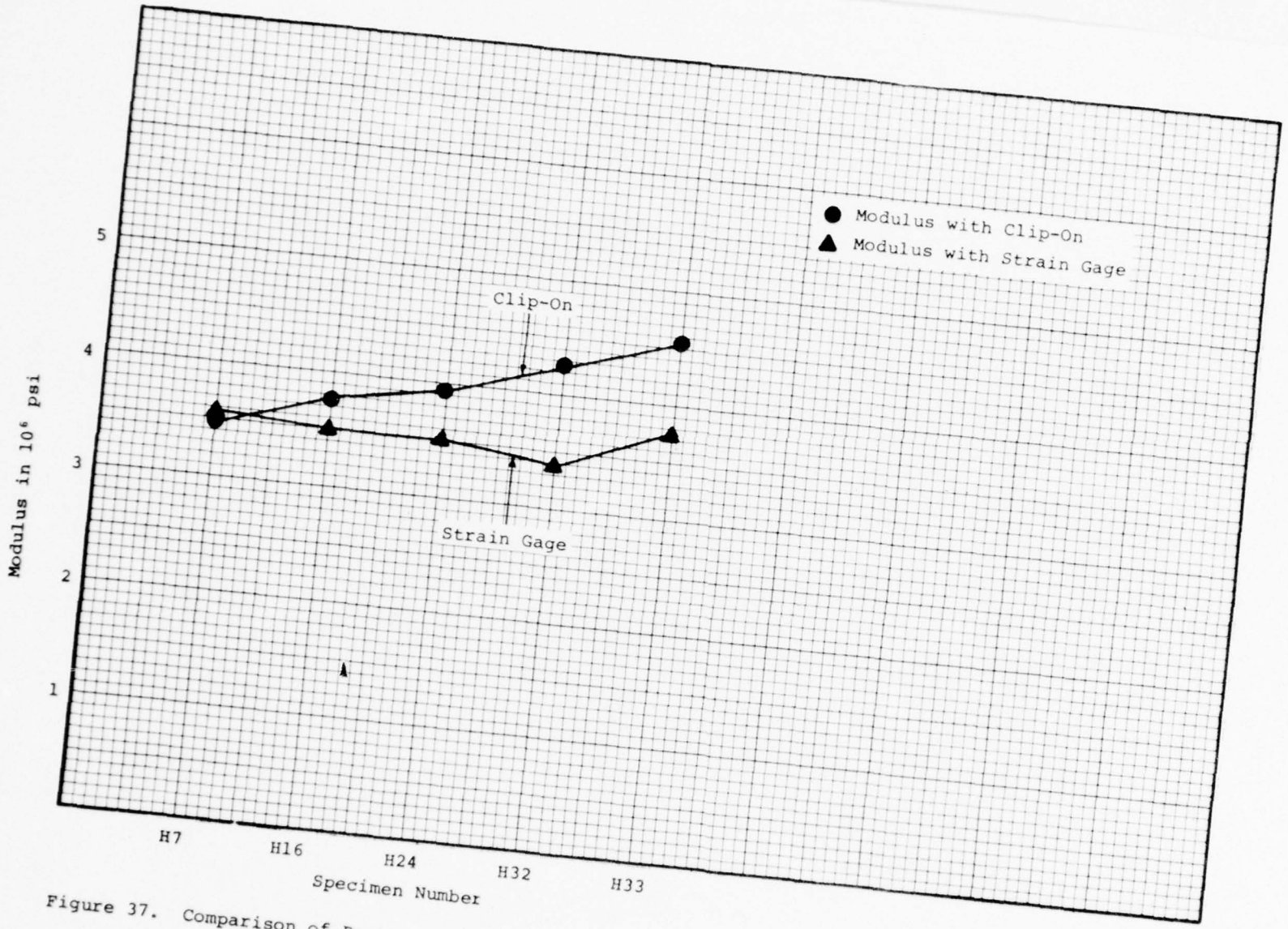

Figure 37. Comparison of Rectangular Circumferential Clip-On versus Strain Gage Data 4.1.18

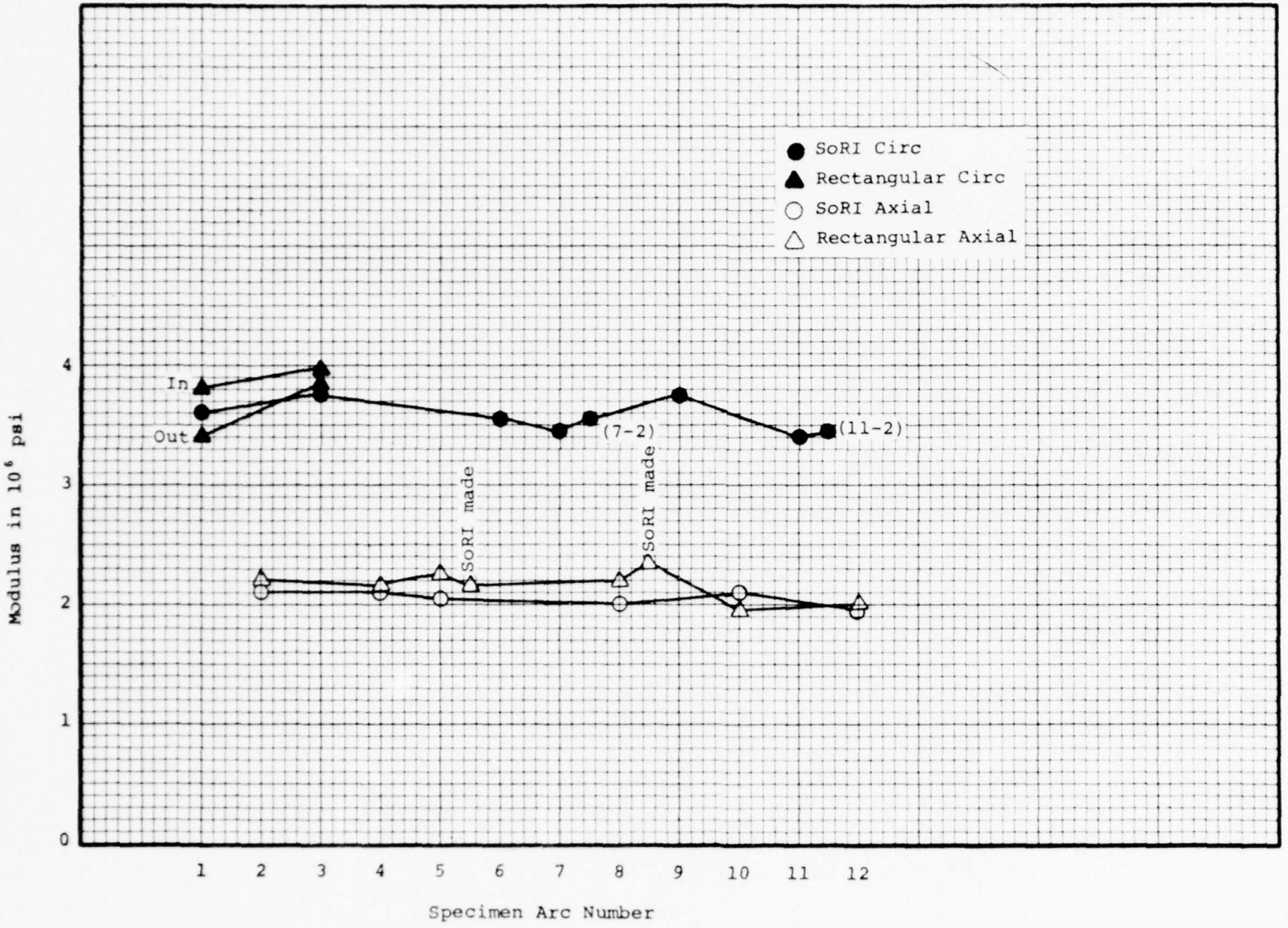

Figure 38. Rectangular versus SoRI Design Specimens Modulus Calculated From Clip-on

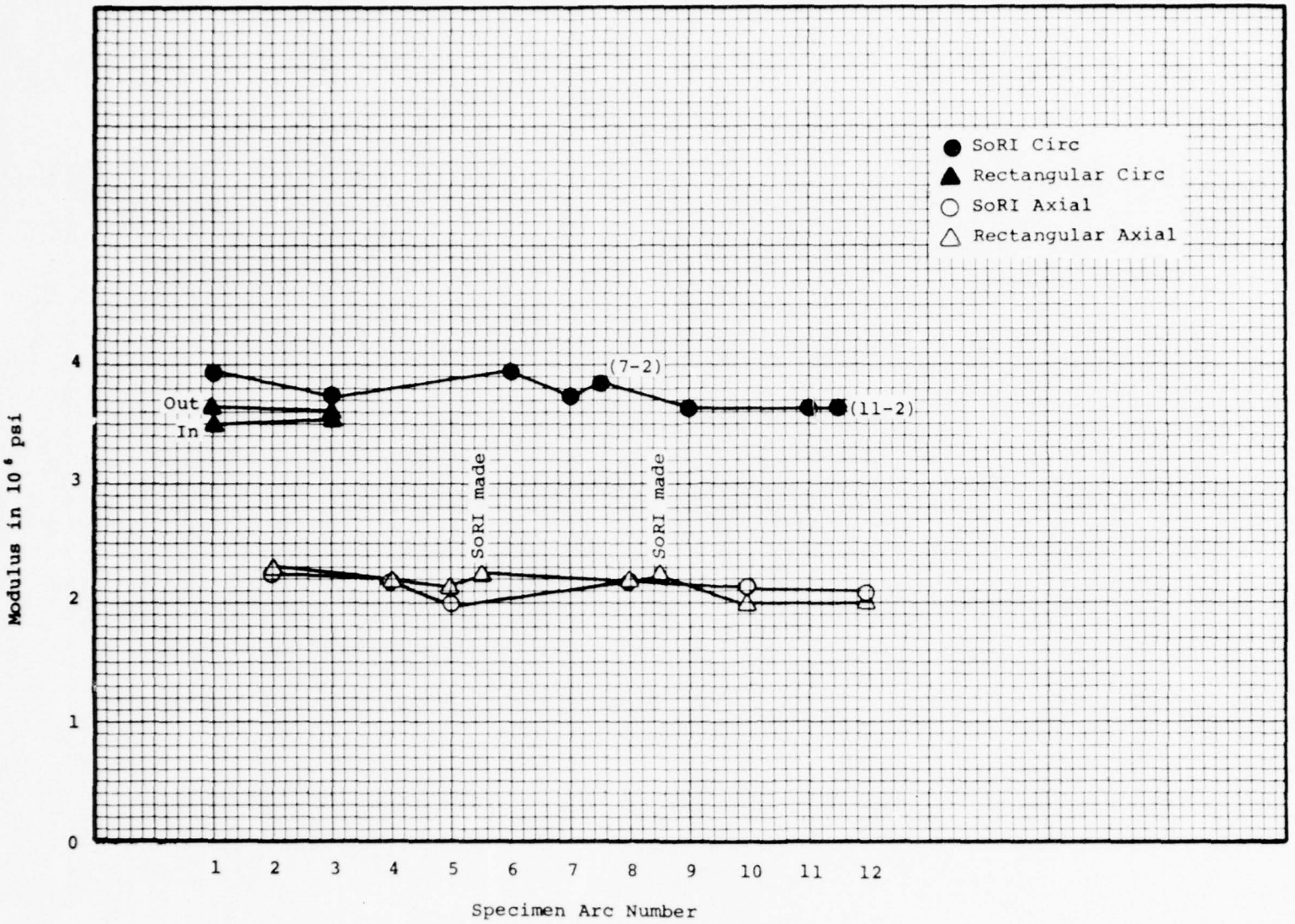

Figure 39. Rectangular versus SoRI Design Specimens Modulus Calculated From Strain Gage

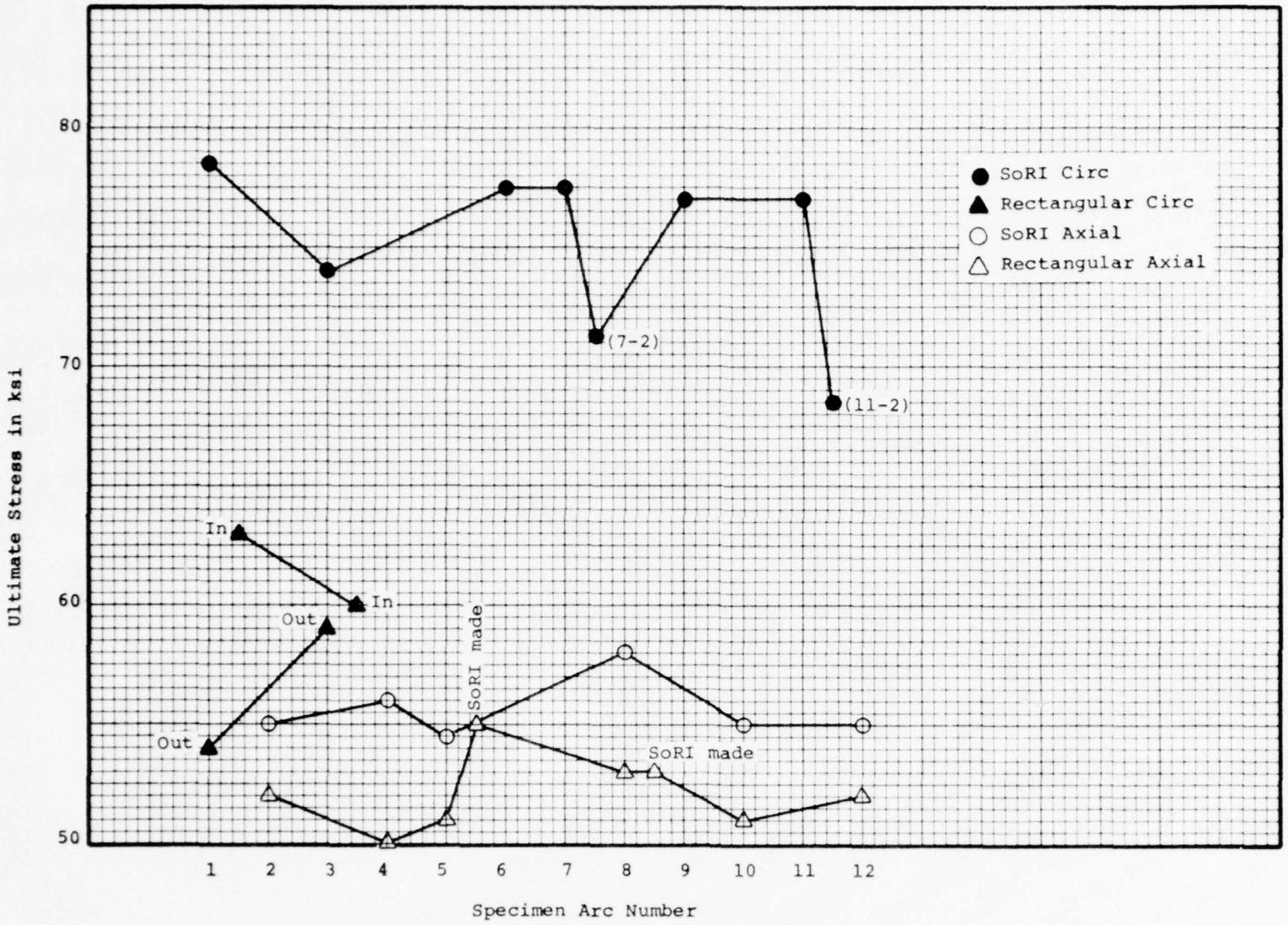

Figure 40. Rectangular versus SoRI Design Specimens Ultimate Stress

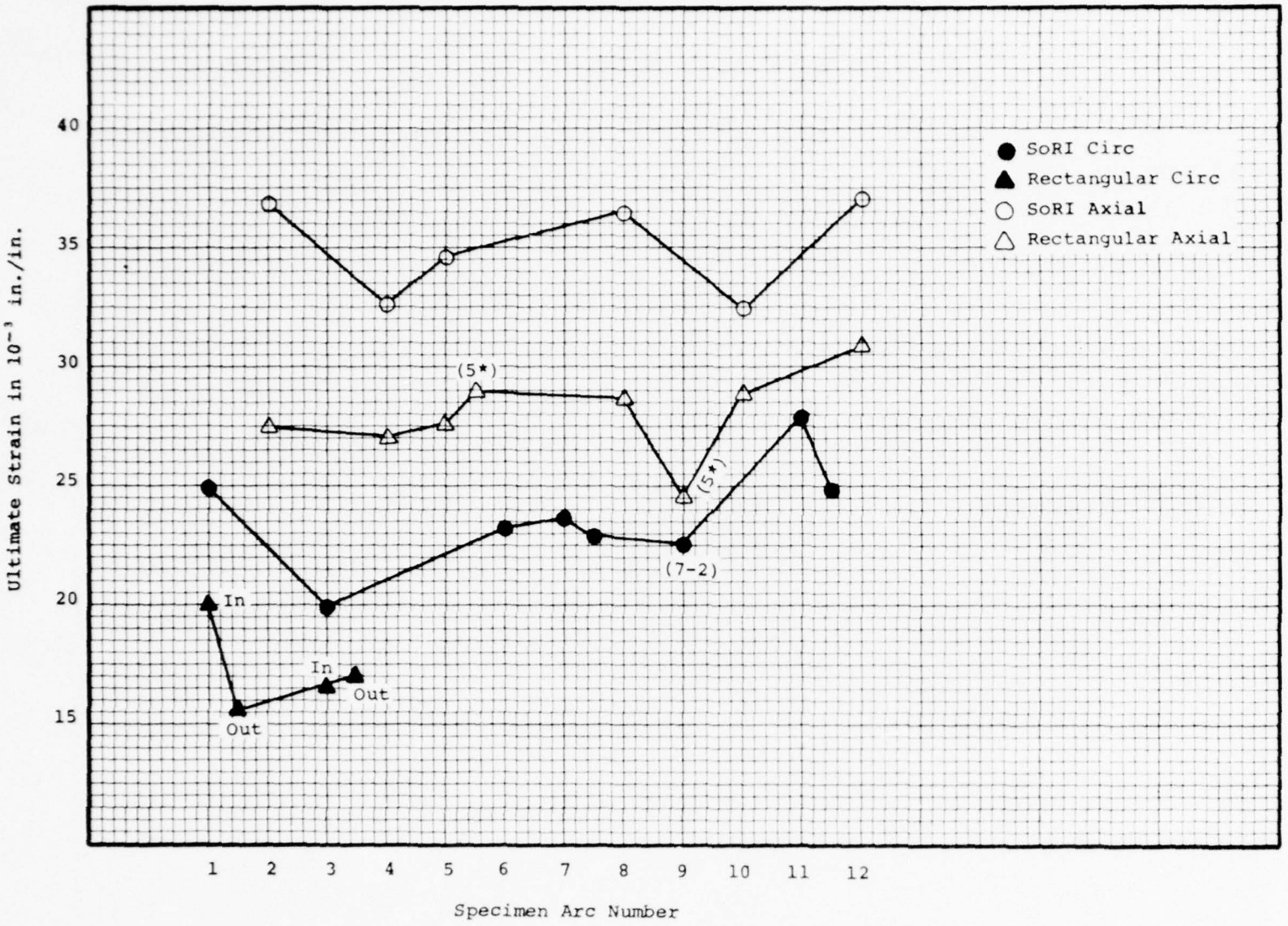

Figure 41. Comparison of Rectangular versus SoRI Design Specimens Ultimate Strain from Clip-ons

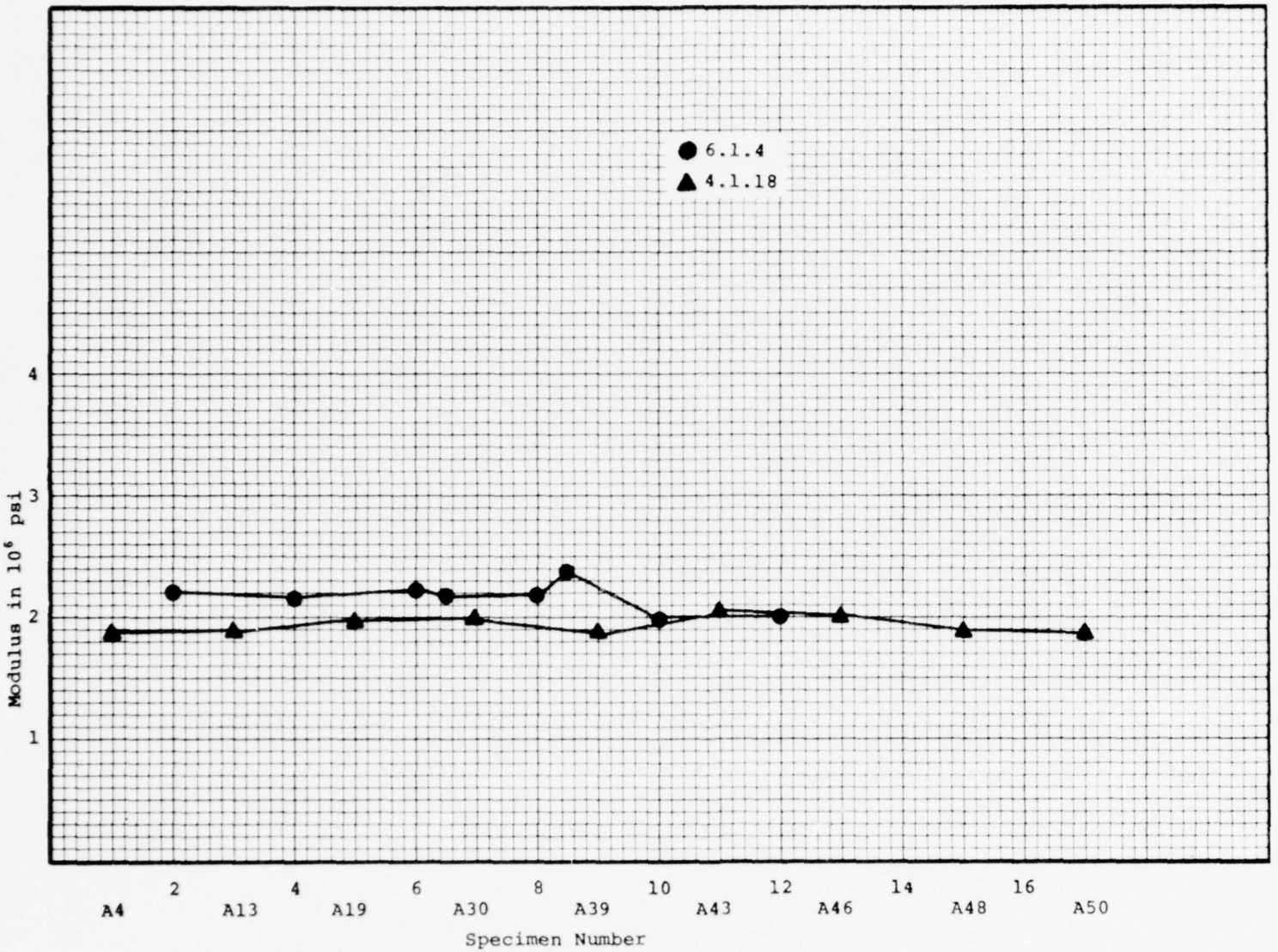

Figure 42. Rectangular Axial Specimens 6.1.4 versus 4.1.18 Modulus (Clip-on)

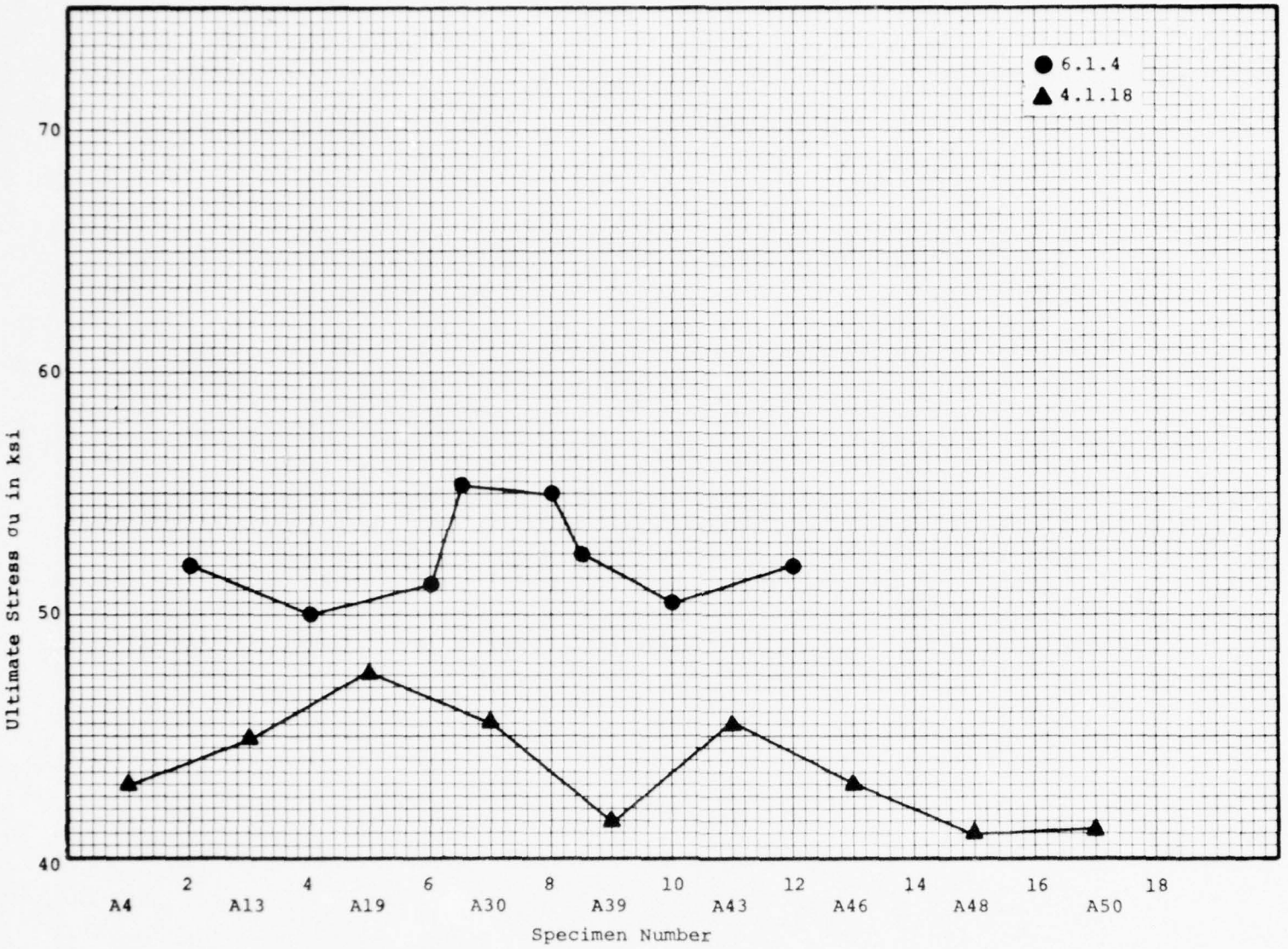

Figure 43. Rectangular Axial Specimens 6.1.4 versus 4.1.18

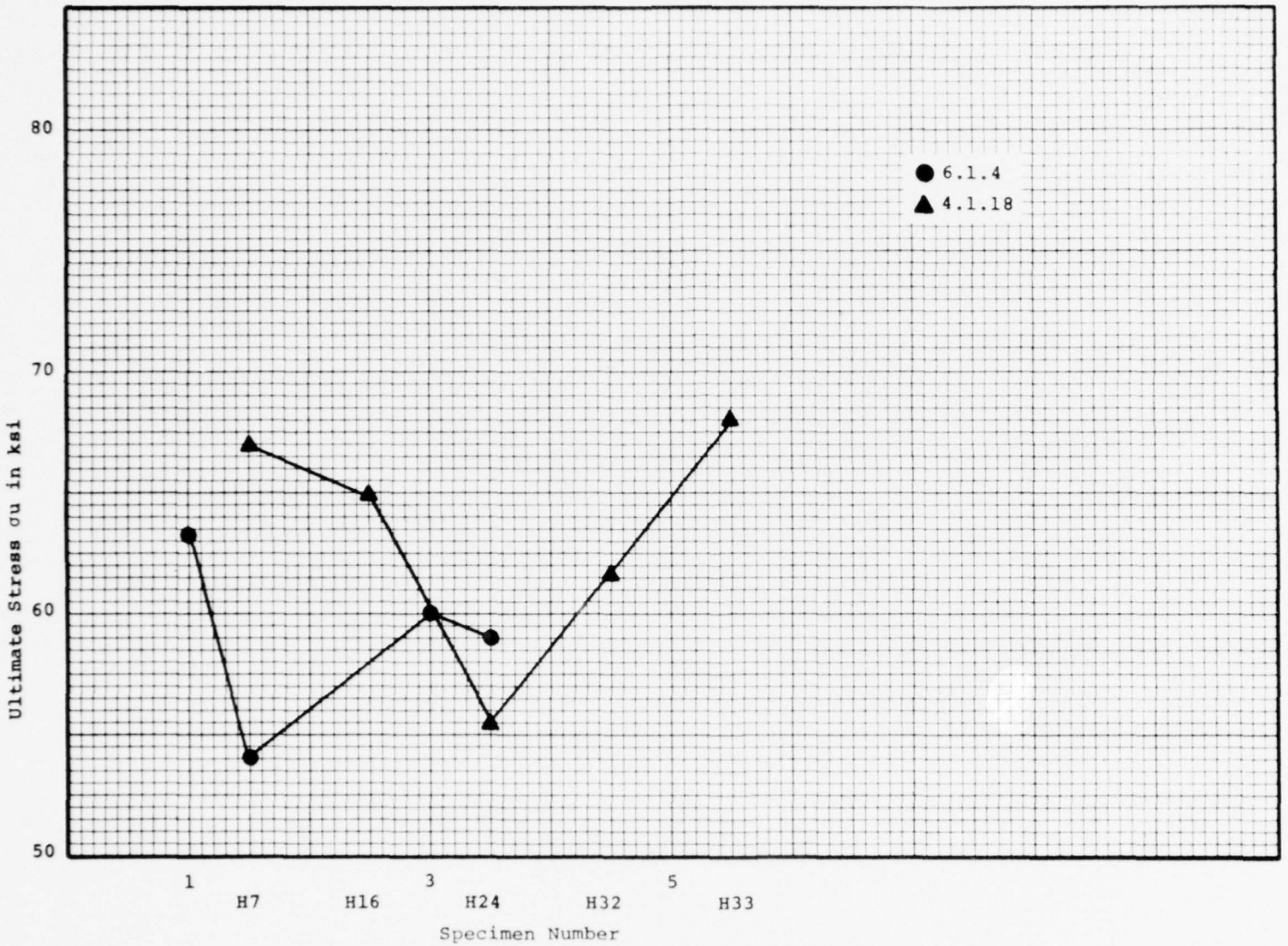

Figure 44. Rectangular Circumferential Specimens 6.1.4 versus 4.1.18

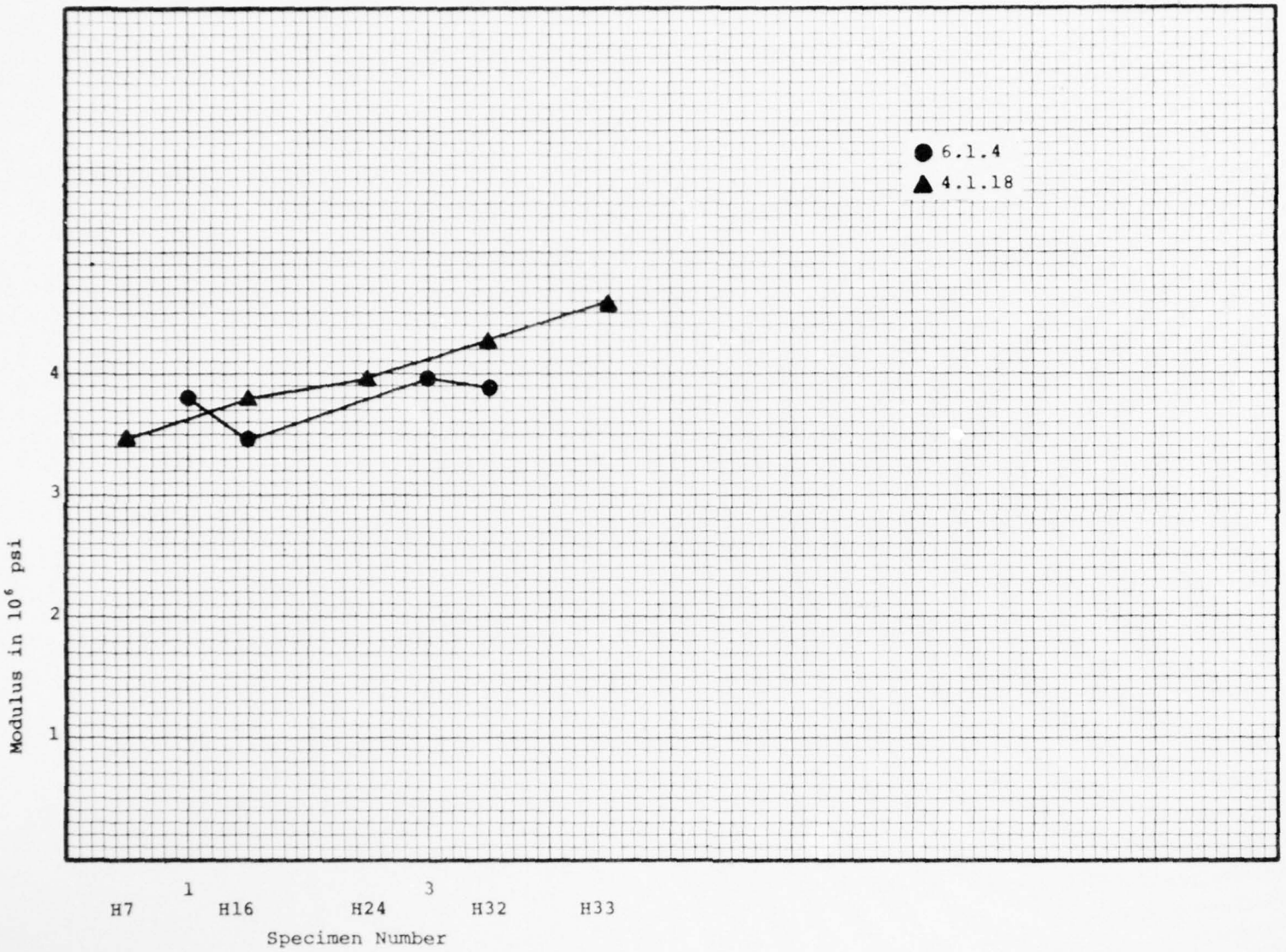

Figure 45. Rectangular Circumferential Specimens 6.1.4 versus 4.1.18 Modulus (Clip-on)

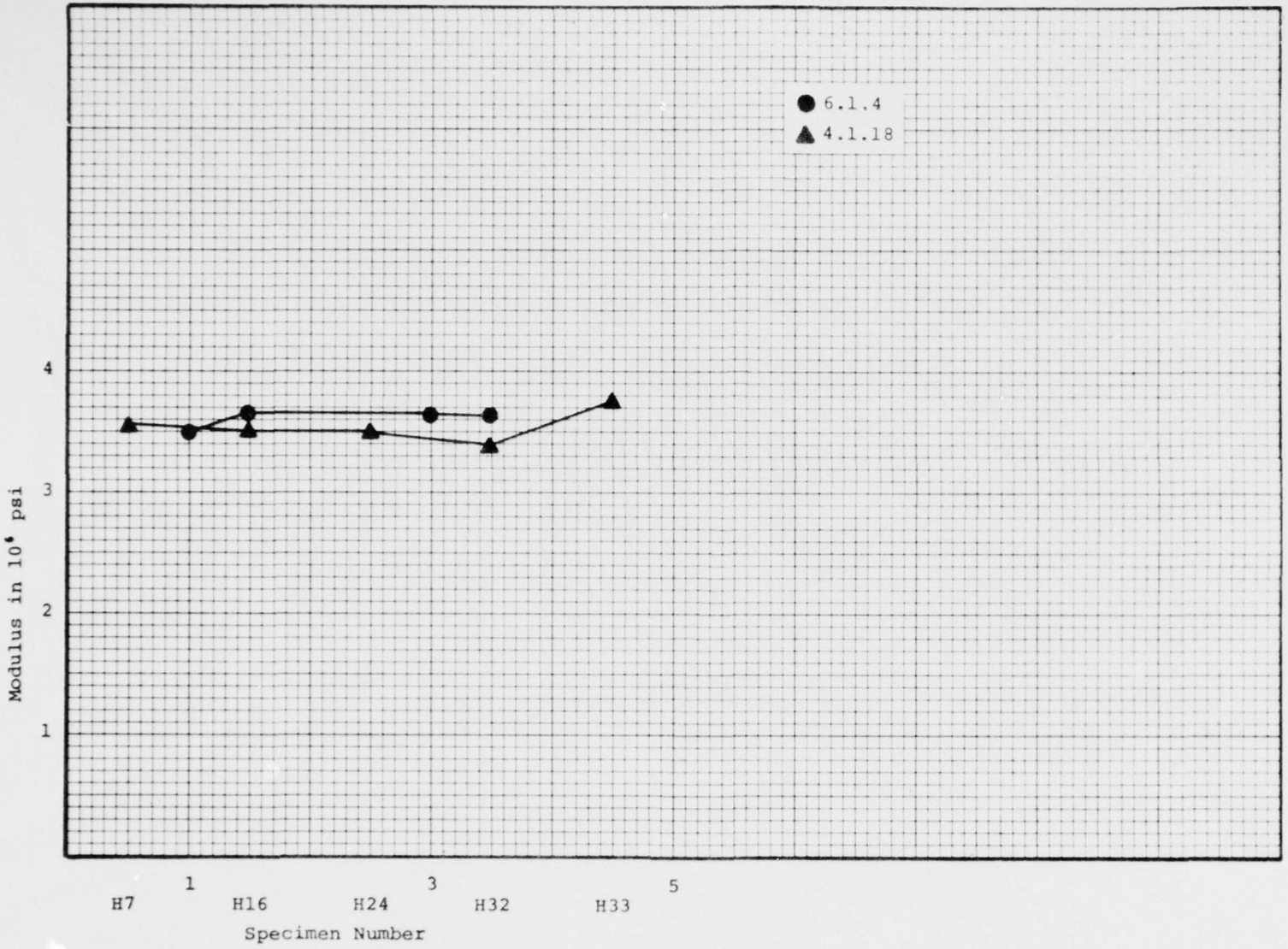

Figure 46. Rectangular Circumferential Specimens 6.1.4 versus 4.1.18 Modulus (Strain Gage)

Table 1

TEST MATRIX

		SoRI Design SoRI Machined	Rectangular Design Pre-Machined	Rectangular Design SoRI Machined
6.1.4	Hoop	8	--	4
	Axial	6	6	2
4.1.18	Hoop	--	5	--
	Axial	--	9*	--

*only 0.5 inch wide

Table 2

NONDESTRUCTIVE CHARACTERIZATION RESULTS ON TWELVE ARCS FROM CYLINDER 6.1.4

Arc	Circs/in.	Density gm/cm^3	Axial Velocity in./μsec	Circ Velocity in./μsec	Radial Velocity in./μsec
C1	96	1.680		0.1807	0.1913
A2	96	1.688	0.1790		
C3	96	1.687		0.1804	0.1917
A4	96	1.679	0.1797		
A5	92	1.685	0.1803		
C6	96	1.685		0.1821	0.1990
C7	92	1.676		0.1798	0.1932
A8	100	1.695	0.1802		
C9	96	1.683		0.1812	0.1918
A10	96	1.685	0.1792		
C11	96	1.689		0.1801	0.1951
A12	92	1.688	0.1801		
	Average	1.685	0.1798	0.1809	0.1937
	SD	0.005	0.0008	0.0012	0.0036

Table 3

DENSITIES OF HOOP AND AXIAL SPECIMENS
FROM CYLINDER 4.1.18

Specimen		Density gm/cm^3
H7-CC-Rect	a	1.614
	b	1.611
H16-CC-Rect	a	1.621
	b	1.634
H24-CC-Rect	a	1.633
	b	1.634
H32-CC-Rect	a	1.631
	b	1.638
H33-CC-Rect	a	1.623
	b	1.623
Average		1.626
A4-AC-Rect		1.628
A13-AC-Rect		1.620
A19-AC-Rect		1.623
A30-AC-Rect		1.624
A39-AC-Rect		1.626
A43-AC-Rect		1.625
A46-AC-Rect		1.625
A48-AC-Rect		1.623
A50-AC-Rect		1.621
Average		1.624

Table 4

DENSITIES OF FIVE SPECIMENS MACHINED FROM THE INSIDE SURFACE ADJACENT TO RESPECTIVE ARCS IN CYLINDER 6.1.4

Specimen	Density gm/cm^3
2-AC-Rect	1.660
4-AC-Rect	1.660
5-AC-Rect	1.665
8-AC-Rect	1.663
10-AC-Rect	1.661
12-AC-Rect	1.660
Average	1.662

Table 5

AXIAL COMPRESSIVE TESTS
SoRI SPECIMEN CONFIGURATION 3DQP 6.1.4

Specimen Number	Tangent Modulus E (x 10^6 psi)		Ultimate Stress σ_u (psi)	Ultimate Strain ε_u (x 10^{-3} in./in.)
	Clip-on	S.G.		Clip-on
2-AC-SoRI	2.10	2.24	55,400	36.8
4-AC-SoRI	2.10	2.20	56,000	32.6
5-AC-SoRI	2.07	2.00	54,500	34.6
8-AC-SoRI	2.05	2.20	58,000	36.4
10-AC-SoRI	2.09	2.15	55,000	32.4
12-AC-SoRI	1.92	2.10	55,500	37.0
$\bar{X}$	2.06	2.15	55,733	35.0
S	0.07	0.09	1,219	2.1

Table 6

AXIAL COMPRESSIVE TESTS
RECTANGULAR SPECIMEN CONFIGURATION 3DQP 6.1.4

Specimen Number	Tangent Modulus E ($\times 10^6$ psi)		Ultimate Stress σ_u (psi)	Ultimate Strain ε_u ($\times 10^{-3}$ in./in.)
	Clip-on	S.G.		Clip-on
2-AC-Rect	2.20	2.26	52,000	27.4
4-AC-Rect	2.16	2.20	50,000	27.0
5-AC-Rect*	2.18	2.25	55,400	28.9
5-AC-Rect	2.23	2.13	51,200	27.6
8-AC-Rect*	2.38	2.28	52,500	24.5
8-AC-Rect	2.19	2.20	55,000	28.7
10-AC-Rect	1.98	2.00	50,600	28.8
12-AC-Rect	2.00	2.02	52,000	30.8
$\overline{X}$	2.17	2.17	52,338	28.0
S	0.13	0.11	1,946	1.8

*Specimen from same arc number machined at SoRI

Table 7

AXIAL COMPRESSIVE TESTS
RECTANGULAR SPECIMEN CONFIGURATION 3DQP 4.1.18

Specimen Number	Tangent Modulus E (x 10^6 psi)		Ultimate Stress σ_u (psi)	Ultimate Strain ε_u (x 10^{-3} in./in.)
	Clip-on	S.G.		Clip-on
A4-AC-Rect	1.88	1.89	43,000	23.6
A13-AC-Rect	1.88	1.91	44,800	25.0
A19-AC-Rect	1.96	1.98	47,600	26.4
A30-AC-Rect	1.99	2.00	45,500	24.1
A39-AC-Rect	1.88	1.77	41,400	22.8
A43-AC-Rect	2.05	1.90	45,500	24.4
A46-AC-Rect	2.00	1.86	43,000	22.9
A48-AC-Rect	1.88	1.71	41,000	25.6
A50-AC-Rect	1.86	1.76	41,100	24.3
$\bar{X}$	1.93	1.86	43,656	24.3
S	0.07	0.10	2,324	1.2

Table 8

CIRCUMFERENTIAL COMPRESSIVE TESTS
SoRI SPECIMEN CONFIGURATION 3DQP 6.1.4

Specimen Number	Tangent Modulus E (x 10^6 psi)		Ultimate Stress σ_u (psi)	Ultimate Strain ε_u (x 10^{-3} in./in.)
	Clip-on	S.G.		Clip-on
1-CC-SoRI	3.60	3.91	78,500	24.9
3-CC-SoRI	3.73	3.78	73,800	19.9
6-CC-SoRI	3.55	3.96	77,400	23.2
7-1-CC-SoRI	3.45	3.76	77,600	23.7
7-2-CC-SoRI	3.54	3.85	70,800	22.9
9-CC-SoRI	3.70	3.65	77,000	22.6
11-1-CC-SoRI	3.40	3.66	68,500	27.8
11-2-CC-SoRI	3.35	3.63	76,800	24.8
$\bar{X}$	3.54	3.78	75,050	23.7
S	0.14	0.12	3,651	2.3

Table 9

CIRCUMFERENTIAL COMPRESSIVE TESTS
RECTANGULAR SPECIMEN CONFIGURATION 3DQP 6.1.4

Specimen Number	Tangent Modulus E (x 10^6 psi)		Ultimate Stress σ_u (psi)	Ultimate Strain ε_u (x 10^{-3} in./in.)
	Clip-on	S.G.		Clip-on
1 (In)-CC-Rect	3.80	3.50	63,200	19.9
1 (Out)-CC-Rect	3.45	3.65	54,000	15.6
3 (In)-CC-Rect	3.95	3.63	60,000	16.6
3 (Out)-CC-Rect	3.88	3.64	59,000	17.0
$\bar{X}$	3.77	3.61	59,050	17.3
S	0.22	0.07	3,814	1.9

Table 10

CIRCUMFERENTIAL COMPRESSIVE TESTS
RECTANGULAR SPECIMEN CONFIGURATION 3DQP 4.1.18

Specimen Number	Tangent Modulus E (x 10^6 psi)		Ultimate Stress σ_u (psi)	Ultimate Strain ε_u (x 10^{-3} in./in.)
	Clip-on	S.G.		Clip-on
H7-CC-Rect	3.47	3.53	67,000	17.7
H16-CC-Rect	3.78	3.50	65,000	19.3
H24-CC-Rect	3.94	3.50	55,400	16.0
H32-CC-Rect*	4.25	3.37	61,700	15.8
H33-CC-Rect	4.55	3.75	68,000	17.8
$\bar{X}$	4.00	3.53	63,420	17.3
S	0.42	0.14	5,088	1.4

*Apparent bending in specimen

Table 11

70°F AXIAL COMPRESSIVE DATA COMPARISON

Program	AHP	CRS	6.1.4	6.1.4
Material				
Process	A	C	C	C
A_r/A_t	0.48	0.607	0.700	0.700
S/P	P	P	S	S
Density	1.67	(1.64)*	1.685	1.685
Velocity				
Radial	(0.197)	(0.173)	(0.194)	(0.194)
Axial	0.1732 (0.1840)	(0.171)	0.180	0.180
Circ	0.1894	-	(0.179)	(0.179)
Type Test	Coupon	Coupon (Inners & Full)	SoRI Design	Rectangular Design
Specimen Gage (in.)	4 cells/0.5/ 1.2	(0.6 x 0.5 x 0.8) (0.6 x 0.2 x 0.8)	(0.6 x 0.5 x 0.8)	3 cells x 0.2 x 1.0
No. of Tests	3	9	6	8
$\bar{E}$ in 10^6 psi	2.23	2.60	2.06	2.17
$\bar{\sigma}_u$ in 10^6 psi	32.2	45.0	55.7	52.3
$\bar{\varepsilon}_u$ in 10^{-3} $\frac{in.}{in.}$	28.0	21.0	35.0	28.0

*Data not from these particular specimens in parenthesis

Table 12

70°F HOOP COMPRESSIVE DATA COMPARISON

Program	Coated Disc	Coated Disc	AHP	CRS	CRS	CRS/Spades	6.1.4	6.1.4
Material								
Process	A	A	A	C	C	C	C	C
A_r/A_t	0.40	0.40	0.48	0.607	0.607	0.45		
S/P	P	P	P	P	P	S	S	S
Density	1.61	1.61	1.66 (1.67)	(1.64)	(1.64)	-	1.685	1.685
Velocity								
Radial	0.1988	0.1988	(0.1971)*	(0.173)	(0.173)	0.166	0.194	0.194
Axial	-	-	(0.1840)	(0.171)	(0.171)	0.166	(0.180)	(0.180)
Circ	-	-	0.1780 (0.1894)	-	-	-	0.179	0.179
Type Test	Inner/100% CCC	Outer/100% CCC	Full/0% CCC	I, O, & Full/ 100% CCC	Hydrostatic	Hydrostatic	SoRI Design	Rectangular Design
Specimen Gage (in.)	0.2 x 0.4 x 0.6	0.2 x 0.4 x 0.6	0.4 x 0.4 x 0.625 and 0.4 x 0.2 x 0.625	0.6 x 0.5 x 0.8 0.6 x 0.2 x 0.8	2.0 x 0.5 x 1.0	2.0 x 0.5 x 1.0	0.6 x 0.5 x 0.8	2(0.3 x 0.15 x 1.0)
No. of Tests	4	3	3	9	12	2	8	4
$\bar{E}$ in 10^6 psi	3.07	3.02	2.42	3.81	3.53	3.66	3.54	3.61
$\bar{\sigma}_u$ in 10^3	39.3	37.6	31.2	58.6	-		75.1	59.1
$\bar{\varepsilon}_u$ in 10^{-3} $\frac{in.}{in.}$	16.5	16.1	20.0	14.3	-		23.7	17.3

*Data not from these particular specimens in parenthesis

Table 13

OUTSIDE/INSIDE COMPARISON

Property	ID	OD	Full
Density on full Arcs compared to ID Specimen (Axials) (Adjacent)	1.662	-	1.685
Clip-on Modulus on Circ Specimens (2)	3.87	3.66	(3.54)
S.G. Modulus on Circ Specimens (2)	3.57	3.65	(3.78)
Ultimate Stress on Circ Specimens (2)	61,600	57,000	(75,050)
Ultimate Strain on Circ Specimens (2)	18.2	16.3	(23.7)

Note: Data in parenthesis not truly comparable due to specimen design

Table 14

COMPARISON OF RECTANGULAR AND SoRI SPECIMEN CONFIGURATIONS 6.1.4

	Configuration	Tangent Modulus E ($\times 10^6$ psi)		Ultimate Stress σ_u (psi)	Ultimate Strain ε_u ($\times 10^{-3}$ in./in.)
		Clip-on	S.G.		Clip-on
Axial	SoRI	2.06	2.15	55,733	35.0
	Rectangular	2.17	2.17	52,338	28.0
Circ	SoRI	3.54	3.78	75,050	23.7
	Rectangular*	3.77	3.61	59,050	17.3

*Inside and outside specimens

Table 15

COMPARISON OF 6.1.4 VERSUS 4.1.18 RECTANGULAR SPECIMEN CONFIGURATION 3DQP

	Cylinder Number	Tangent Modulus E ($\times 10^6$ psi)		Ultimate Stress σ_u (psi)	Ultimate Strain ε_u ($\times 10^{-3}$ in./in.)
		Clip-on	S.G.		Clip-on
Axial	6.1.4	2.17	2.17	52,338	28.0
	4.1.18	1.93	1.86	43,656	24.3
Circ	6.1.4*	3.88	3.57	61,600	18.3
	4.1.18	4.00	3.53	63,420	17.3

*Specimens from inside surface of cylinder only

APPENDIX A

Raw Data

A1

Axial Compressive Tests
SoRI Specimen Configuration

6.1.4

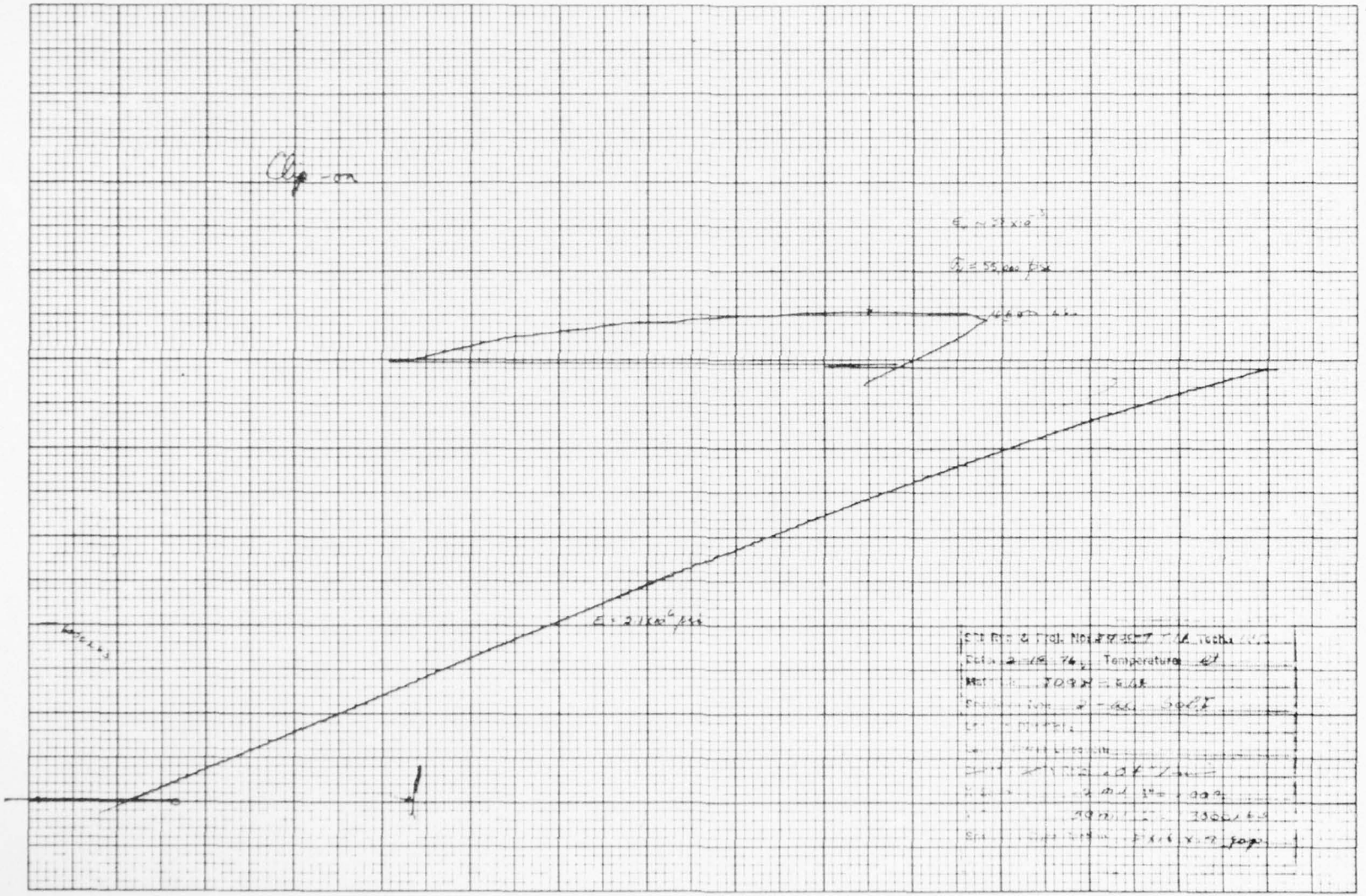

Figure A1 . Test results for Specimen 2-AC-SubB1

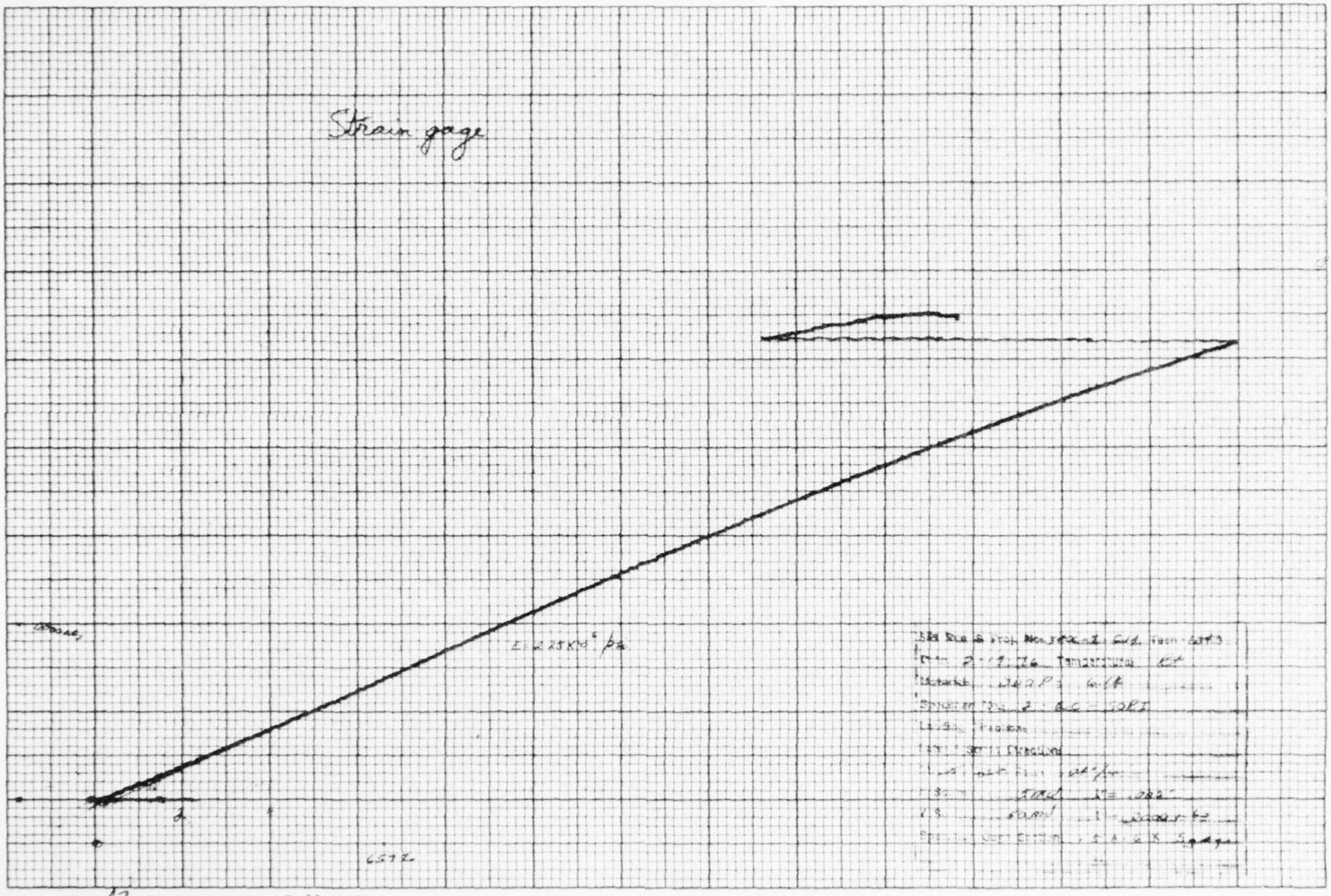

Figure 12 Test Results for Specimen 2-AC-S4R1

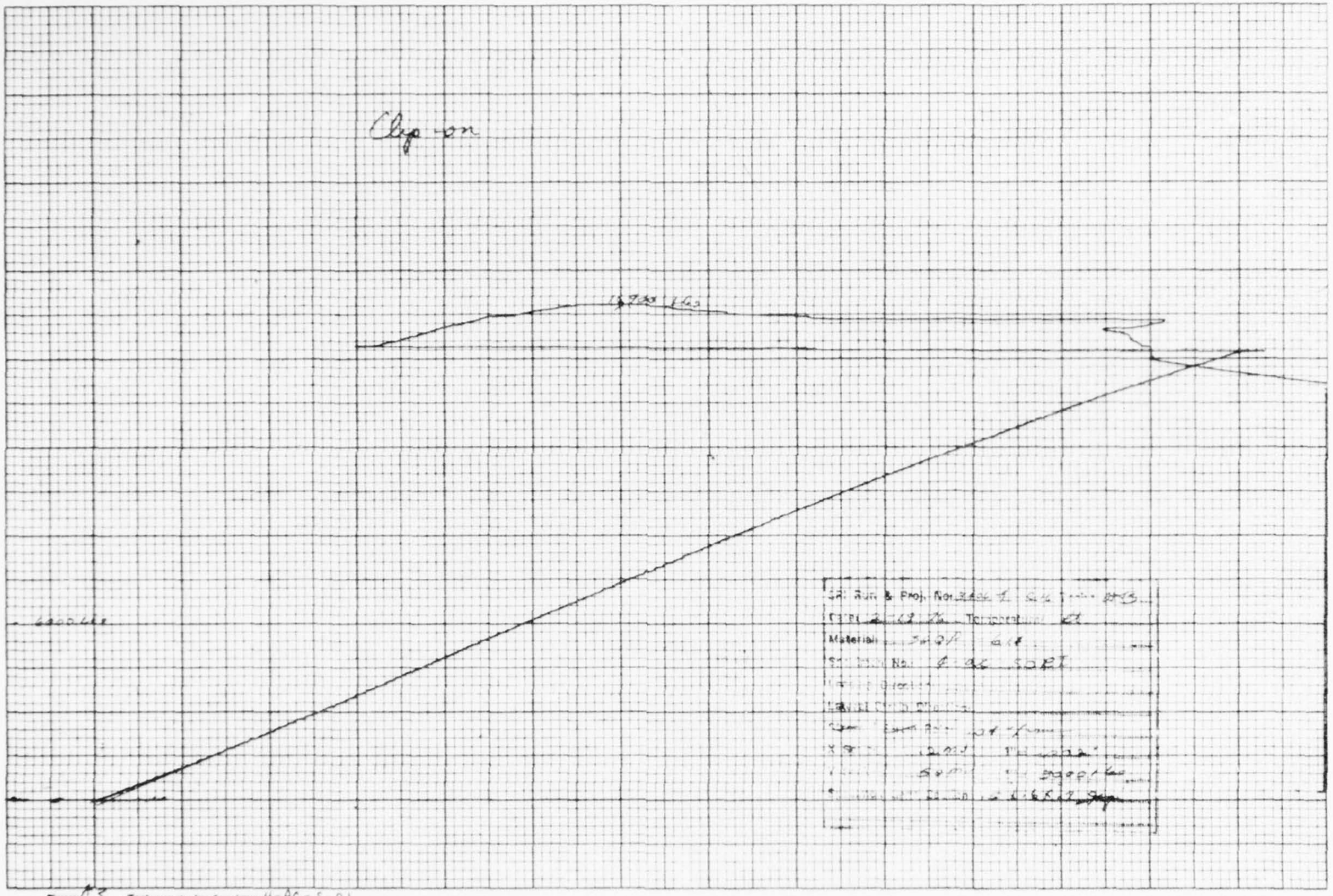

Fig. 3 Test results for Specimen 4-AC-SeB1

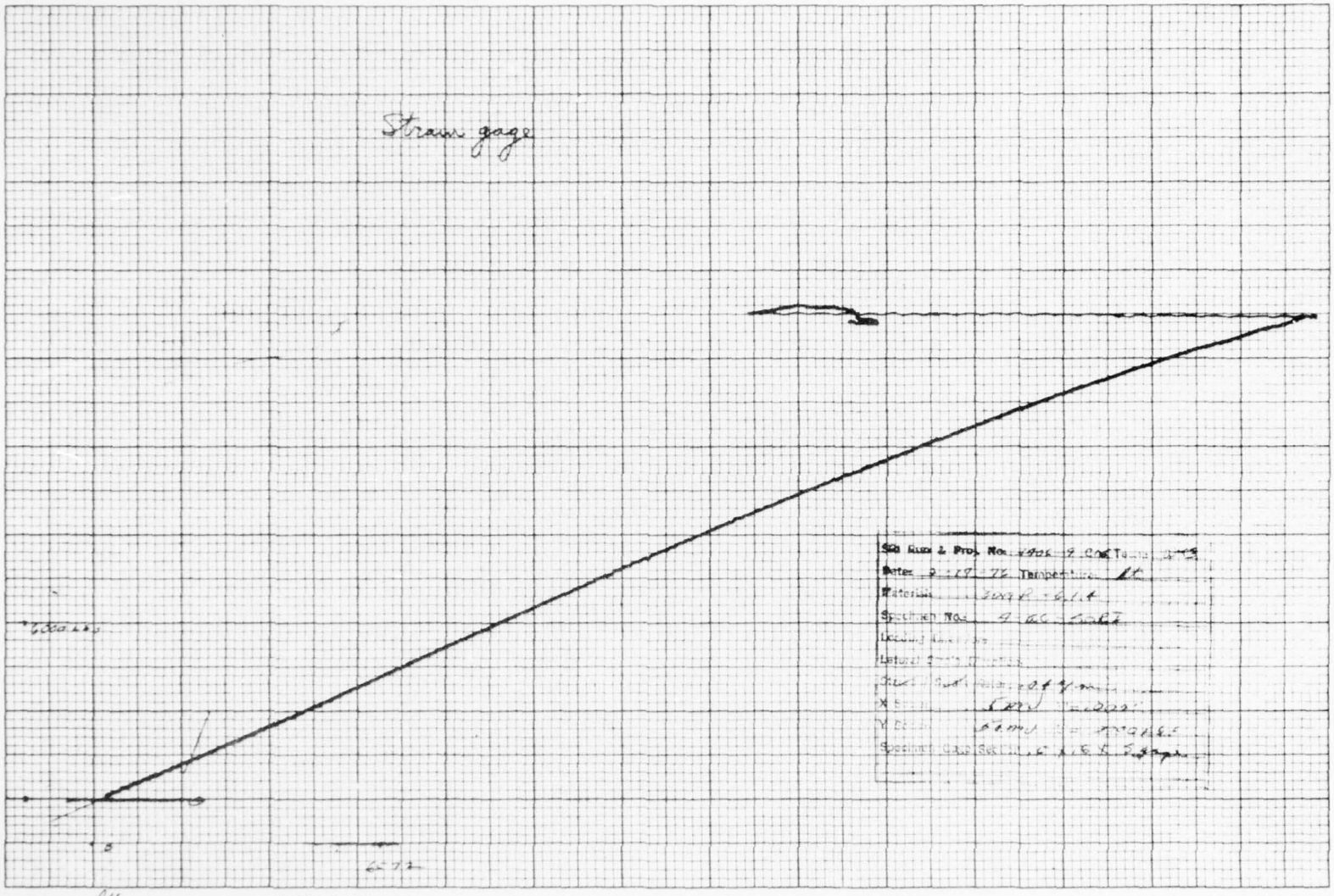

Figure 14 Test Results for Specimen 4-AC-SaB1

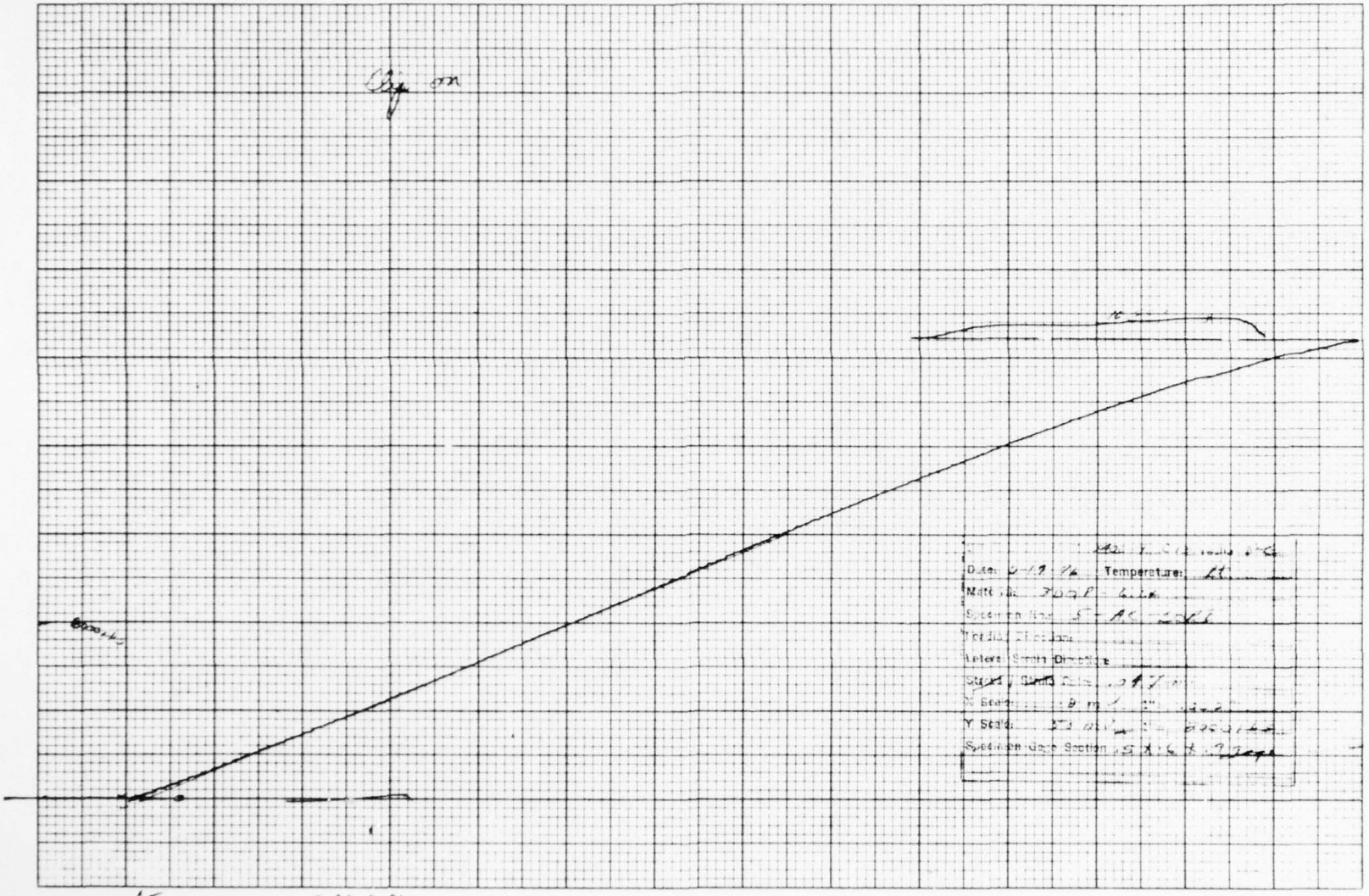

Figure A5. Test Results for Specimen S-AC-S0R1

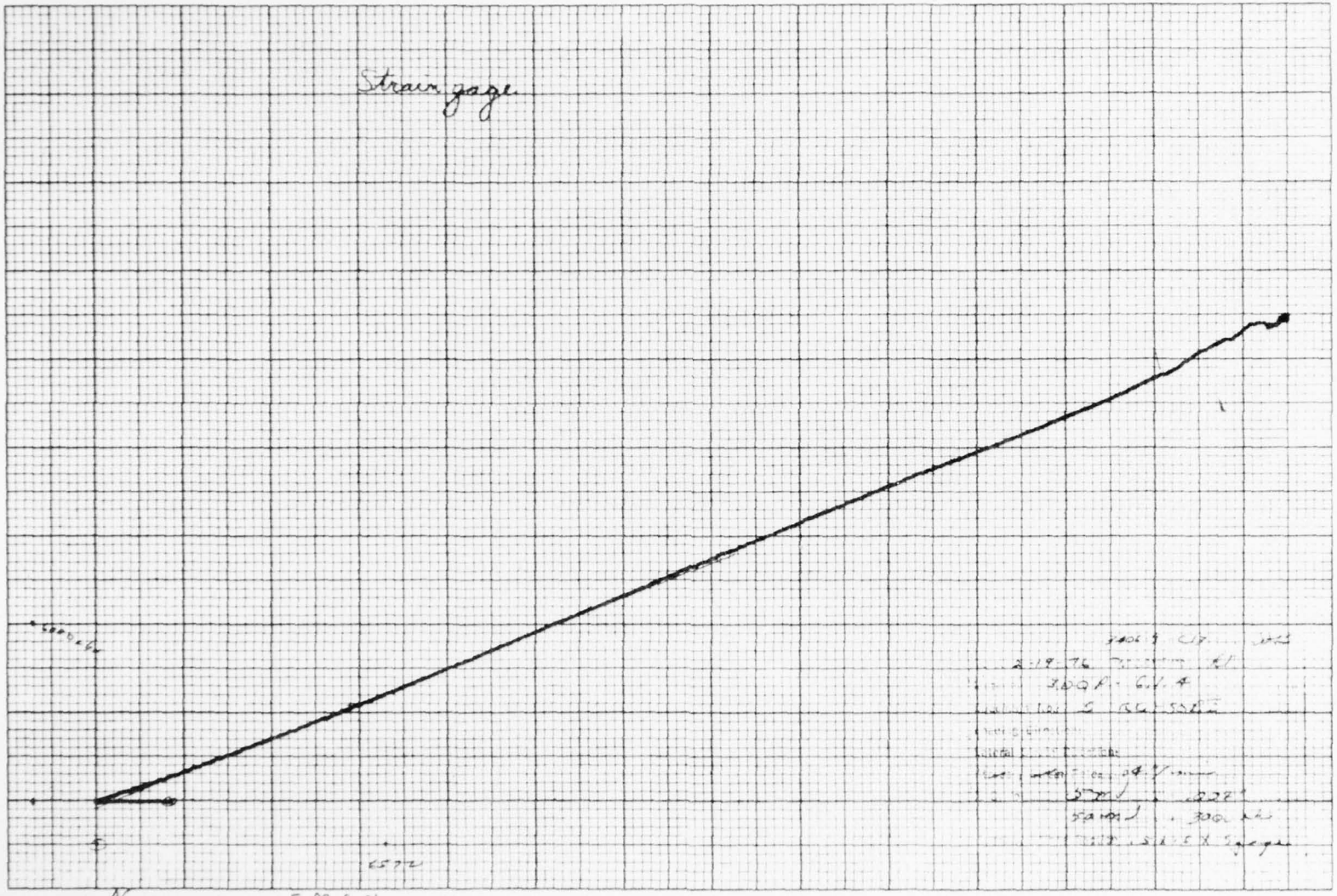

Figure A6 . Test Results for Specimen S-AC-SSR1

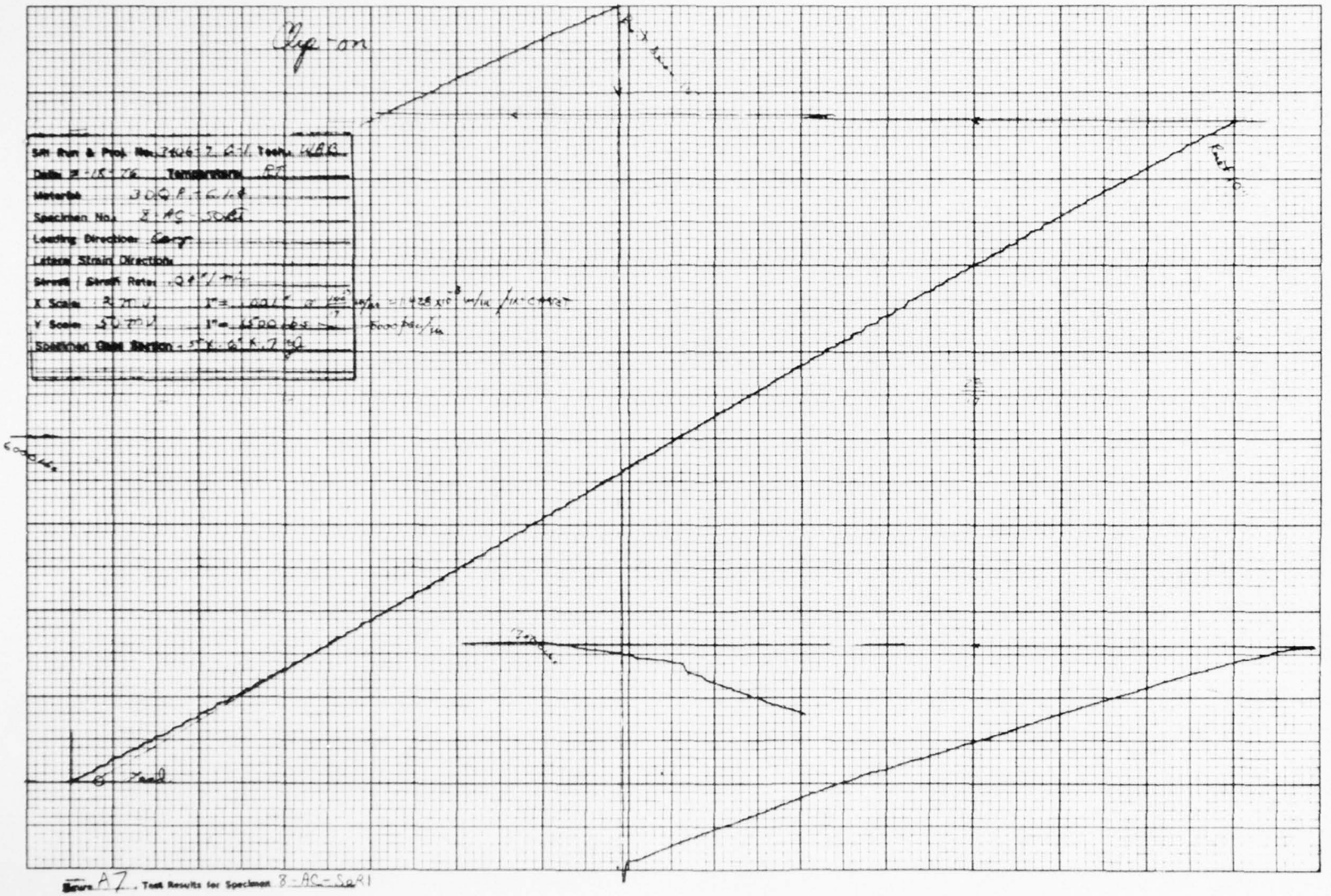

Figure A7. Test Results for Specimen 8-AC-Soil

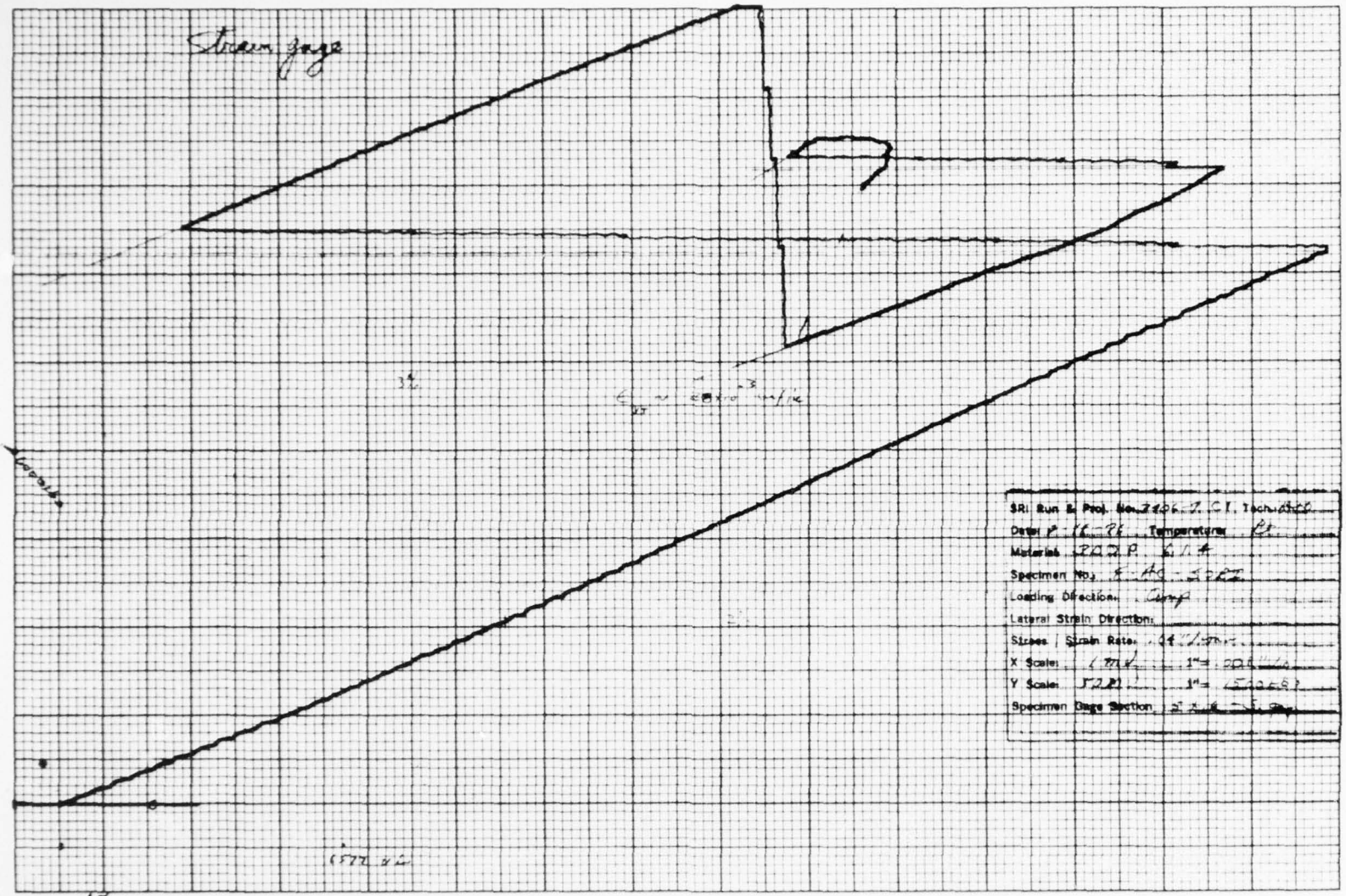

Figure A8 Test Results for Specimen 8-AC-SwRI

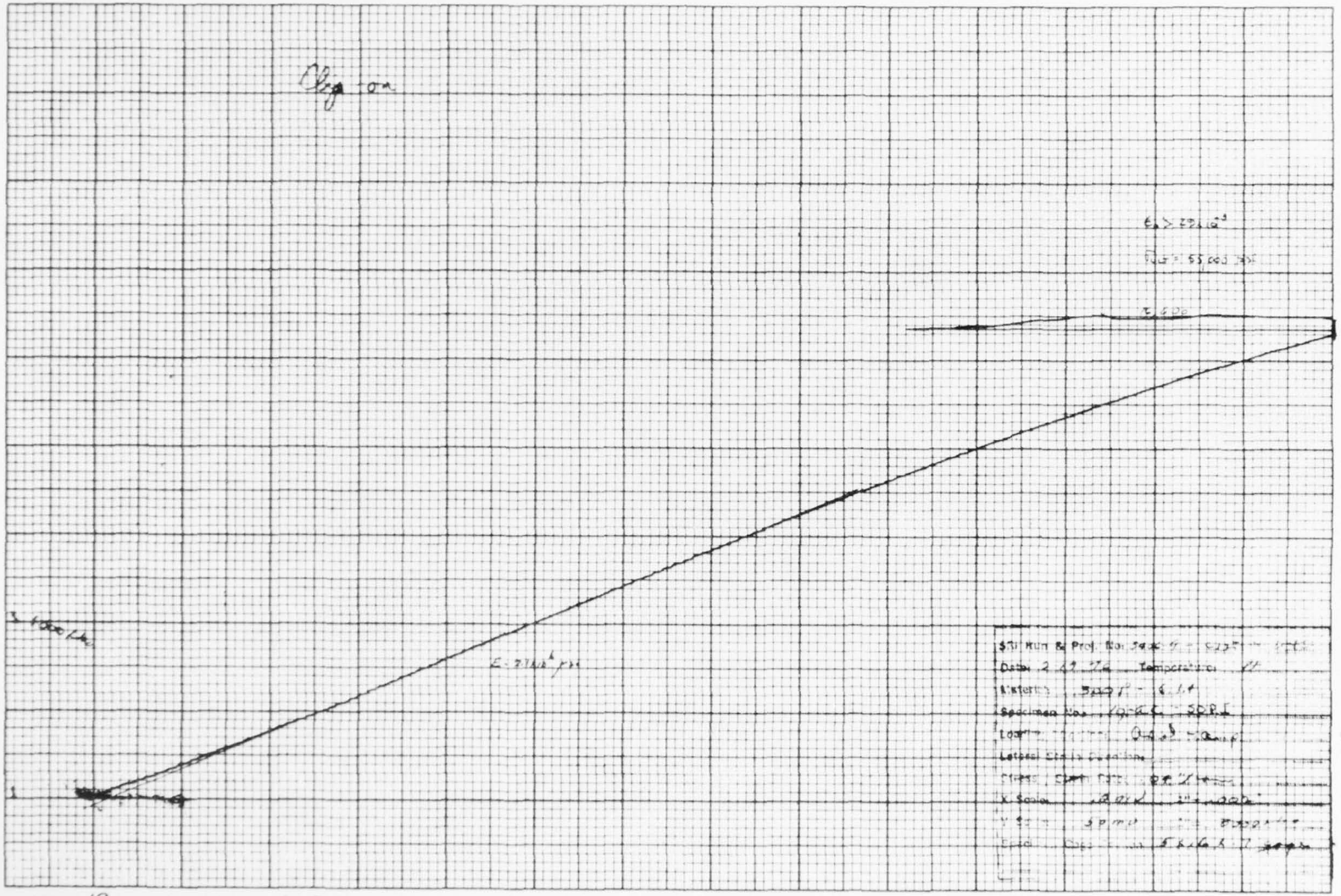

Figure 19. Test Results for Specimen 10-AC-SmR1

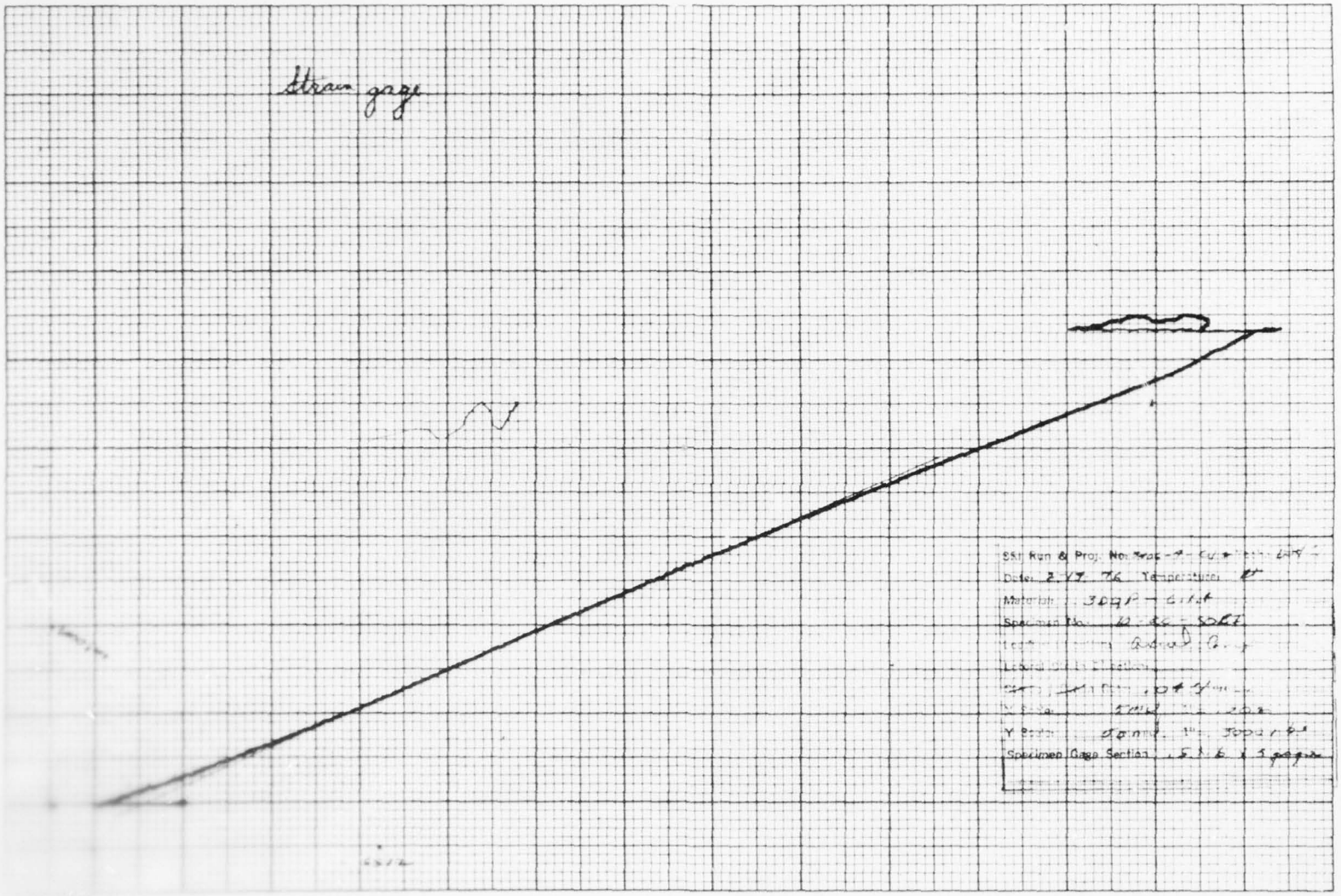
Strain gage

AD-A044 031 SOUTHERN RESEARCH INST BIRMINGHAM ALA F/G 11/9
EVALUATION OF THE COMPRESSIVE PROPERTIES OF A SPECIAL 3DQP.(U)
SEP 76 J R KOENIG, G F FORNARO DNA001-75-C-0037
UNCLASSIFIED SORI-76-483-3406-9-I-F DNA-4174F NL

2 OF 2
AD
A044031

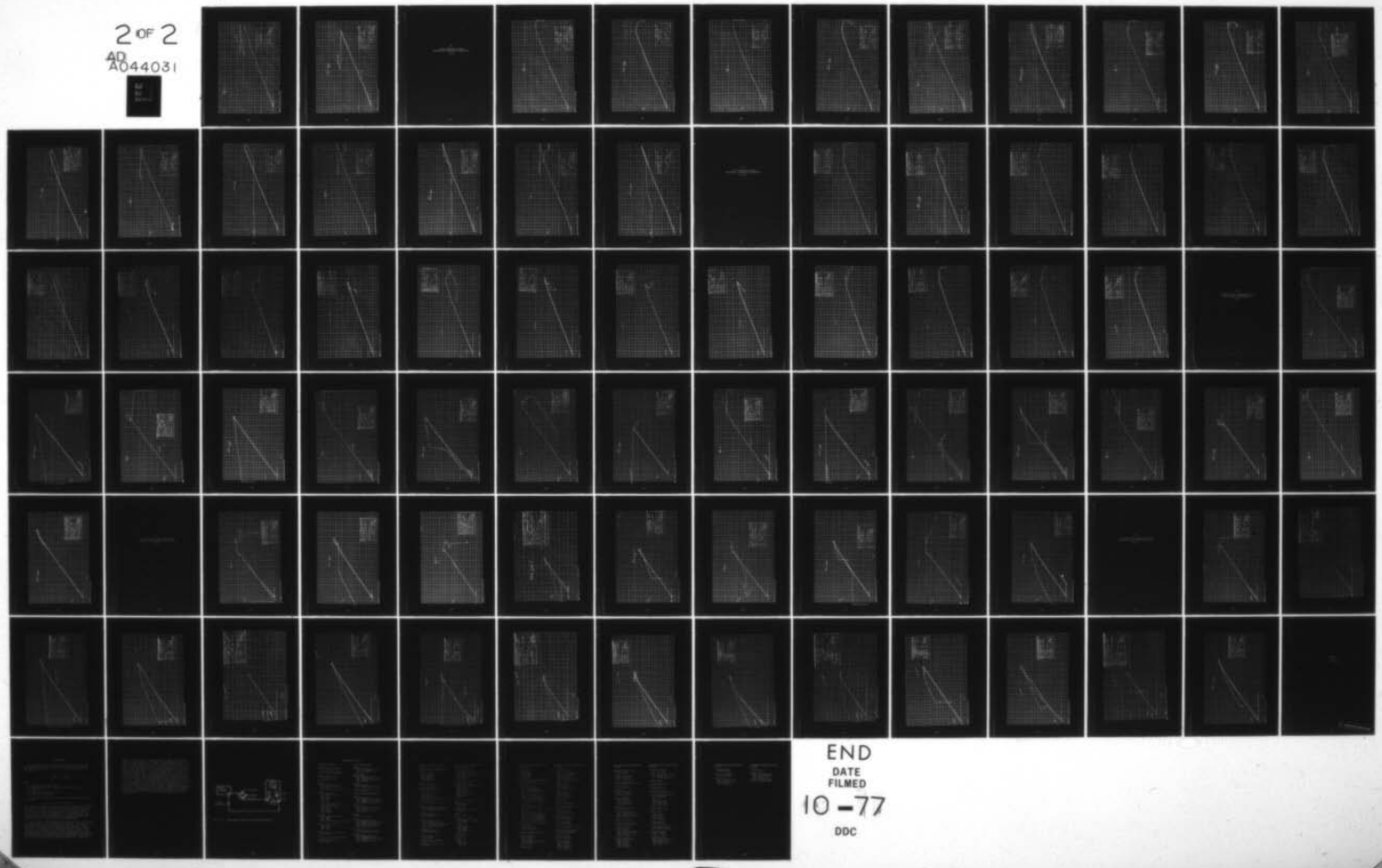

END
DATE
FILMED
10-77
DDC

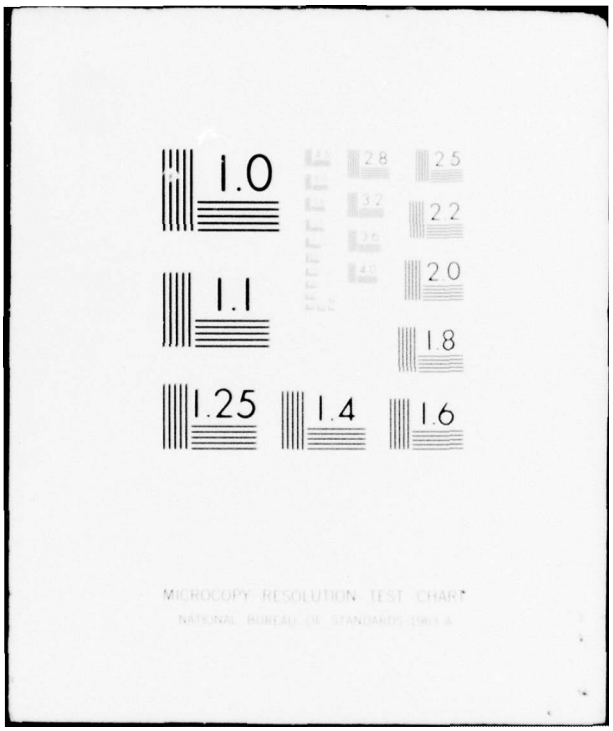
1.0
1.1
1.25
1.4
1.6
2.8
3.2
3.6
4.0
2.5
2.2
2.0
1.8
MICROCOPY RESOLUTION TEST CHART
NATIONAL BUREAU OF STANDARDS 1963 A

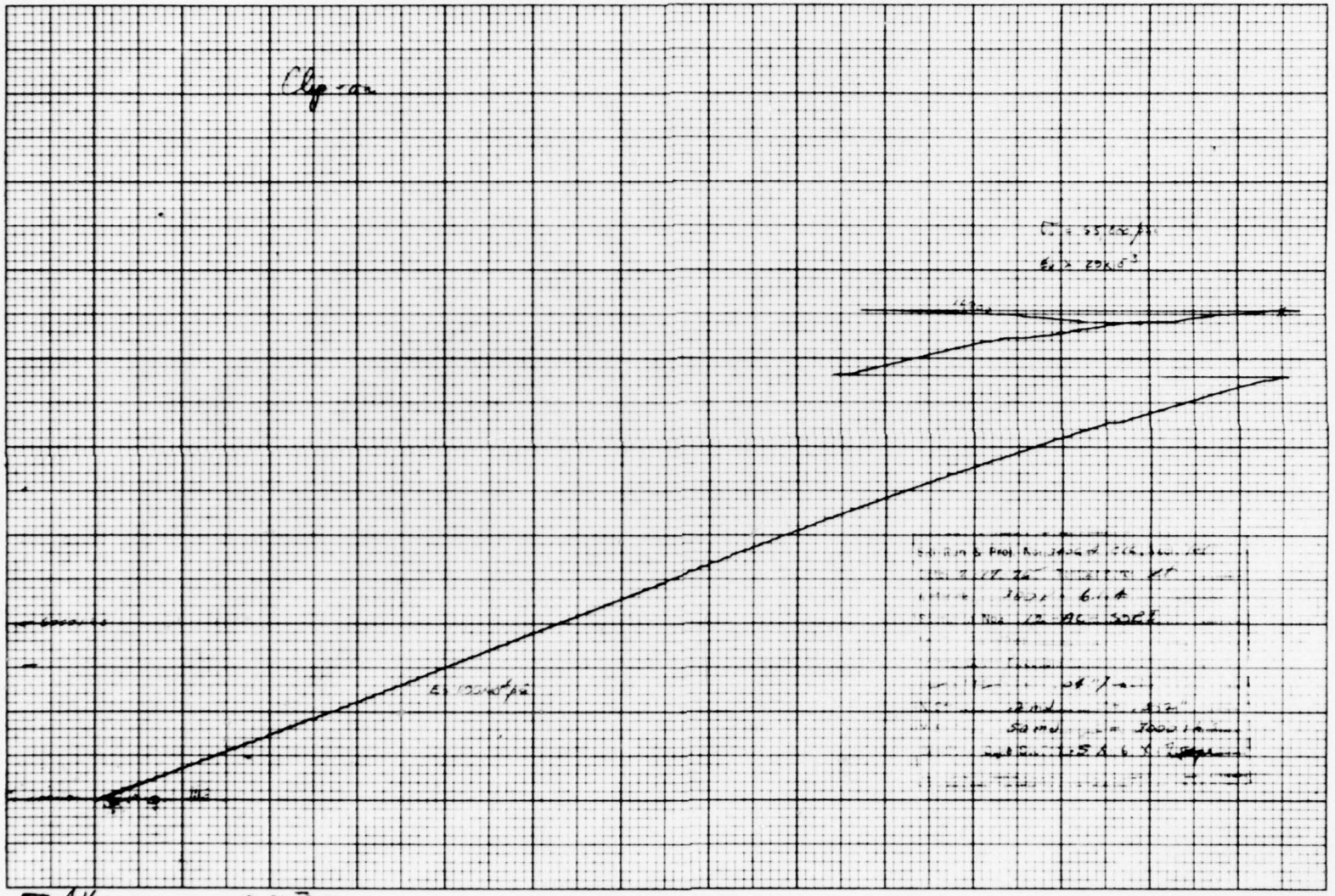

Figure A11. Test Results for Specimen 12-AC-30R1

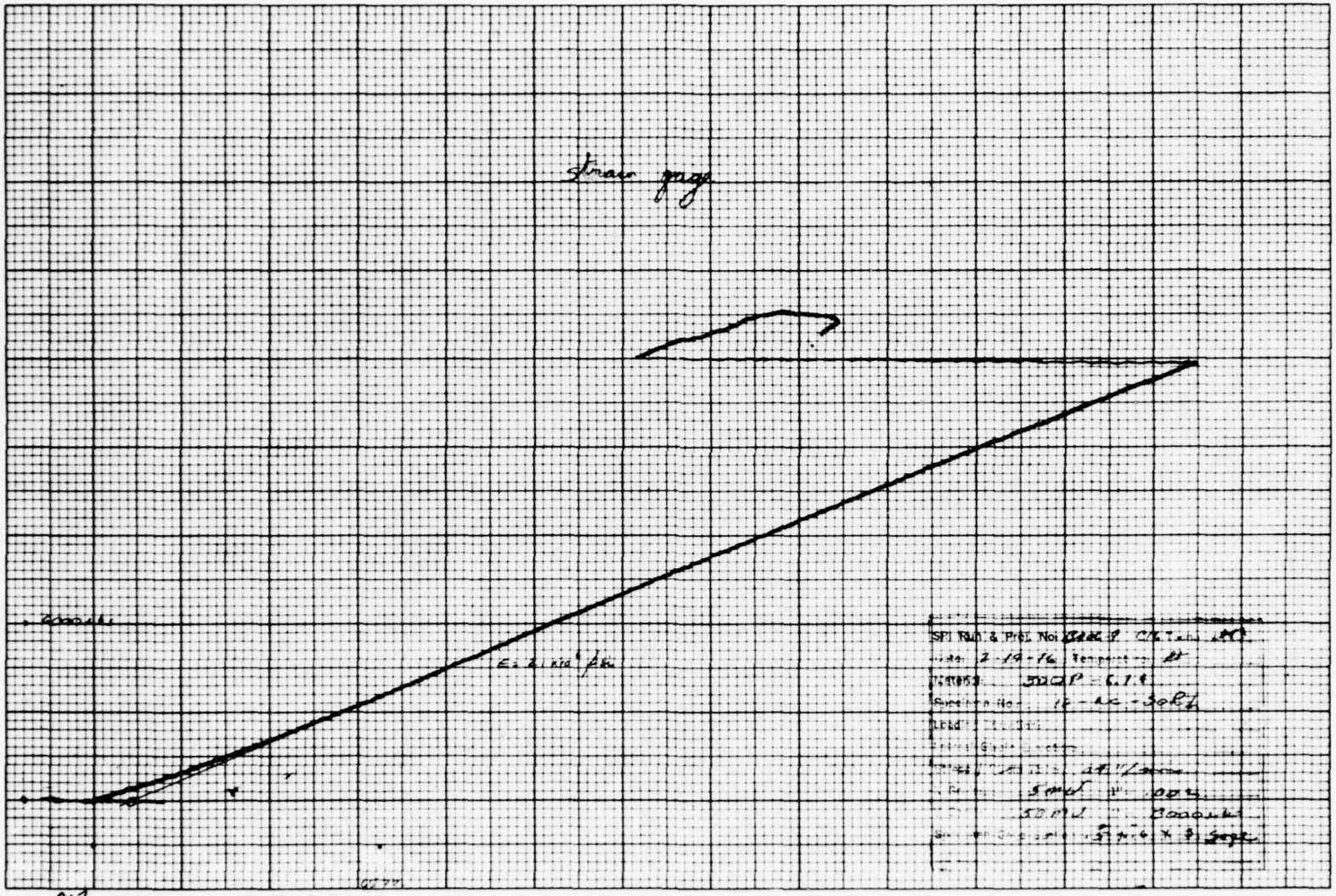

Figure A-2 Test Results for Specimen 12-AC-SoR1

A2

Axial Compressive Tests
Rectangular Specimen Configuration

6.1.4

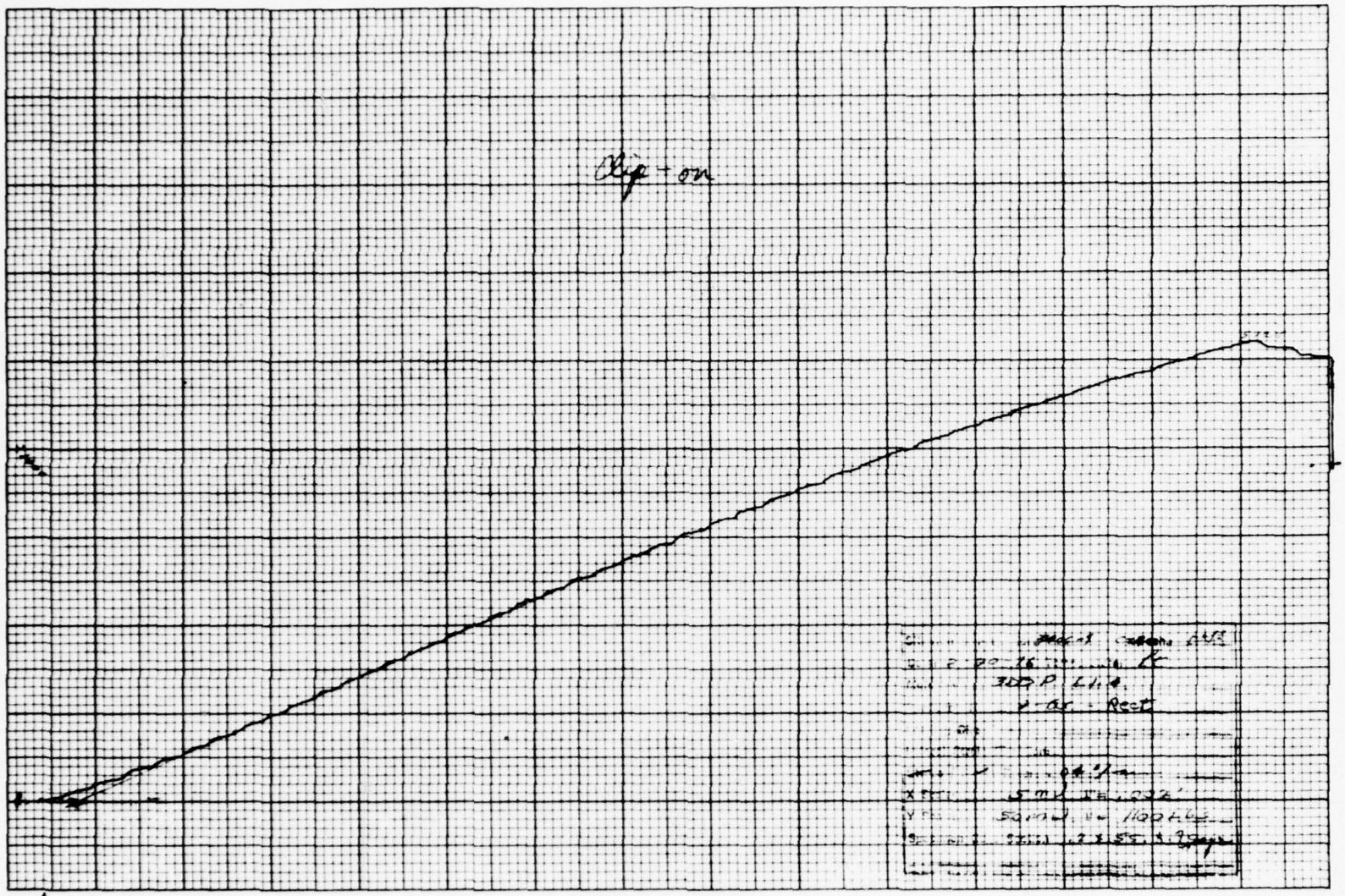

Figure A.13 Test Results for Specimen 2-AC-Rect

Figure A.19. Test Results for Specimen 2-AC-Rect

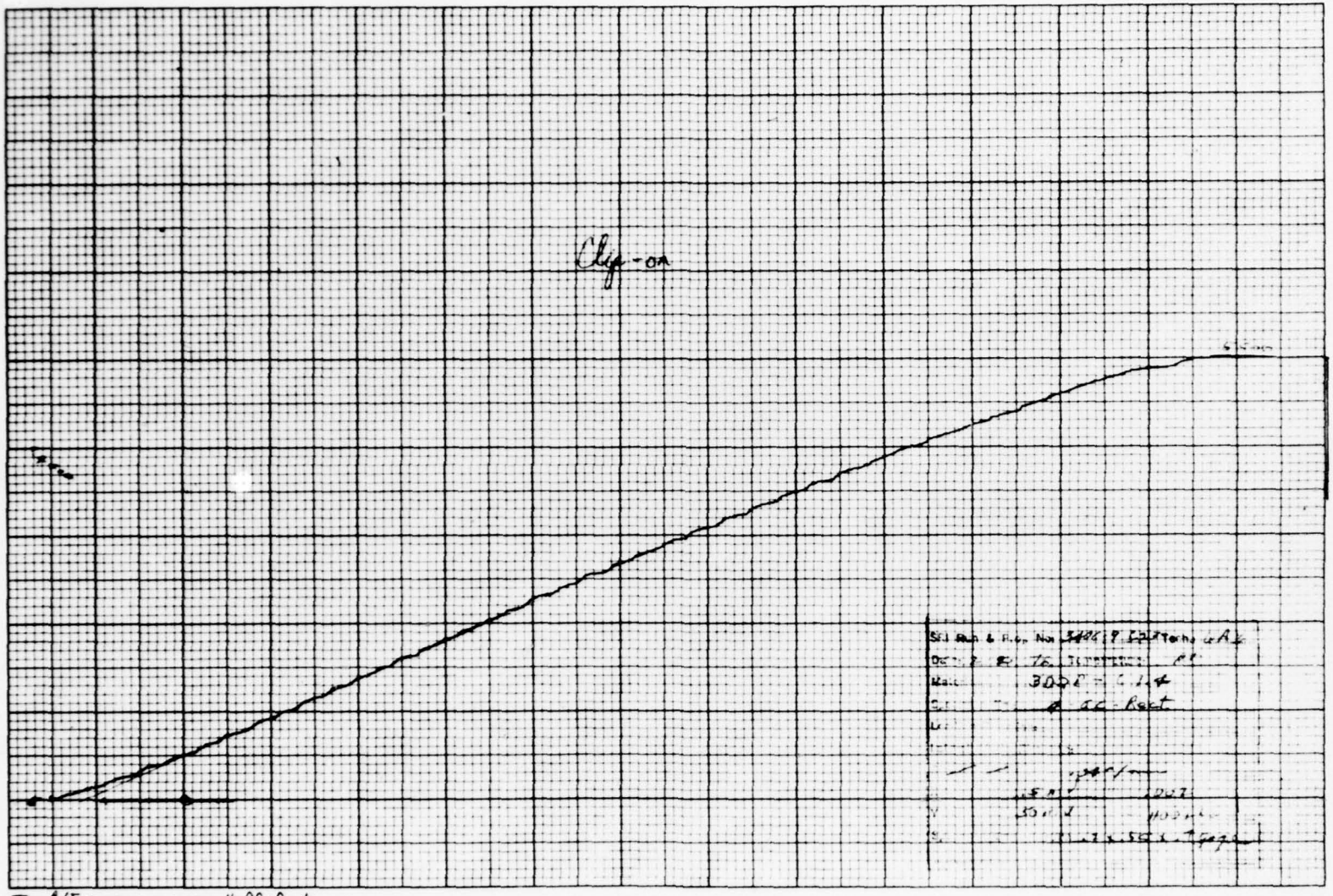

Figure A15. Test Results for Specimen 4-AC-Rect

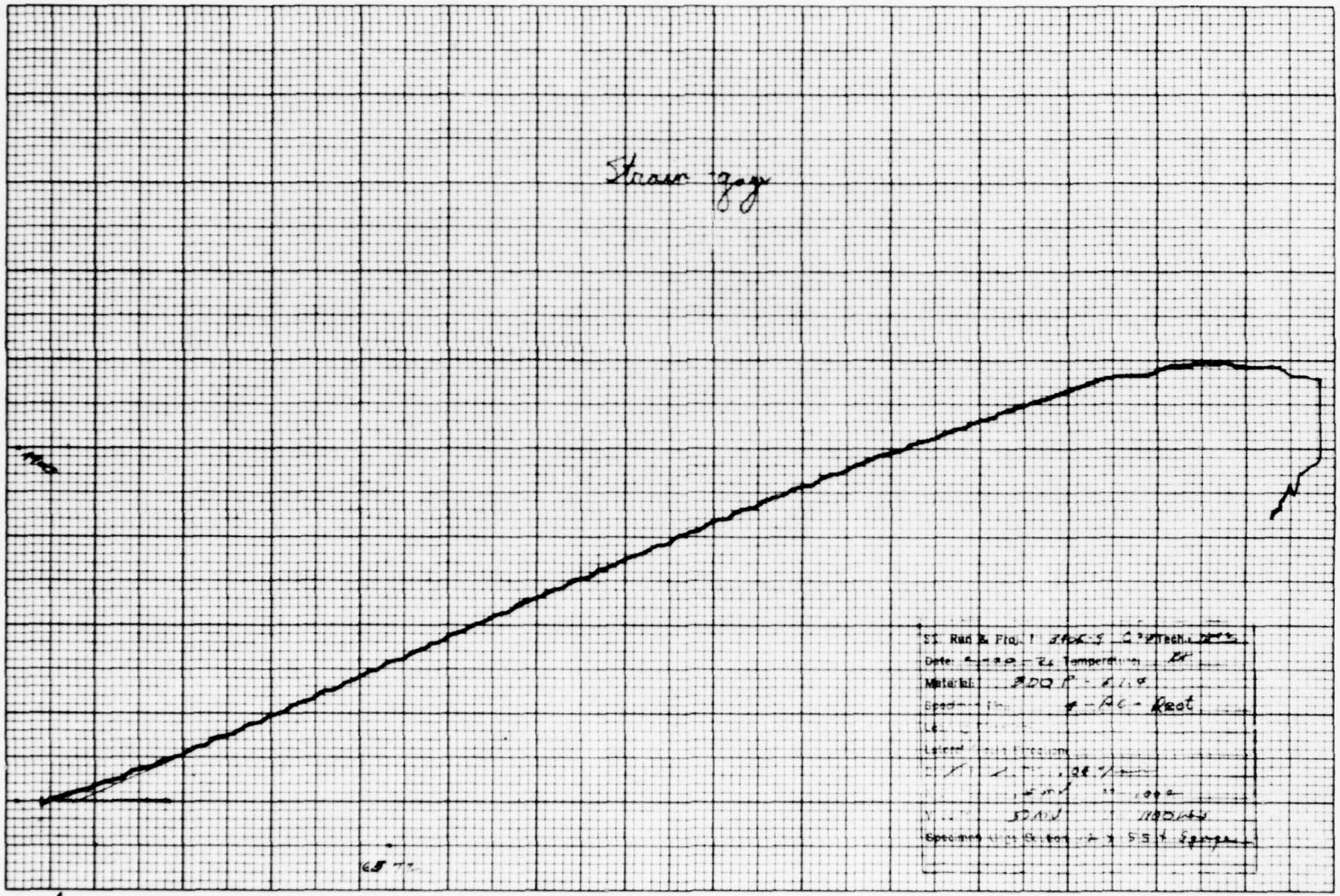

Figure A16 Test Results for Specimen 4-AC-Heat

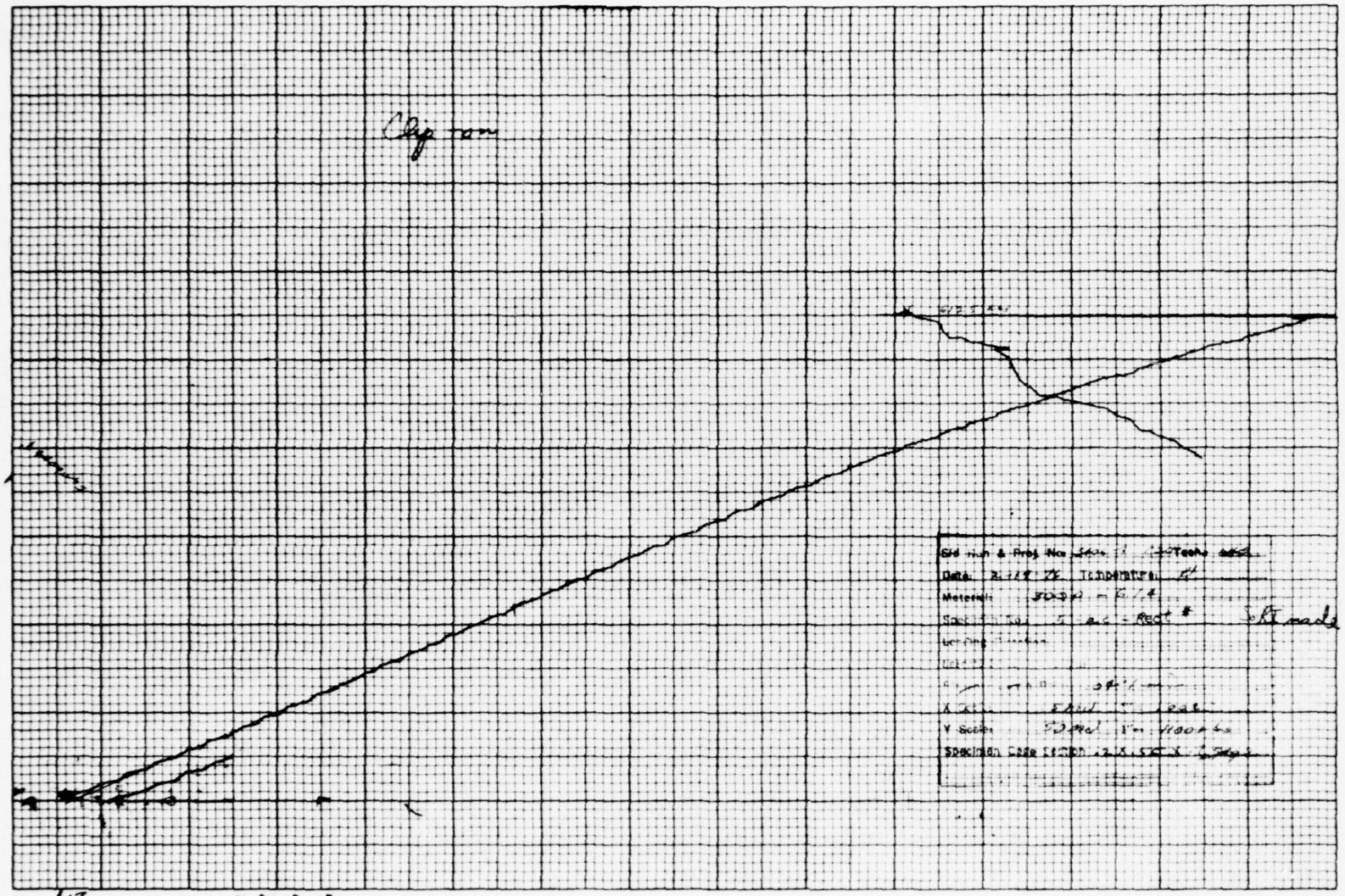

Figure 117. Test Results for Specimen 5-AC-Rest*

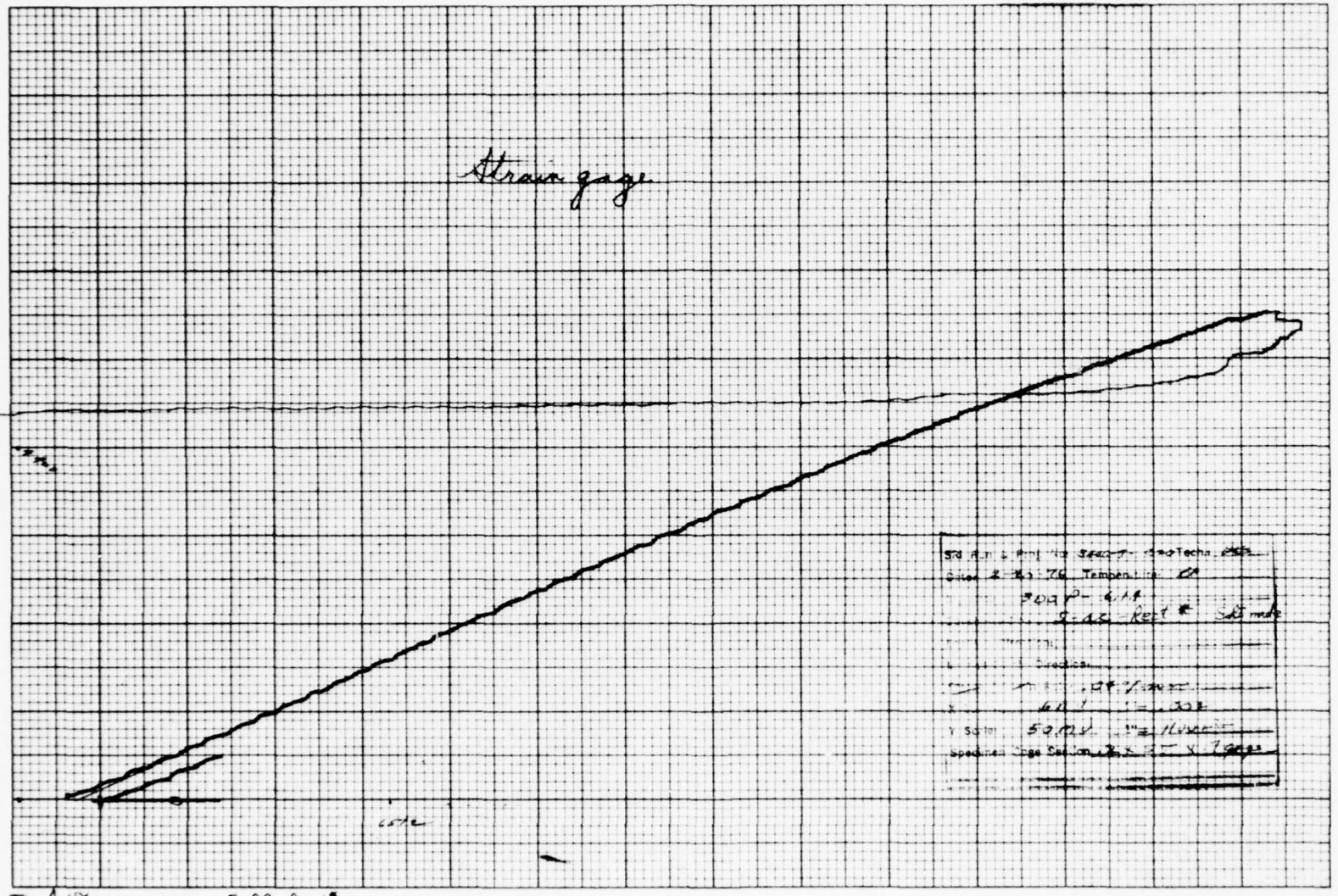

Figure A.18 Test Results for Specimen S-AC-Rect*

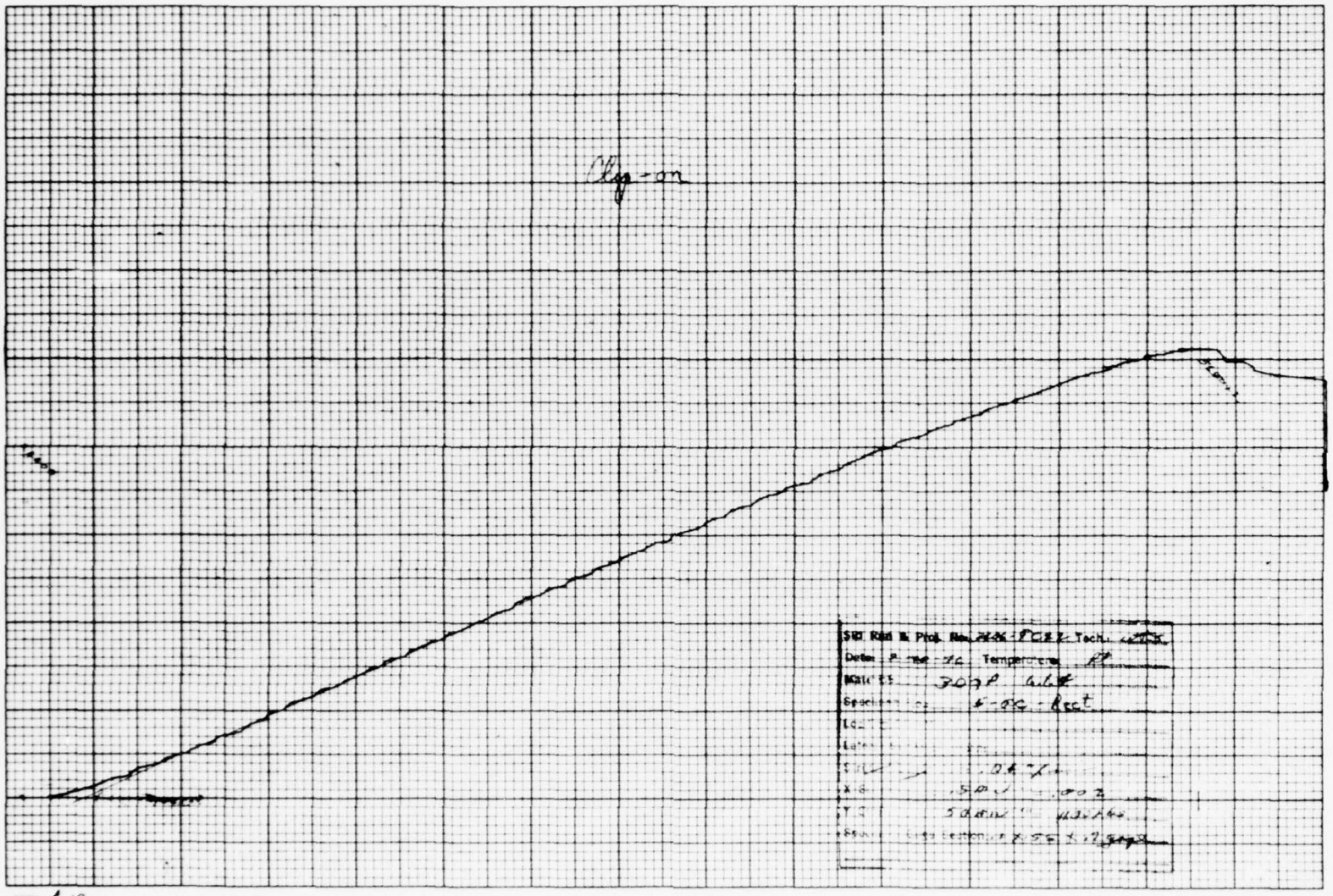

Figure A.19 Test Results for Specimen S-AC-Rect

Figure A20 Test Results for Specimen 5-AC-Rect

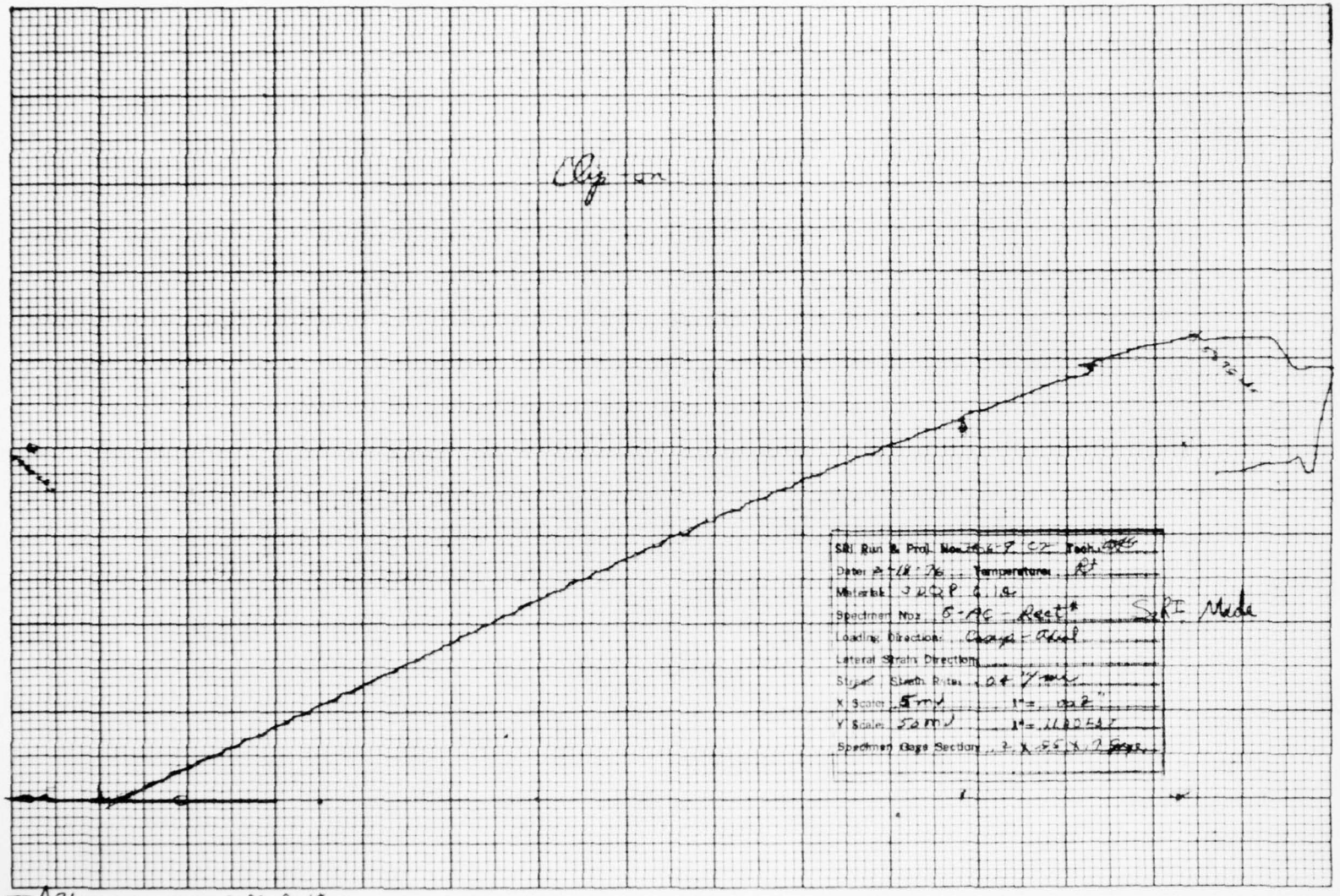

Fig. A21. Test Results for Specimen 6-AC-Rect*

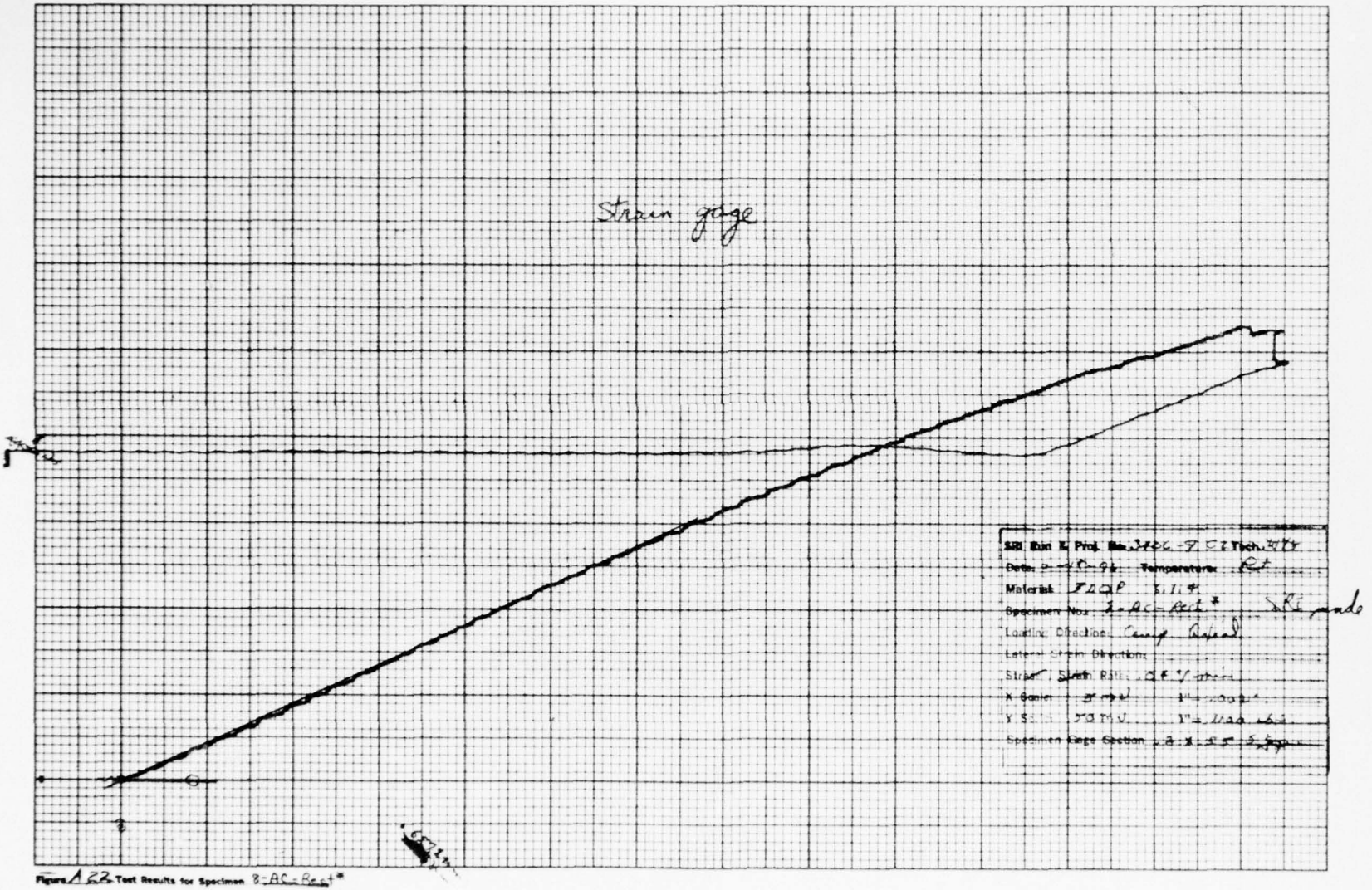

Figure A.22 Test Results for Specimen 8-AC-Rect*

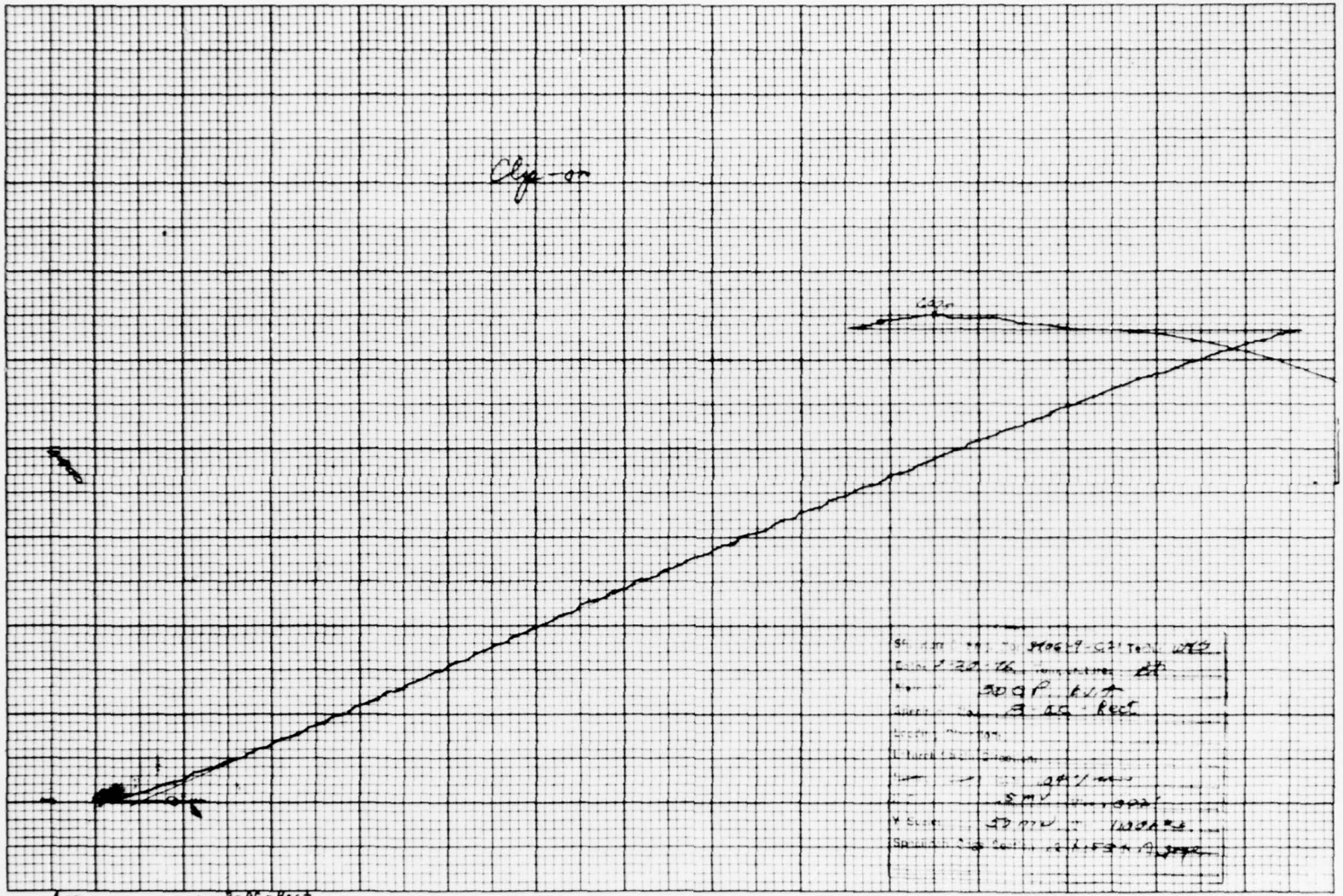

Figure A23 Test Results for Specimen 8-AL-Rect

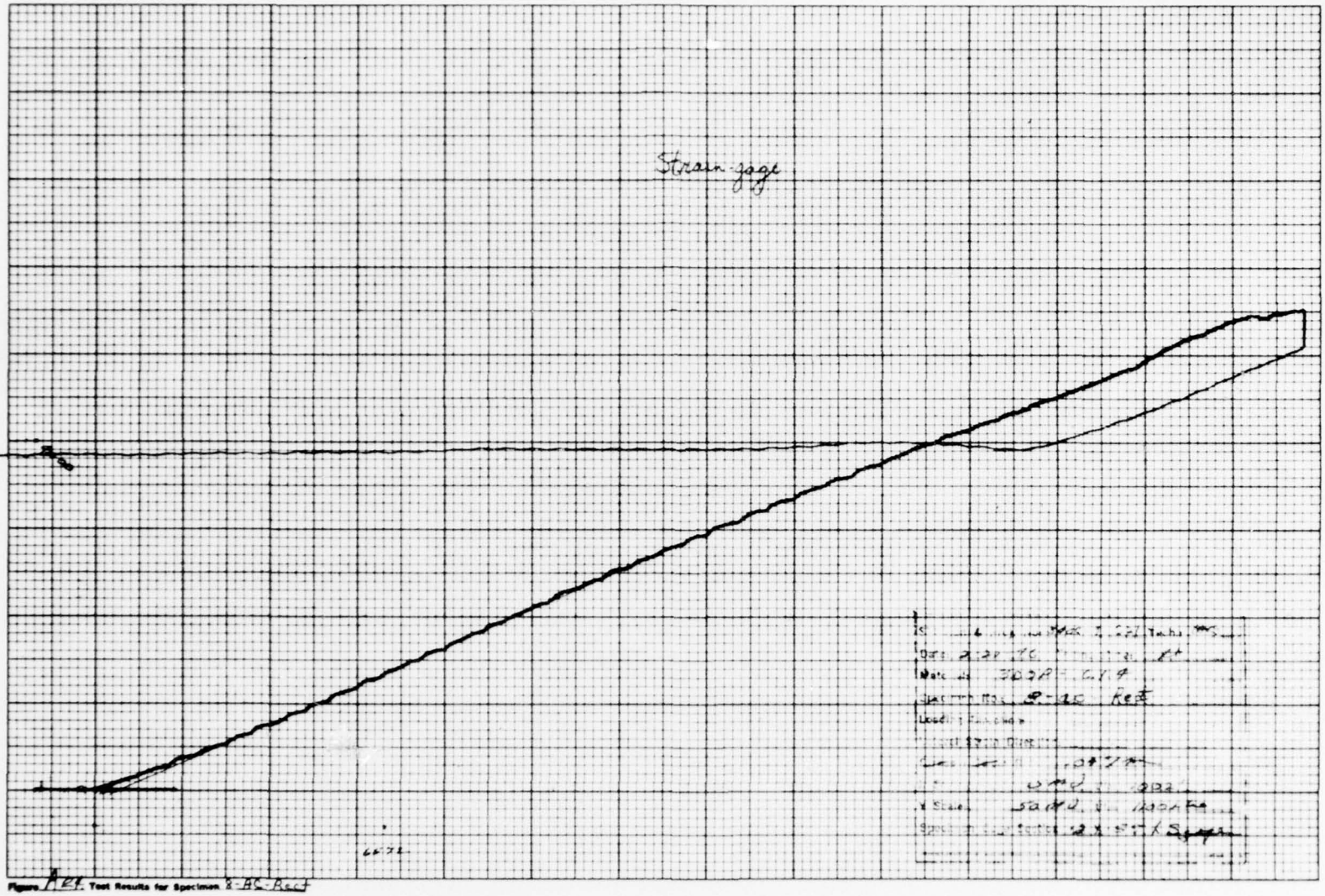

Figure A24. Test Results for Specimen 8-AS-Rect

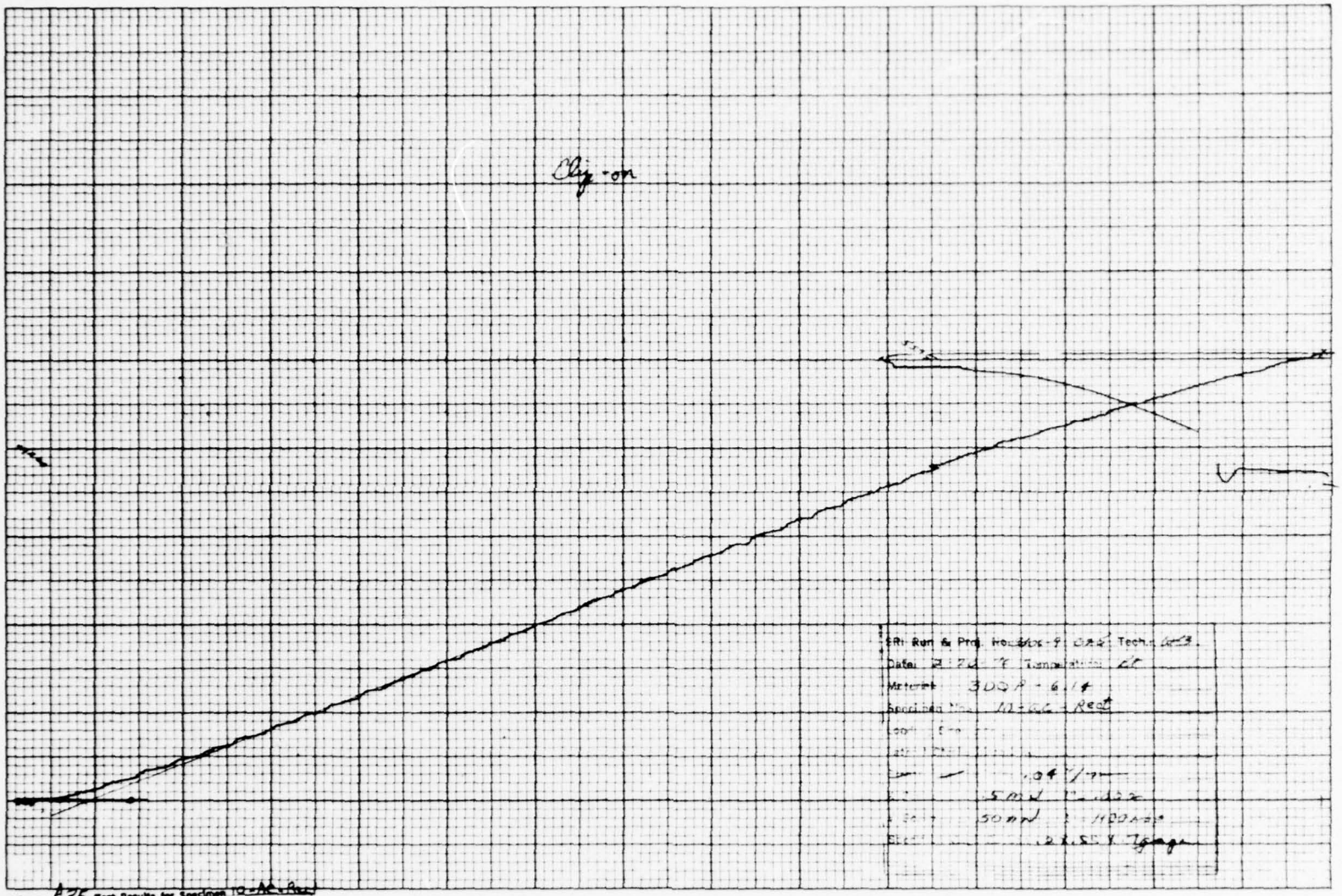

Figure A25 Test Results for Specimen TD-AC-Rect

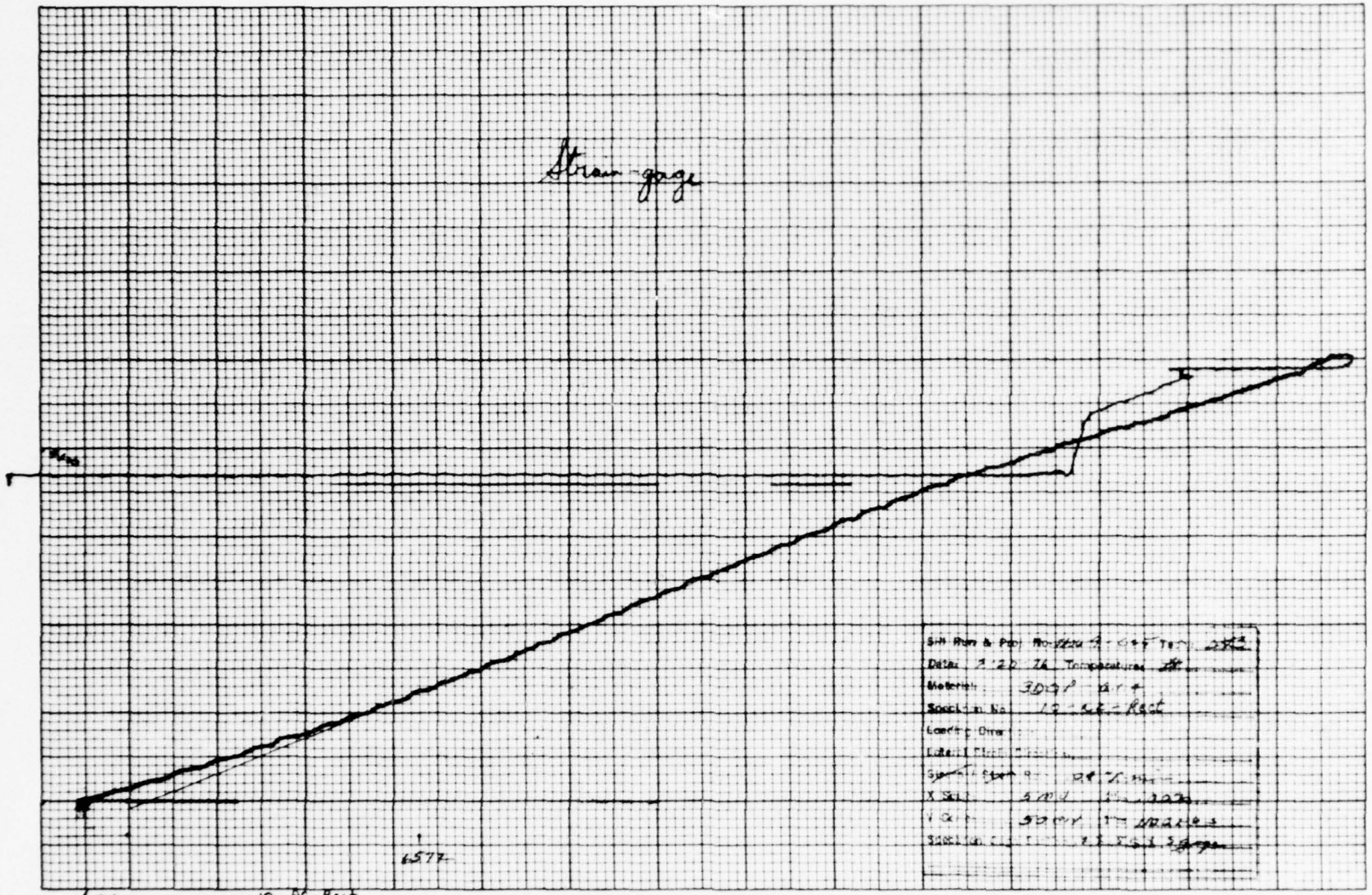

Figure A 26 Test Results for Specimen 10 - RC - Rect

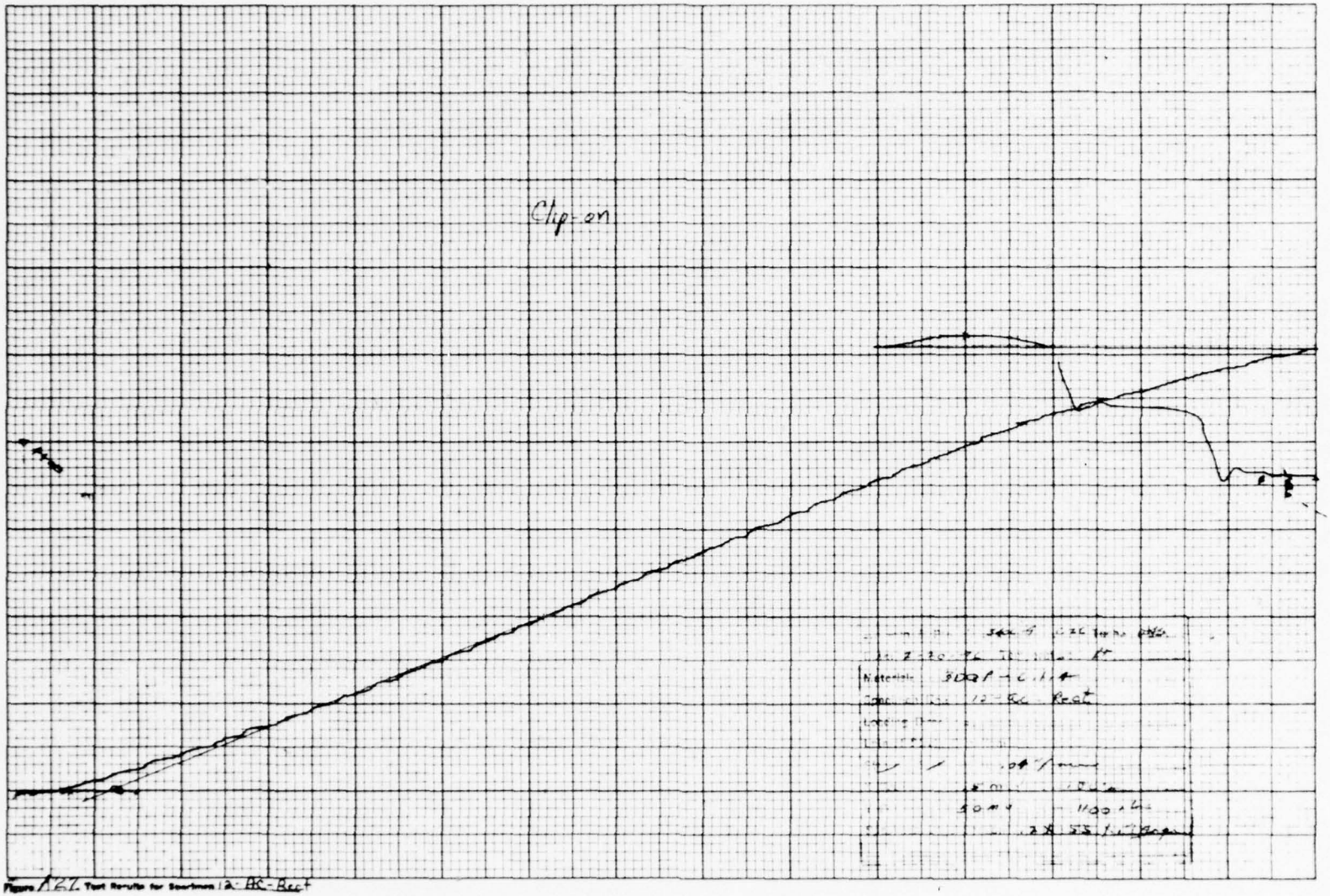

Figure A.6.7. Test Results for Specimen 12: AC-Bent

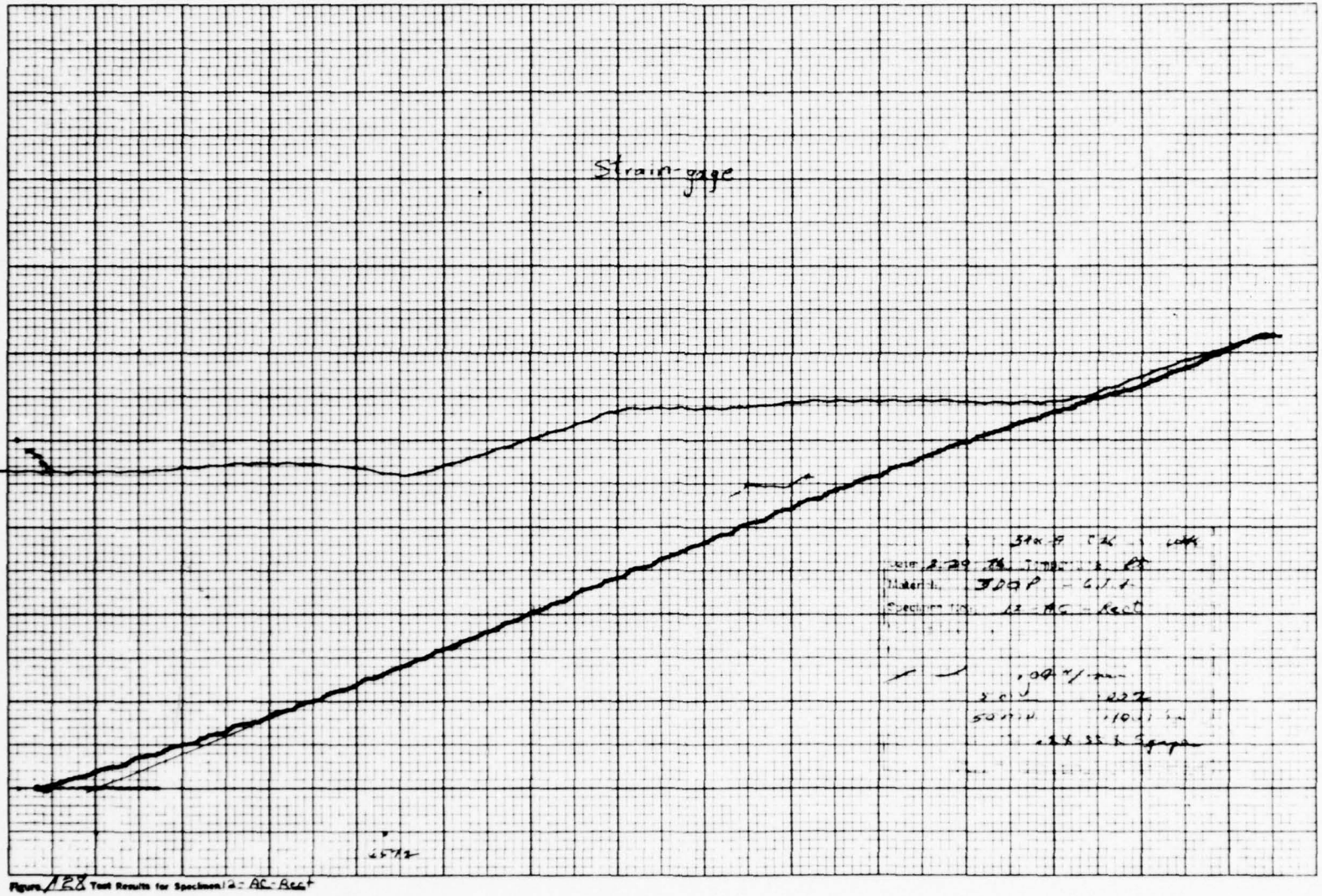

Figure A2.8 Test Results for Specimen 12 - AC - Rect

A3

Axial Compressive Tests
Rectangular Specimen Configuration

4.1.18

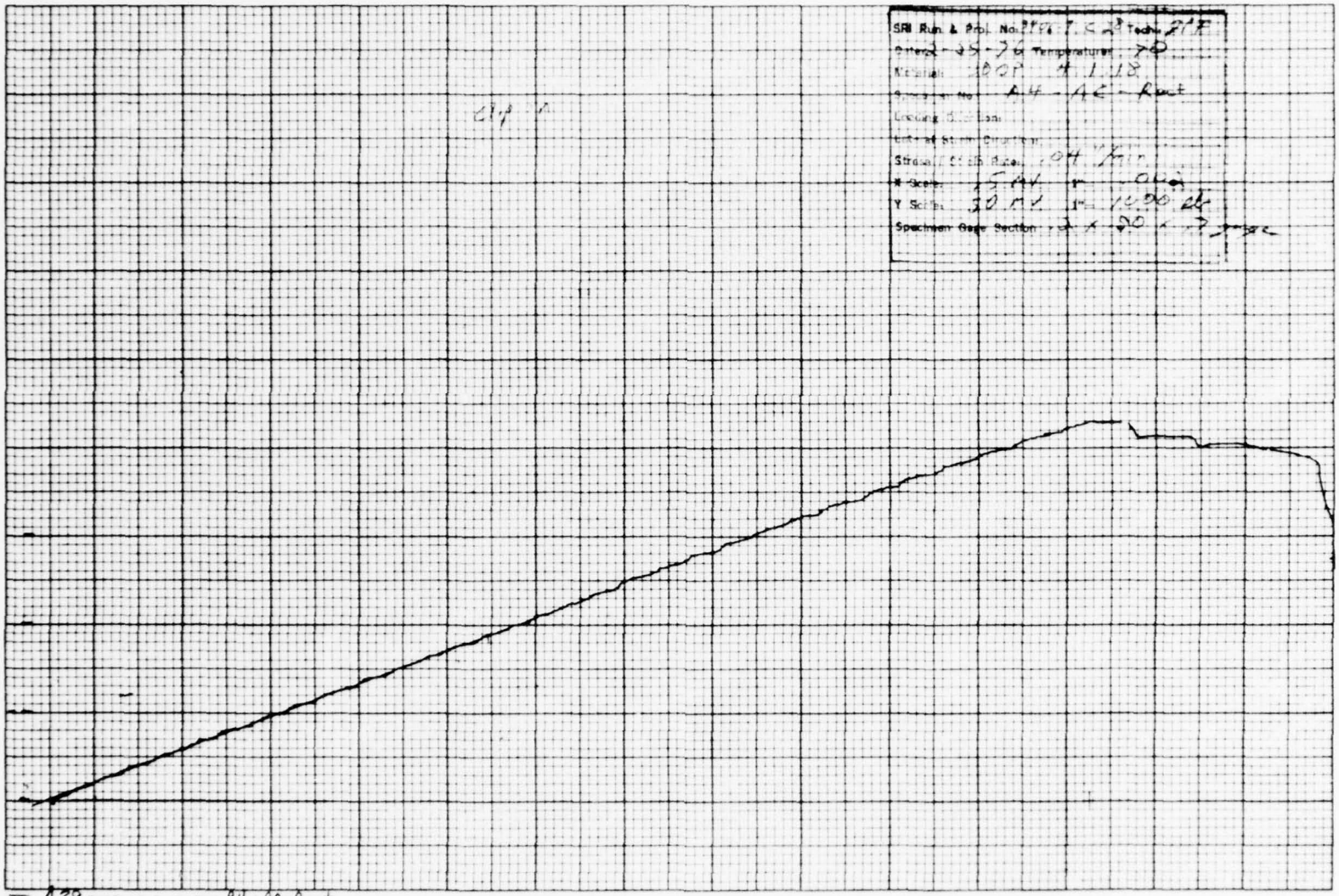

Figure A29 Test Results for Specimen A4-AC-Bect

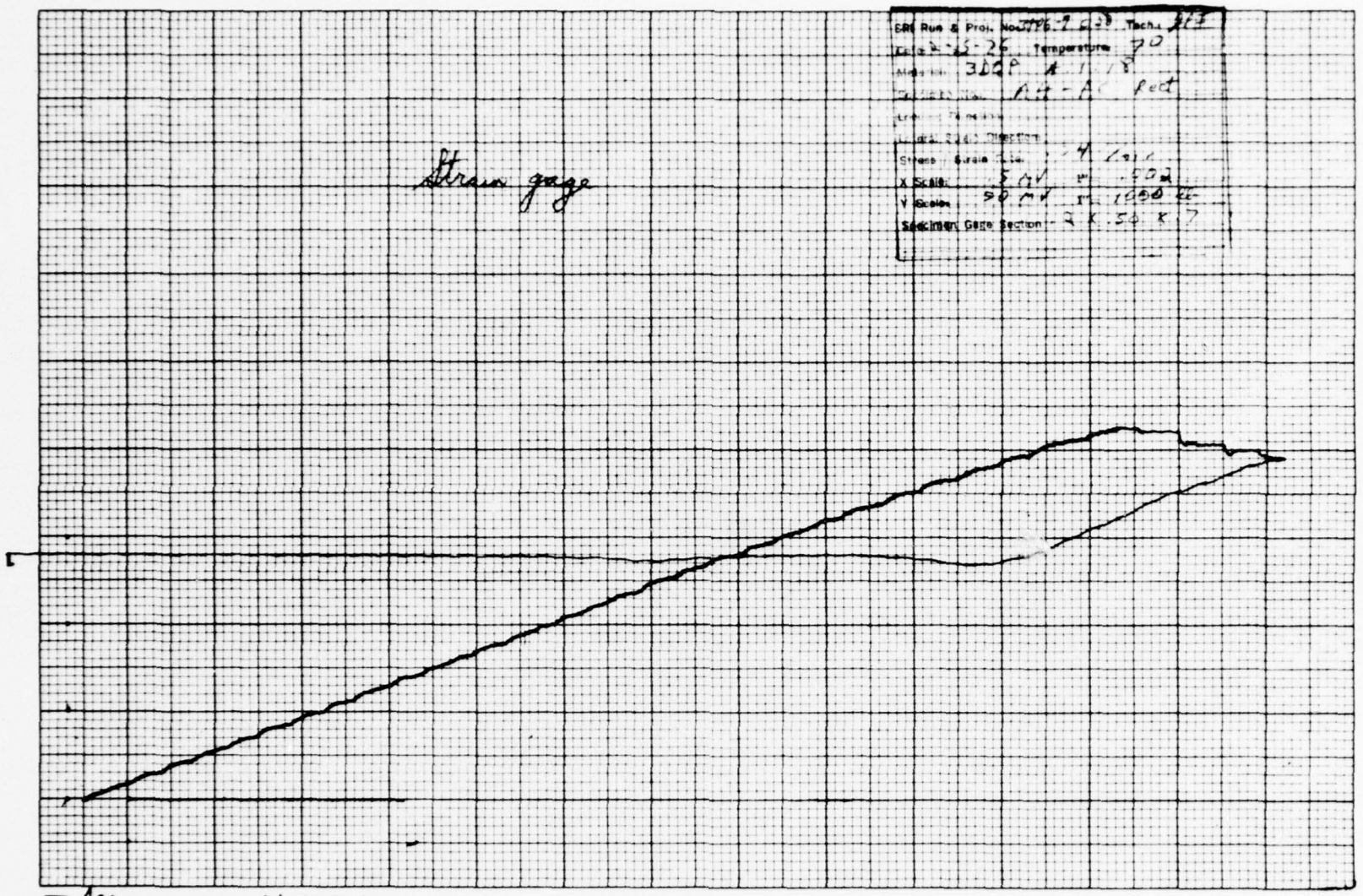

Figure A30 Test Results for Specimen A4-AC-Rect

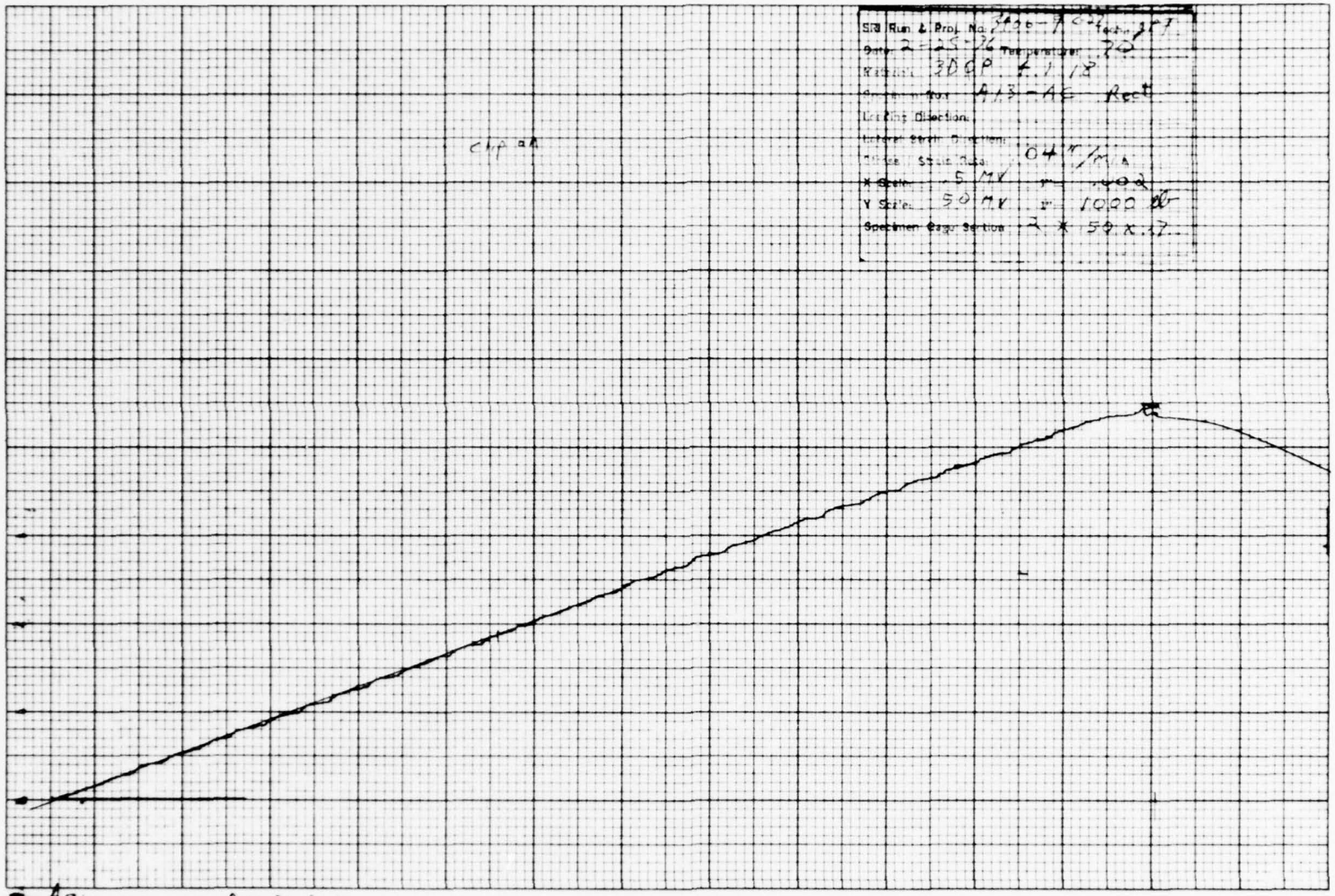

Figure A31. Test Results for Specimen A13-AC-Rect

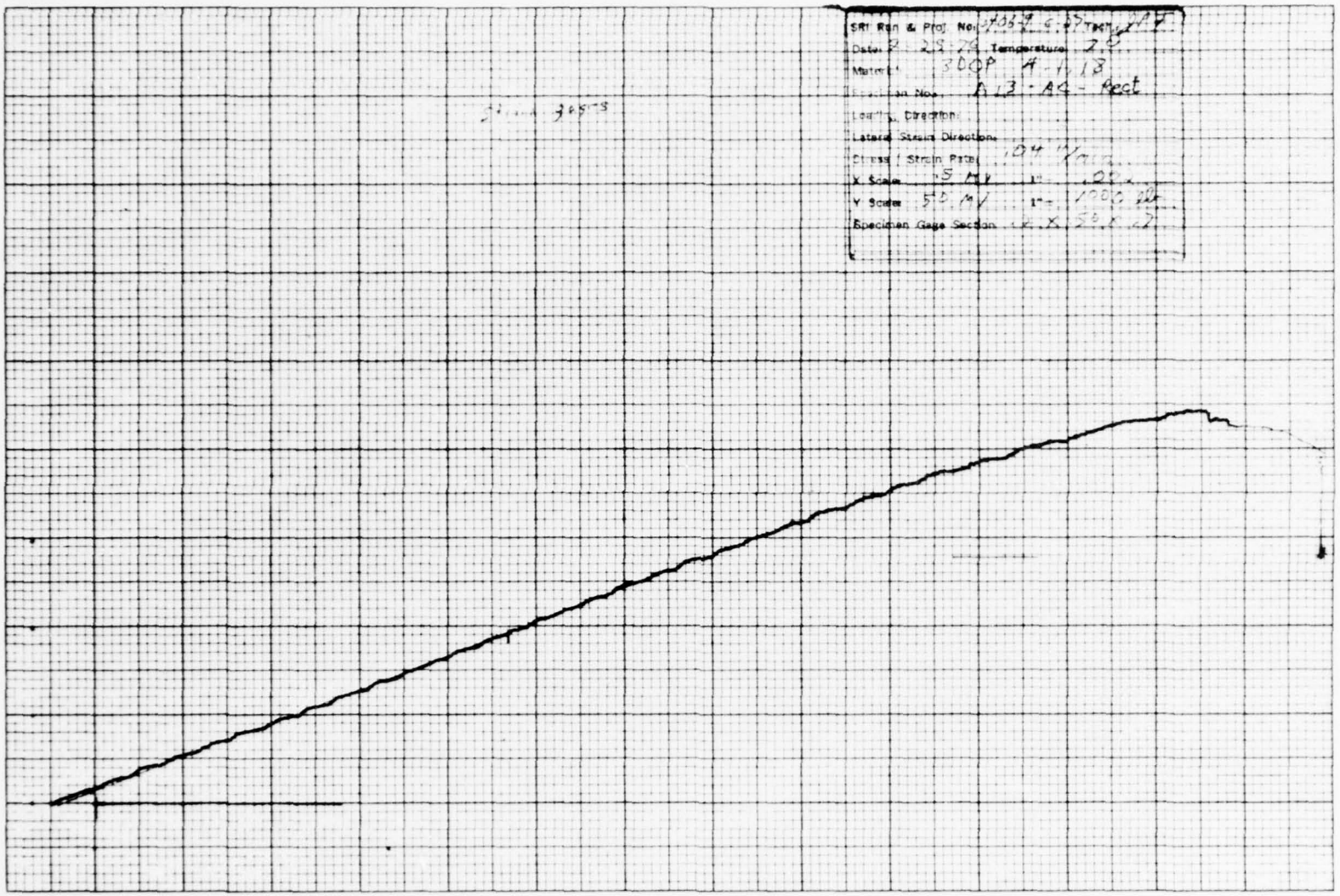

Figure A.32 Test Results for Specimen A13-A5-Rect

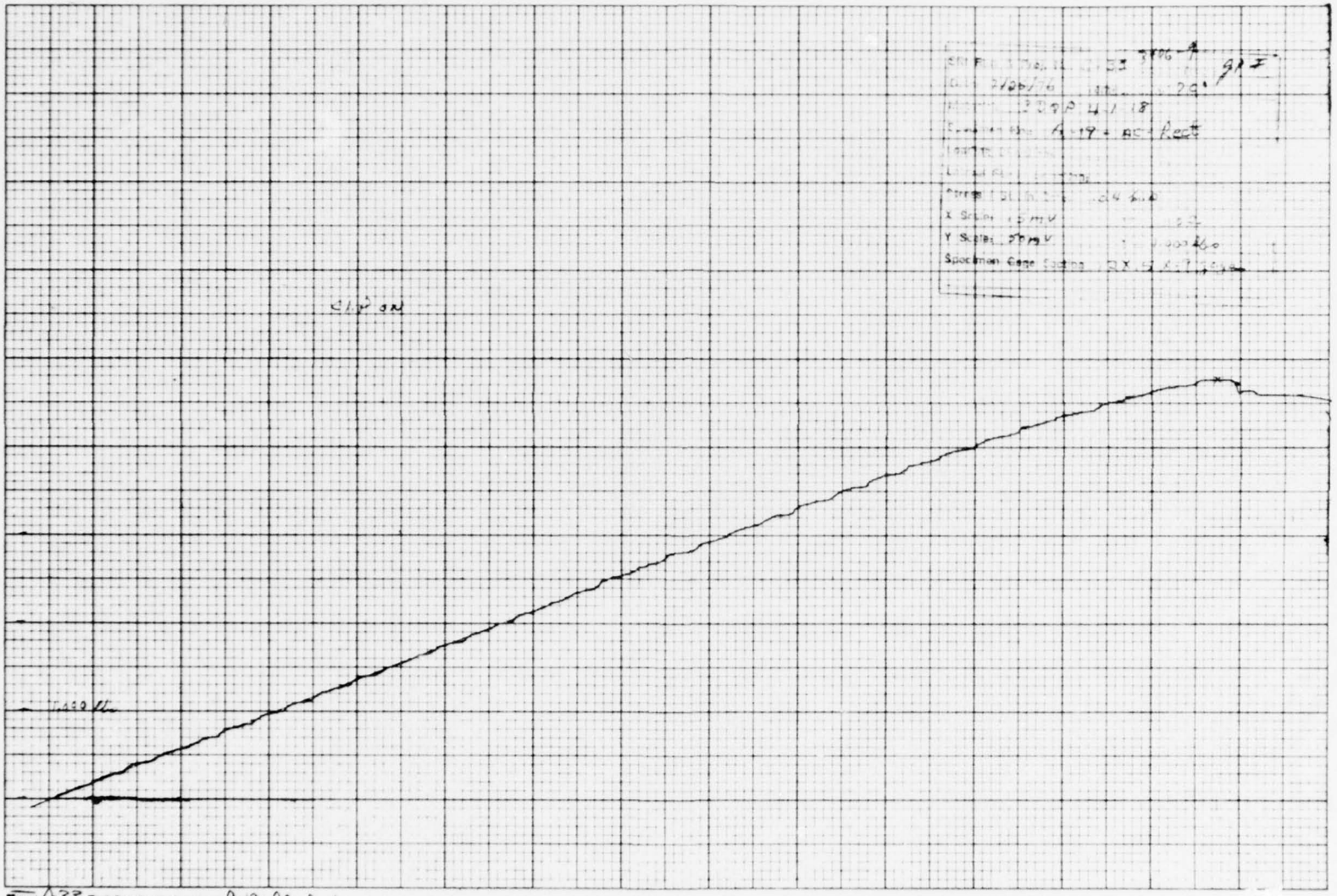

Figure A.33 Test Results for Specimen A-19-AG-Rect

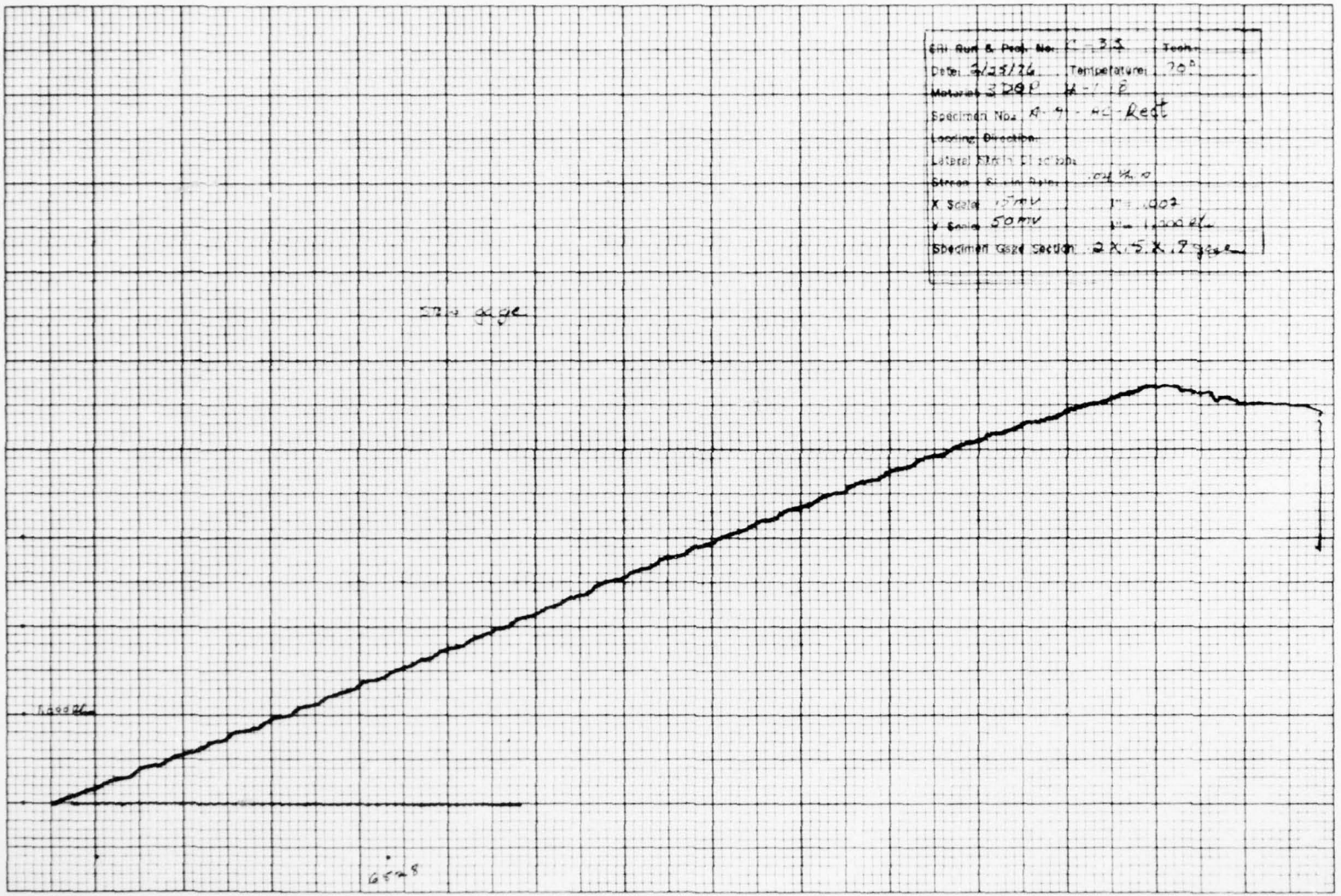

Figure A34 Test Results for Specimen A-19-AC-Rect

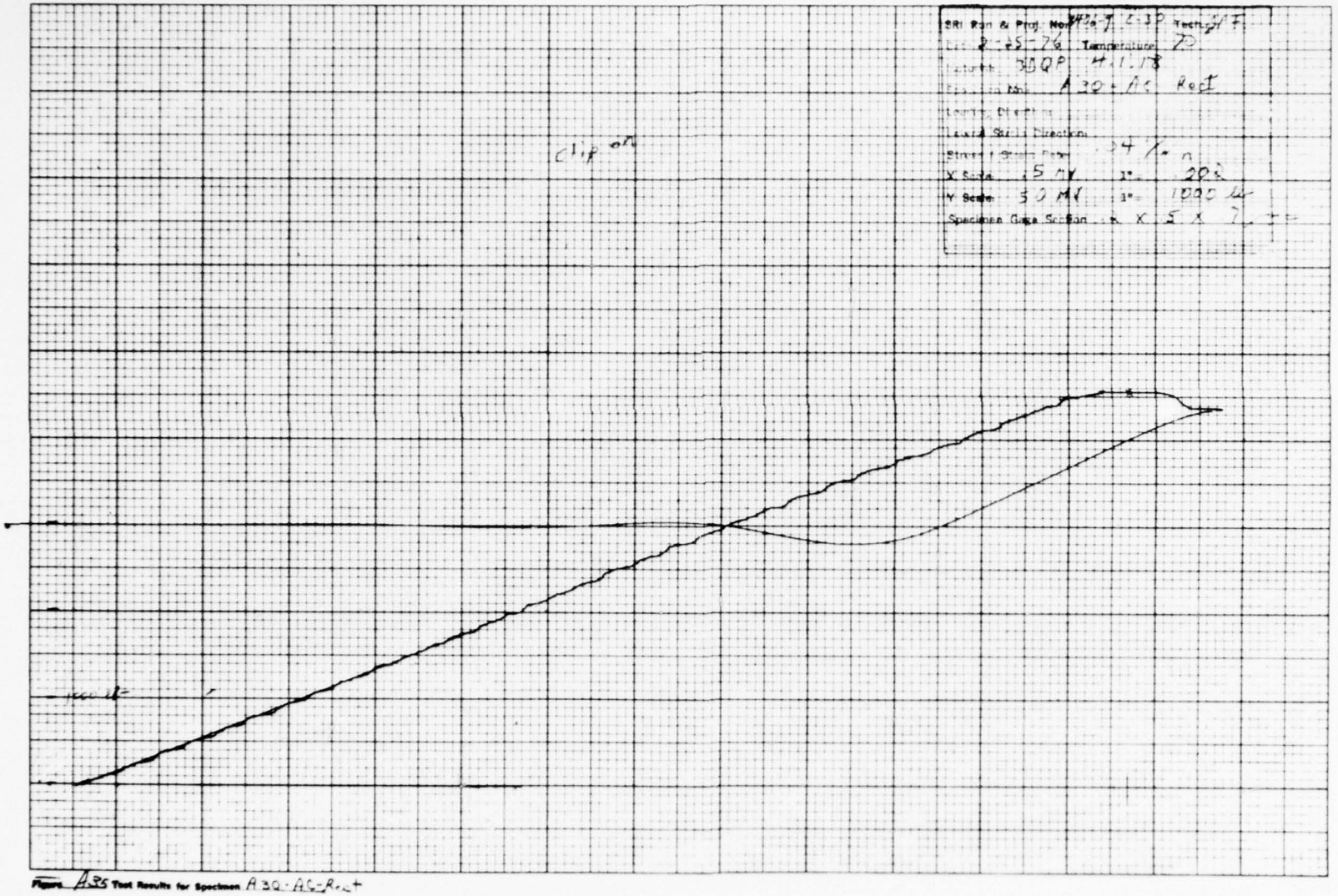

Figure A35 Test Results for Specimen A30-AC-Rect

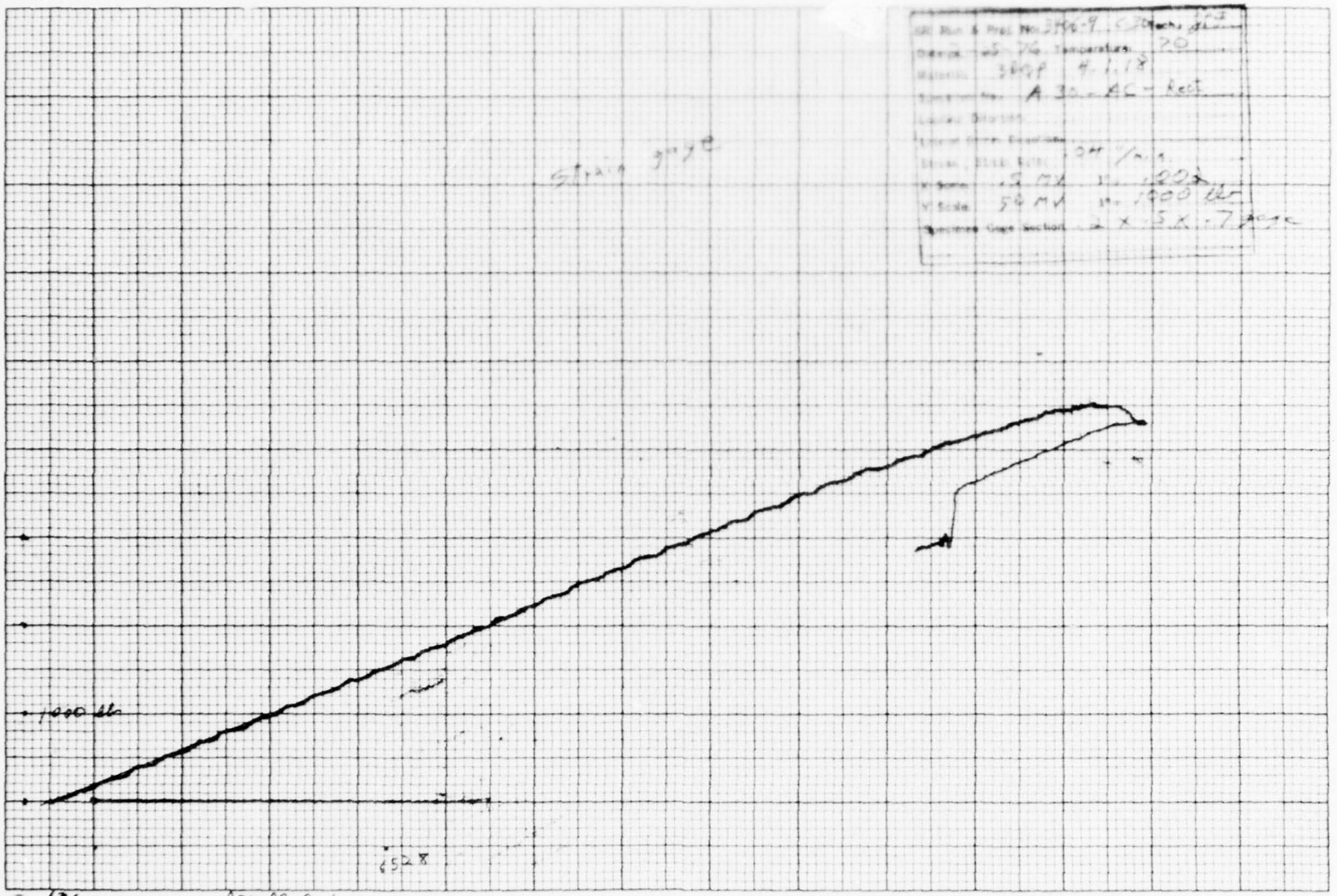

Figure A-36. Test Results for Specimen A30-AC-Rect

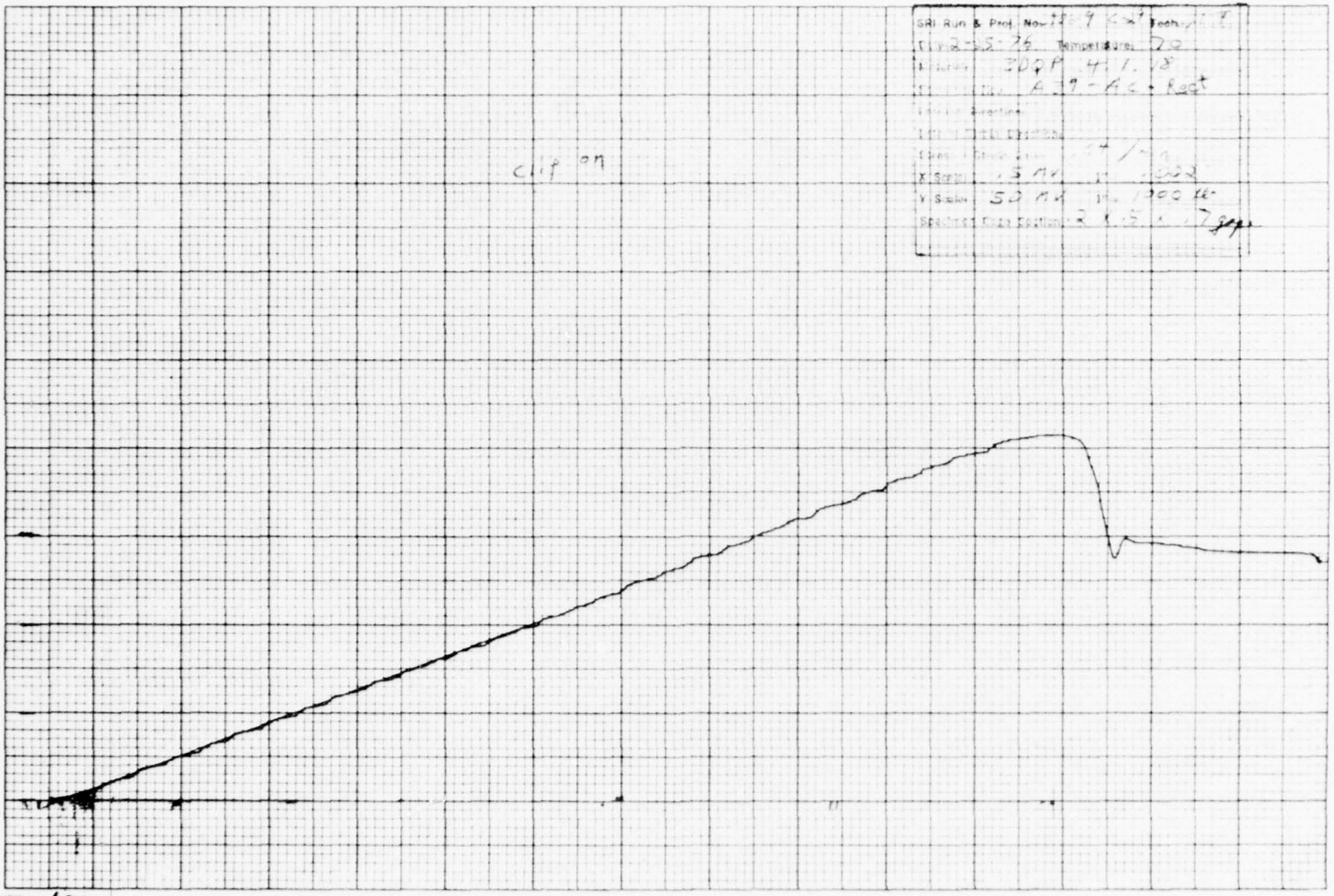

Figure A.37 Test Results for Specimen A.39-AC-Rect

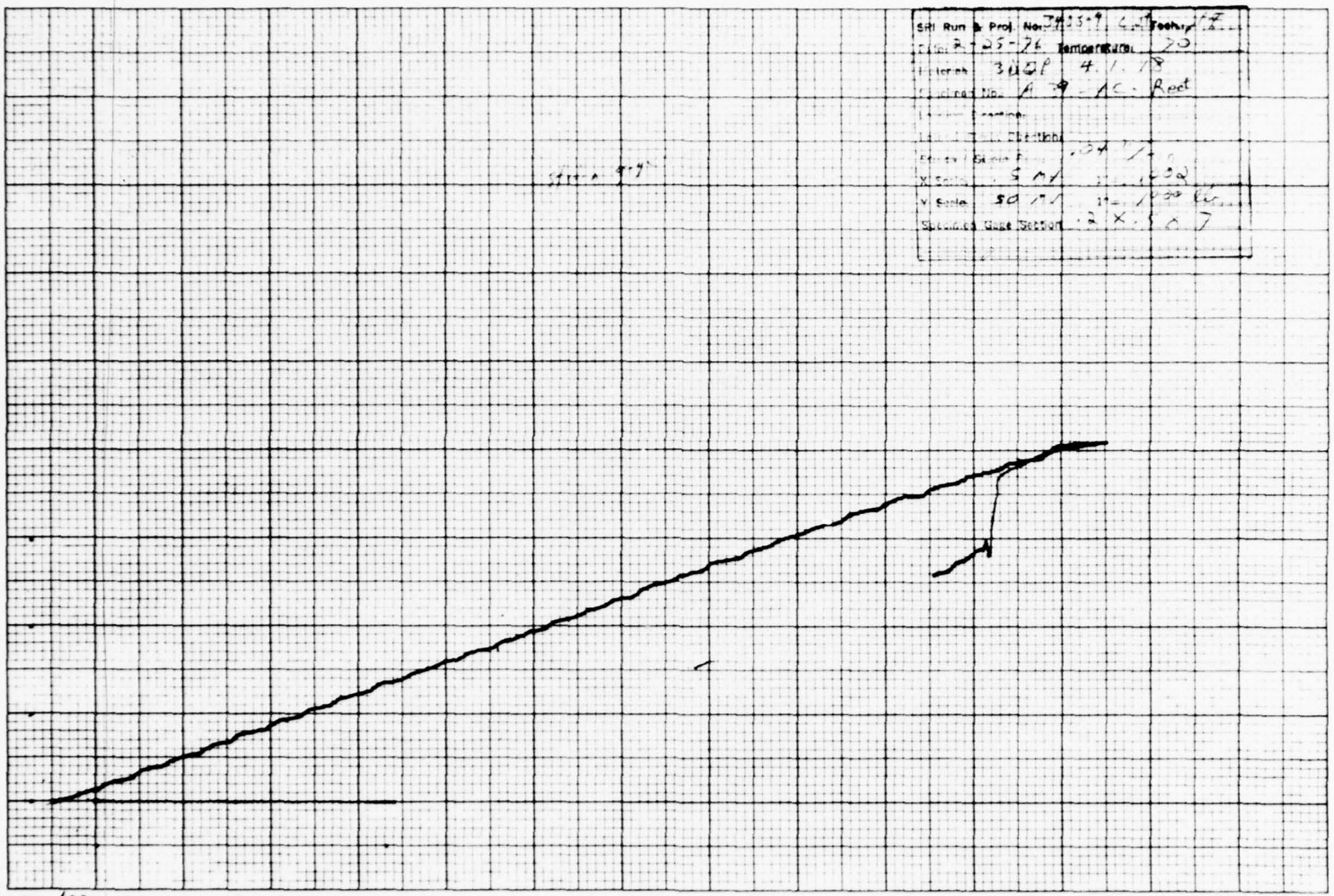

Figure A38. Test Results for Specimen A39-AC-Rect

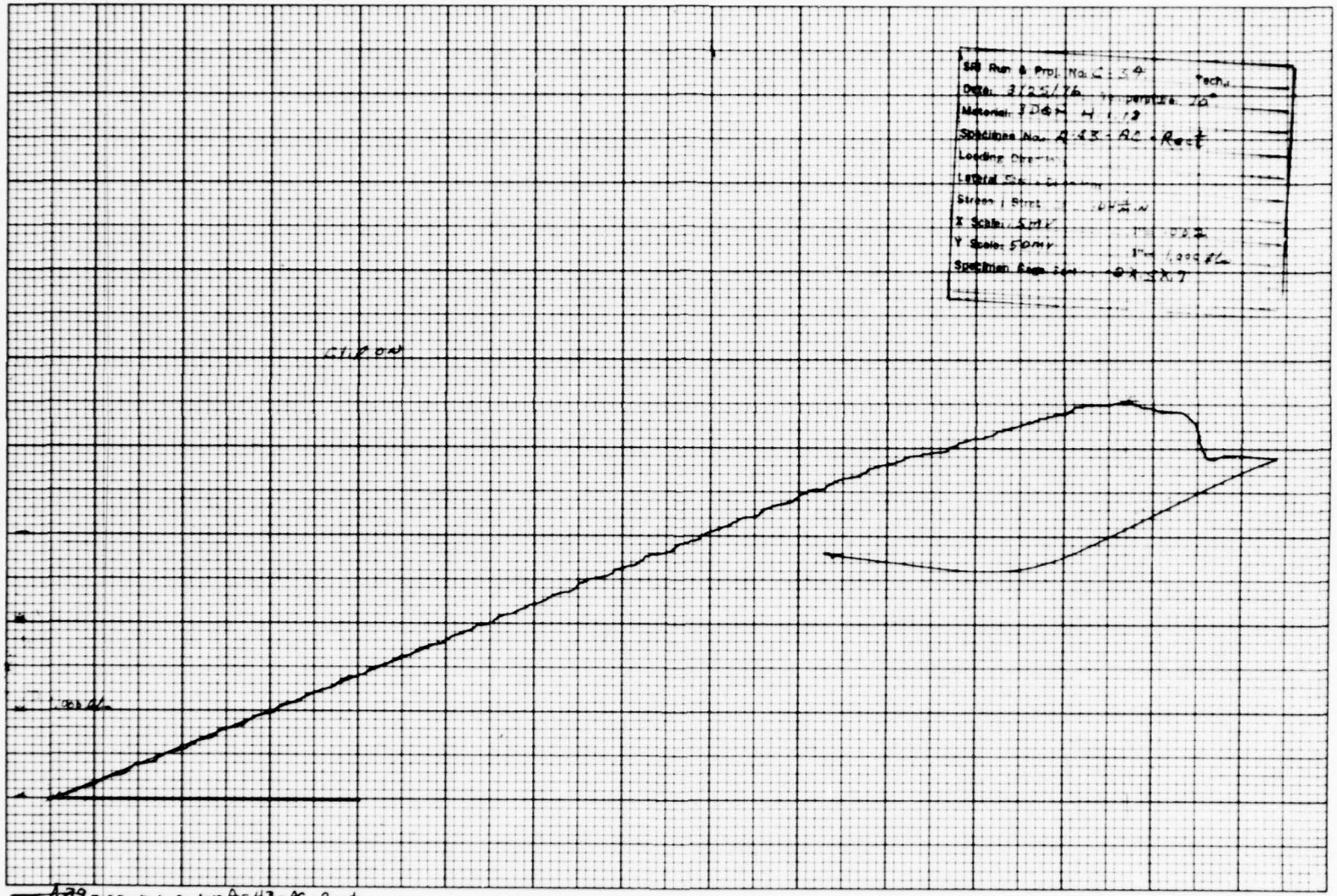

Figure A-39 Test Results for Specimen A-43-AC-Rect

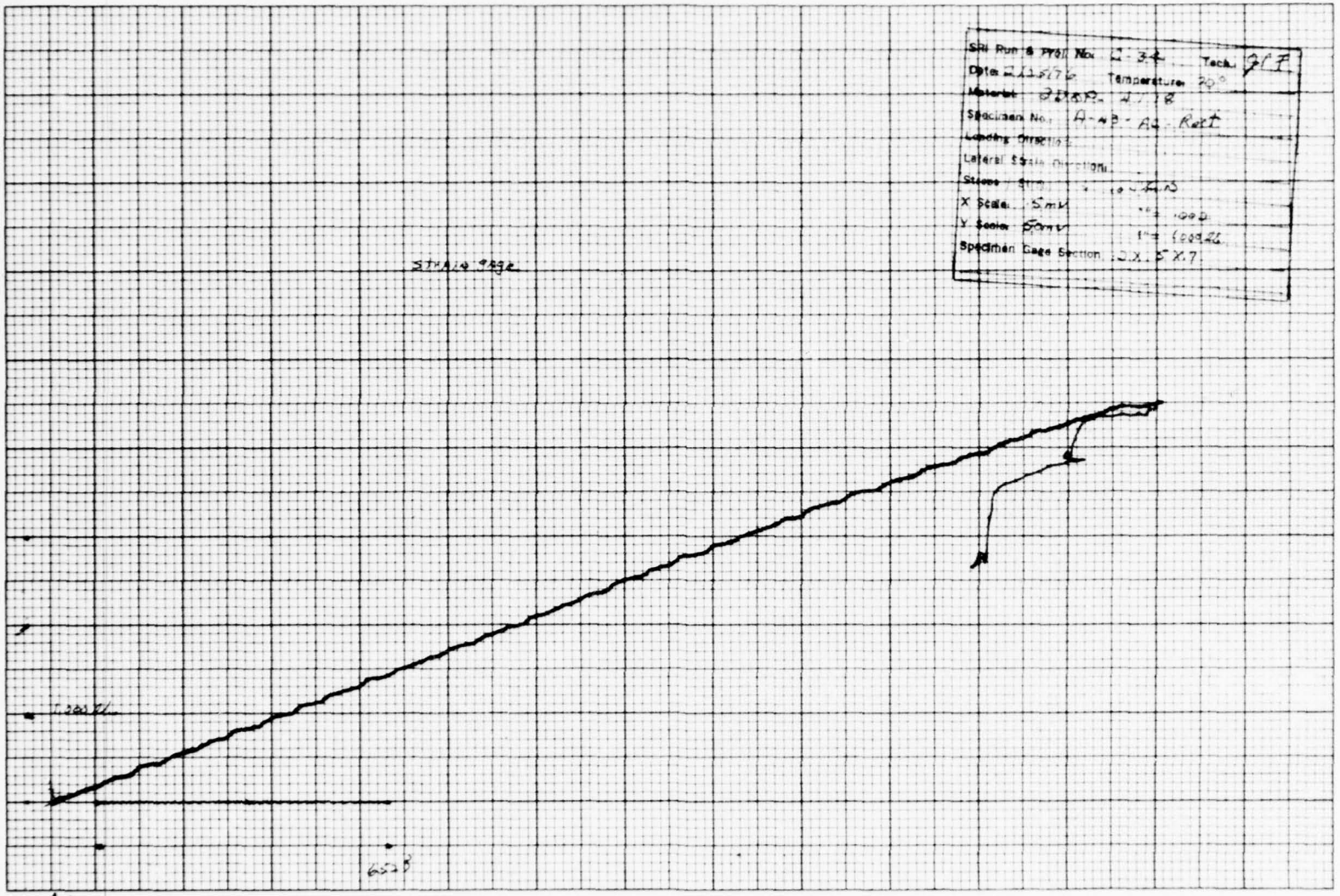

Fig. A90. Test results for specimen A-43-AC-Rect

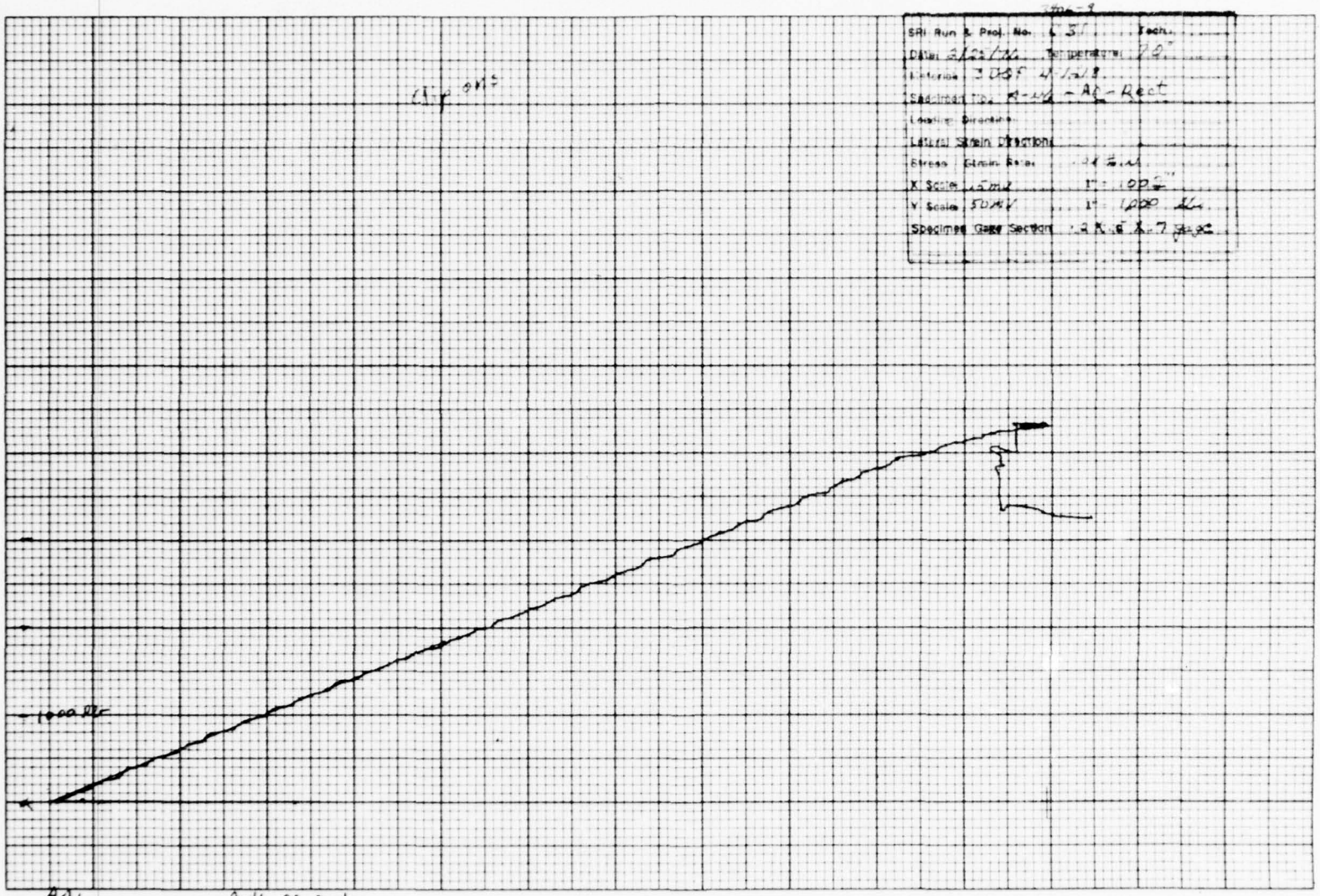

Figure A-46 Test Results for Specimen A-46-AC-Rect

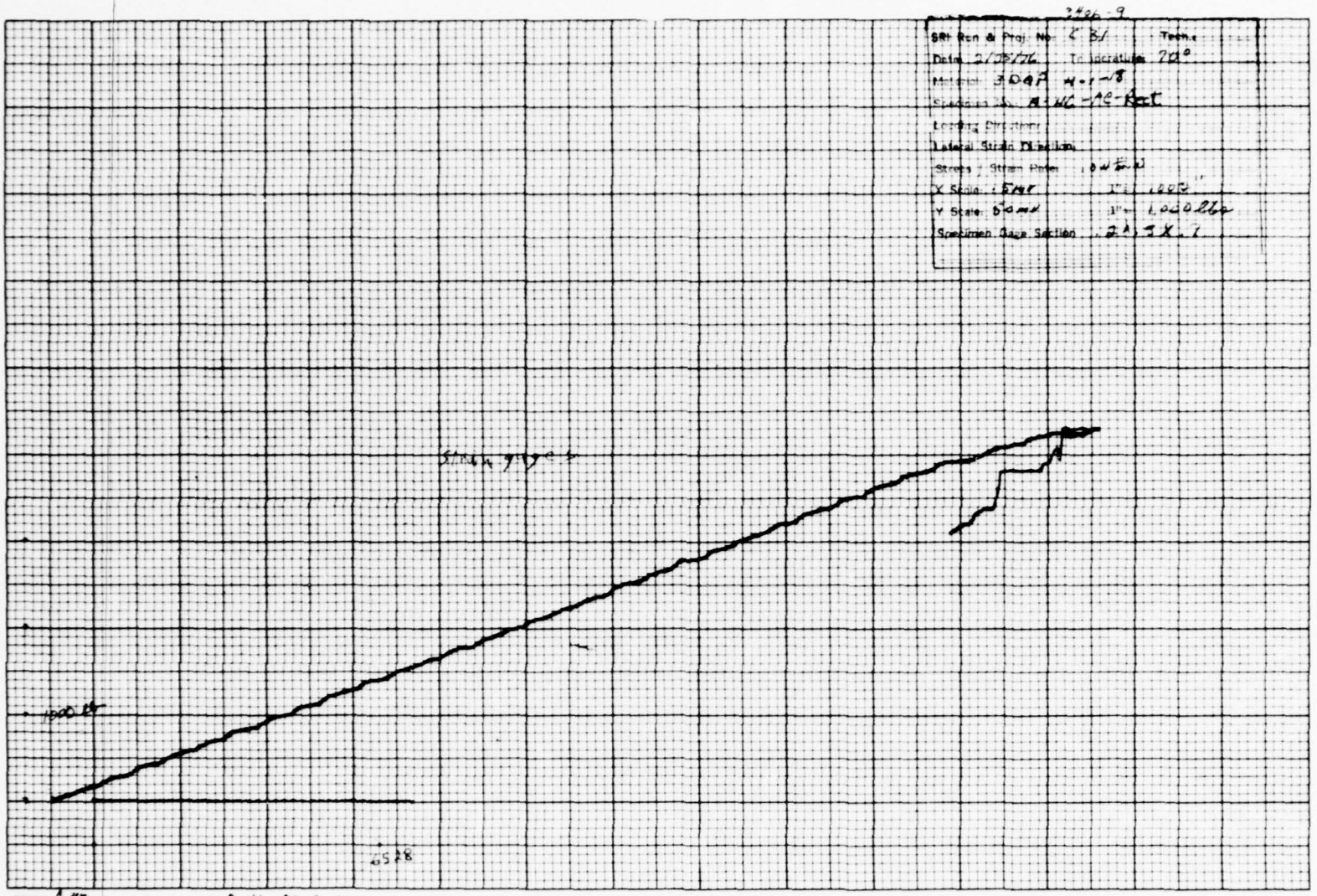

Figure A-47 Test Results for Specimen A-46-AS-Rect

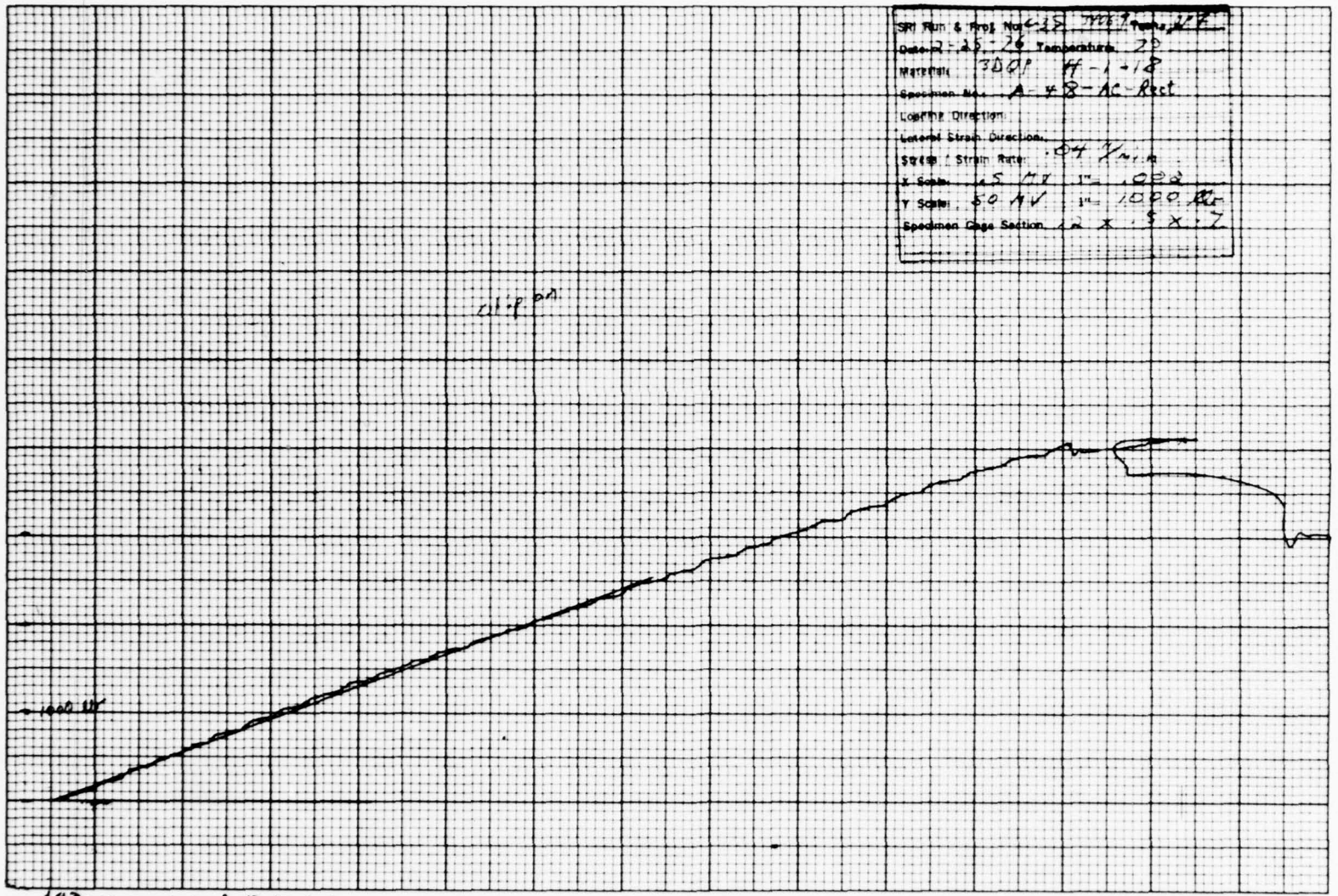

A93 Test Results for Specimen A-48-AC-Rect

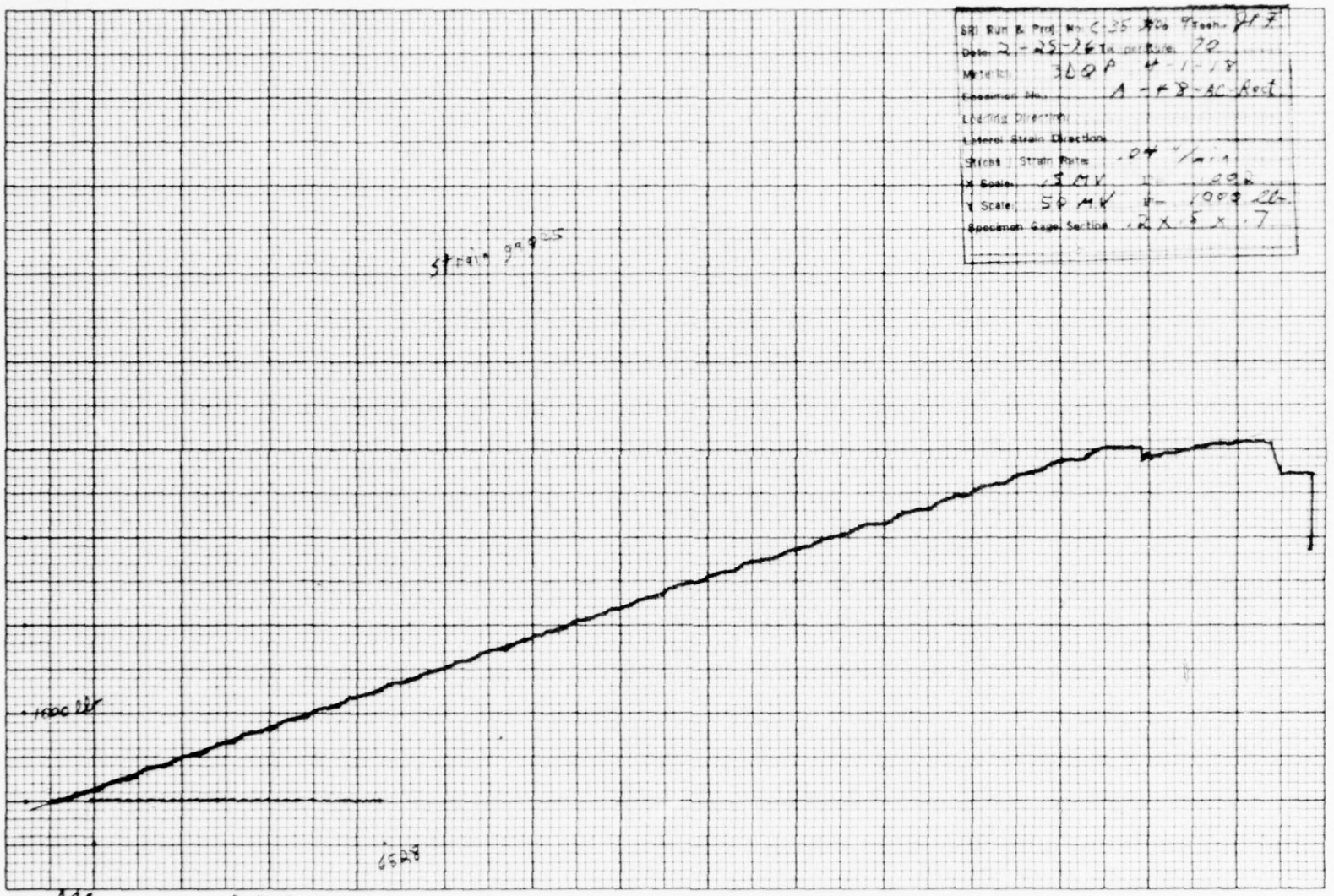

Test Results for Specimen A-48-AC-Rect

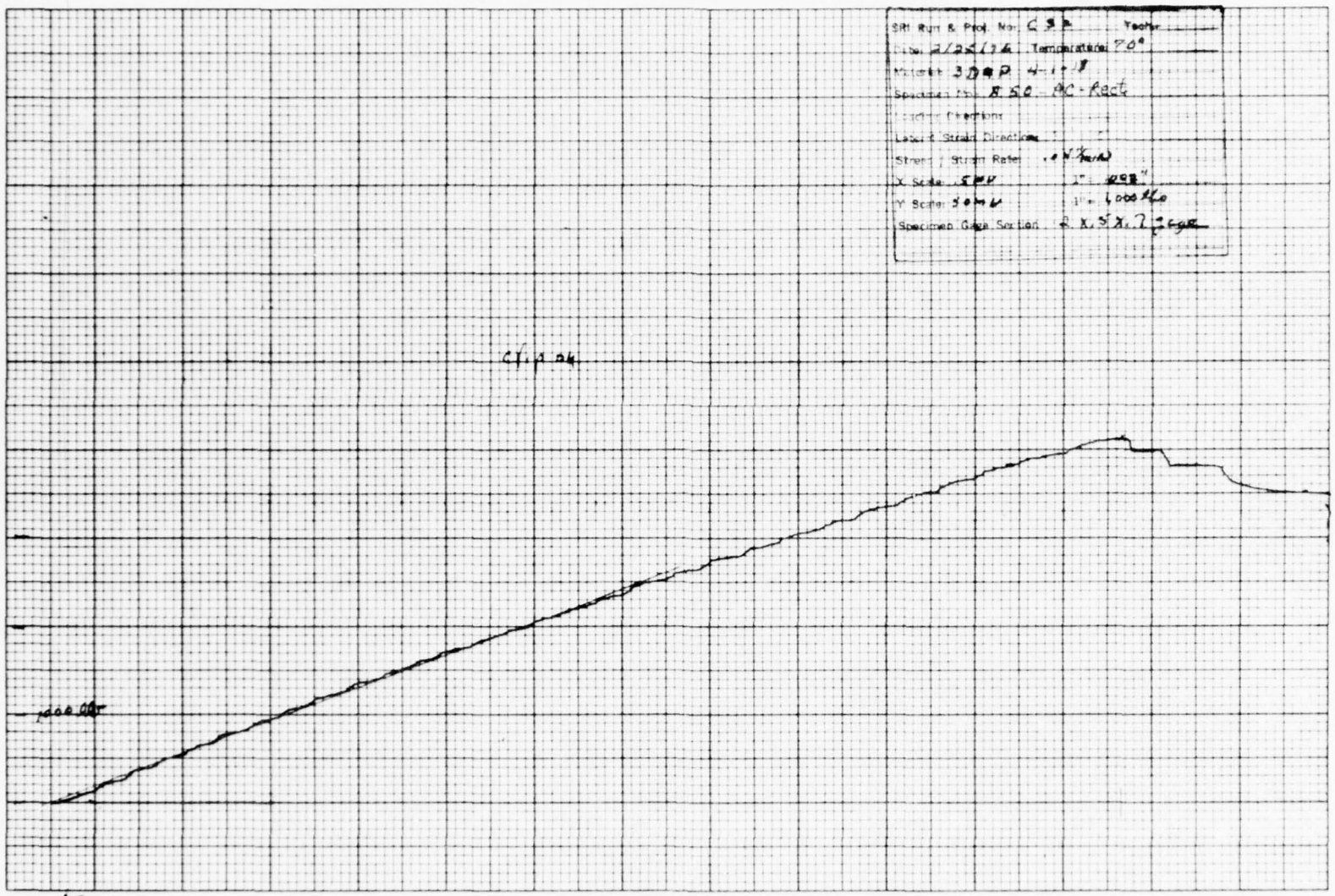

Figure A 95. Test Results for Specimen A 50-AC-Rect

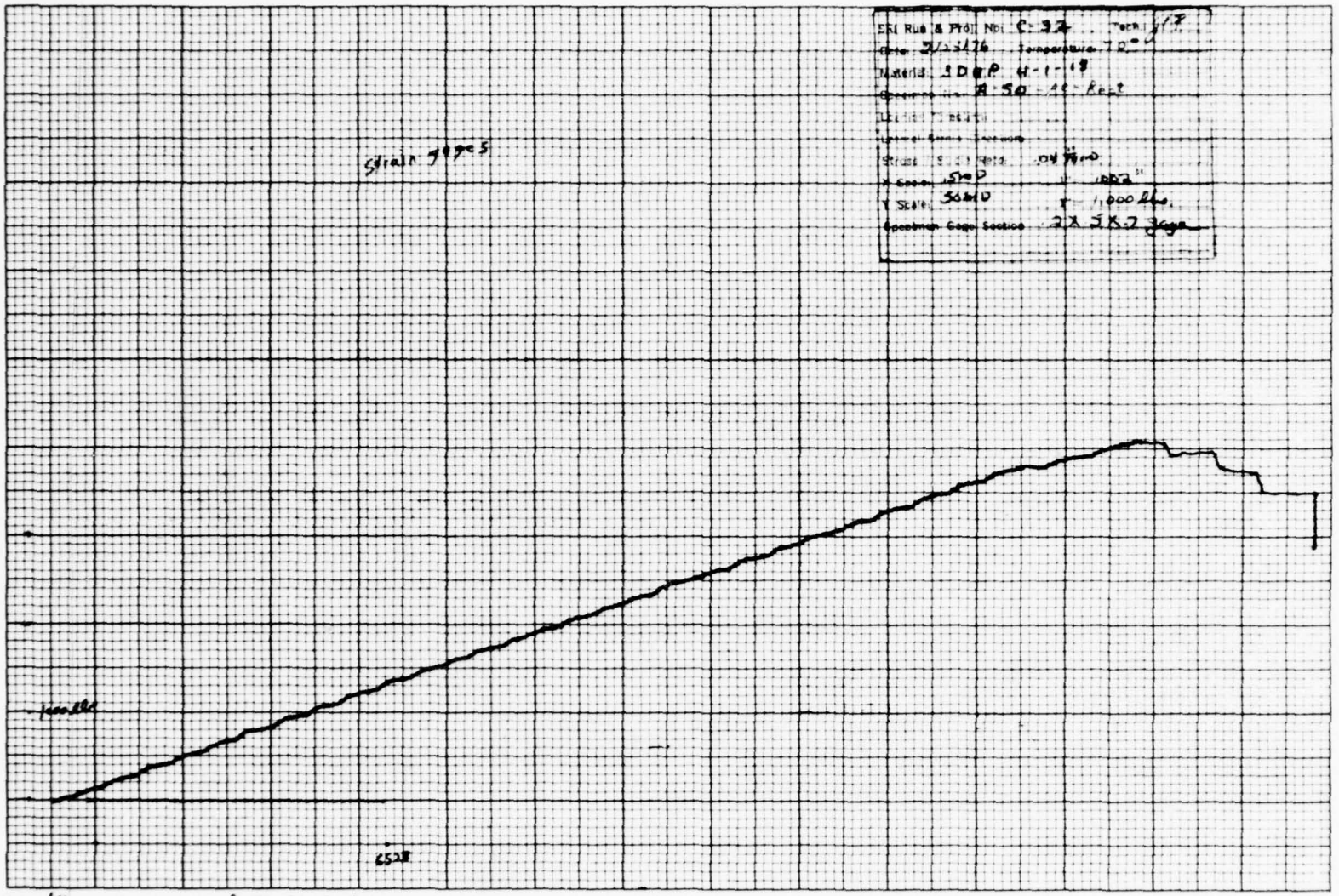

A46. A-50-AC-Rect

A4

Circumferential Compressive Tests
SoRI Specimen Configuration

6.1.4

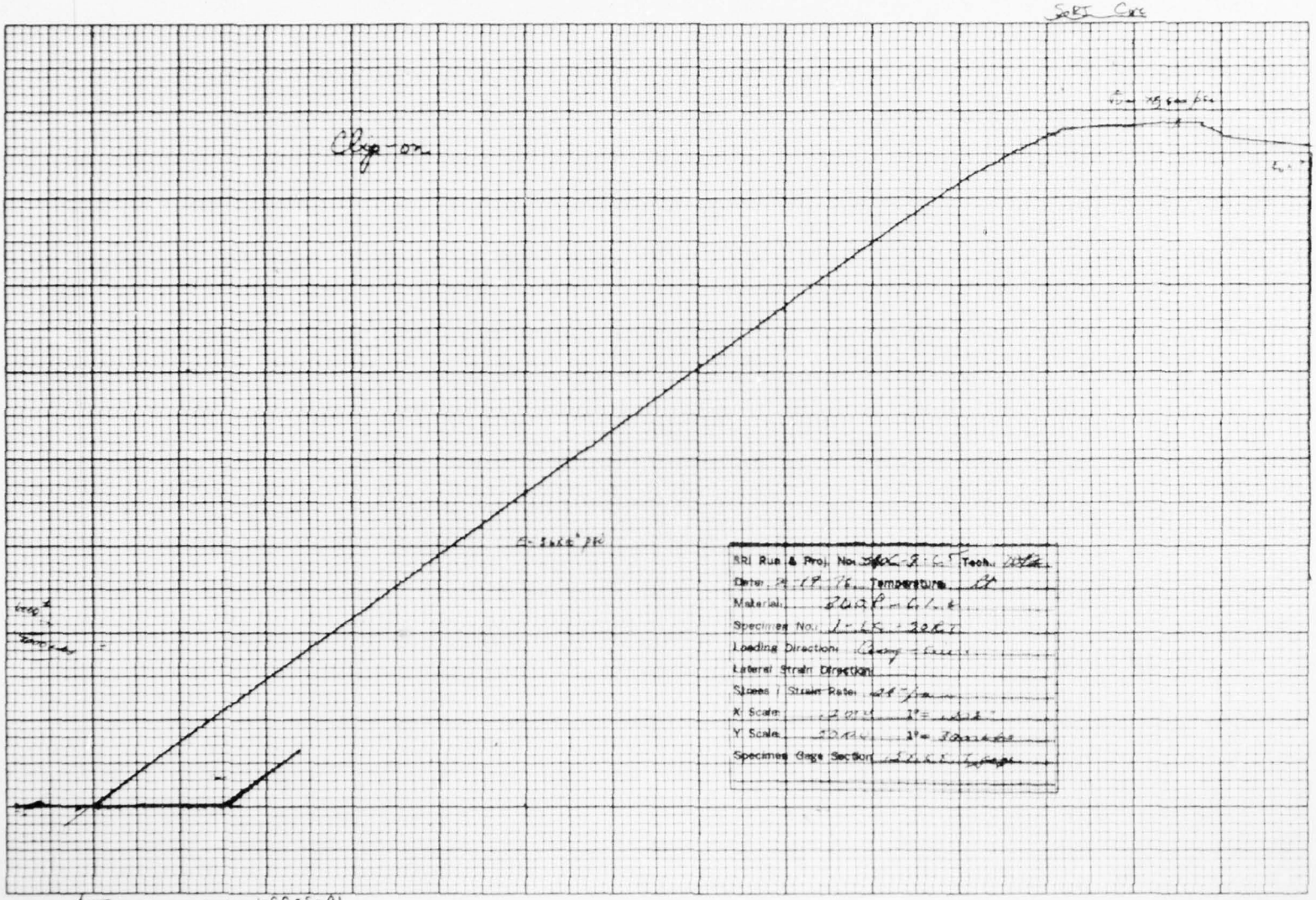

Figure A-47. Test Results for Specimen 1-CC-SoBI

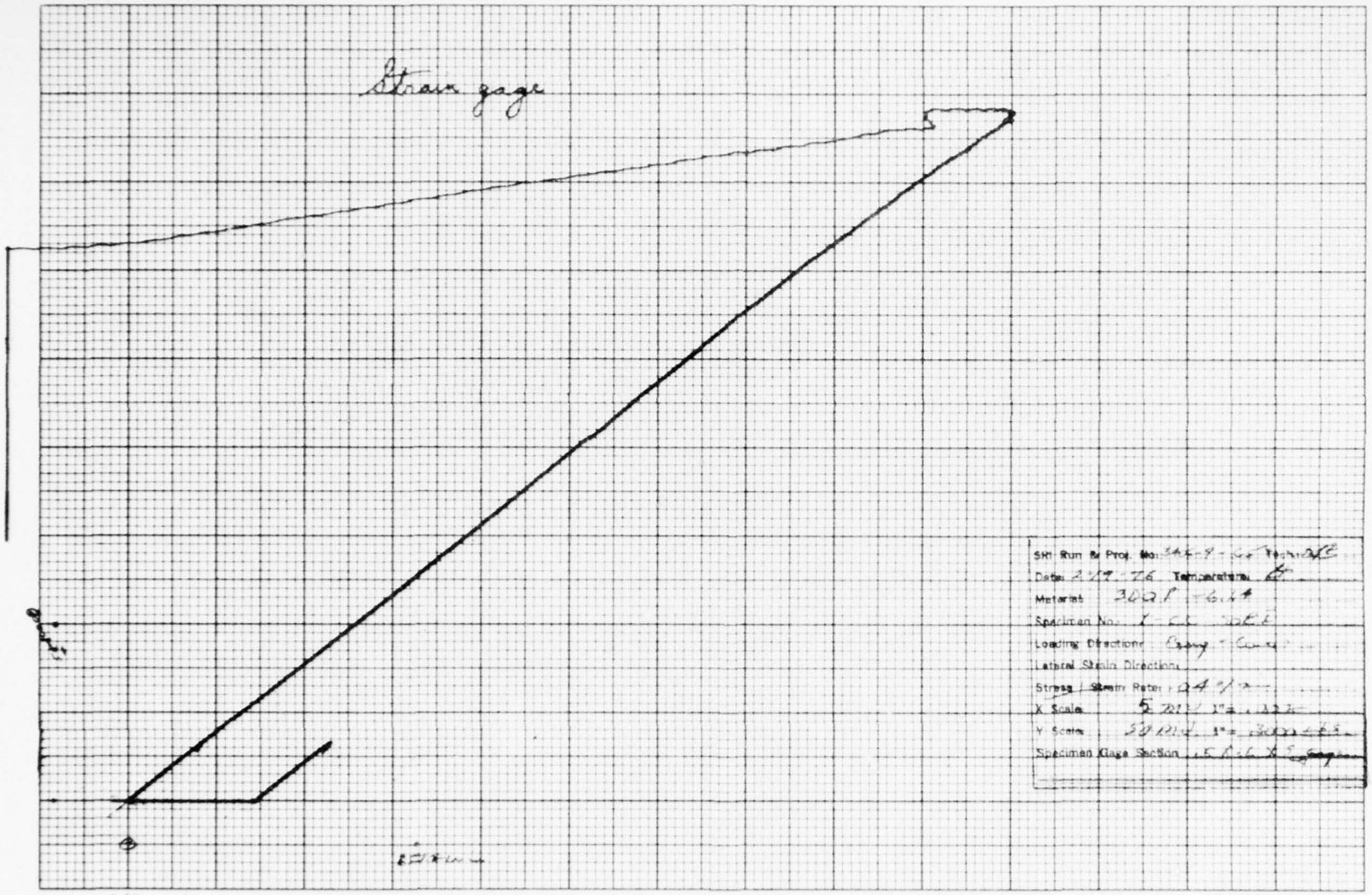

Figure 148 Test Results for Specimen 1-CC-S2R1

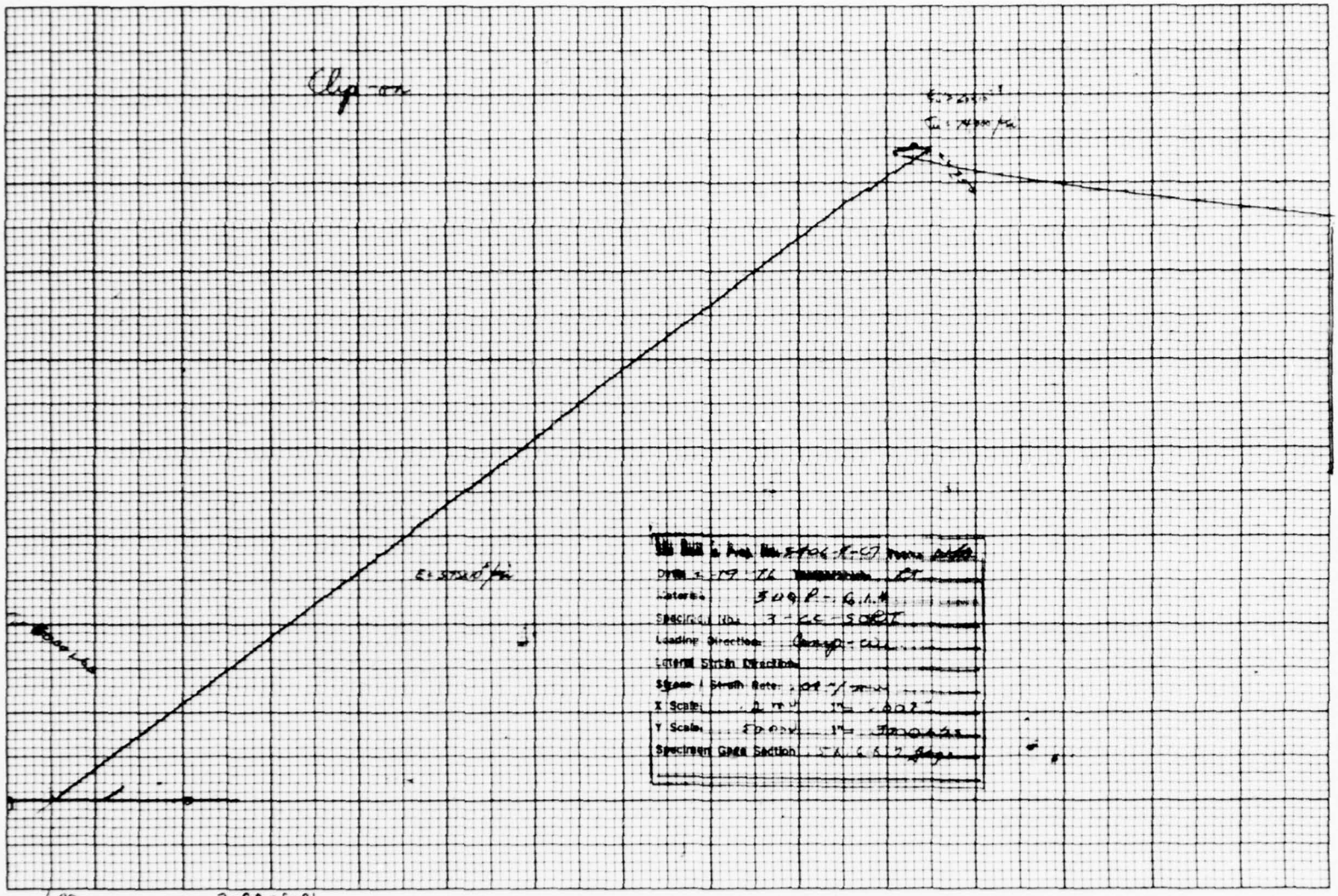

/49 Test Results for Specimen 3-CC-SaA1

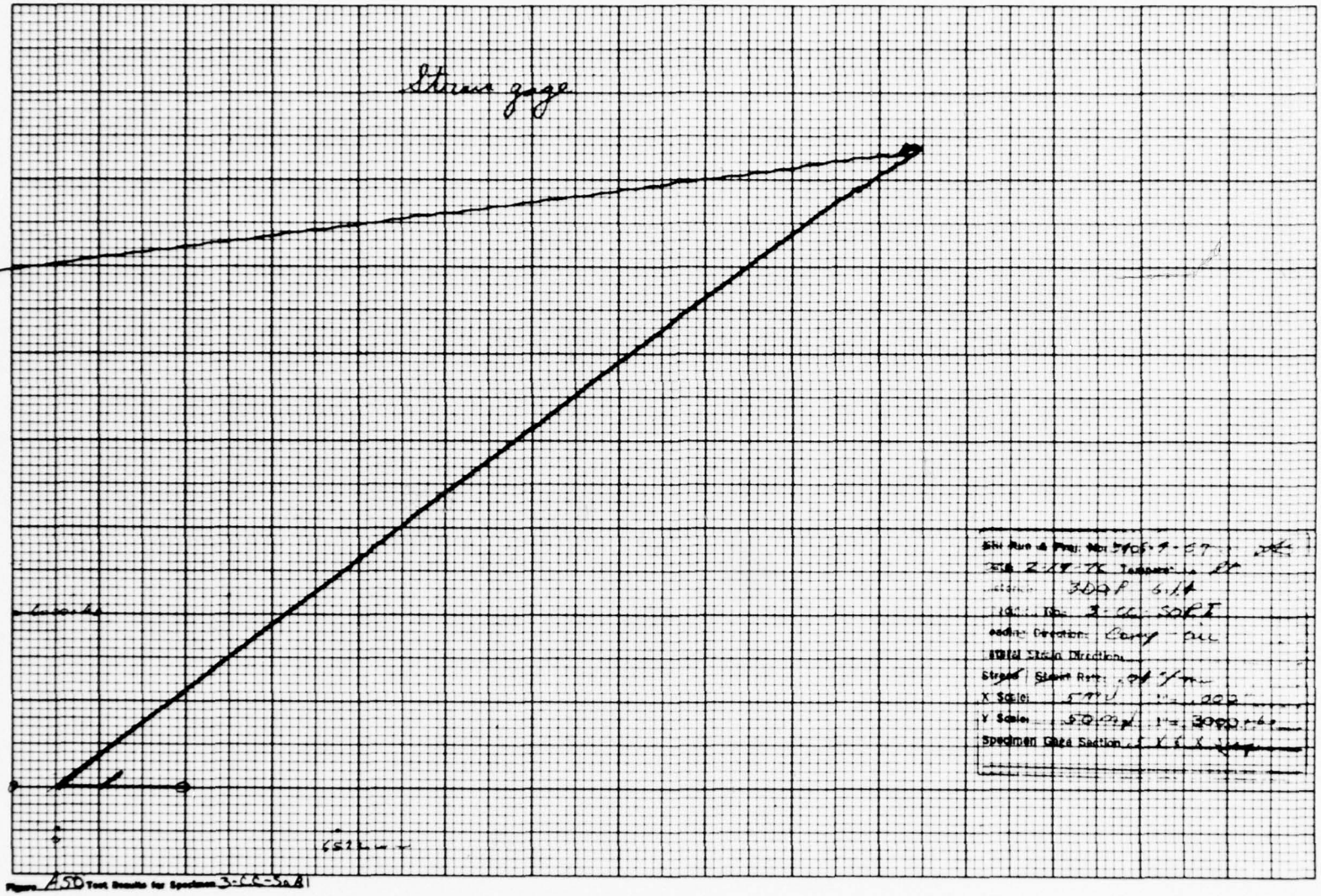

Figure A.50 Test Results for Specimen 3-CC-5aB1

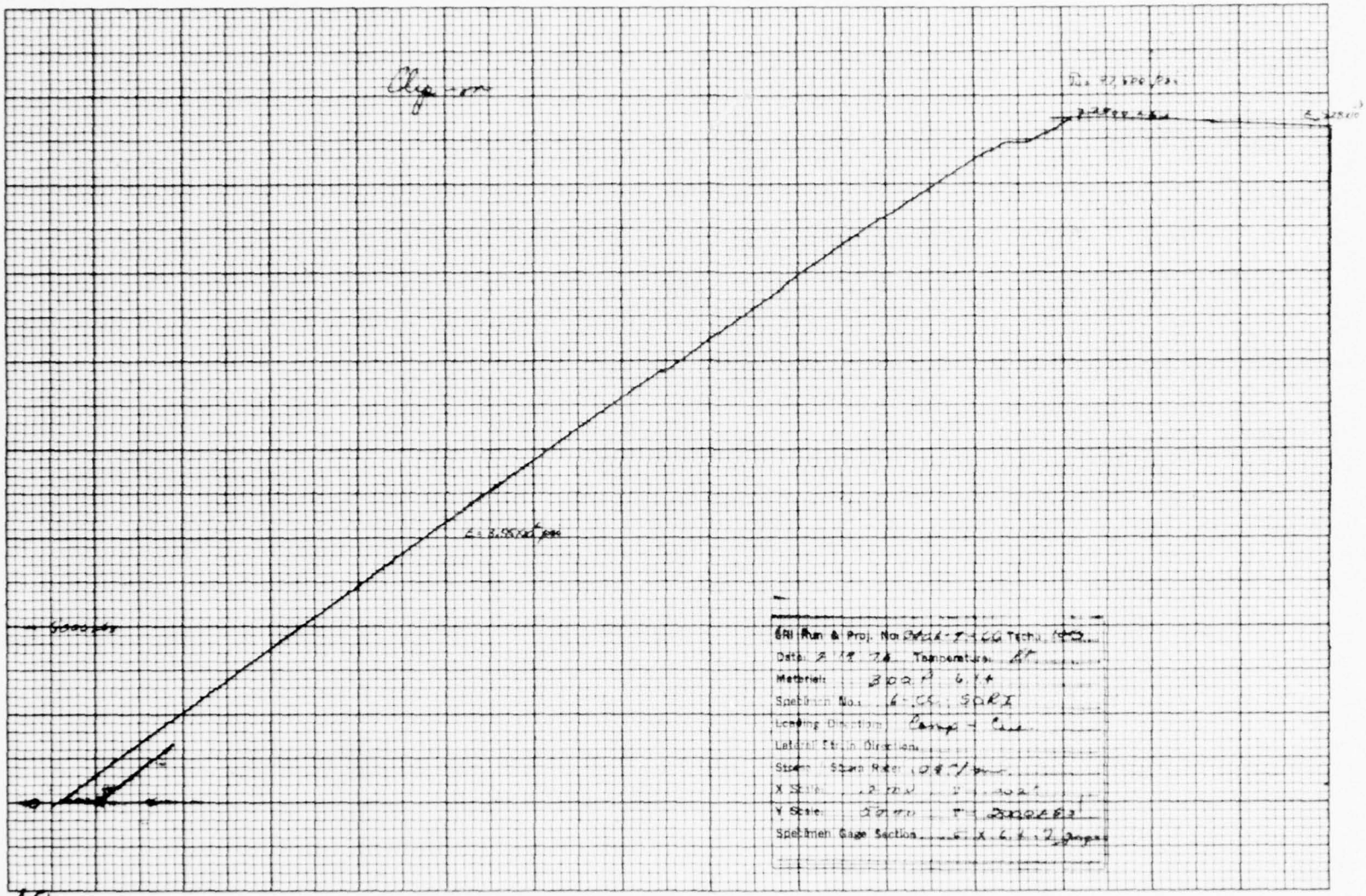

Figure A31. Test Results for Specimen G-CC-SnR1

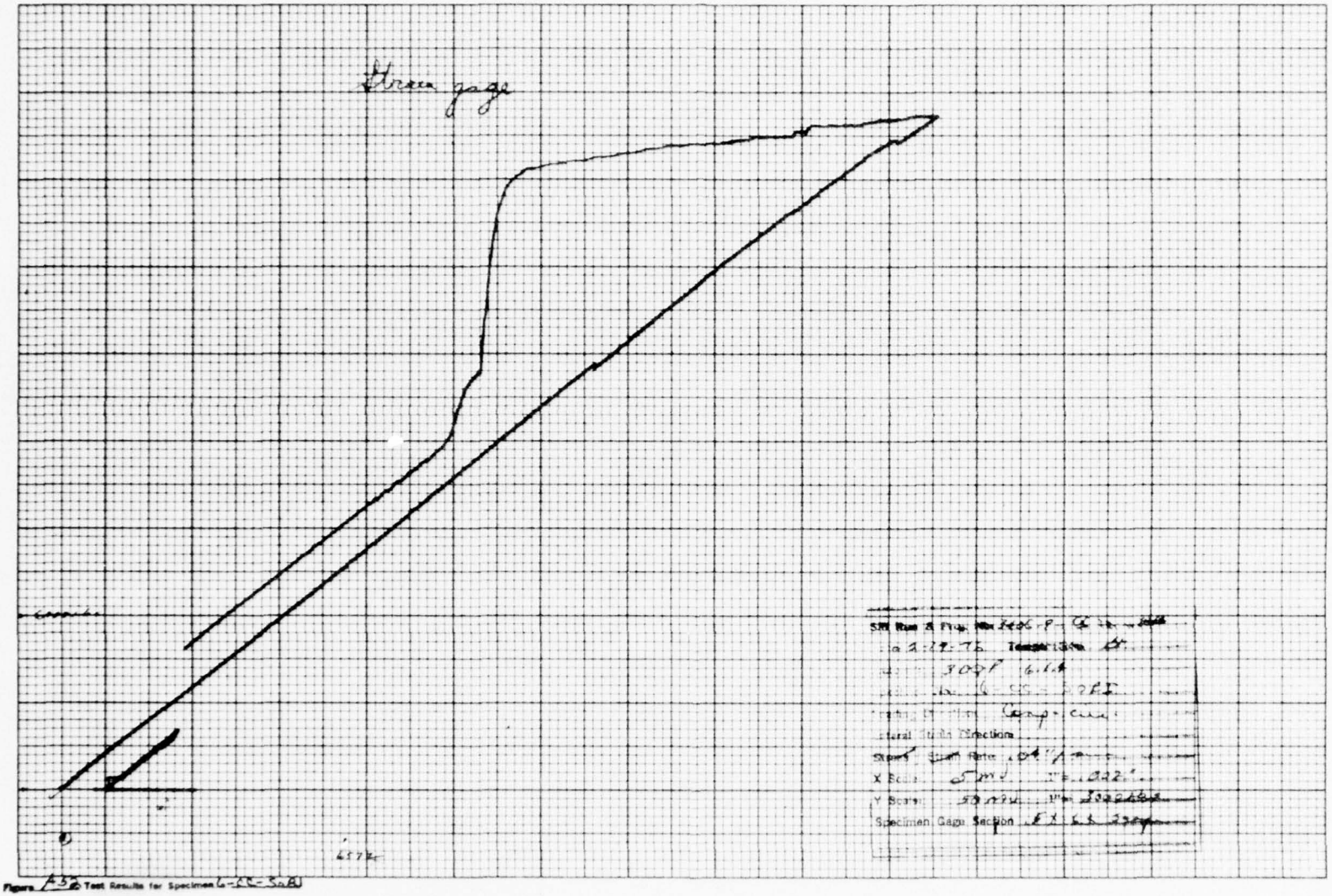

Figure A-32 Test Results for Specimen G-RE-SAB

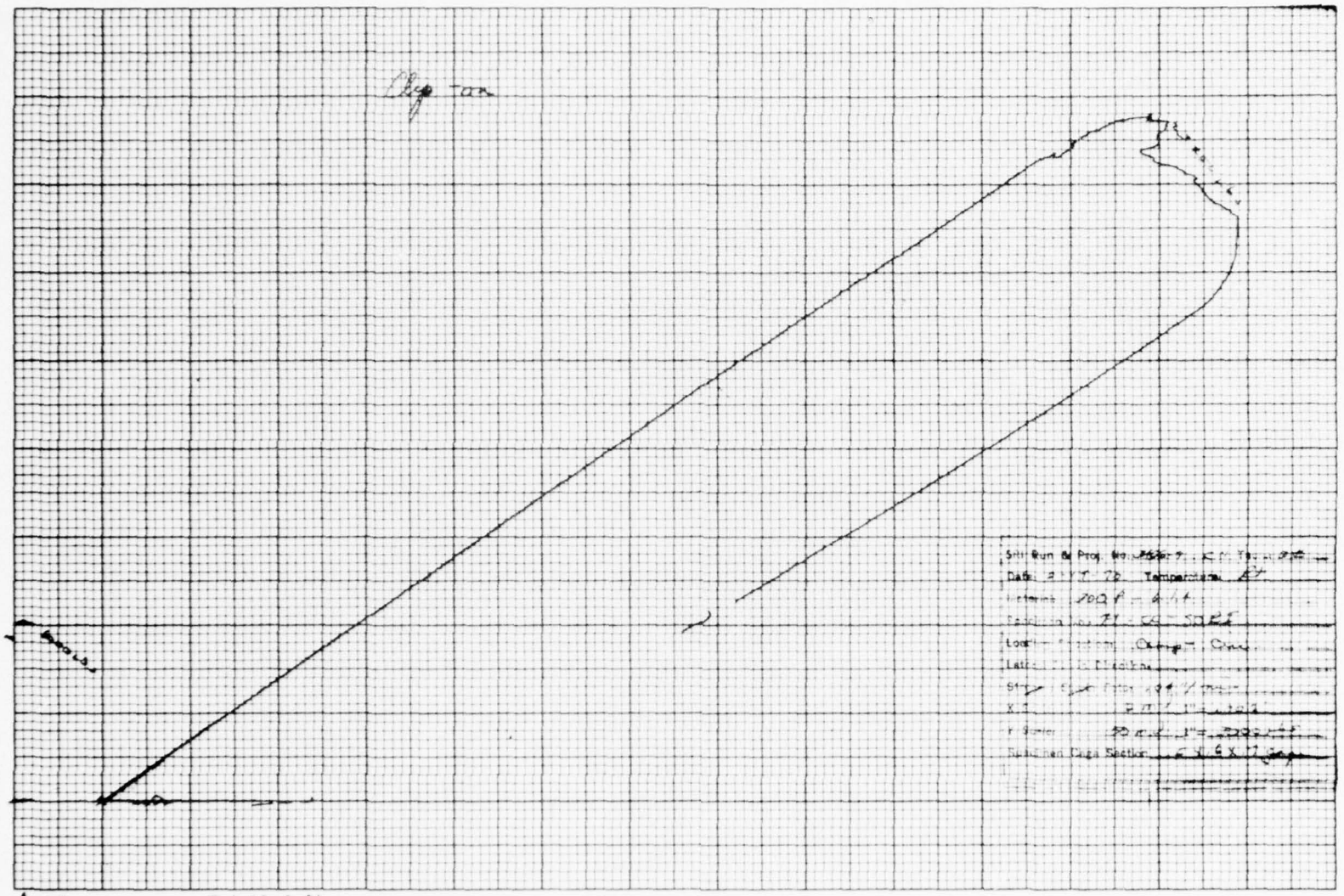

Figure A 53 Test Results for Specimen 7-1-CC-S-R1

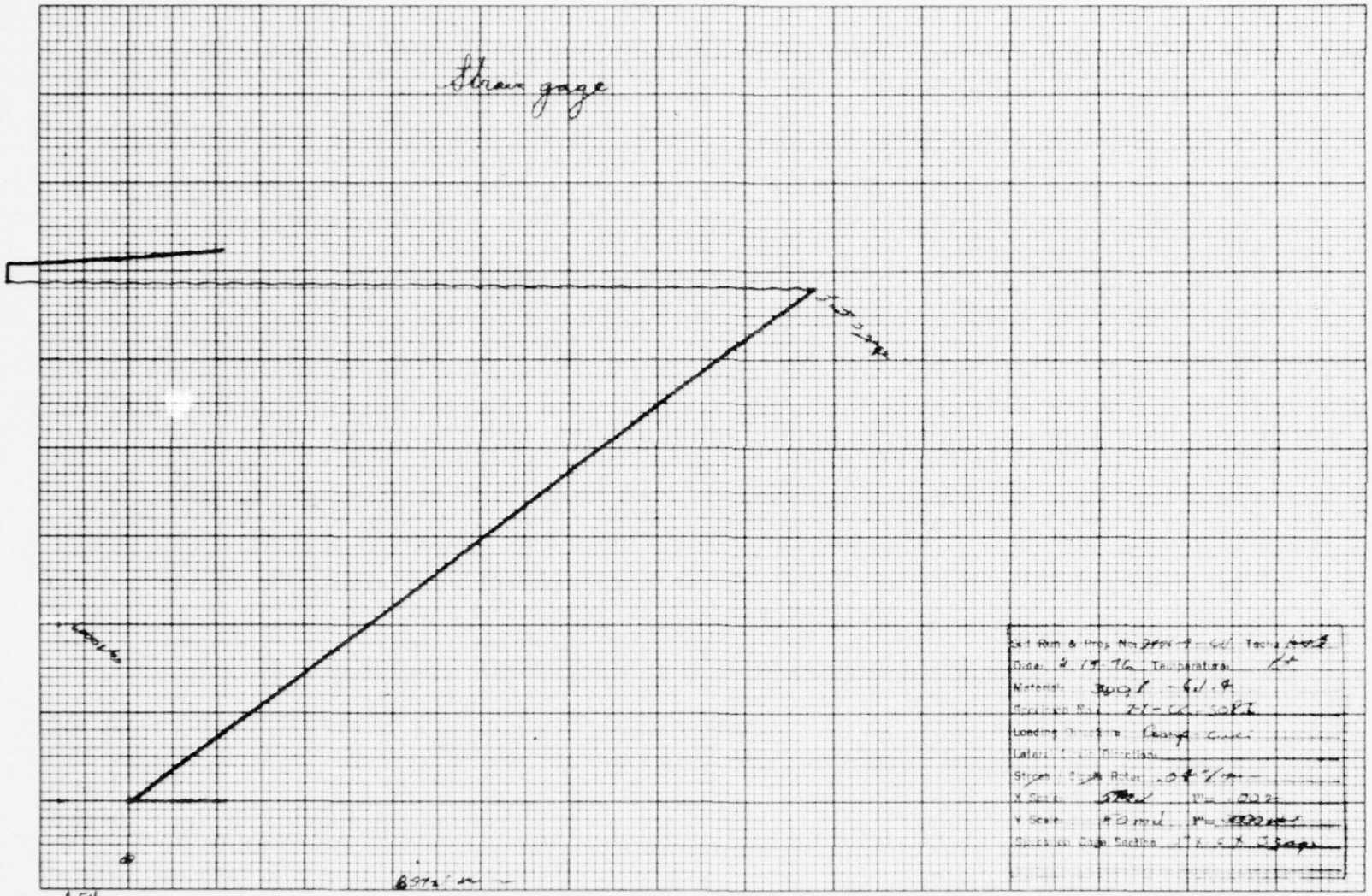

Figure A.54 Test Results for Specimen 7-1-CC-3-R1

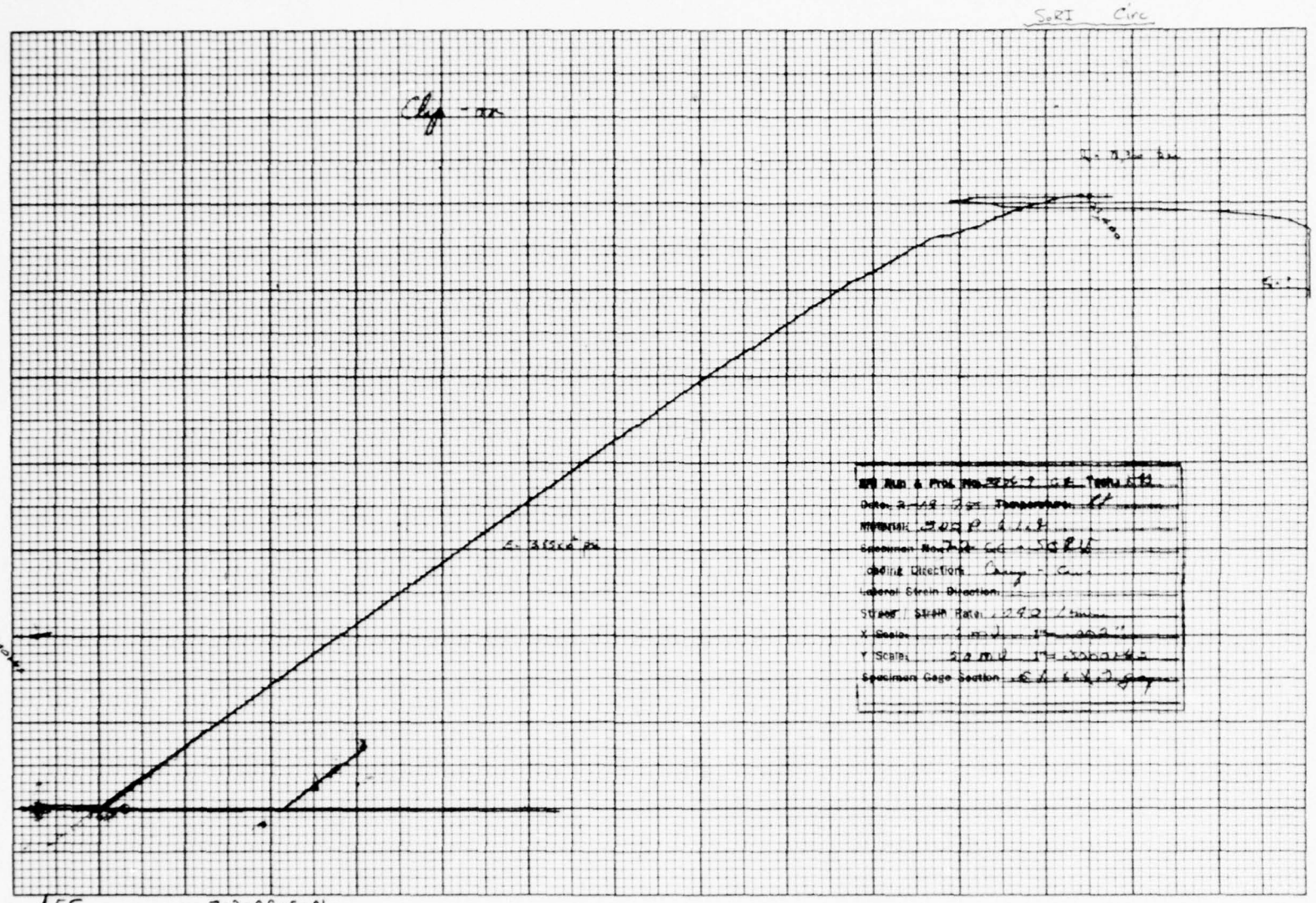

Figure 155 Test Results for Specimen 7-2-CS-30 A1

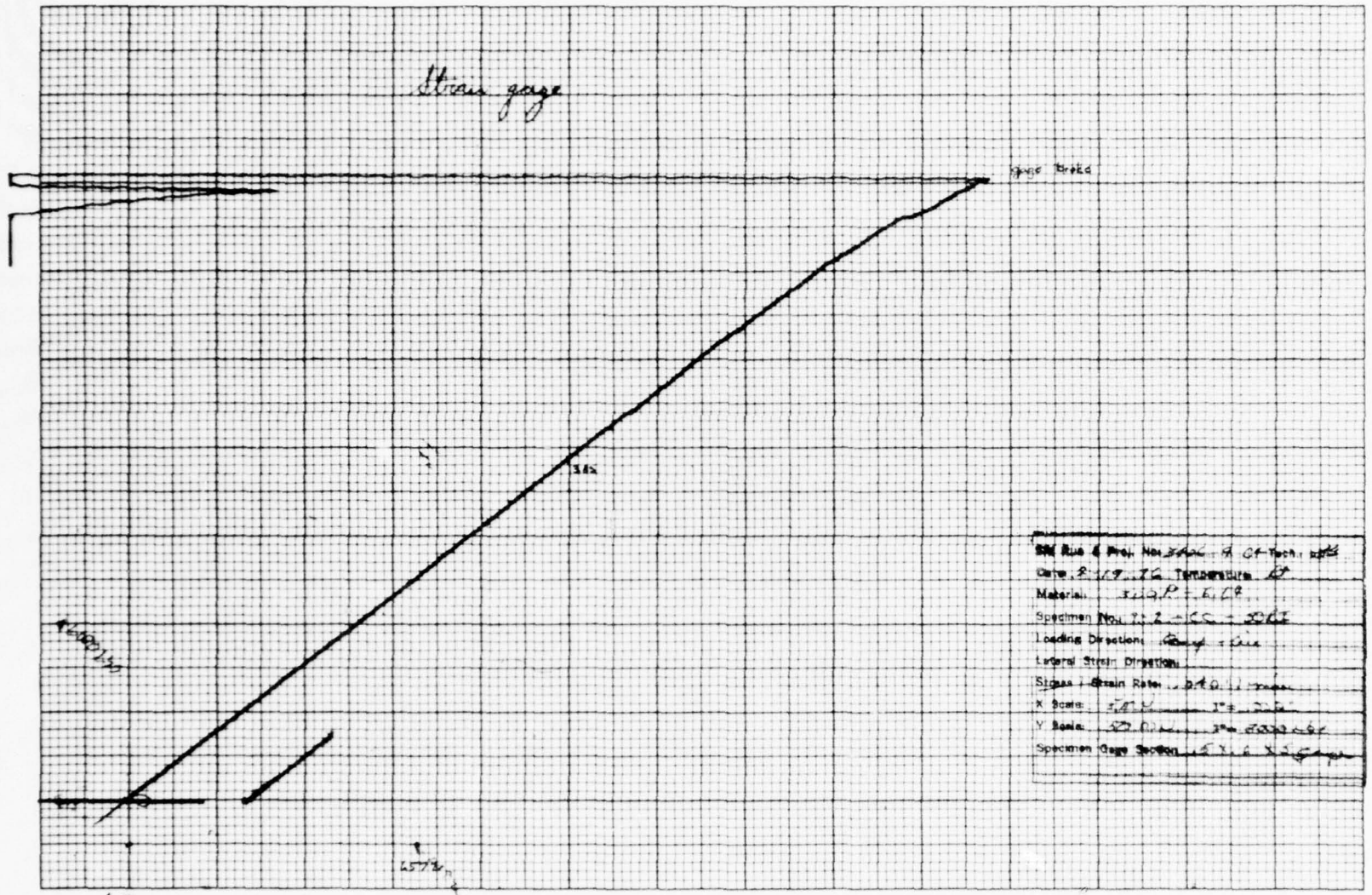

Fig. A56 Test Results for Specimen 7-2-SS-SoAl

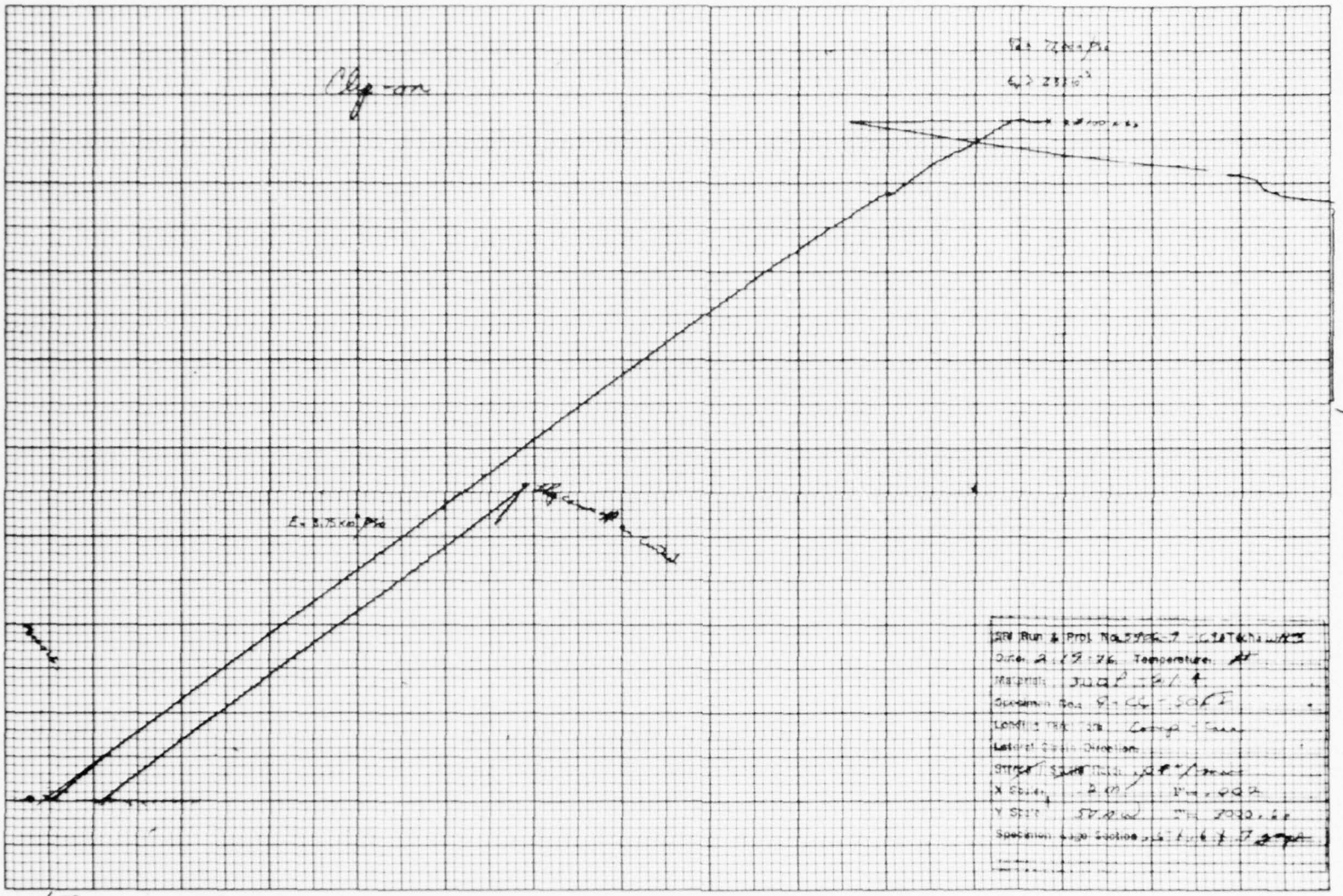

Figure 157 Test Results for Specimen 9-CC-SaR1

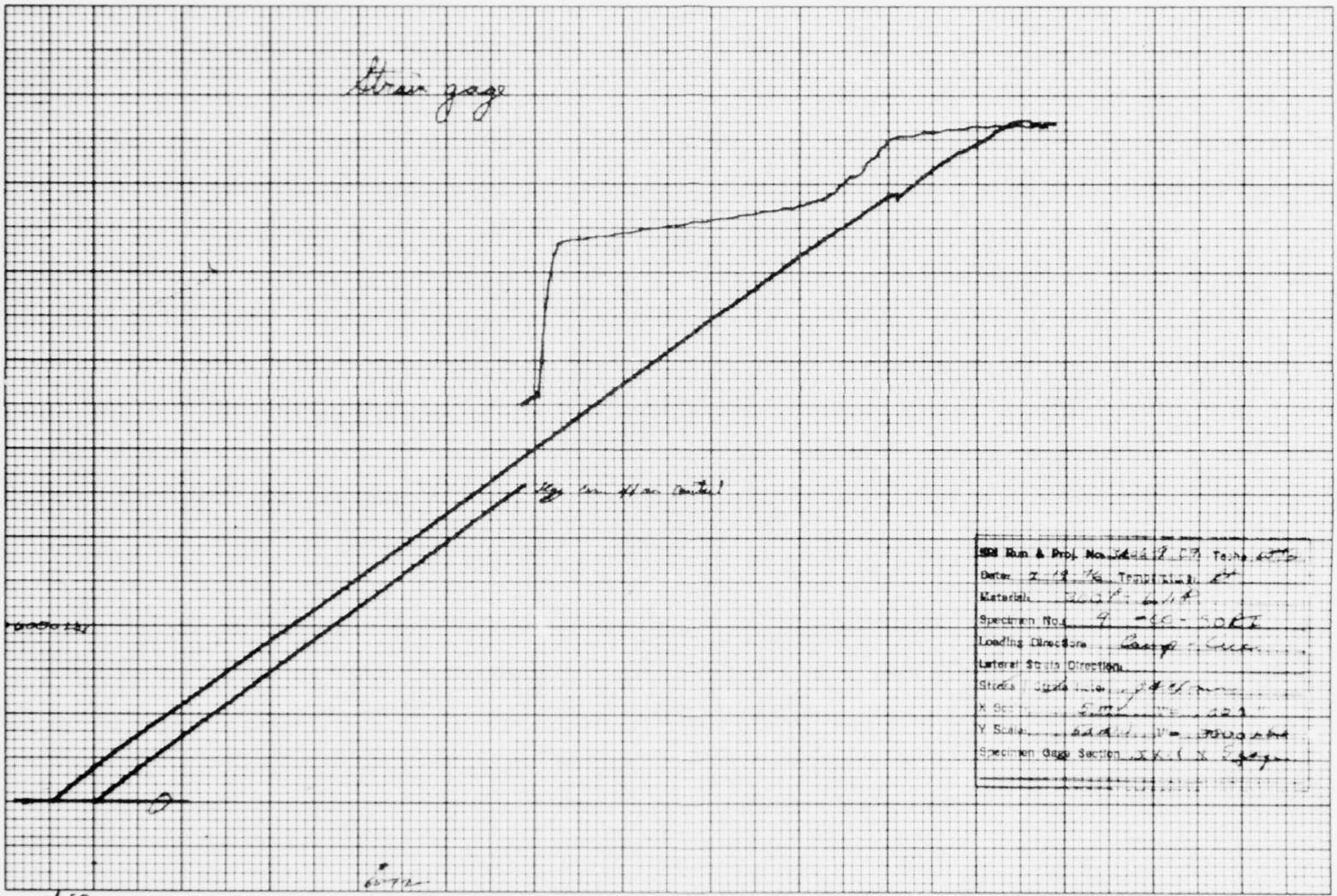

Figure 58. Test Results for Specimen 9-66-S2R1

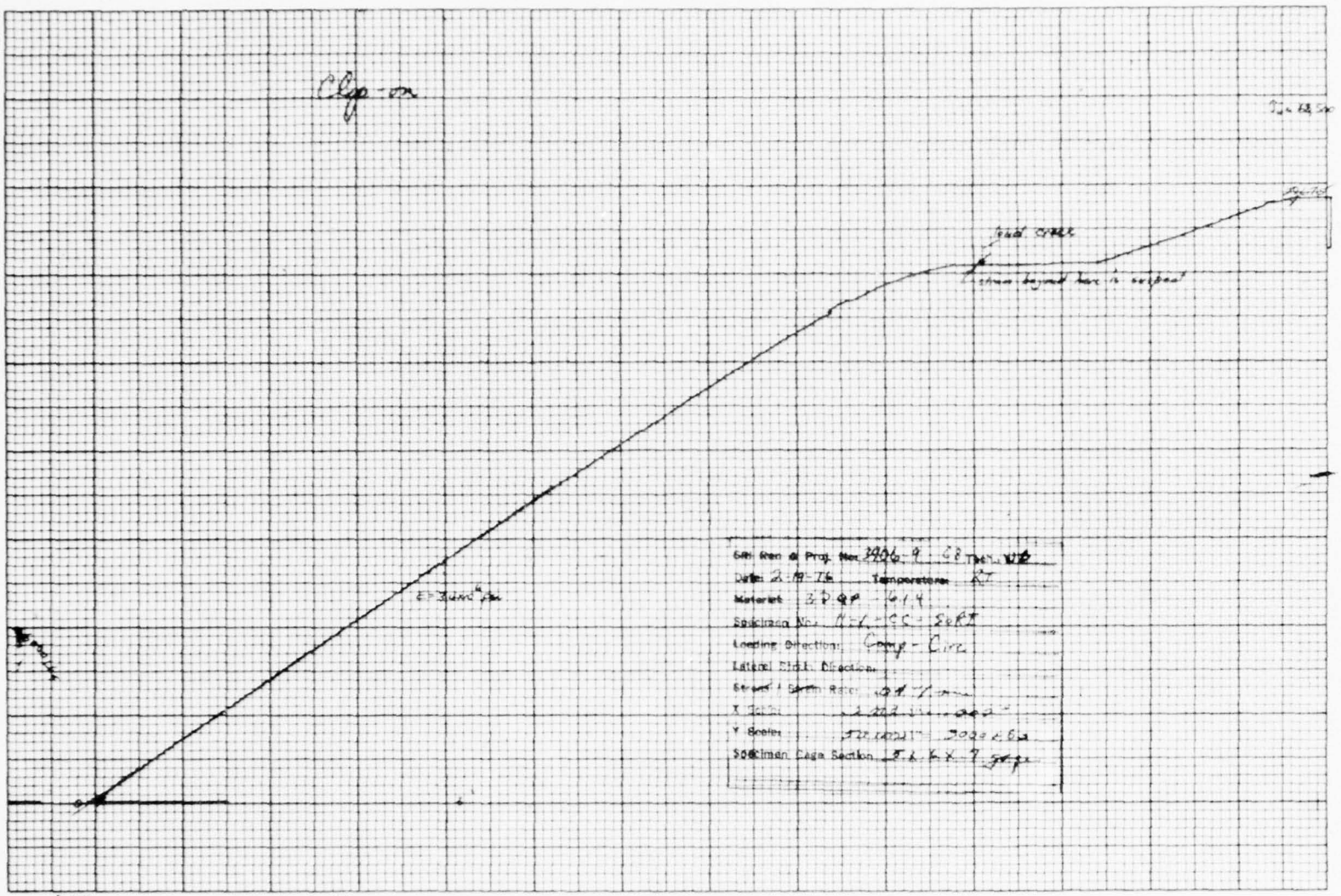

Figure A.53 Test Results for Specimen

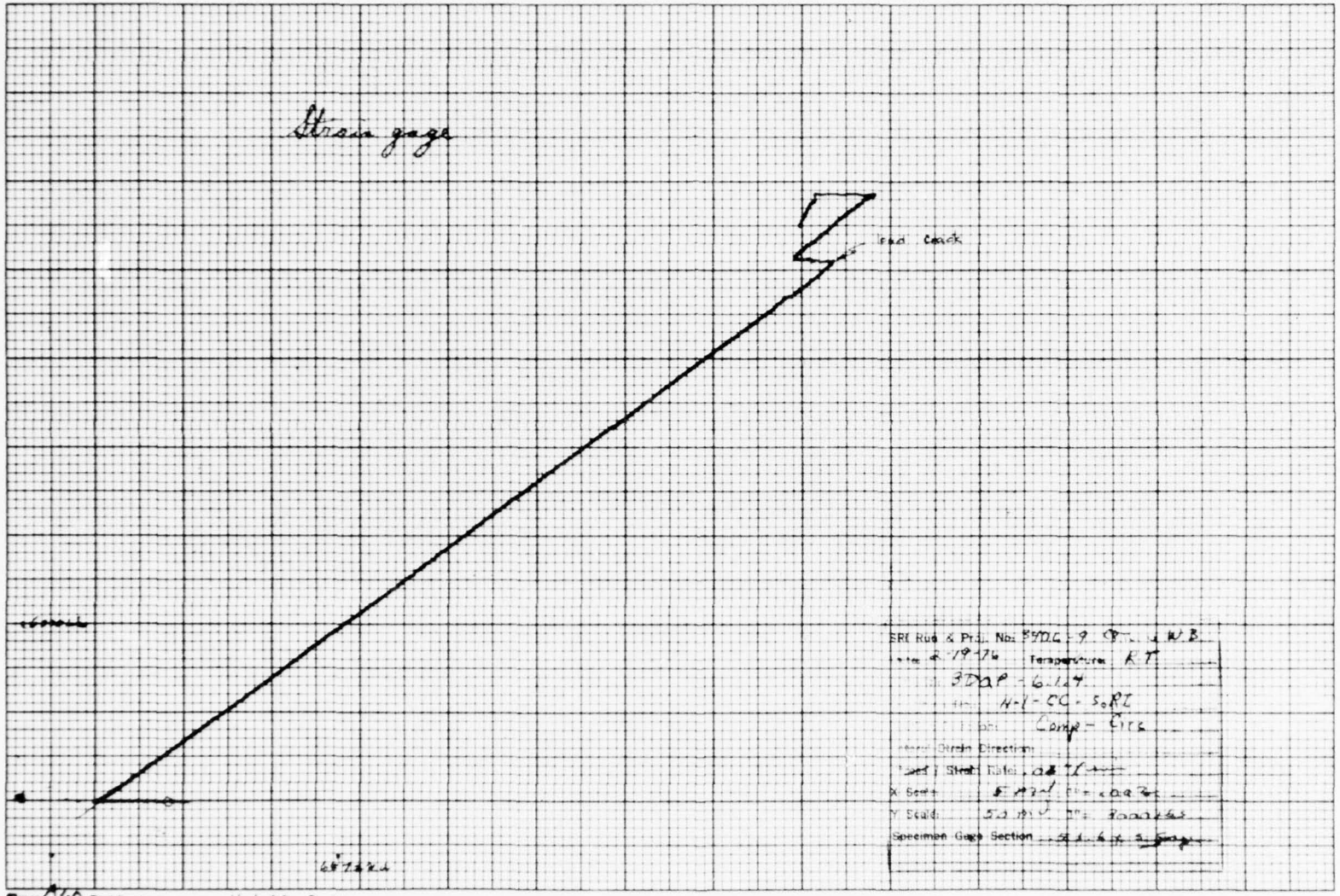

Figure A-20. Test Results for Specimen H-1-CC-50RI

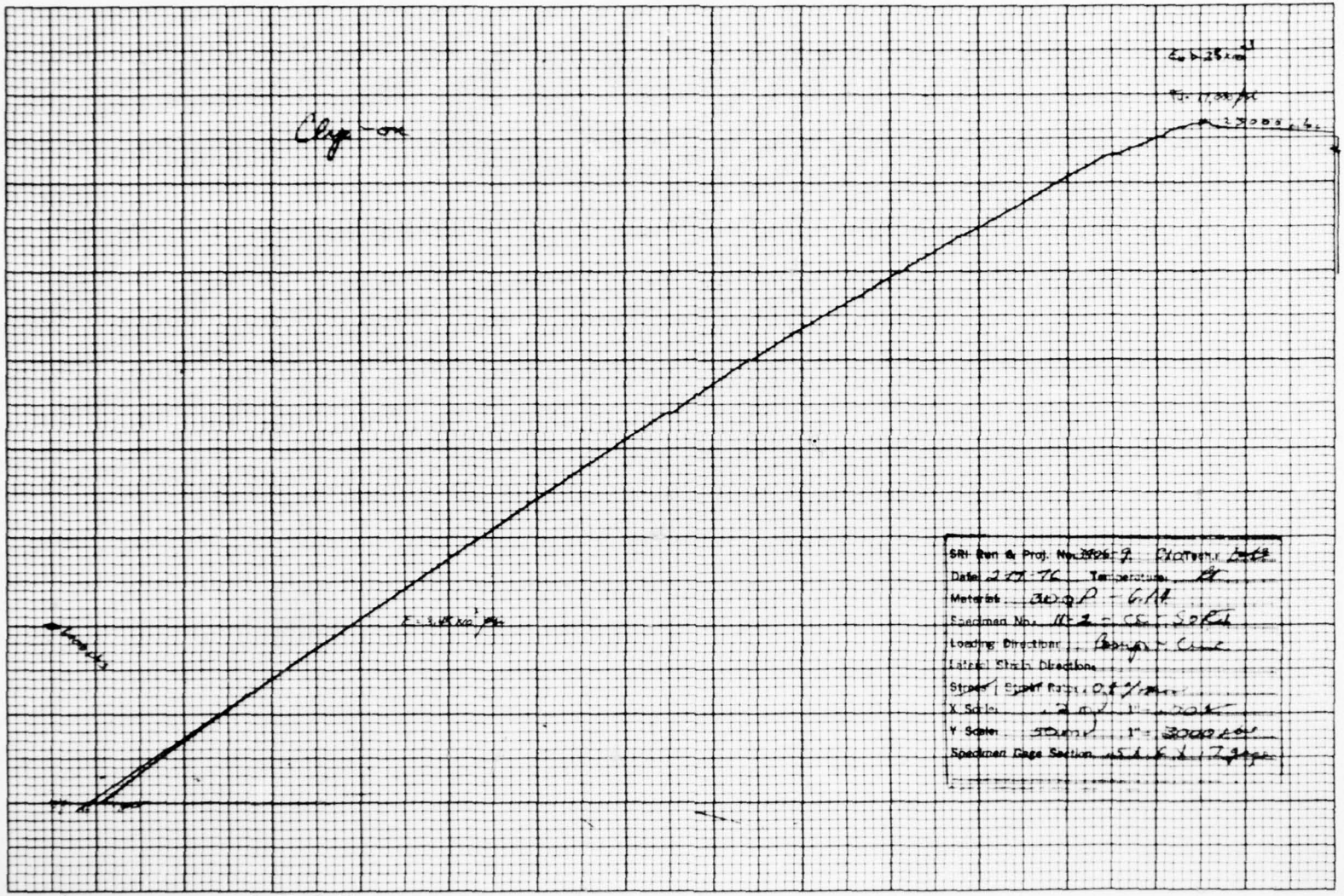

Figure A61 Test Results for Specimen IL-2-CC-S0R1

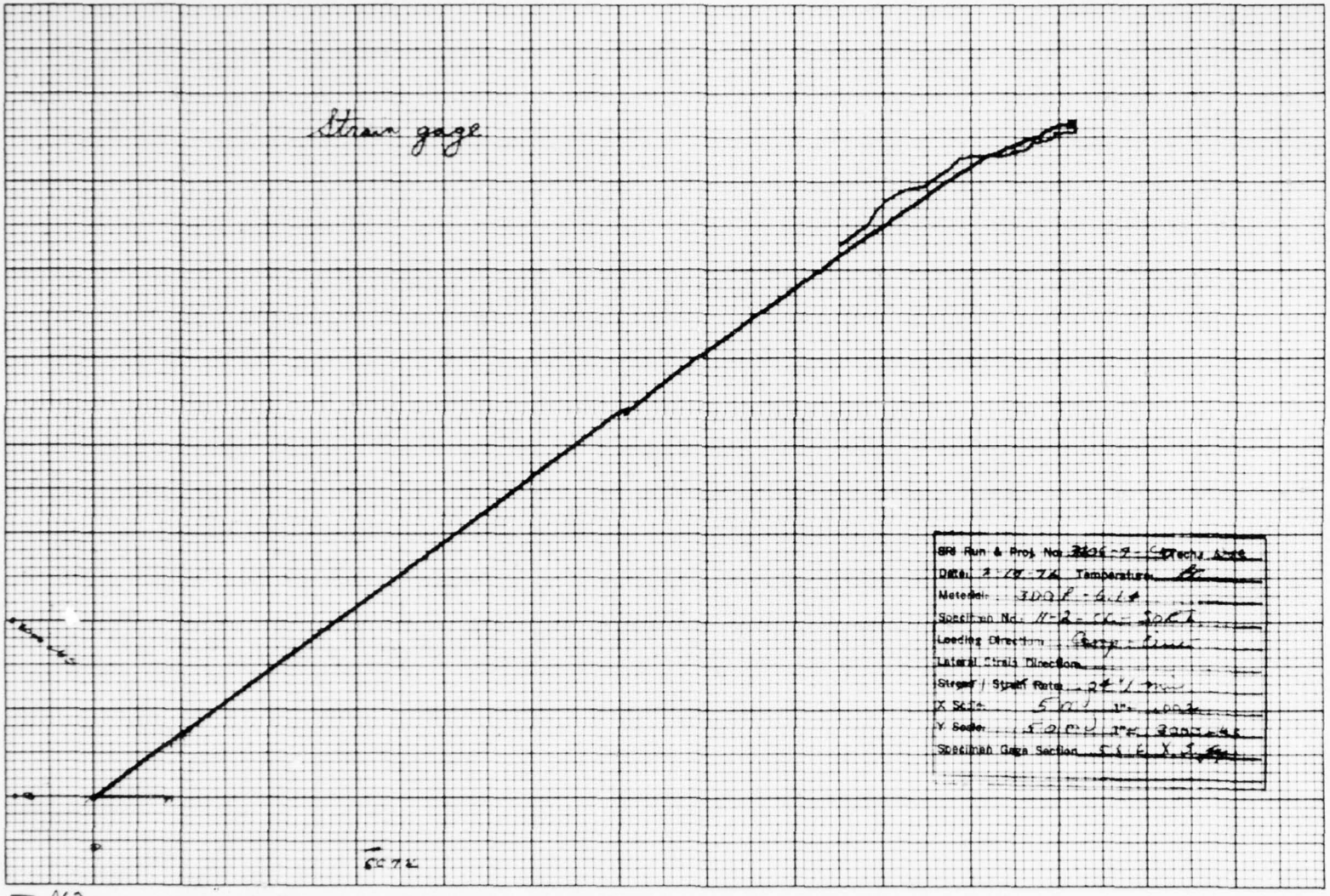

Figure A62 Test Results for Specimen II-2-CC-SoR1

A5

Circumferential Compressive Tests
Rectangular Specimen Configuration

6.1.4

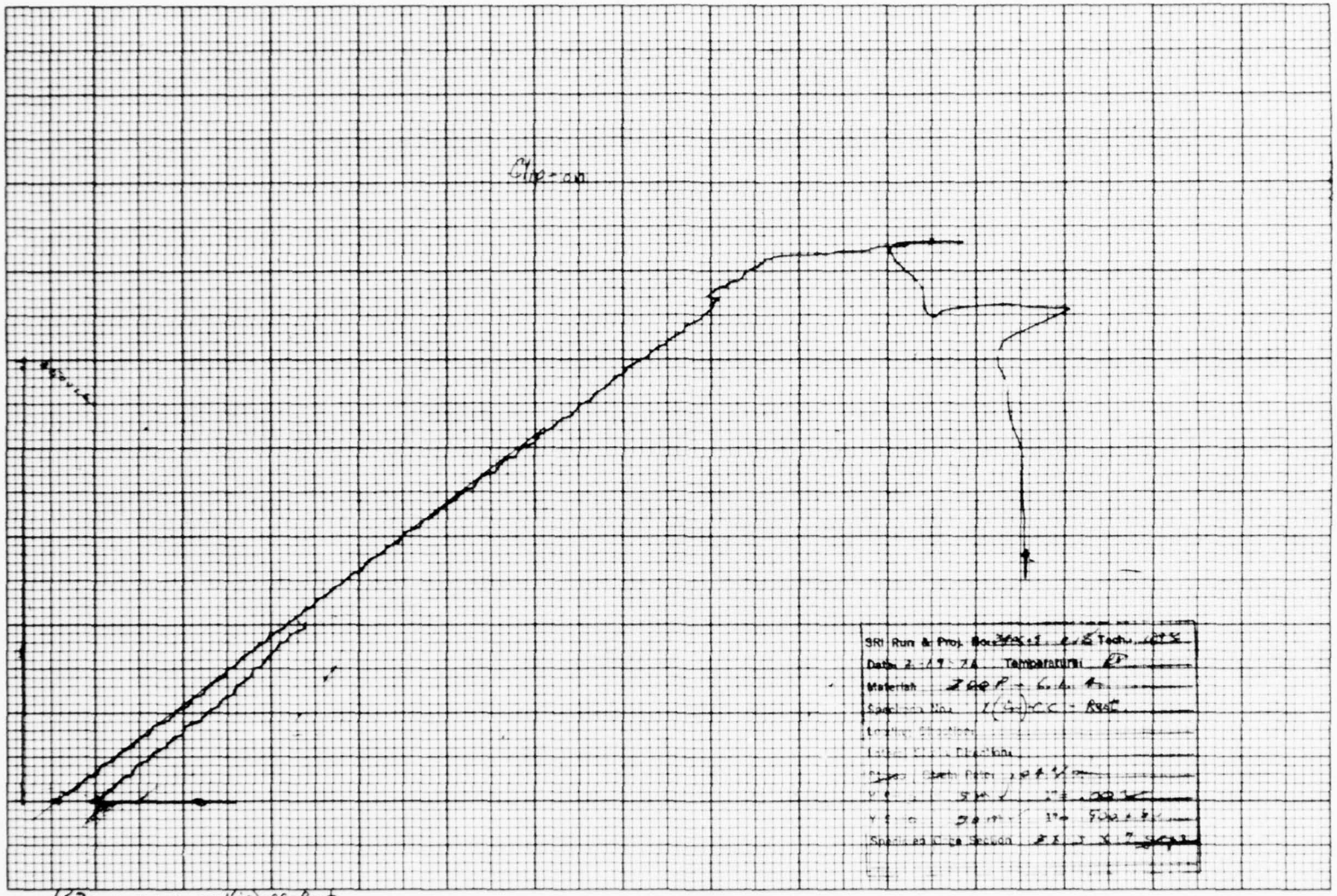

Figure A63 Test Results for Specimen 11(10)-CC-Beet

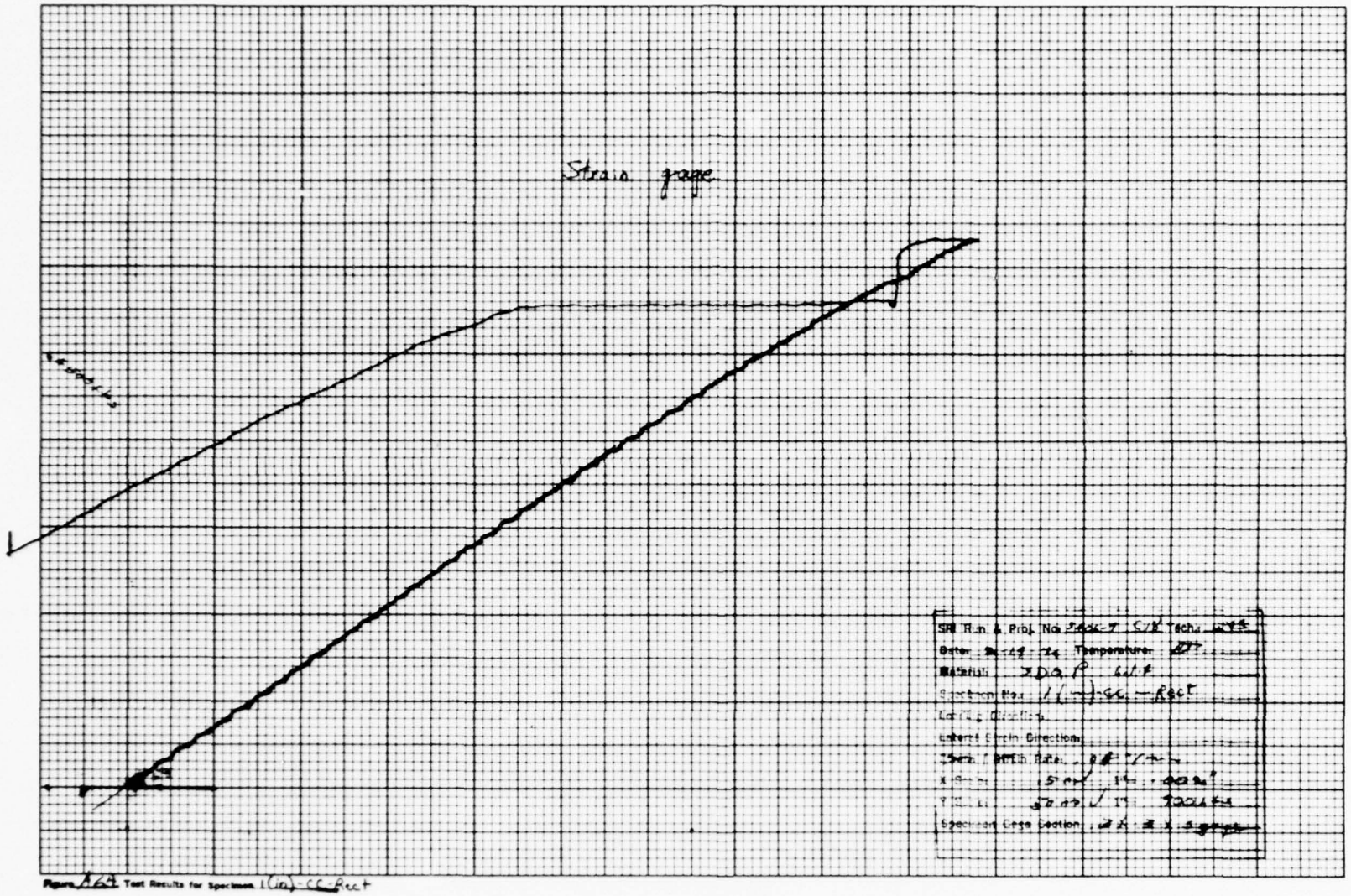

Figure A64 Test Results for Specimen 1(in)-CC-Rect

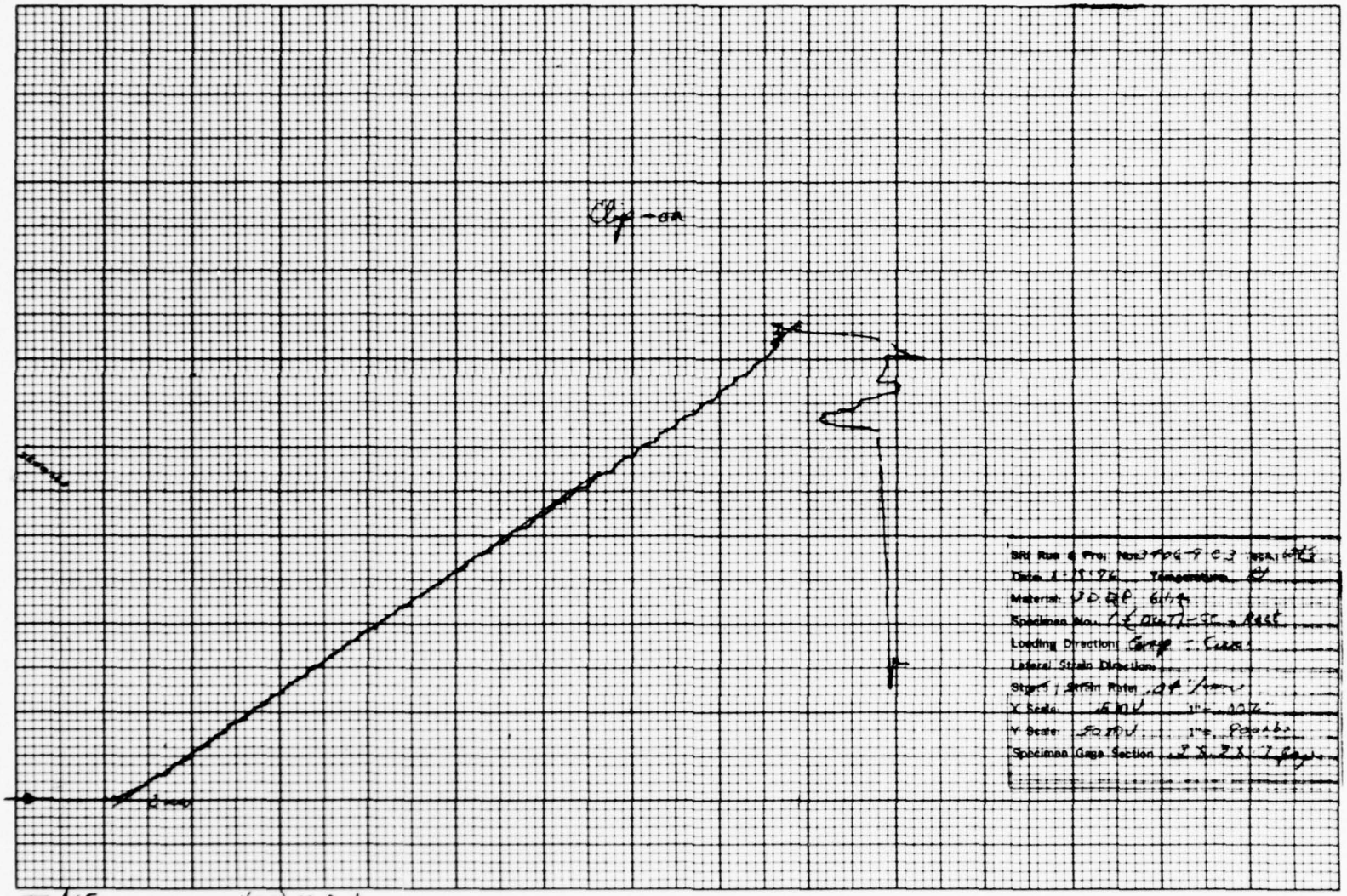

Figure A65 Test Results for Specimen 1(CAUT)-CC-Rect

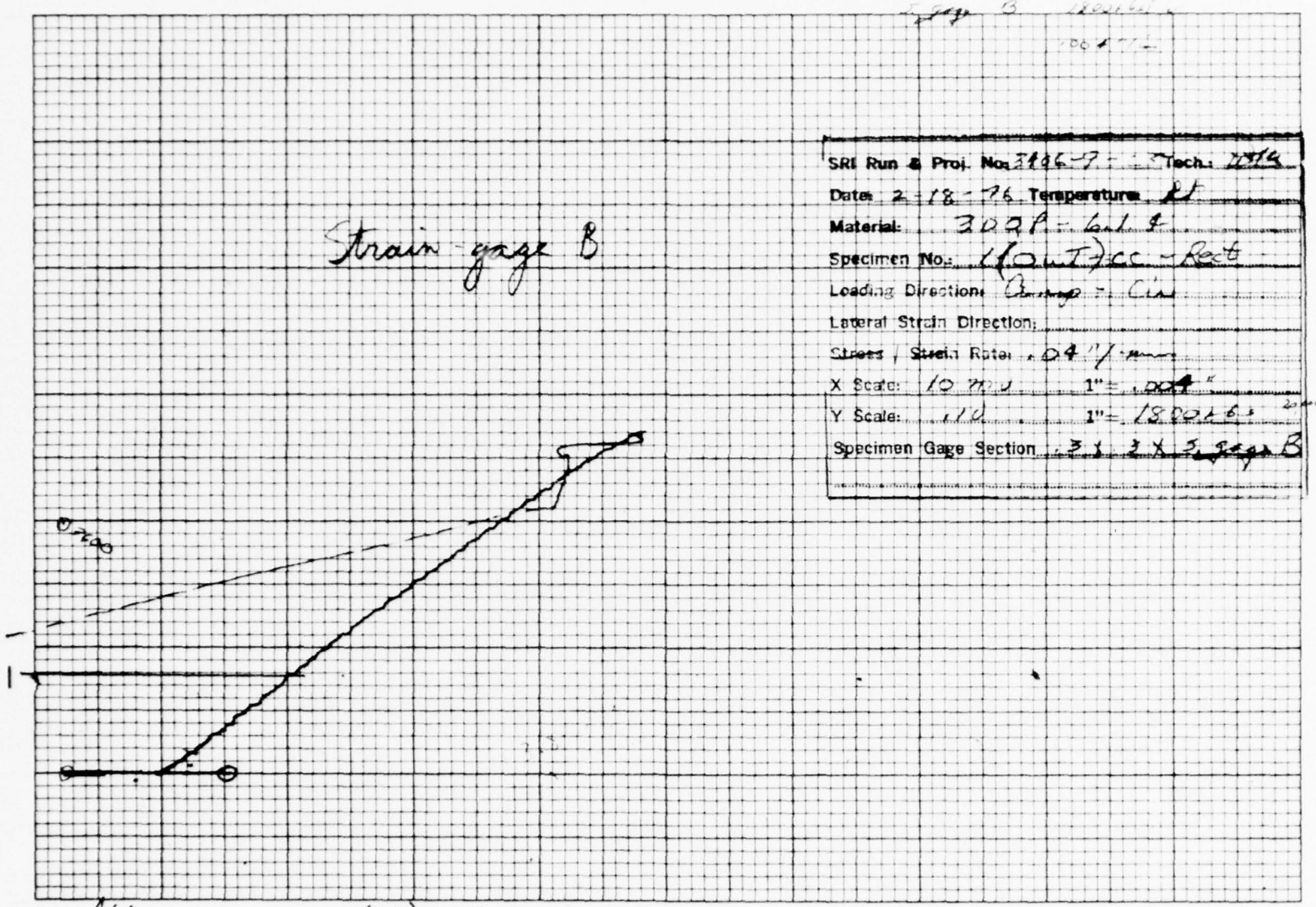

Figure A6b6 Test Results for Specimen 1(OUT)-CC-Rect

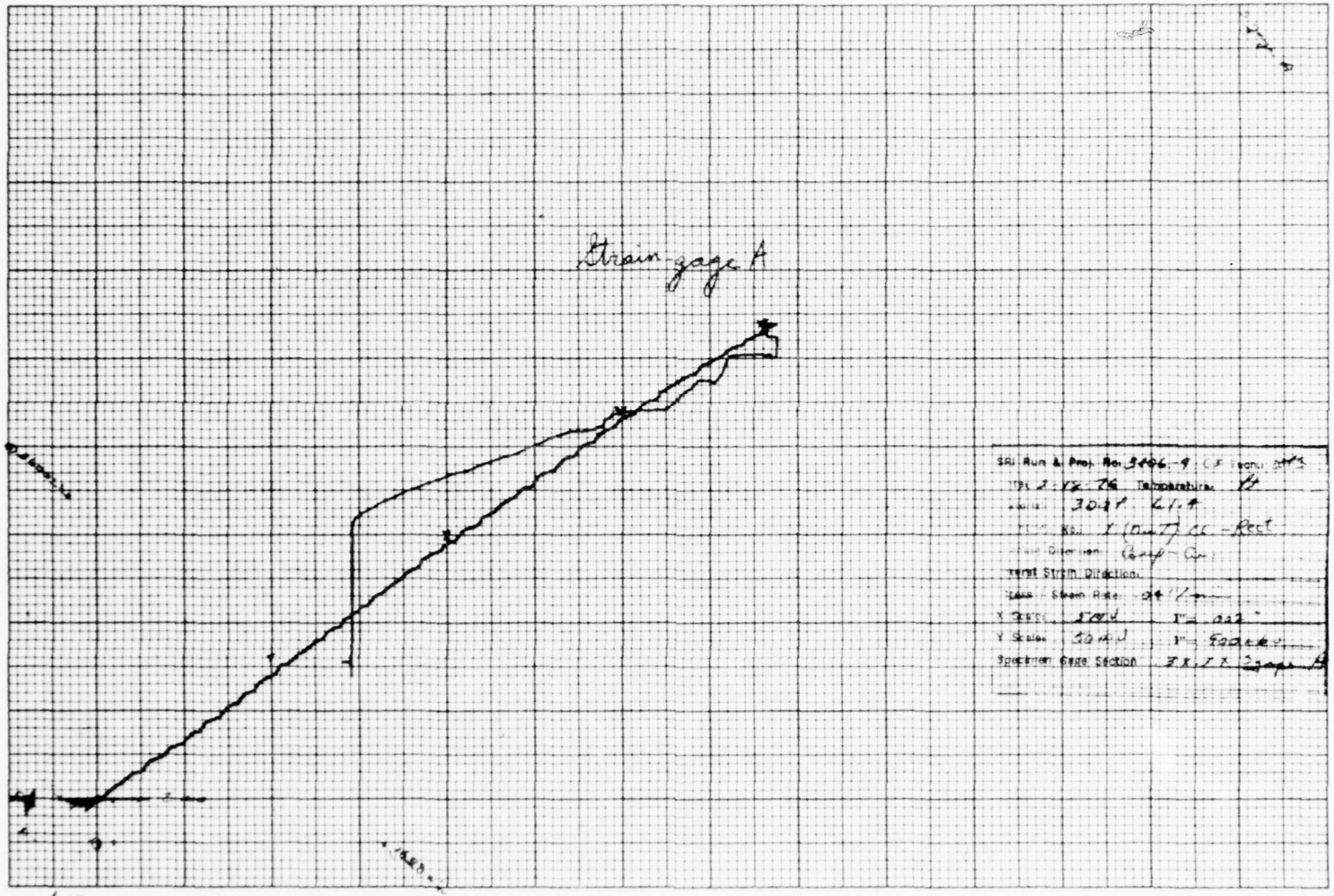

Figure A-67 Test Results for Specimen: (QVT)-CC-Rect

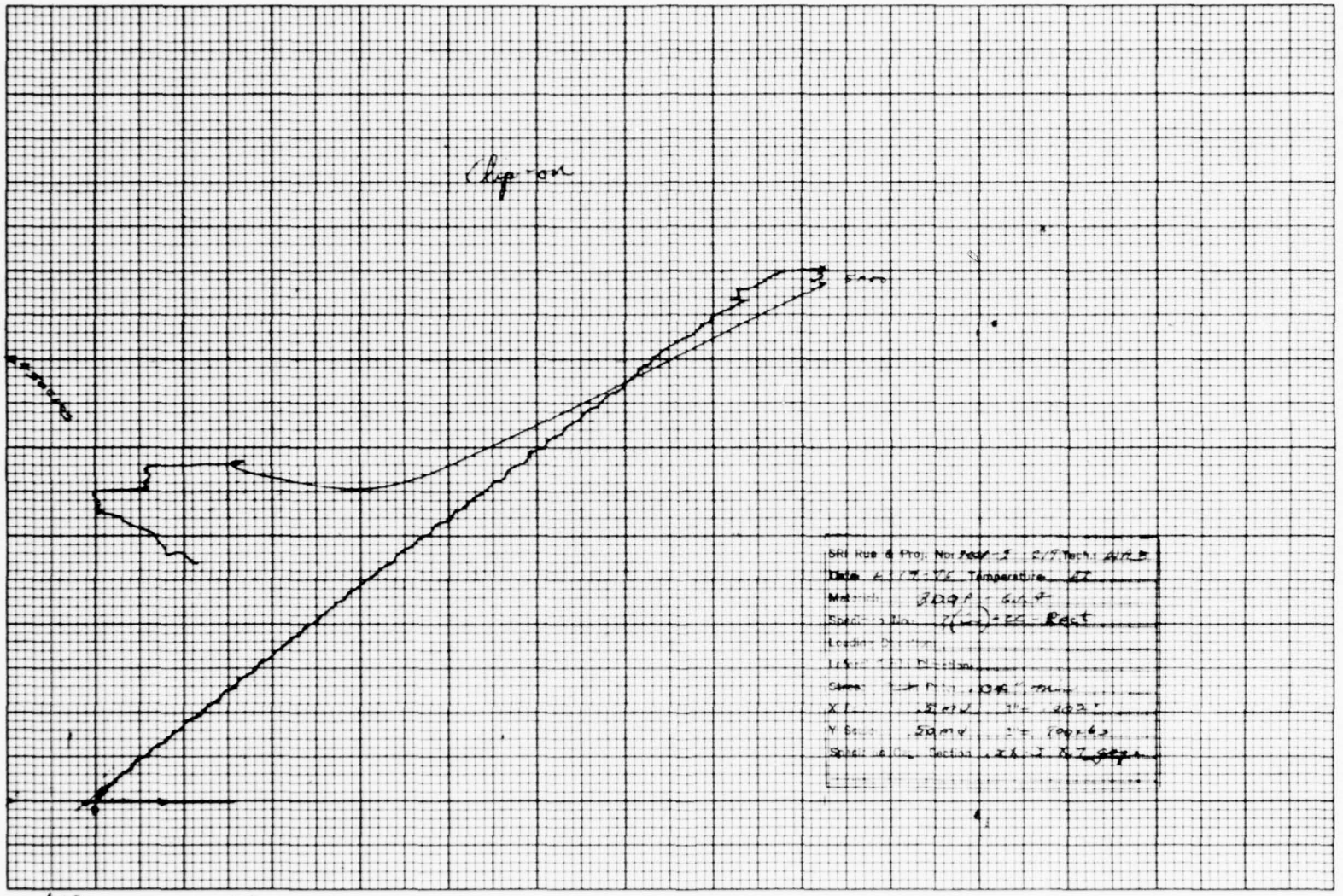

Figure A68 Test Results for Specimen 3(in)-CC-Rect

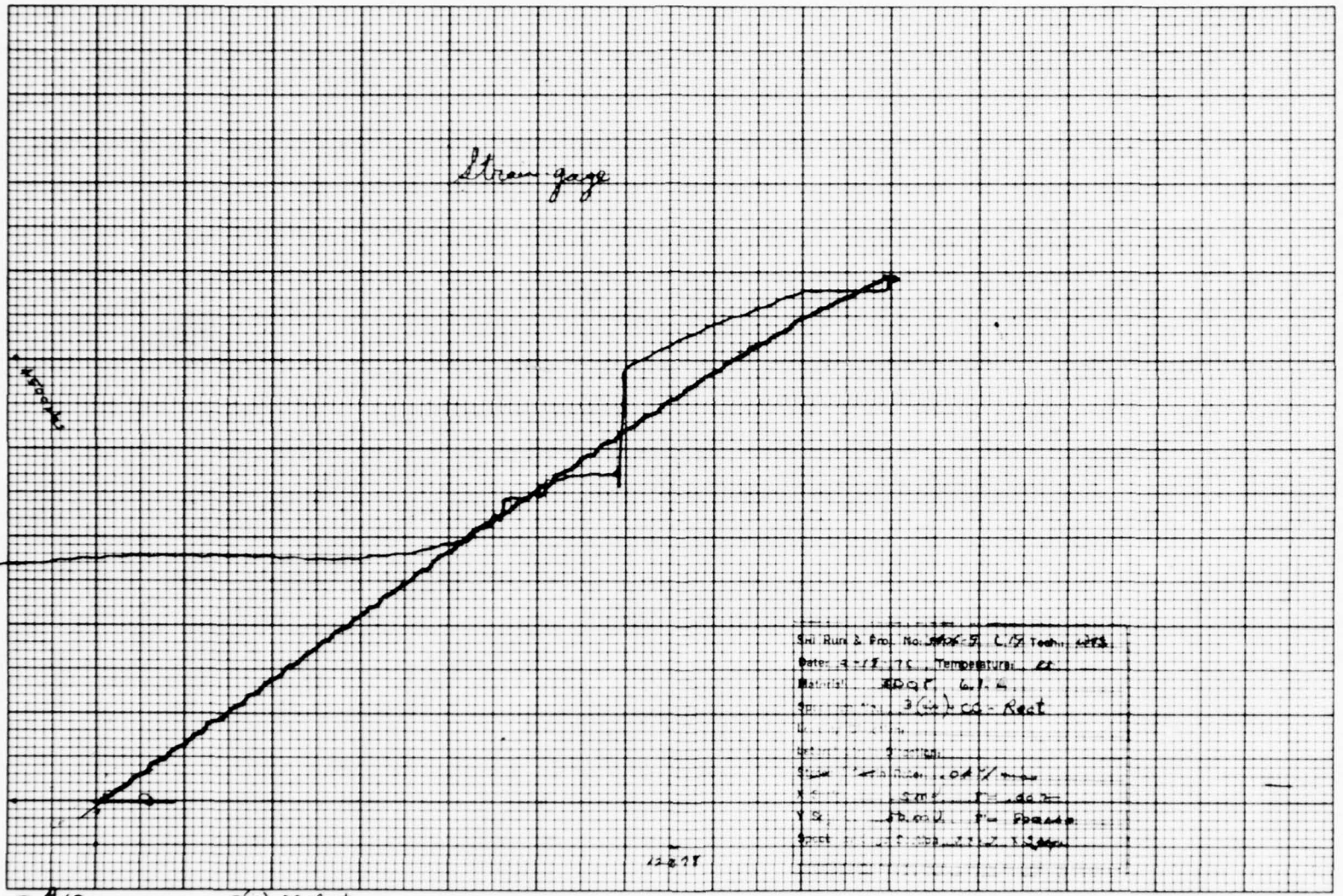

Figure A69. Test Results for Specimen 3(in)-CC-Rect

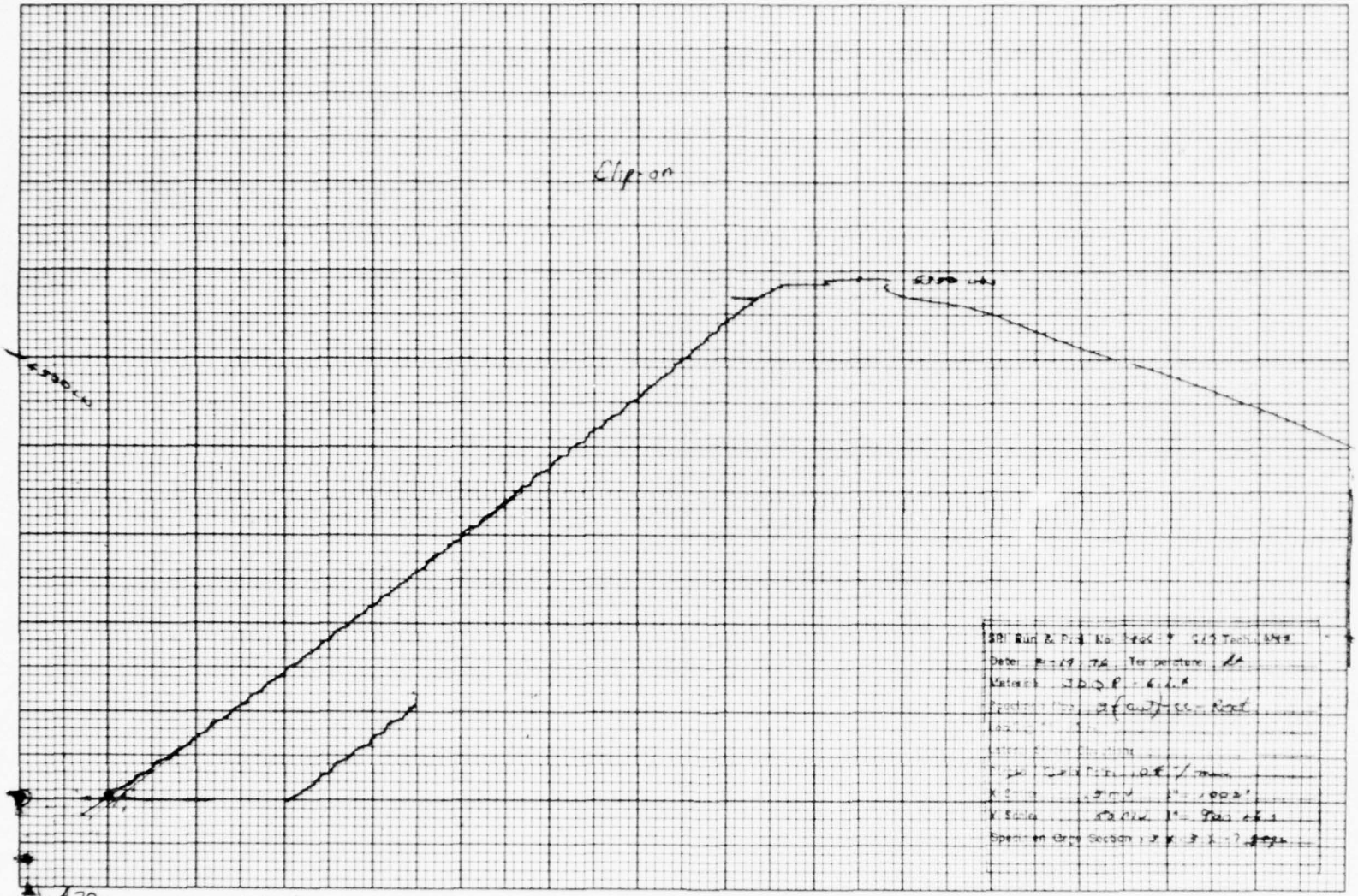

Figure A.70 Test Results for Specimen 3-(out)-CC-Acct

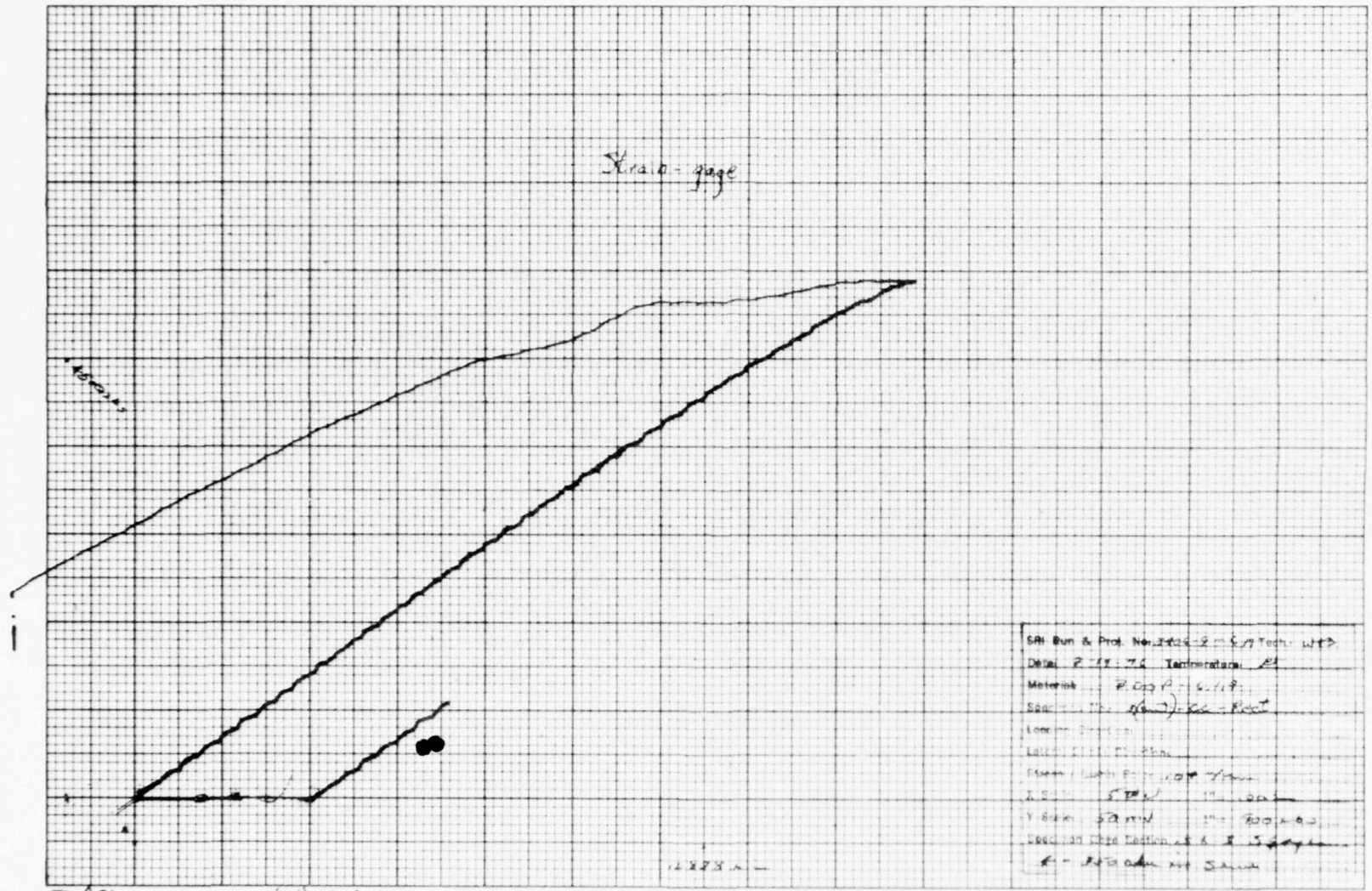

Figure A.71. Test Results for Specimen 3(Aut)-CC$_{Trans}$-Rect

A6

Circumferential Compressive Tests
Rectangular Specimen Configuration

4.1.18

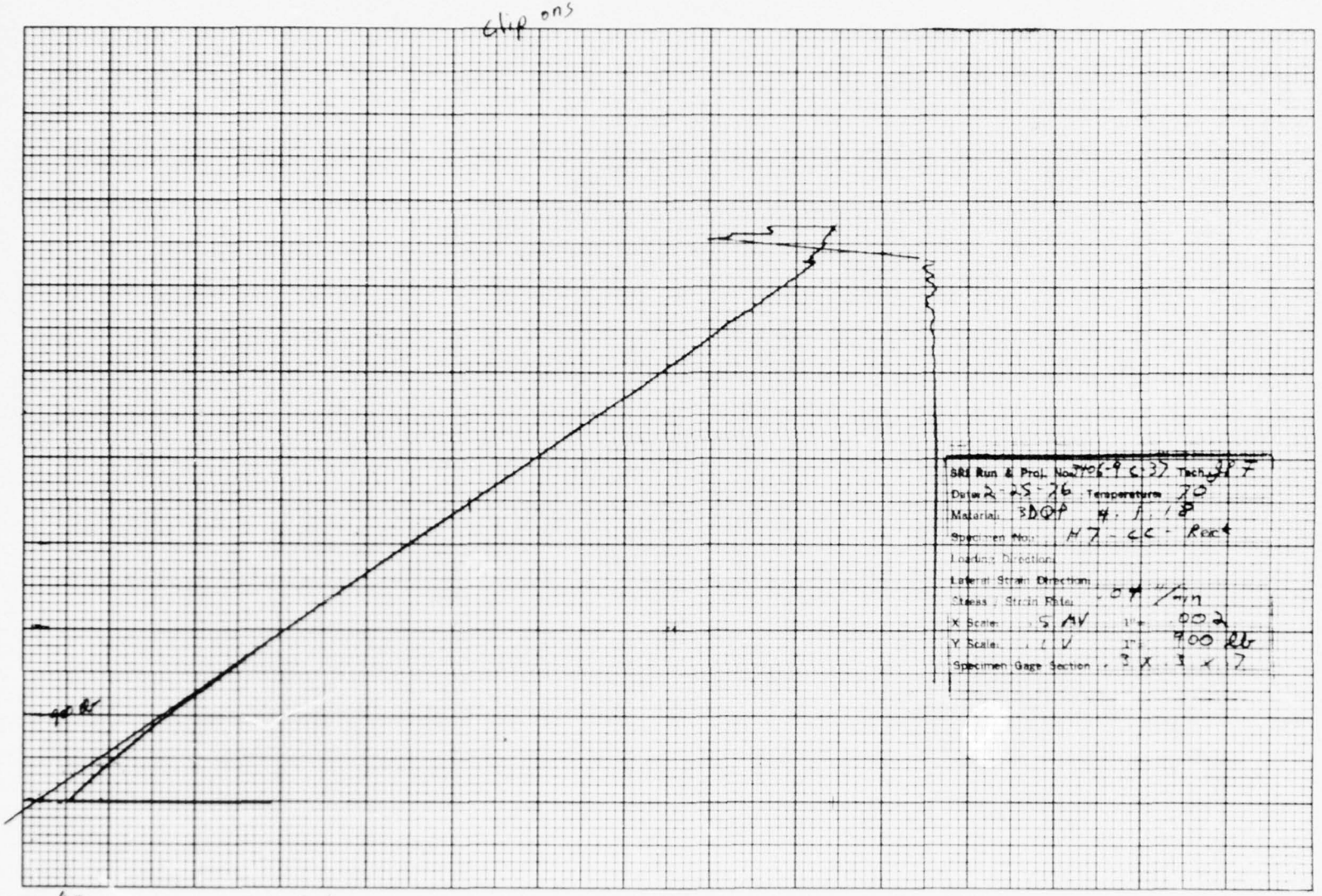

Figure A22 Test Results for Specimen H7-CC-Rect

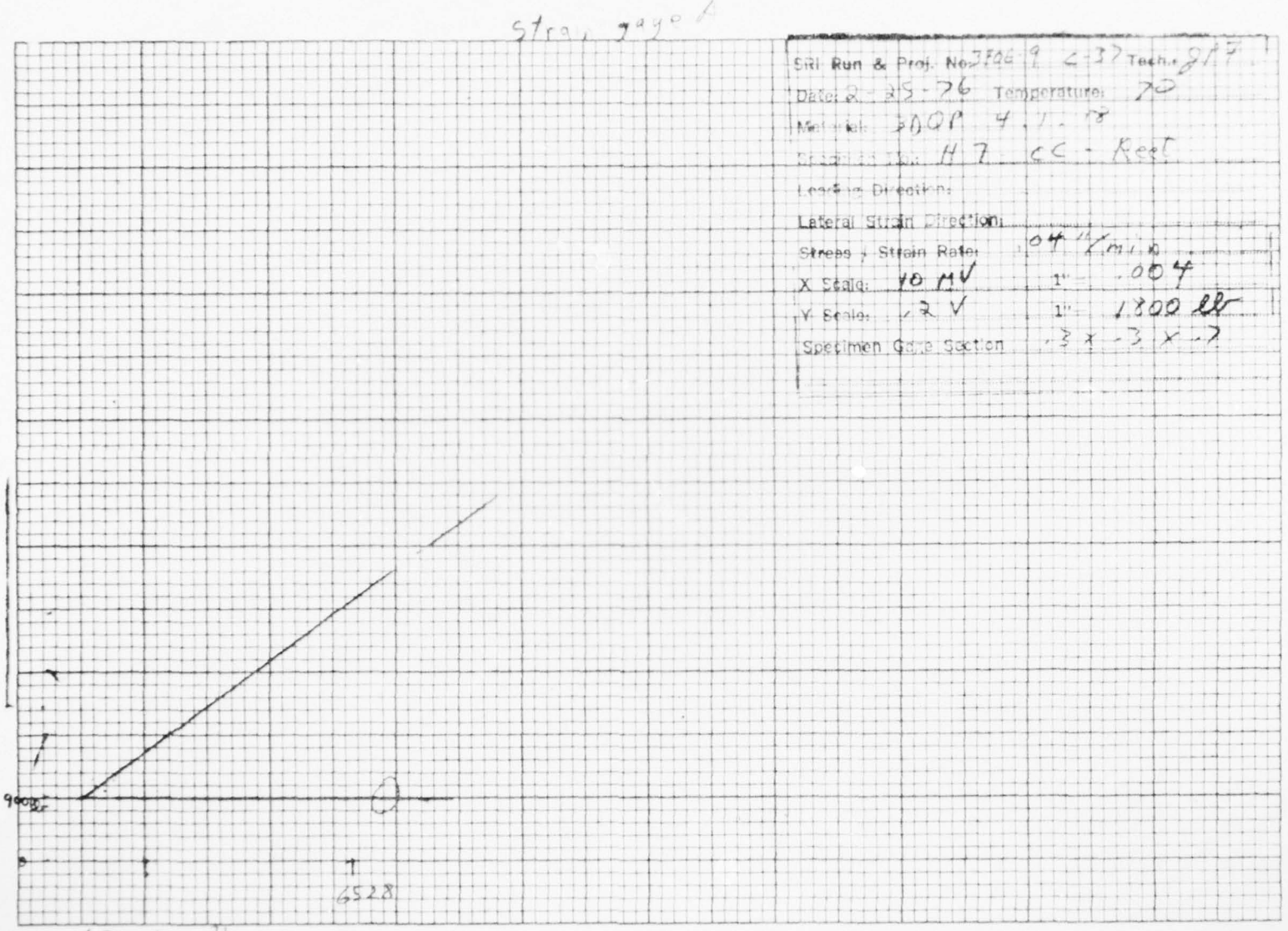

Figure A-73. Test Results for Specimen H7-CC-Rect

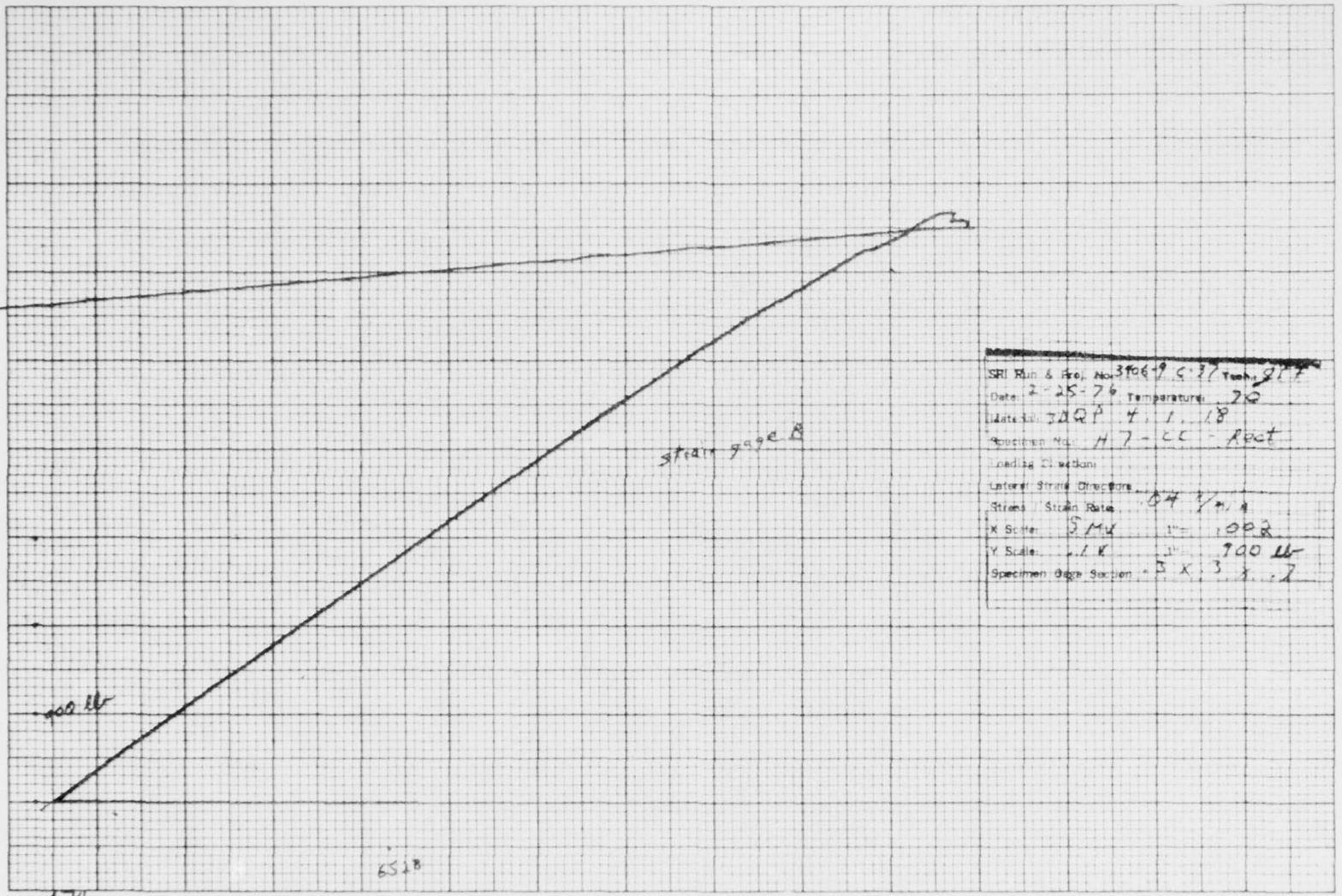

Figure 474 Test Results for Specimen H7-CC-Rect

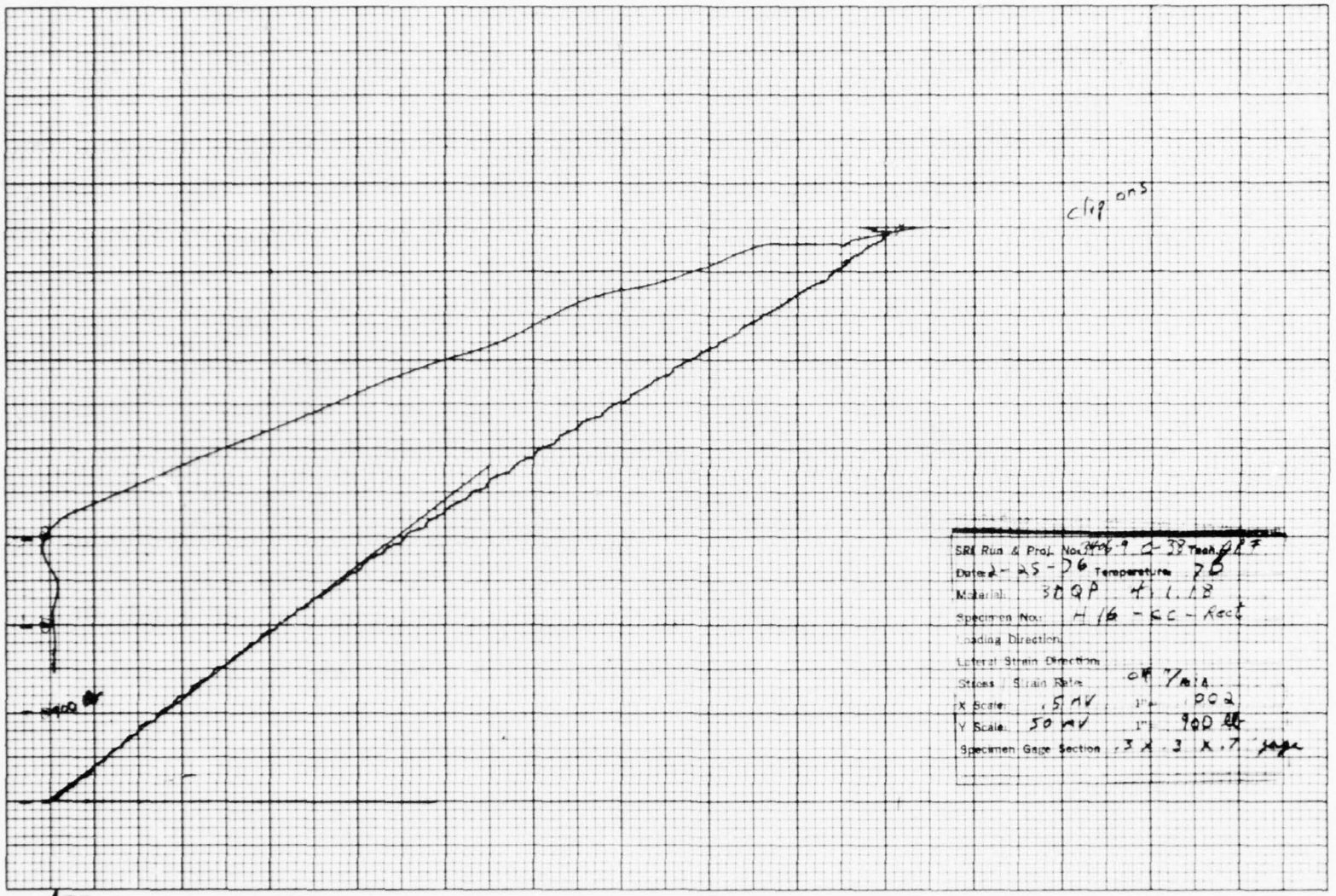

Figure A75 Test Results for Specimen H16-CC-Rect

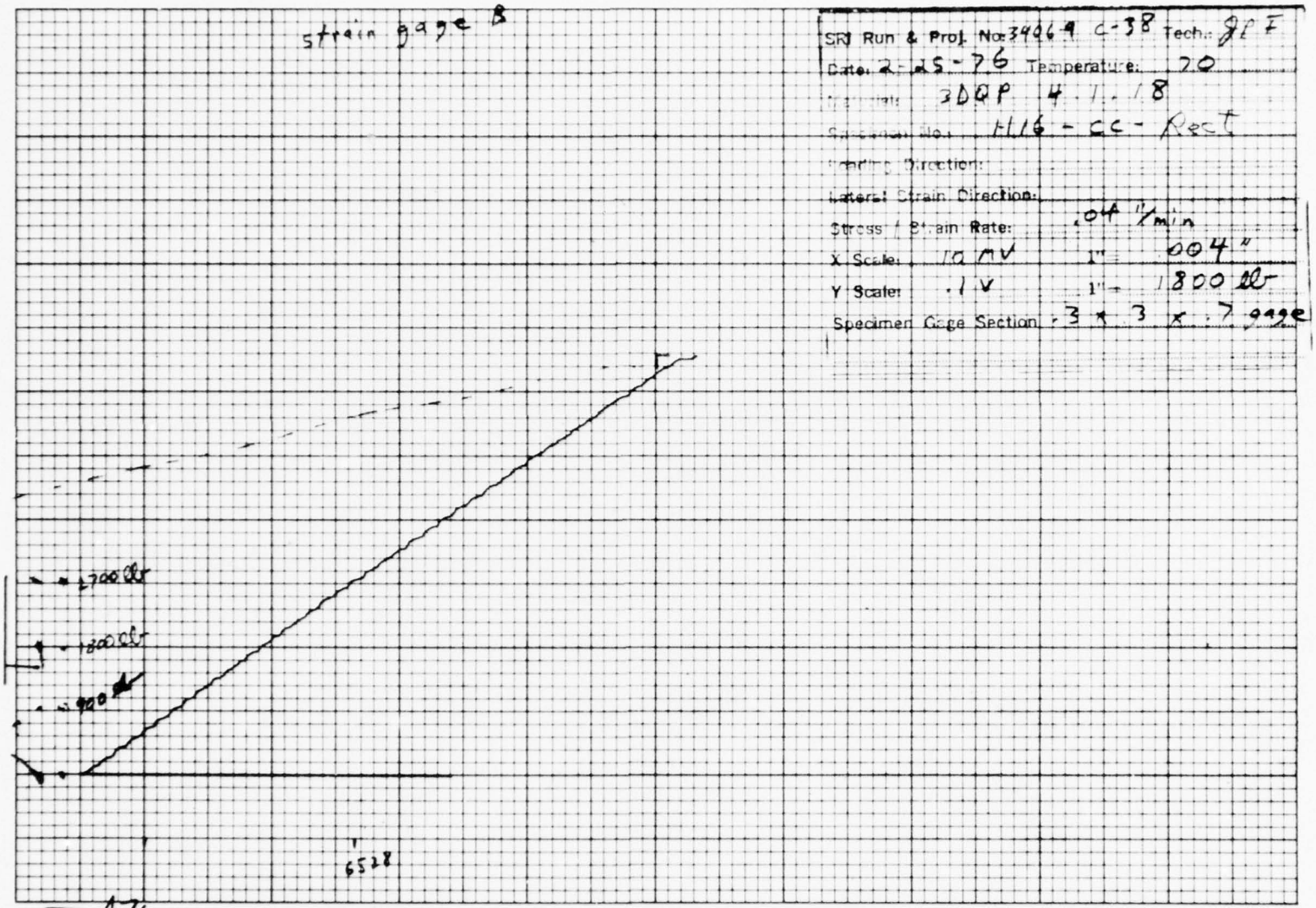

Figure A76 Test Results for Specimen H16-CC-Rect

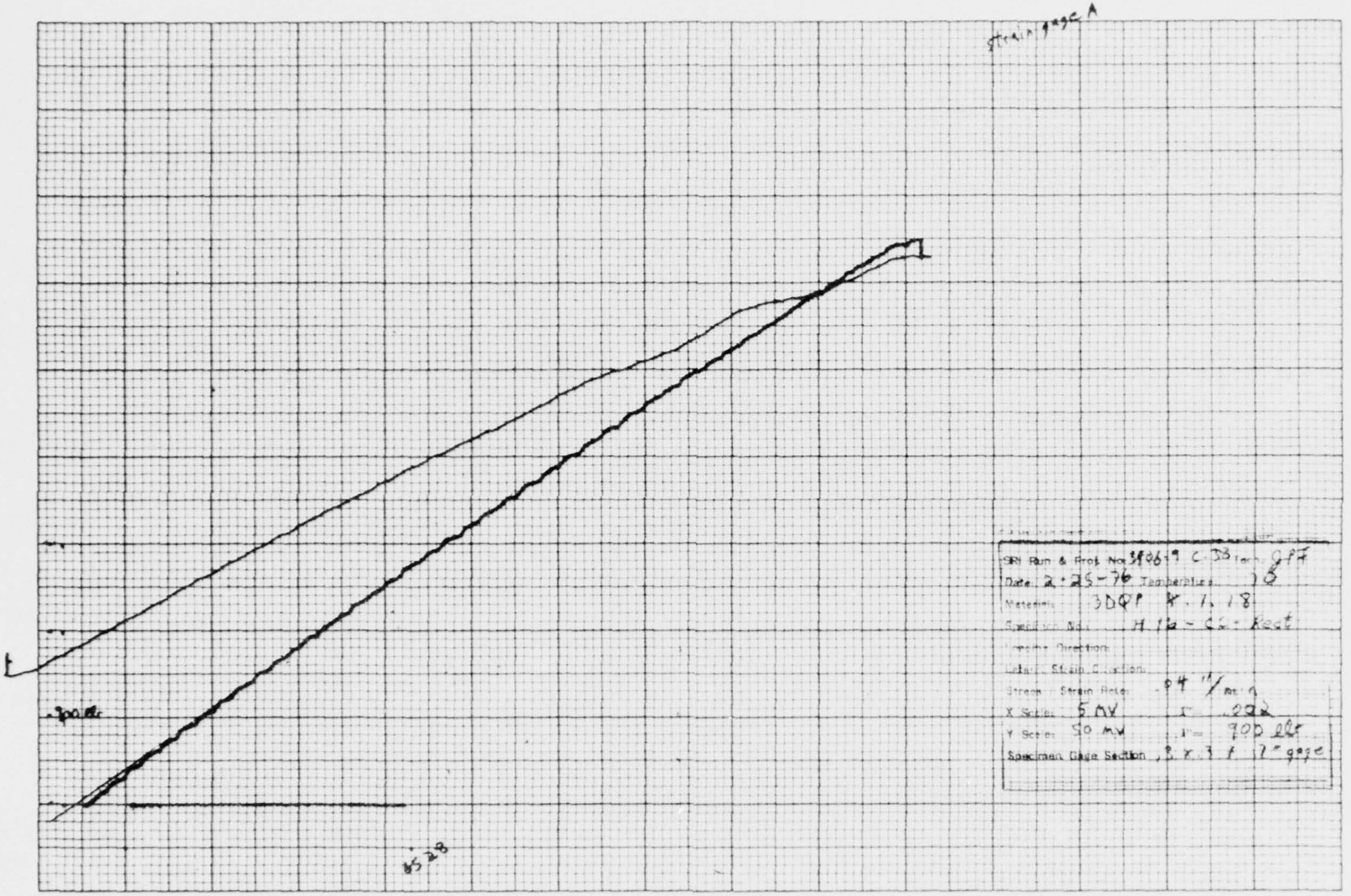

Figure A.77 Test Results for Specimen H-11a-CC-Rect

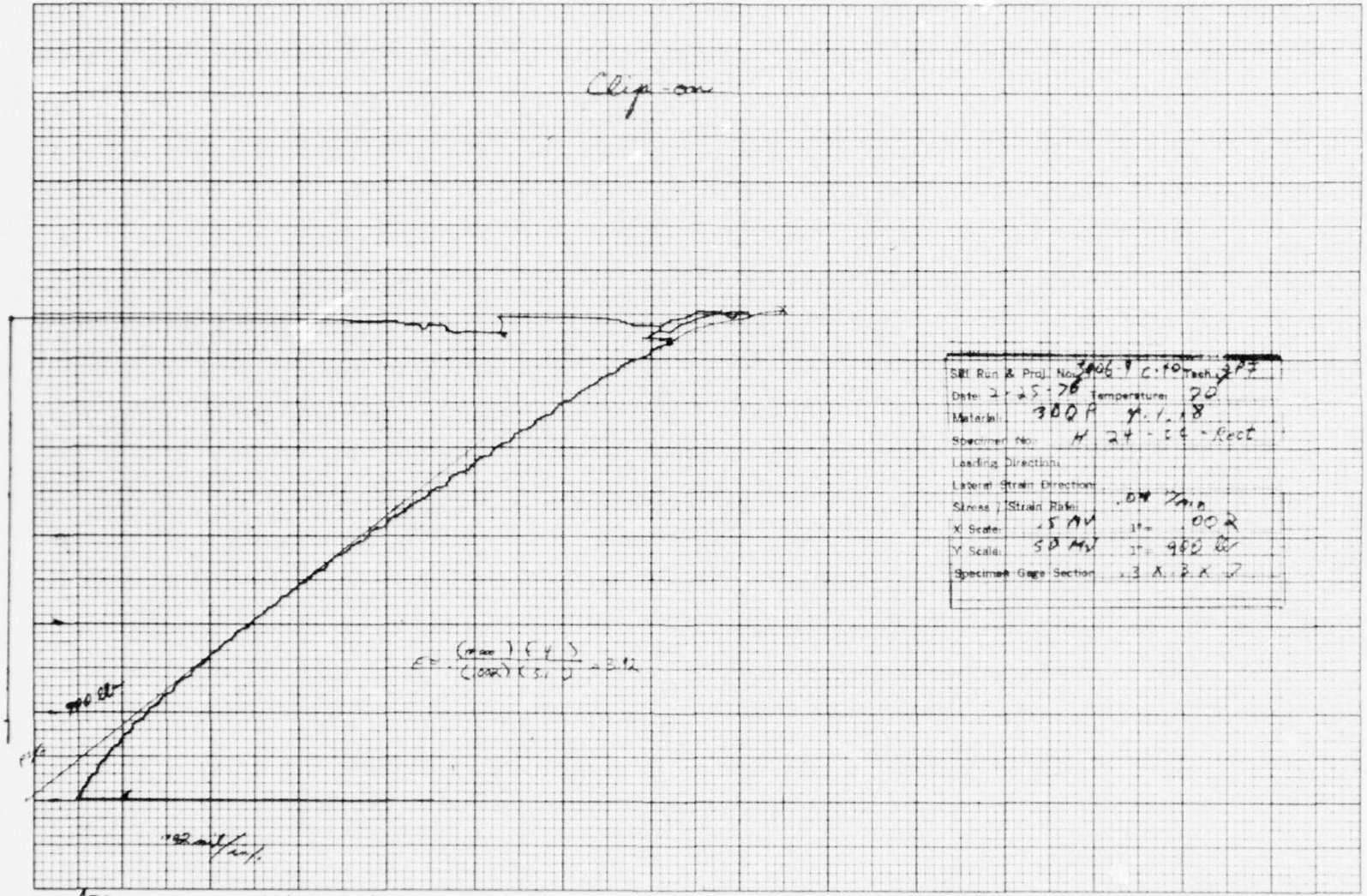

Figure A78. Test Results for Specimen H24-CC-Rect

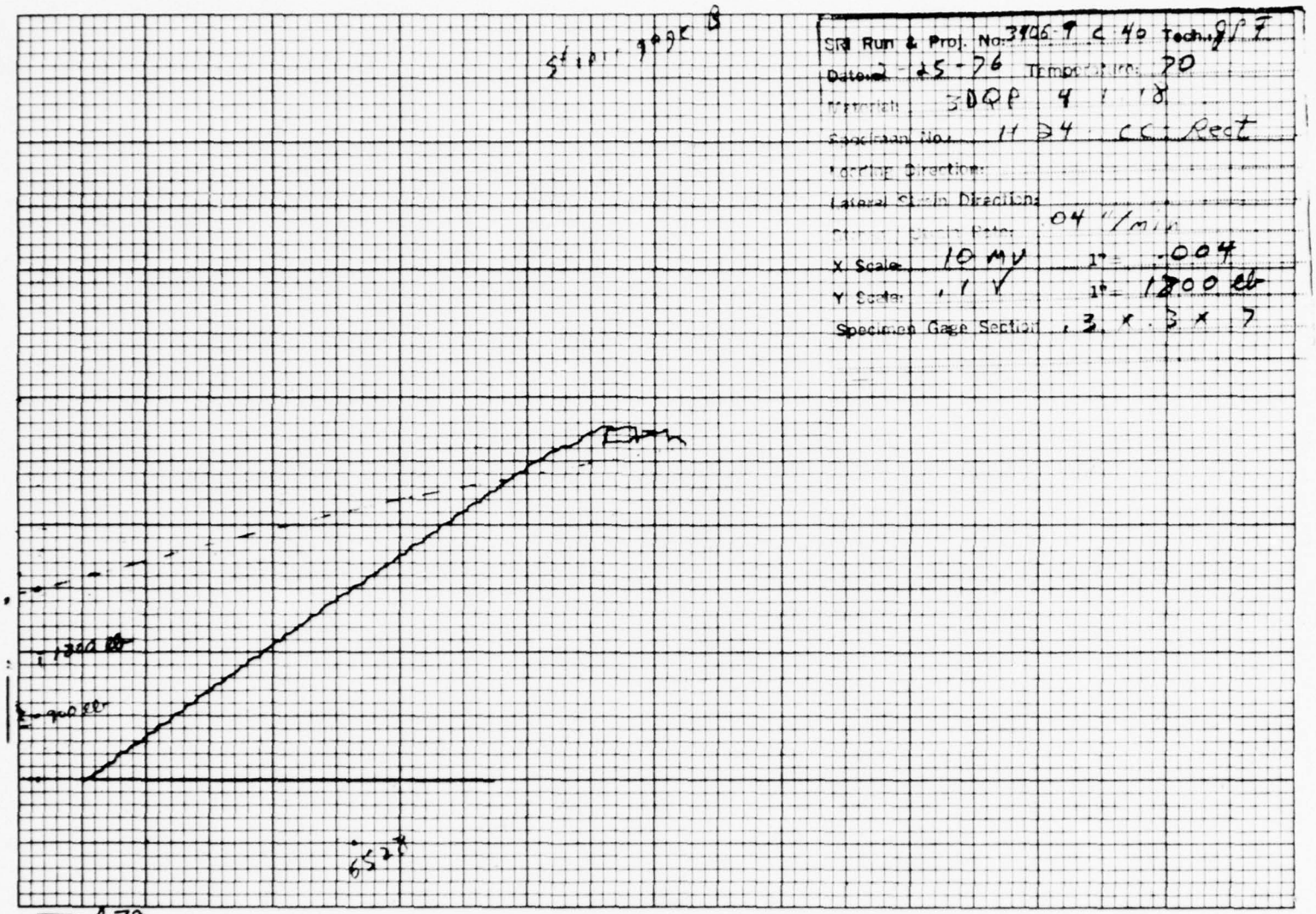

Figure A79 Test Results for Specimen .....

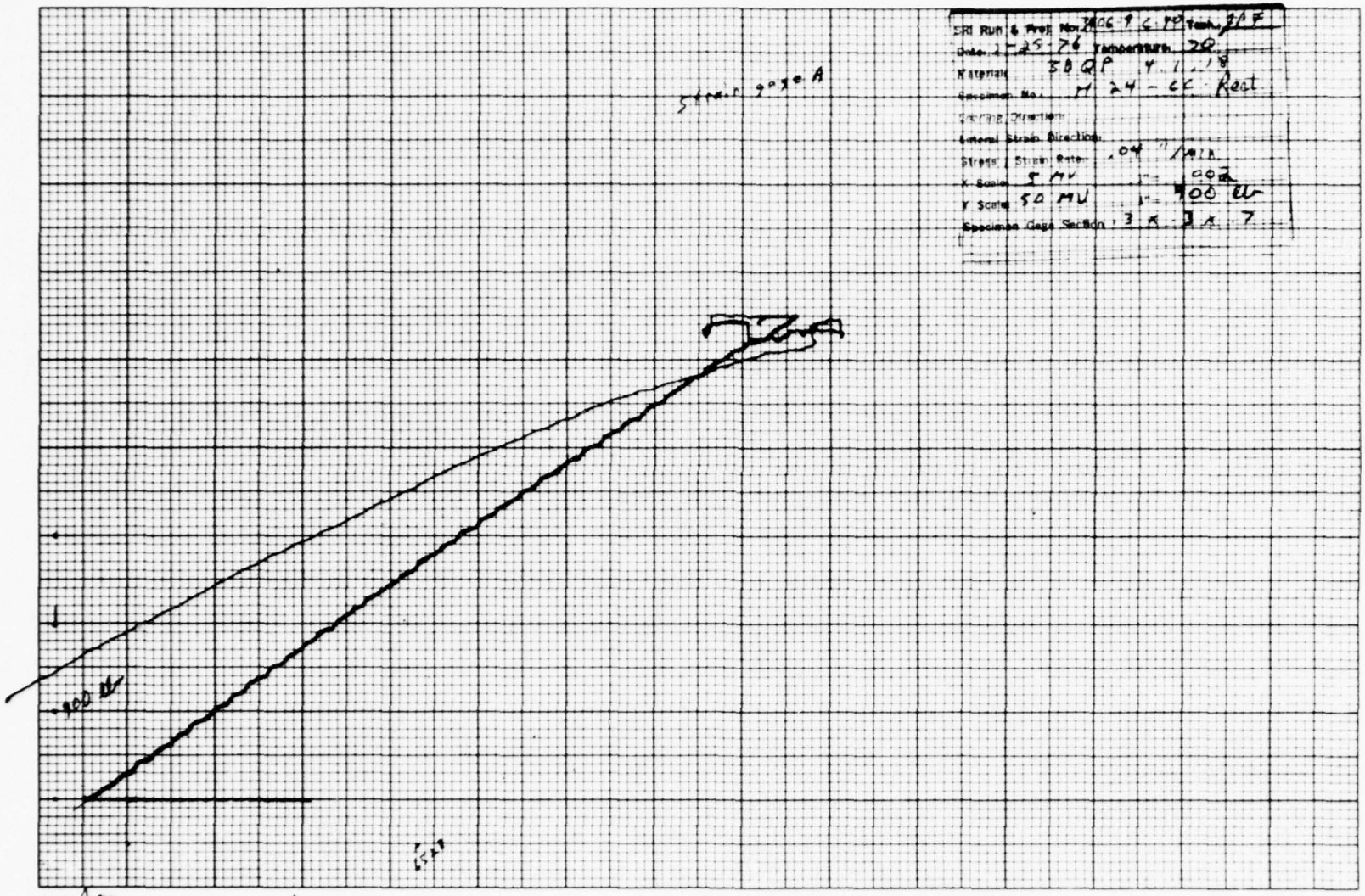

Figure A-80 Test Results for Specimen H24-CC-Rect

2nd run of spec

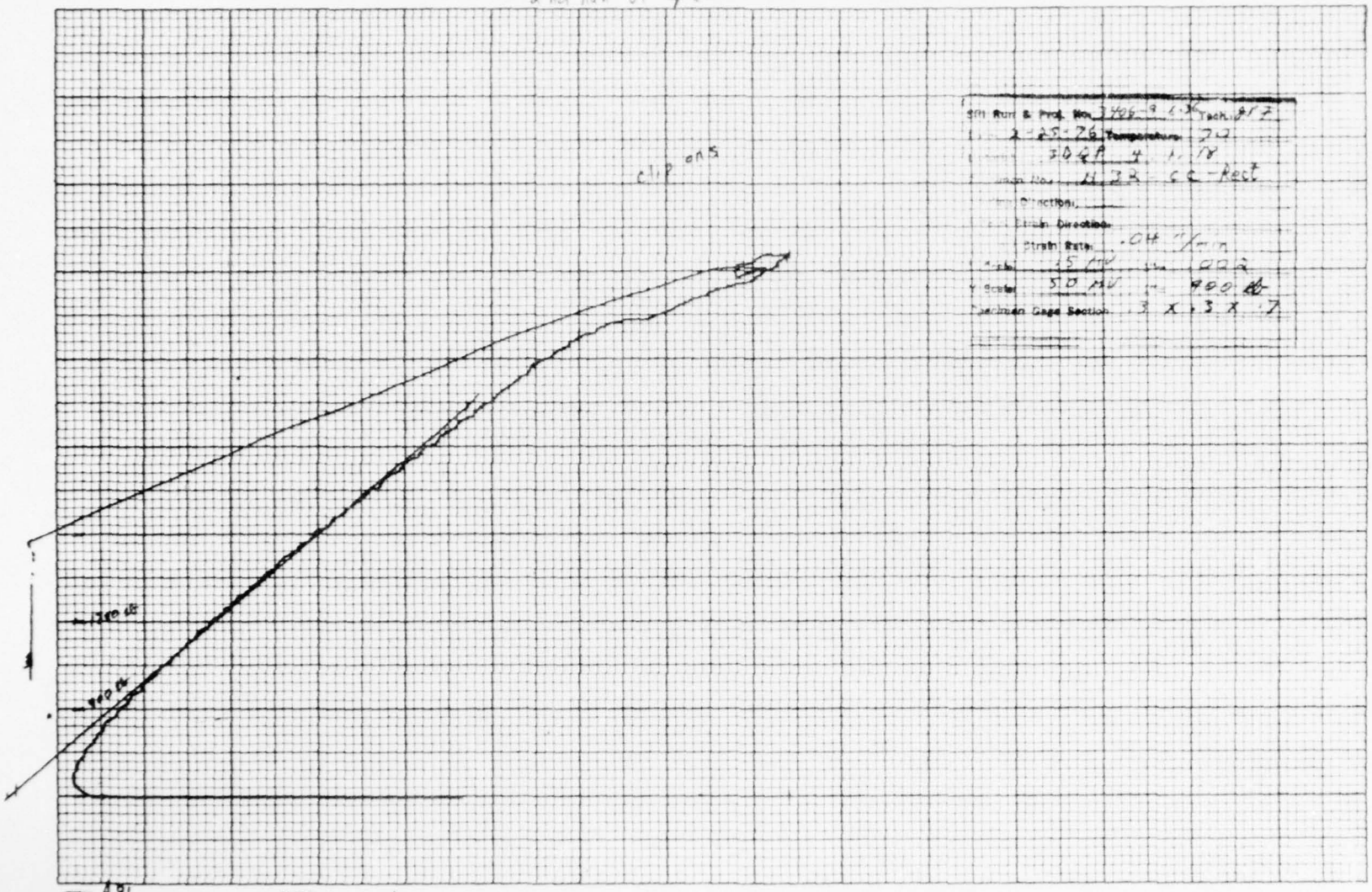

Figure A81 Test Results for Specimen H32-CC-Rect

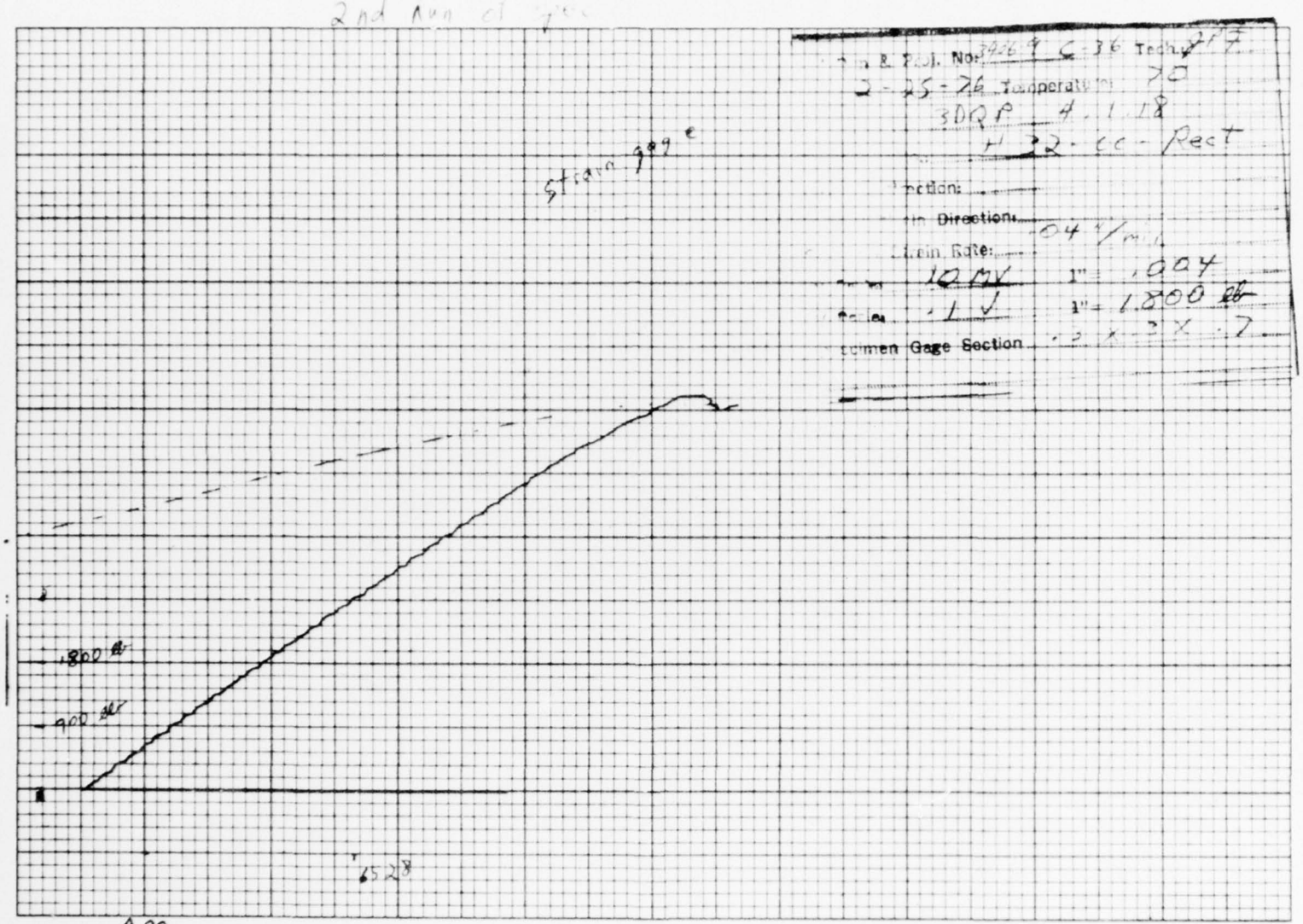

Figure A82 Test Results for Specimen H 32-CC-Rect

2nd Run of Spec

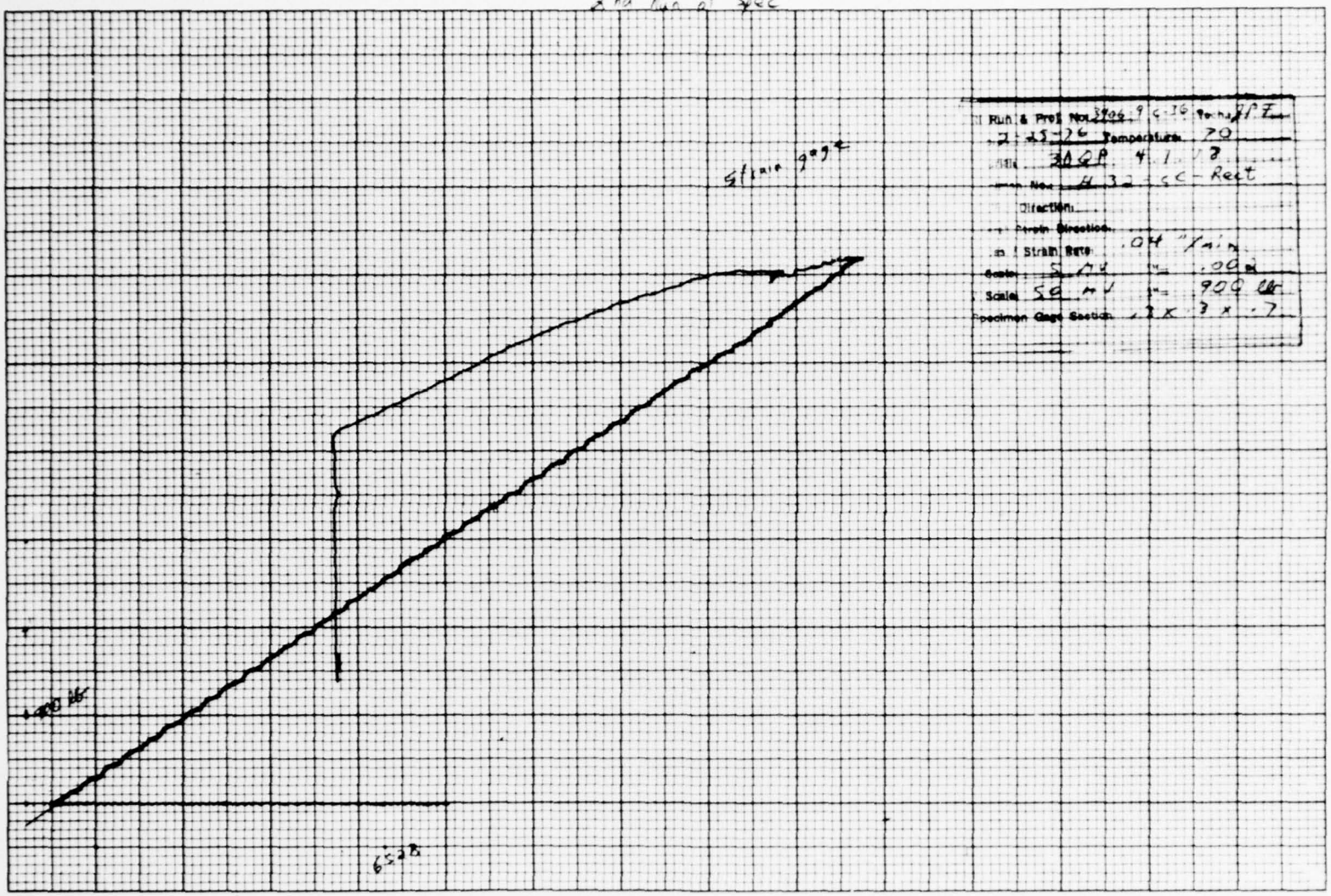

Figure A83 Test Results for Specimen H 32-CC-Rect

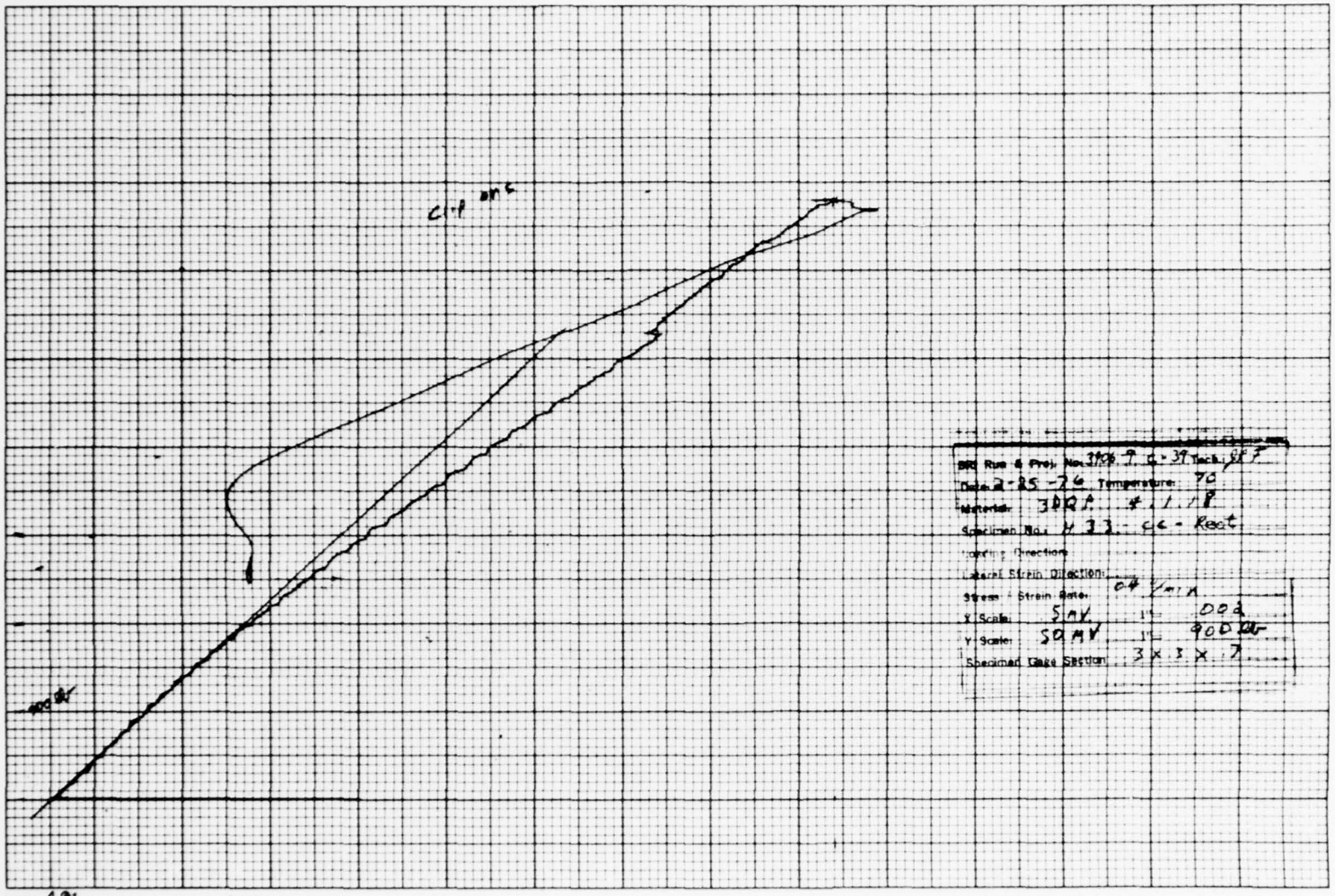

Figure A84. Test Results for Specimen H33-CC-Rect

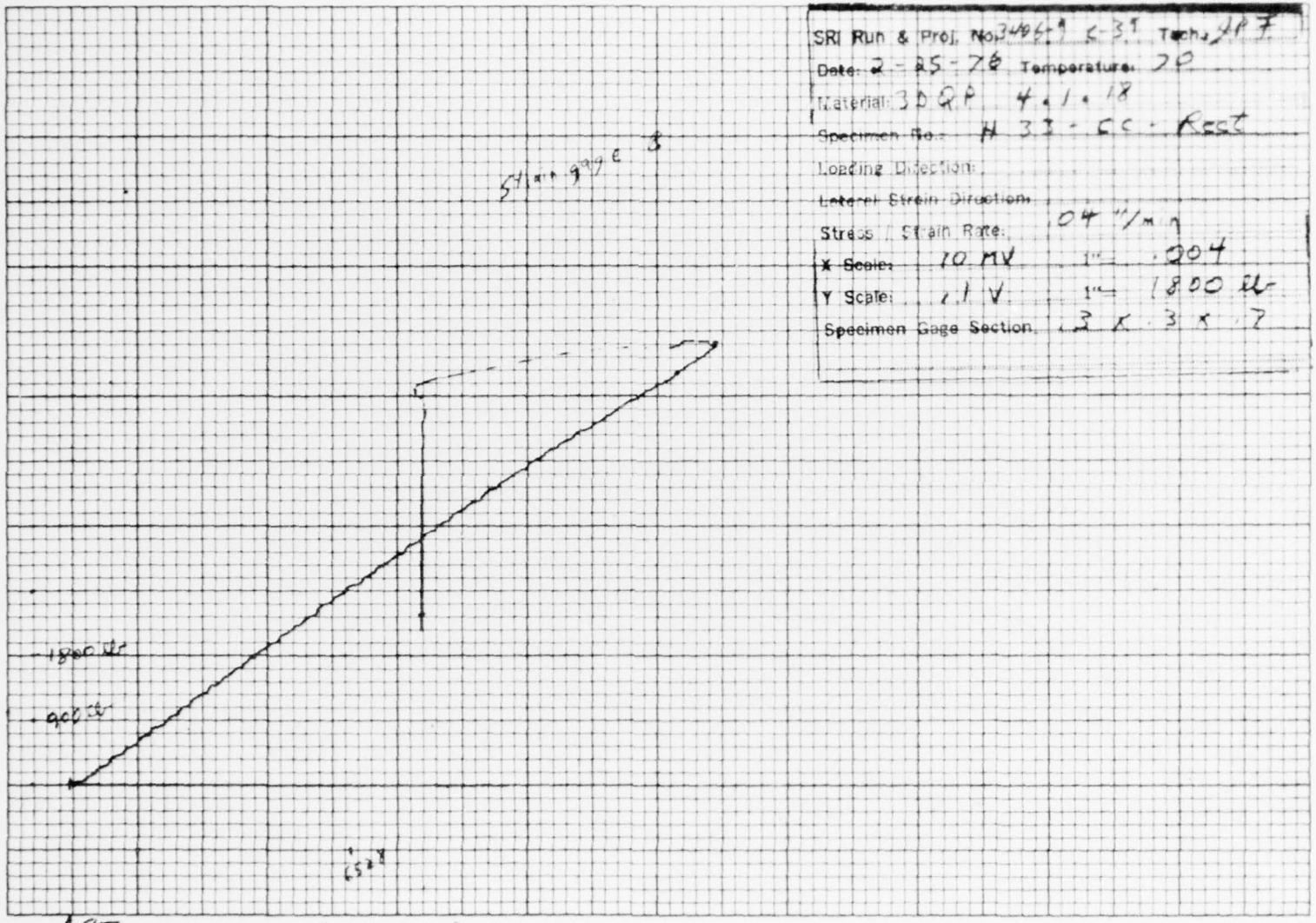

Figure A85 Test Results for Specimen H 33-CC-Rect

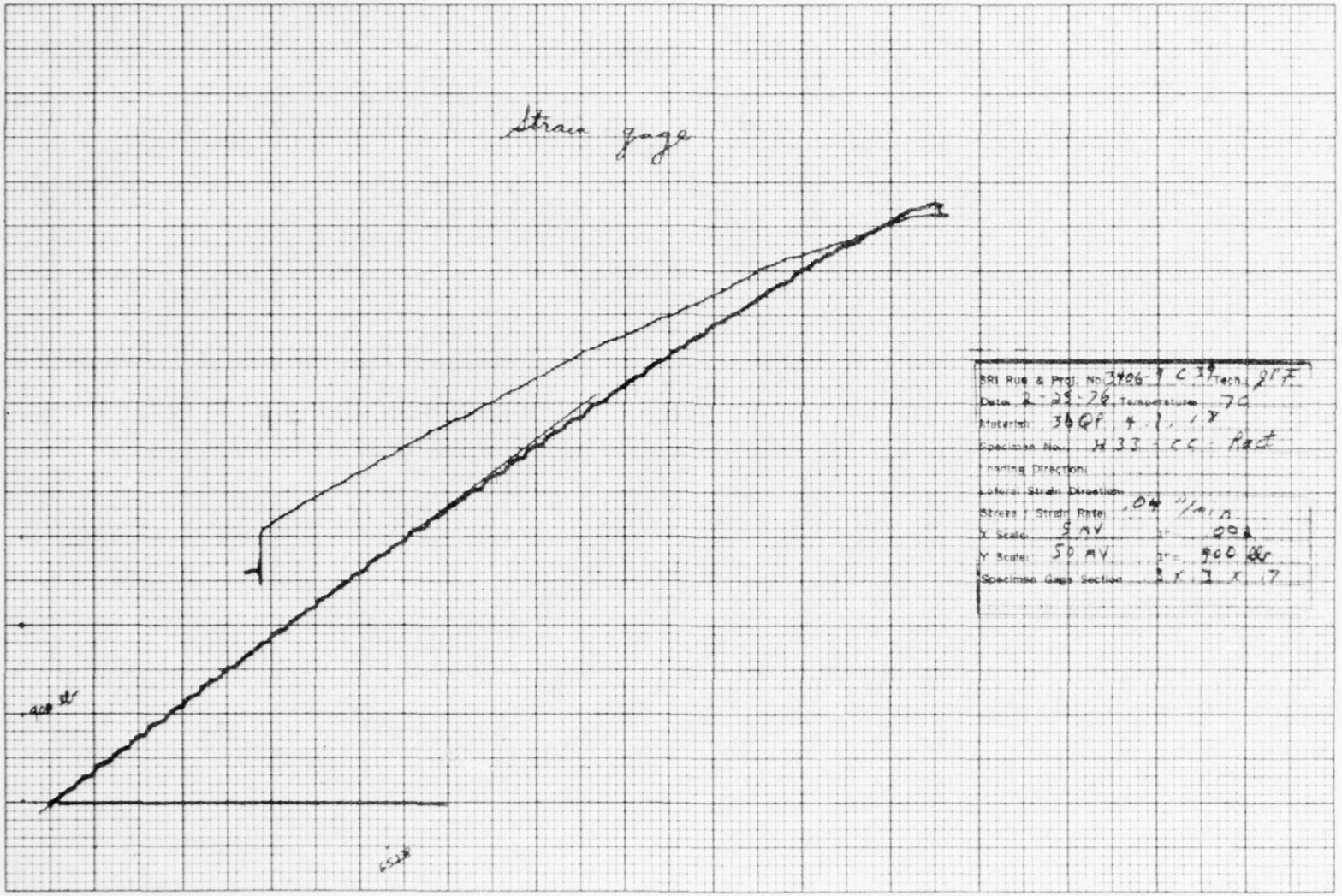

Figure A86 Test Results for Specimen H-33-CC-Rect

APPENDIX B

Ultrasonics

ULTRASONICS

The classical theory of the propagation of waves in elastic solid media describes the longitudinal motion of an element between two adjacent cross sections in a long prismatical bar by the equation

$$\frac{\partial^2 u}{\partial t^2} = V_o^2 \frac{\partial^2 u}{\partial x^2}$$

where

u = longitudinal displacement
x = distance along the longitudinal axis of the bar
t = time
$V_o = (E/\rho)^{1/2}$
E = modulus of elasticity, and
ρ = mass per unit volume

The general solution to the equation of motion can be written in the form

$$u = f(x + V_o t) + g(x - V_o t)$$

and is seen to represent two waves traveling in opposite directions along the longitudinal axis of the bar with constant velocity V_o. Thus V_o is the velocity of wave propagation and depends only on the modulus of elasticity and the density. It must be kept in mind, of course, that the assumption of a long prismatical bar infers that the transverse dimensions of the bar are small when compared to the length, and it is also assumed that the cross sections of the bar remain plane during deformation.

Sound transmission measurements for flaw detection and velocity are made utilizing a Sperry UM721 reflectoscope. The pulsed echo, reflection technique is used for detecting flaws. At 1 MHz, propagation is limited to a distance of approximately 12 inches -- or to state it another way -- a discontinuity at a depth below 6 inches of the surface is out of range. Sound velocity is determined by the through-transmission, elapsed-time method using the Sperry UM721 as a pulser unit and a Tektronix 564 oscilloscope complete with a 3B3 time base unit (time base precision of 1%) and a 3A3 vertical amplifier as measuring devices. Using this

method, a short pulse of longitudinal mode sound is transmitted through the specimen. An electrical pulse originates in a pulse generator and is applied to a ceramic piezoelectric crystal (SFZ). The pulse generated by this crystal is transmitted through a short delay line and inserted into the specimen. The time of insertion of the leading edge of this sound beam is the reference point on the time base of the oscilloscope which is used as a "high-speed stop watch". When the leading edge of this pulse of energy reaches the other end of the specimen, it is displayed on the oscilloscope. The difference between the entrance and exit times is used with the specimen length in calculating ultrasonic velocity. A short lucite delay line is used to allow time isolation of the sound wave from electrostatic coupling and to facilitate clear presentation of the leading edge of the entrant wave resulting in a more accurate "zero" in time. Reading time to inital rise portion of the sound wave gives some freedom from frequency distortion. This ultrasonic test system utilizes a longitudinal wave motion at frequencies near 1 MHz for graphites. A block diagram of the ultrasonic velocity measuring apparatus is shown in Figure B-1.

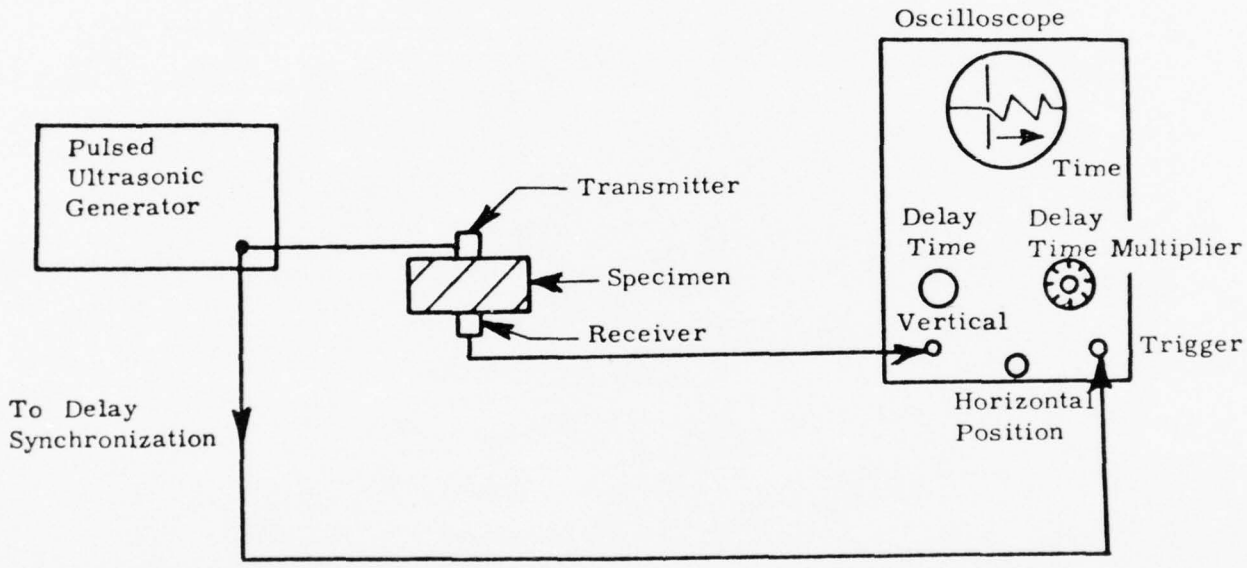

Figure B-1. Block Diagram of Ultrasonic Velocity Measuring Apparatus

DISTRIBUTION LIST

DEPARTMENT OF DEFENSE

Director
Defense Advanced Rsch. Proj. Agency
ATTN: Strategic Tech. Office

Defense Communication Engineer Center
ATTN: Code 720, John Worthington

Director
Defense Communications Agency
ATTN: NMCSSC Code 510

Defense Documentation Center
12cy ATTN: TC

Director
Defense Intelligence Agency
ATTN: DT-1C, Nuc. Eng. Branch
ATTN: DIA-DT-2, Tony Dorr
ATTN: DI-7D
ATTN: DT-2, Wpns. & Sys. Division

Director
Defense Nuclear Agency
ATTN: STSI, Archives
3cy ATTN: STTL, Tech. Library
ATTN: SPSS
ATTN: SPAS
ATTN: DDST
ATTN: STSP
ATTN: SPTD

Director of Defense Rsch. & Engineering
ATTN: George R. Barse
ATTN: DD/S&SS, John B. Walsh
ATTN: AD/ET, J. Persh
ATTN: AD/ET
ATTN: AD/OS
ATTN: DD/S&SS
ATTN: DD/R&AT
ATTN: AD/DS

Commander
Field Command, Defense Nuclear Agency
ATTN: FCTMOF
ATTN: FCPR
ATTN: FCTMD
ATTN: FCTMOT, Lieutenant Commander Strode

Director
Joint Strat. Tgt. Planning Staff, JCS
ATTN: JPTP
ATTN: JPTM
ATTN: JLTW-2
ATTN: JPST

Chief
Livermore Division, Field Command, DNA
ATTN: FCPRL

OJCS/J-5
ATTN: J-5, Plans & Policy, R & D Division

Studies Analysis and Gaming Agency
Joint Chiefs of Staff
ATTN: SDEB

DEPARTMENT OF THE ARMY

Director
BMD Advanced Tech. Center
ATTN: CRDABH-S, William C. Loomis
ATTN: ATC-T, Melvin T. Capps
ATTN: Marcus Whitfield

Program Manager
BMD Program Office
ATTN: DACS-BMT, John Shea
ATTN: DACS-BMT, Clifford E. McLain
ATTN: Technology Division
ATTN: DACS-BMZ-D, Julian Davidson
ATTN: DACS-BMZ

Commander
BMD System Command
ATTN: BDMSSC-TEB, R. Simpson
ATTN: BDMSC-TEN, Noah J. Hurst

Deputy Chief of Staff for Rsch. Dev. & Acq.
ATTN: NCB Division

Deputy Chief of Staff for Ops. & Plans
ATTN: Director of Nuc. Plans & Policy

Commander
Harry Diamond Laboratories
ATTN: DRXDO-NP, Francis N. Wimenitz
ATTN: DRXDO-NP, Louis J. Belliveau
ATTN: DRXDO-RBH, James H. Gwaltney
ATTN: DRXDO-RC, Robert B. Oswald, Jr.

Commander
Picatinny Arsenal
ATTN: SARPA-FR-E, Louis Avrami
ATTN: SARPA-ND-C-T, Donald Miller
ATTN: Al Loeb
ATTN: SMUPA-MD, Henry Opat
ATTN: F. Cotton

Director
TRASANA
ATTN: R. E. DeKinder, Jr.

Director
U.S. Army Ballistic Research Labs.
ATTN: DRXBR-TB, J. T. Frasier
ATTN: DRXRD-BVL, William J. Schuman, Jr.
ATTN: DRXBR-TL-IR, J. H. Keefer
ATTN: Robert E. Eichelberger
ATTN: DRXBR-X, Julius J. Meszaros
ATTN: Richard Vitali

Commander
U.S. Army Mat. & Mechanics Rsch. Center
ATTN: DRXMR-HH, John F. Dignam

Commander
U.S. Army Missile Command
ATTN: DRSMI-XS, Chief Scientist
ATTN: DRSMI-RRR, Bud Gibson
ATTN: DRCPM-PE-EA, Wallace O. Wagner
ATTN: Troy Smith
ATTN: DRS-RKP, W. B. Thomas

DEPARTMENT OF THE ARMY (Continued)

Commander
U.S. Army Materiel Dev. & Readiness Command
ATTN: DRCDE-D, Lawrence Flynn

Commander
U.S. Army Nuclear Agency
ATTN: COL Deverill
ATTN: ATCA-NAW
ATTN: MONA-WE
ATTN: CDC-NVA
ATTN: MAJ J. Vecke
ATTN: MONA-SA

Chief
U.S. Army Research Office
ATTN: Technical Library

DEPARTMENT OF THE NAVY

Chief of Naval Material
ATTN: MAT 0323, Irving Jaffe

Chief of Naval Operations
ATTN: OP 62
ATTN: Robert A. Blaise
ATTN: OP 981
ATTN: Code 604C3, Robert Piacesi
ATTN: OP 981

Chief of Naval Research
ATTN: Code 464, Thomas P. Quinn

Director
Naval Research Laboratory
ATTN: Code 7770, Gerald Cooperstein
ATTN: Code 2600, Tech. Library
ATTN: Code 5180, Mario A. Persechino

Commander
Naval Sea Systems Command
ATTN: ORD-0333A
ATTN: 0333A, Marlin A. Kinna
ATTN: Code 0351

Commander
Naval Surface Weapons Center
ATTN: Code 2302, Leo F. Gowen
ATTN: Code 322, Victor C. Dawson
ATTN: Code WA501, Navy Nuc. Prgms. Off.
ATTN: Code 323, W. Carson Lyons
ATTN: Code 241, Joseph Petes

Commanding Officer
Naval Weapons Evaluation Facility
ATTN: Peter Hughes
ATTN: Lawrence R. Oliver

Director
Strategic Systems Project Office
ATTN: NSP-272
ATTN: NSP-273

DEPARTMENT OF THE AIR FORCE

Commandant
AF Flight Dynamics Laboratory, AFSC
ATTN: FXG

DEPARTMENT OF THE AIR FORCE (Continued)

AF Geophysics Laboratory, AFSC
ATTN: Chan Touart

AF Materials Laboratory, AFSC
ATTN: MBC, Donald L. Schmidt
ATTN: MAS
ATTN: MBE, George F. Schmitt
ATTN: LPH, Gordon Griffith
ATTN: T. Nicholas
ATTN: LTM
ATTN: Bill Kessler

AF Rocket Propulsion Laboratory, AFSC
ATTN: RTSN, G. A. Beale

AF Weapons Laboratory, AFSC
ATTN: ALO, Maj Lawrence T. James
ATTN: SUL
ATTN: SAB
ATTN: Al Sharp
ATTN: Dr. Minge
2cy ATTN: NTO
ATTN: Tech. Review
ATTN: DYS, Lt E. J. Burns
ATTN: DYT
ATTN: DYV

AFTAC
ATTN: Col Earnest F. Dukes, Jr.

Headquarters
Air Force Systems Command
ATTN: SOSS
ATTN: XRTO

Commander
Arnold Engineering Development Center
ATTN: XOA

Commander
ASD
4cy ATTN: EWES, D. Ward

Commander
Foreign Technology Division, AFSC
ATTN: TDPTN
ATTN: TDFBD, J. D. Pumphrey
ATTN: PDBG

HQ USAF/RD
ATTN: RDQSM
ATTN: RDPM
ATTN: RDQ
ATTN: RDQSM
ATTN: David S. Hyman
ATTN: RD

HQ USAF/XO
ATTN: XOOSS

SAMSO/DY
ATTN: DYS

SAMSO/RS
ATTN: RSSE
ATTN: RSS
ATTN: RST

DEPARTMENT OF THE AIR FORCE (Continued)

SAMSO/ MN
ATTN: MNNR

Commander in Chief
Strategic Air Command
ATTN: XPFS
ATTN: DOXT
ATTN: XPQM
ATTN: XOBM
ATTN: NRI

ENERGY RESEARCH AND DEVELOPMENT ADMIN

Division of Military Application
ATTN: Doc. Con. for Res. & Dev. Branch

University of California
ATTN: G. Staihle, L-24
ATTN: Joseph B. Knox, L-216
ATTN: C. Joseph Taylor, L-92
ATTN: Larry W. Woodruff, L-96
ATTN: Joseph E. Keller, Jr., L-125

Los Alamos Scientific Laboratory
ATTN: Doc. Con. for J. W. Taylor
ATTN: Doc. Con. for Richard A. Gentry
ATTN: Doc. Con. for T. Talley
ATTN: Doc. Con. for John McQueen
ATTN: Doc. Con. for Donald Kerr
ATTN: Doc. Con. for R. S. Thurston

Sandia Laboratories
ATTN: Doc. Con. for T. Gold
ATTN: Doc. Con. for C. S. Hoyle
ATTN: Raymond Ng
ATTN: Doc. Con. for 8131, H. F. Norris, Jr.

Sandia Laboratories
ATTN: Doc. Con. for B. Caskey
ATTN: Doc. Con. for A. W. Snyder
ATTN: Doc. Con. for Albert Chabai
ATTN: Doc. Con. for Thomas B. Cook
ATTN: Doc. Con. for R. R. Boade
ATTN: Doc. Con. for Walter Herrmann
ATTN: Doc. Con. for D. McCloskey
ATTN: Doc. Con. for M. L. Merritt

DEPARTMENT OF DEFENSE CONTRACTORS

Acurex Corporation
ATTN: J. Huntington
ATTN: C. Nardo
ATTN: Robert M. Kendall
ATTN: J. Courtney

Aeronautical Rsch. Assoc. of Princeton, Inc.
ATTN: Coleman Donaldson

Aerospace Corporation
ATTN: J. McClelland
ATTN: W. Barry
ATTN: R. Allen
ATTN: R. Mortensen
ATTN: Richard Crolius, A2-Rm1027
ATTN: W. Mann
ATTN: R. Strickler

Analytic Services, Inc.
ATTN: Jack Selig

DEPARTMENT OF DEFENSE CONTRACTORS (Continued)

Aro, Incorporated
ATTN: John C. Adams

Avco Research & Systems Group
ATTN: John E. Stevens, J100
ATTN: S. Skemp, J200
ATTN: George J. Davis
ATTN: George Weber, J230
ATTN: Doc. Control
ATTN: William G. Reinecke, K100
ATTN: J. Patrick
ATTN: John Gilmore, J400

Battelle Memorial Institute
ATTN: E. Unger
ATTN: W. Pfeifer
ATTN: Richard Castle
ATTN: Merwyn R. Vanderlind

The Boeing Company
ATTN: Brian Lempriere
ATTN: Ed York
ATTN: William Crist
ATTN: Robert Dyrdahl
ATTN: Robert Holmes

The Boeing Company
ATTN: T. Swaney

Brown Engineering Company, Inc.
ATTN: Ronald Patrick

California Research & Technology, Inc.
ATTN: Ken Kreyenhagen

Calspan Corporation
ATTN: M. S. Holden
ATTN: M. G. Dunn
ATTN: Romeo A. Deliberis

University of Dayton
Industrial Security Super KL-505
ATTN: D. Gerdiman
ATTN: Hallock F. Swift

Effects Technology, Inc.
ATTN: Robert Wengler
ATTN: Richard Parise

Ford Aerospace & Communications Operations
ATTN: P. Spangler

General American Transportation Corp
General American Research Division
ATTN: Marion J. Balcerzak
ATTN: W. F. Byrne

General Dynamics Corp.
Convair Aerospace Division
ATTN: R. Shemensky

General Electric Company
ATTN: Phillip Cline
ATTN: Carl Anderson
ATTN: C. Kyriss
ATTN: B. M. Maguire
ATTN: A. Martellucci
ATTN: G. Harrison
ATTN: Daniel Edelman

DEPARTMENT OF DEFENSE CONTRACTORS
(Continued)

General Electric Company
TEMPO-Center for Advanced Studies
ATTN: DASIAC
ATTN: B. Gambill

General Research Corporation
ATTN: T. Stathacopoulos
ATTN: John Ise, Jr.
ATTN: Robert E. Rosenthal

Institute for Defense Analyses
ATTN: IDA Librarian, Ruth S. Smith
ATTN: Joel Bengston

Ion Physics Corporation
ATTN: Robert D. Evans

Kaman Avidyne
Division of Kaman Sciences Corp.
ATTN: Ray Reutinick
ATTN: E. S. Criscione
ATTN: Norman P. Hobbs

Kaman Sciences Corporation
ATTN: R. Keefe
ATTN: John Keith
ATTN: John R. Hoffman
ATTN: Thomas Meagher
ATTN: Donald C. Sachs
ATTN: Frank H. Shelton

LFE Corporation
Environmental Analysis Lab. Division
ATTN: Marcel Nathans

Lockheed Missiles & Space Co., Inc.
ATTN: Gerald T. Chrusciel
ATTN: Charles M. Lee
ATTN: Arthur Collins, Dept. 81-14
ATTN: Art Thomas, Dept. 85-85
ATTN: L. D. Hull

Lockheed Missiles and Space Co.
ATTN: T. R. Fortune

Lockheed Missiles and Space Company
ATTN: F. G. Borgardt
ATTN: Raymond R. Capiaux

Martin Marietta Aerospace
ATTN: Laird Kinnaird
ATTN: G. Fotieo
ATTN: William A. Gray, MP-61
ATTN: Joyce Legare, MP-328
ATTN: H. Rosenthal
ATTN: James M. Potts, MP-61
ATTN: Gene Aiello

McDonnell Douglas Corporation
ATTN: Robert W. Halprin
ATTN: L. Cohen
ATTN: R. J. Reck
ATTN: Ken Kratch
ATTN: J. Kirby
ATTN: J. F. Garibotti
ATTN: H. Hurwicz

DEPARTMENT OF DEFENSE CONTRACTORS
(Continued)

McDonnell Douglas Corporation
ATTN: Jean McGrew

National Academy of Sciences
ATTN: Nat. Mat. Advisory Board for Donald G. Groves
ATTN: Nat. Mat. Advisory Board for Edward R. Dyer

Northrop Corporation
ATTN: Don Hicks

Pacific-Sierra Research Corp.
ATTN: Gary Lang

Physical Sciences, Inc.
ATTN: M. S. Finson

Physics International Company
ATTN: Doc. Con. for James Shea

Prototype Development Associates, Inc.
ATTN: John McDonald
ATTN: John Slaughter

R & D Associates
ATTN: Jerry Carpenter
ATTN: F. A. Field
ATTN: Harold L. Brode
ATTN: Albert L. Latter
ATTN: Cyrus P. Knowles

The Rand Corporation
ATTN: R. Robert Rapp

Raytheon Company
ATTN: Library

Science Applications, Inc.
ATTN: R. Fisher
ATTN: G. Ray
ATTN: John Warner
ATTN: Dwane Hove

Science Applications, Inc.
ATTN: Carl Swain
ATTN: Lyle Dunbar

Science Applications, Incorporated
ATTN: William M. Layson
ATTN: William R. Seebaugh

Southern Research Institute
ATTN: C. D. Pears
ATTN: J. R. Koenig
ATTN: G. F. Fornaro

Stanford Research Institute
ATTN: D. L. Huestis
ATTN: George R. Abrahamson
ATTN: Donald Curran
ATTN: Herbert E. Lindberg
ATTN: OAI
ATTN: Philip J. Dolan

DEPARTMENT OF DEFENSE CONTRACTORS
(Continued)

Stanford Research Institute
ATTN: Harold Carey
ATTN: W. B. Reuland

Systems, Science and Software, Inc.
ATTN: G. A. Gurtman
ATTN: Russell E. Duff

TRW Systems Group
ATTN: E. Y. Wong, 527/712
ATTN: William Polich
ATTN: Earl W. Allen, 520/141
ATTN: L. Berger
ATTN: V. Blankenship

DEPARTMENT OF DEFENSE CONTRACTORS
(Continued)

Terra Tek, Inc.
ATTN: Sidney Green

TRW Systems Group
ATTN: R. K. Plebuch, R1-2078
ATTN: Peter K. Dai, R1-2170
ATTN: Thomas G. Williams
ATTN: W. W. Wood
ATTN: D. H. Baer, R1-2136
2cy ATTN: I. E. Alber, R1-1008
ATTN: Peter Brandt, F1-2006